Characterization of the Upper Arkansas River Basin, Chaffee County Colorado

CSM/BSU Geophysics Field Camp 2008

June 5, 2008

Abstract

Each year, students in the department of Geophysics at the Colorado School of Mines participate in a summer field session upon completion of their junior year. For the fourth year in a row, the 2008 summer field session took place in Chaffee County, Colorado from May 11th through the 23rd before returning to Golden, Colorado for processing until June 6th.

Twenty-seven students from the Colorado School of Mines along with two additional students from Boise State University used a variety of geophysical methods in an attempt to characterize the subsurface geology of the Upper Arkansas River Valley. More specifically, they attempted to describe both the depth and location of the water table and to map the faulting structures. They spent the first three days studying the geology of the area, in order to better understand their geophysical approach, using the tools and techniques they learned at the Colorado School of Mines and Boise State University.

Very little is known about the subsurface structure, except for what past field sessions have discovered. Methods such as deep seismic and gravity were used in Chalk Creek Canyon along Road 90 and Highway 162 and near Highway 50 west of Salida. From this, students attempted to gain a better understanding of the faulting structures in those areas.

Other electrical methods were implemented which utilized electromagnetics, self potential, ground penetrating radar, and shallow seismic techniques in order to image the near-subsurface. This was carried out with the intention of gaining a better understanding of the location of the water table as well as the direction of flow which will help in identifying some spots to drill for hot water that can be used as a geothermal source of energy. A drainage ditch site was also inspected with the intention of determine the direction and amount of discharge from an irrigation channel.

Following a thirteen day period of data acquisition in Chaffee County, the students returned to the Colorado School of Mines in Golden, Colorado for an additional two weeks of data processing and interpretation. They drew many conclusions and made interpretations from both the north and south sites, where both deep and shallow geophysical methods were implemented.

Acknowledgements

Our geophysics field camp could not have been possible without the support of many organizations and individuals. We greatly appreciate the generous financial contributions made by the SEG Foundation to this year's field camp. In addition, Chaffee County not only let us use their roads for our measurements, but also granted support which helped pay for our meals (a well-fed student is a good student). We also want to thank those companies who donated not only funds but also knowledge and equipment, including CGG/Veritas and Sercel. CGG/Veritas lent Vibroseis trucks operated by Jose and Rolando, and kept in good running order by Marty. Rod Kellaway not only supervised the vib operation, but provided a great deal of insight on their use. Sercel USA lent us Tom Chatham and Malcolm Lansley who guided us through the tangle of seismic data acquisition. GX Technologies (now Ion) made available software and equipment for the formidable task of processing the deep seismic data with specific contributions in time given by Hans Ecke, Sissy Theisen, Rose Byrnes, And Gerardo Garcia (and Don Chitwood allowed it to happen). Roger and Barbara from the USGS logged wells in the Mt. Princeton and Cottonwood areas.

Many individuals offered their valuable time and know-how to advance our understanding of the area's geology and hydrology. Fred Henderson and Jordan Dimick supplied their experienced take on what is occurring geologically within the Valley and what they believe to be the hydrological situation. We are also grateful for the accommodations provided by Deer Valley Ranch.

Many local private citizens and organizations allowed access to their property. Bill Moore made his geothermal well (and bathroom!) available. Paul Jensen gave us the run of his hayfield down south. Mount Princeton Hot Springs Resort opened space to drop off and tune the vibrators. Many others allowed us to plant little flags and make measurements across or near their property. Many helped out by expressing enthusiasm for our project. We apologize if we left anyone out.

Karen Adams
Taylor Adams
A. W. & Ellen Altorfer
Ralph & Elizabeth Baker
Frank & Jody Bentz
Robert Butler
Dallas Campbell &
Claudia McNamara
Jack & Mary Crawford
Tom Crocombe
Robert Daniel
Eric Danforth
Richard Deckard
Lauri Deloca
Jeff Detterman
Rose Detterman
Brock DeWalt
Warren Dieslin
Gary & Deborah Dittrich
Bill & Lauri Donovan
Dr. Roberta Edwards
Terry Frank
Toni Gerdes
Gary Gilman
Merrie Ann Hahn
Kim Hansen
Charles Holland
Lloyd Johnson
Greg Kettering
Martha Langfitt
Charles & Bev Liddle
Steve Long
Mrs. Joe Loper
Steve Lundgren
Irene Fehtig Lynch
Cathy Manning
Frank McMurray
Ernest McNabb
Glan & Bonnie Merrifield
Richard & Joan Michaud
Myron & Kren Mizell
Bill & Janelle Moore
Patrick Murphy
Jim & Maureen Nichols
Eric Opplinger
Harold Palmer
John Peeples
Steve Proulix

Sherry Radway
Budd Rice
Max & Ardin Roth
Jim & Sharon Schutz
George Sebastian
Alan & Barbara Seeling
Syd & Erin Shieren
Ron Southard
Denny & Carol Storer
Mary Stroupe
Tom & Delle Sullivan
John Stuart
Bob Verbic
Thomas Warren
Roger Williams
Jeff Webb
John & Carol Woolington

Many professors or staff members from both CSM and Boise State contributed their valuable time and assisted us with our geophysical examinations: Michael Batzle, Yaoguo Li, Rich Krahenbuhl, Kaspar van Wijk, and Lee Liberty. Dr. Bob Raynolds of the Denver Museum of Nature and Science offered his knowledge and experience of the geology of the entire Upper Arkansas River Valley. Graduate students Brianne Hamm, Merrick Johnston, and Dylan Mikesell worked along side with the students ensuring that the surveys ran smoothly and efficiently. Also, Brian Passerella, the field equipment coordinator, for his tireless efforts to keep equipment running, batteries charged, and wires soldered.

Disclaimer

The information contained in this document is derived from a summer field camp for undergraduates in Geophysical Engineering at the Colorado School of Mines. The primary purpose of this camp is to teach students the hands-on use of a wide variety of geophysical methods. Secondarily, this camp focused on the issues associated with aquifer recharge dynamics in the Upper Arkansas Valley. However, the processing and interpretation of data gathered in the basin was done, mostly on a first-time basis, by students inexperienced in these activities. Therefore, the results should be regarded appropriately. Neither the Department of Geophysics nor the Colorado School of Mines guarantees the validity of the information presented in this document.

Processing Manager: Chris Engelsma
Assistant Processing Manager: Jeremy Brown
Presentation Manager: Sam Nilsson

Processing Teams	
DC Resistivity	Elise Goggin Rebecca Johnson Shawn Meier
Electromagnetics	Elizabeth McEvoy Chad Baillie Raied Al-Sadan
Ground Penetrating Radar	Arianne Dean Chris Lang
Gravity	Tyson Jesser Cericia Martinez Ryan Paynter
Seismic (Deep)	Jeff Godwin David Wilson Hamad Al-Ghenaim Dylan Connell Thomas Blum
Seismic (Shallow, VSP)	Colin Melvin Andy Lamb Faisal Hakeem Xia Qin
Self Potential	Diego Castañeda Iris Tomlinson Jesse Havens Karoline Volker Abdulrahman Alrugaib
Geology	Jeremy Brown Rebecca Johnson
Survey GIS	Sam Nilsson Yong Ma
Well Logs	Colin Melvin

Contents

Chapter 1

Introduction

1.1 Background Information

Each year geophysical engineering students from the Colorado School of Mines participate in a summer field session. The annual geophysics field camp is an invaluable experience for students that allows for the refining of skills and the reinforcing of knowledge gained through the previous school year. The junior class of 2008, in addition to a few graduate students from the Colorado School of Mines and Boise State University, visited Chaffee County, Colorado from May 11 to May 24. The goal is to investigate the geologic structure of the Upper Arkansas Valley to give the county an understanding of groundwater flow, geothermal resources, and geologic structure. The work of the this year's students builds on the previous field camps work to gain a comprehensive understanding of the Upper Arkansas Valley's structure. Approximately two weeks was spent in the field learning the local geology of the area and acquiring geophysical data in the field around Nathrop and Salida, Colorado. The students spent an additional two weeks processing and interpreting the gathered data. The processed data was then presented along with interpretations and understanding of the structure of the Upper Arkansas Valley to Chaffee County on June 6, 2008 on the Colorado School of Mines campus.

The first three days of the field camp were devoted to learning the local geology. This knowledge supplies the basic building blocks for geophysical data and allows for effective interpretation. Dr. Robert Raynolds, a geological consultant with the Denver Museum of Nature and Science, gave the students a comprehensive overview of the structure and stratigraphy of the valley. Several outcrops were visited. Dr. Raynolds encouraged the students to create a geologic cross-section (along a specified line) and to deduce the geology of the subsurface in the Upper Arkansas River Valley Basin. A smaller cross-section was also created, encompassing the geologic structure and the hydrothermal flow of the west side of the valley. After the first three days, participants used the remaining time spent in Chaffee County to perform a variety of geophysical methods, including seismic, electrical, electromagnetic, gravity, and borehole, to support geologic hypotheses and shed light on new theories. Students oversaw and conducted the various surveys, gaining much experience along the way.

The typical day included a morning briefing followed by fieldwork during the day. The

day was then concluded with a short presentation from a variety of people from industry or academia shedding expert on their geophysical expertise. These talks varied over a broad set of topics relevant to fieldwork conducted earlier in the day.

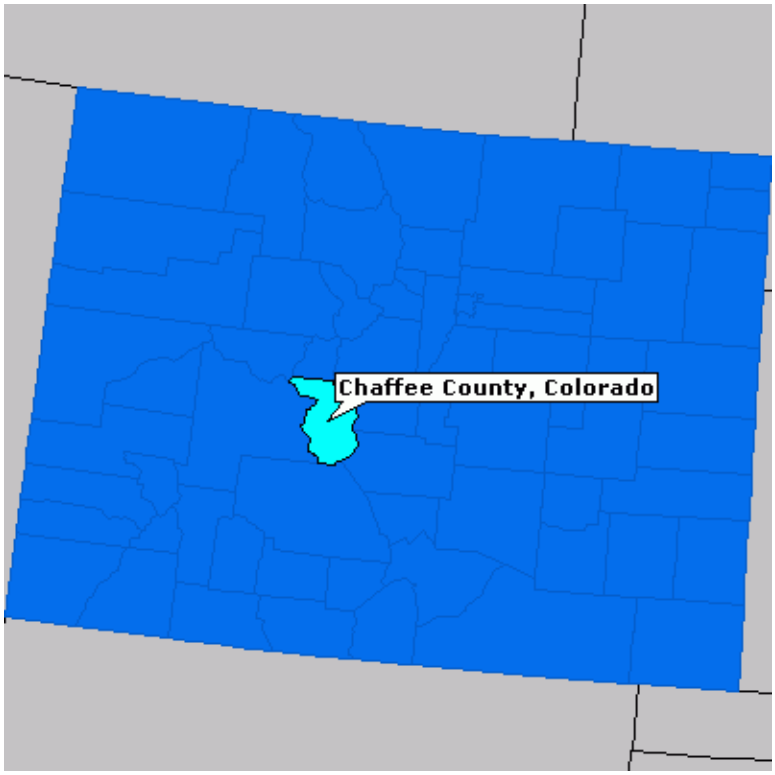

Figure 1.1.1: Map of Colorado showing the location of Chaffee County.[1]

1.2 Problems and Objectives

The area of interest for geophysical surveys is located in Chaffee County, Colorado. The Arkansas River, a major tributary of the Mississippi River, travels through Chaffee County and across the states of Colorado, Kansas, Oklahoma, and Arkansas before flowing into the Mississippi River.[2] Although the river travels through the county, the Prior Appropriation Doctrine restricts the outlying communities of the Upper Arkansas River Valley, including Buena Vista and Salida, from using the river's water.[3] Consequently, the county must rely on groundwater to fulfill the water needs of its residents. With the population projected to increase by 70% by 2030, Chaffee County needs to pinpoint where the groundwater is in their county. Consequently, the knowledge of groundwater flow, recharge, and effect of the Upper Arkansas River Valleys drainage ditches is essential for future planning.[4] Since 2005, the Colorado School Mines geophysical engineering students have been constructing models of the structural geology of the area in addition to potential groundwater locations and flow. Each year, students spend two weeks gathering data and interpret groundwater flow. Data is then built up from on preceding years to make a plausible interpretations. This year's group

produced several figures and interpretations about the groundwater in Chaffee County that complement the work of past field camps.

In addition to groundwater exploration, many residents of the county are interested in the applicability of geothermal energy in the county. Chaffee County has a lot of hot water that reaches the surface, evident in the various hotsprings located on the west side of the valley. This water is a potential renewable energy resource. In order to utilize this resource, the local geology and faulting structures were mapped.

The following report presents the observed data gathered in Chaffee County along with its processing and interpretation. The data, coupled with the interpretation, gives the county a sound model about the geology of the Upper Arkansas River Valley. The students used their knowledge of geophysics and geology to process the raw data gathered in the field. Geophysics theory, incorporating mathematics, computer science, physics, and geology, was applied to produce meaningful models. Methods such as deep seismic, shallow seismic, vertical seismic profiles, and gravity were used to better understand the structural geology of the area. Methods such as self-potential, ground penetrating radar ,DC resistivity, and electromagnetics searched for the water table and aquifers and determined the water flow in the near surface.

Since the county must rely on groundwater, irrigation ditch leakage is detrimental. The students sought to determine whether or not a irrigation ditch in the southern part of the county was leaking. This was done using near surface geophysical methods such as DC resistivity and electromagnetics. The use of both active and passive geophysical methods was used to gather invaluable data that will prove useful to addressing various issues faced by Chaffee County.

Chapter 2

Geologic Background

2.1 Introduction

The geology of Colorado is complex and, in some places, it is still a mystery. Through studying geology we can gain a better idea about what Colorado was like millions of years ago. The geologic interpretation of the subsurface can be difficult because with geology we can only make inferences upon what we can see. Determining the geology of the subsurface can be determined through geophysical methods.

About 300 million years ago (Ma) the Ancestral Rocky Mountains were uplifted but eroded away. Sediments of the Ancestral Rocky Mountains still remain in the present-day Rocky Mountains which were uplifted about 65-70 Ma.

As sediments are deposited on top of each other, the deepest deposits are exposed to high amounts of heat and pressure and become metamorphosed, resulting in what is grouped in general terms as Precambrian basement rock. This basement rock, or granite, is very dense and impermeable and only infiltrated by fractures or faulting. Sediments continue to be deposited on the surface by various methods such as rivers, which deposit well-sorted and organized sediments that are finest at the top. Glaciers deposit rocks of many sizes that have been smoothed and rounded by the movement of the ice against the surface. Debris flows from areas of high relief deposit a poorly organized variety of sediments, from huge and angular boulders to fine silt and mud. In addition to deposition in a region, the terrain can be altered by large scale volcanic and tectonic activity.

2.2 Geology of Upper Arkansas River Valley

The Upper Arkansas River Valley is geologically complex. Millions of years ago the valley looked very different compared to today. It was primarily a flat region with valleys running east-west. Evidence for this is a narrow volcanic flow that extends from Mt. Princeton to near Castle Rock, CO. In the Southern Mosquito Range, there is an igneous extrusive basil substrate of obsidian volcanic rock. This same volcanic rock is seen on the Front Range in Castle Rock, CO (known as the Castle Rock Rhyolite). Consequently, the lava that once

flowed through the present-day Rocky Mountains must have flown from west to east about 36.7 Ma. The volcano that was responsible for the igneous extrusive rock is no longer present due to the substantial uplift that occurred in the area that most likely faulted out the volcano. The basin that exists today, the northern part of the Rio Grande Rift Valley, was formed by major north-south oriented faults. After the uplift of the Sawatch Range (containing the Collegiate Peaks), the valley began to subside to create the present day graben (valley) known as the Upper Arkansas Valley. The subsidence, which occurred 15-20 Ma, of the valley allowed for the entry of the Western Interior Seaway that covered most of Colorado in oceanic water during the Cretaceous period. This allowed for the deposition of marine sediments, including the shale we see in the valley today. The basin is asymmetric, with the dominant faulting in the west. These faults uplifted the Sawatch Range and created the present-day Upper Arkansas Valley. Ultimately, this results in uplifted volcanic and basement rock to the west of the faults (i.e. Mt. Princeton) and a layer of sediments on top of the basement rock to the east of the fault. In the Southern Mosquito Range at Trout Creek Canyon, a stratigraphic sequence of basement rock and sedimentary rock is exposed. The basement rock is exposed. Above the basement rock is a geologic unit known as the Manitou Dolomite (which is Ordovician in age 488-443 Ma). Above the dolomite is a beach quartzite (Paleozoic sandstone) and above the sandstone is a resistive limestone unit. This limestone is called the Leadville Limestone, is a large outcrop that creates the skyline of much of the Trout Creek Canyon. Although it is not seen in abundance today due to erosion, a unit of shale (the Beldon Shale) sits on top of the limestone. It is important to know the geology of the surrounding mountain ranges, particularly the Southern Mosquito Range, because as these sediments are eroded they end up in the Upper Arkansas Valley. When trying to determine the composition and structure of the valley, having an idea about the provenance (source) of the sediments in the valley is invaluable. The Arkansas River began flowing through the valley and carved it deeper, also eroding parts of the valley to expose very deep basement rock and older sediments. Outwash materials from glaciers pushed the river to the east as they extended into the valley, as evidenced by fluvial deposits extending as far west as the base of the mountains. There is heat from the rifting process very deep below the subsurface, resulting in the hot springs in the area. The Chalk Cliffs are hydrothermally altered basement rock that was uplifted by faults. In fact, the Chalk Cliffs were once predominantly feldspar but due to hydrothermal alteration they are now kaolinite.

Along Chalk Creek, the major fault that runs along the western side of the valley has been displaced somewhere between Mt. Princeton and Mt. Antero. The most popular theory is that the displacement is due to a younger east-west running fault. The creek eroded the deep valley where Chalk Creek and the Mt. Princeton Hot Springs are located.

The Upper Arkansas Valley and the surrounding mountain ranges may be a consequence of negative inversion. In geology, negative inversion refers to a change from a thrust fault/compression system to a normal fault/extension system. The uplift that created the Collegiate Range had to be due to compression, but after some time the geologic system could have become extensional to influence the creation of the present-day basin.

Understanding the local geology of the valley is an important step in understanding the

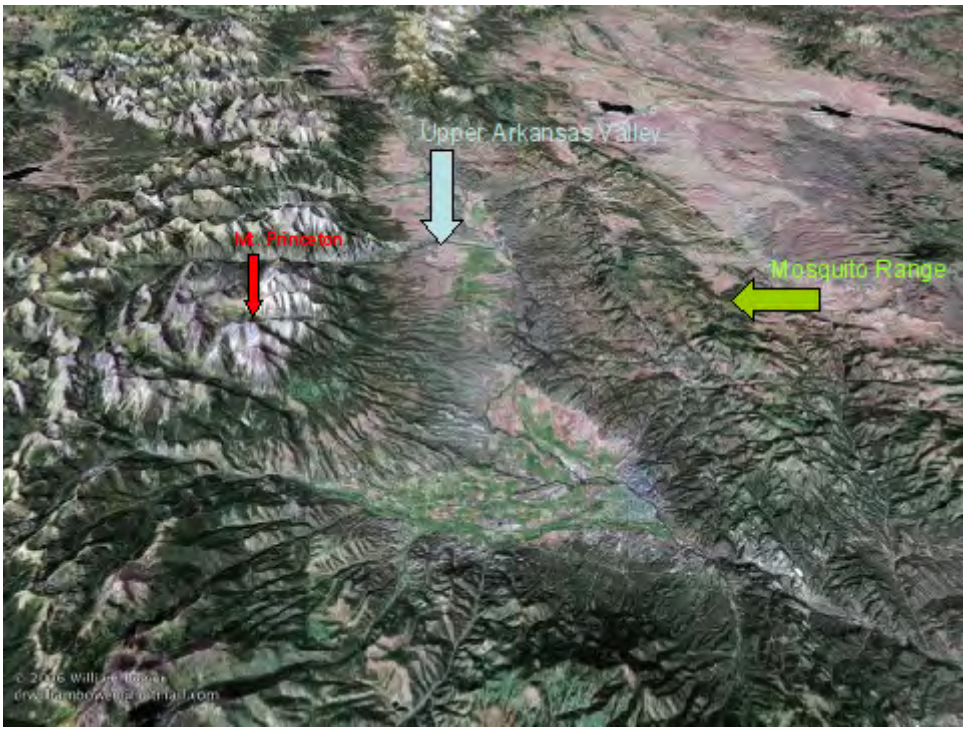

Figure 2.2.1: Upper Arkansas River Valley satellite view

geothermal systems and groundwater. Water infiltration from rain and melt water probably

Figure 2.2.2: The Collegiate Range

Figure 2.2.3: Resistive Limestone Unit

Figure 2.2.4: Chalk Cliffs

occurs near the mountains and logically flows downward into the basin. Some of this water may circulate extremely deep, below the basement rock, where it is heated, expands, and travels back to the surface to form hot springs. The depth the hot spring water travels is indicated in part by its chemical composition. While it is relatively easy for water to infiltrate porous sedimentary rocks, because they are more permeable, water travels through dense basement rock only through faults and fractures. This is why it is very important to understand the number and orientations of the faults near the mountains. Much of the groundwater does not

Figure 2.2.5: Upper Arkansas Valley

experience heating and continues flowing in the form of cold groundwater, accumulating in shallow aquifers. Water accumulation is expected to be in permeable sedimentary rocks. The water flows down-gradient into the low points in the sedimentary rocks, ultimately draining into the Arkansas River. The amount of groundwater that is available varies drastically depending on factors such as annual rainfall and upstream human consumption or redirection for drainage ditches or irrigation.

2.3 Cross Sections

Using the processed gravity data along the deep seismic line near the Chalk Cliffs, we can create a cross-section of the subsurface to determine the structure. This can be valuable in determining how much sediment is overlain on top of basement rock (rock that has been metamorphosed and is Precambrian in age). The gravity data can give us depth to basement based on densities. In Figure 2.3.1, the cross-section of the area along the deep seismic line is shown. There are a few meters of alluvium (alluvial fan deposits) followed by a geologic sandstone formation known as the Dry Union Formation. Below the relatively thin formation is the basement rock. The depth to the basement rock, as expected, is only a few hundred meters.

Figure (2.3.1) only shows the geologic structure along the deep seismic line which was in the western part of the basin near Mt. Princeton. The cross-section does not give the structure of the entire valley. Based on the geology and outcrops in the area, Figure 2.3.3 shows an

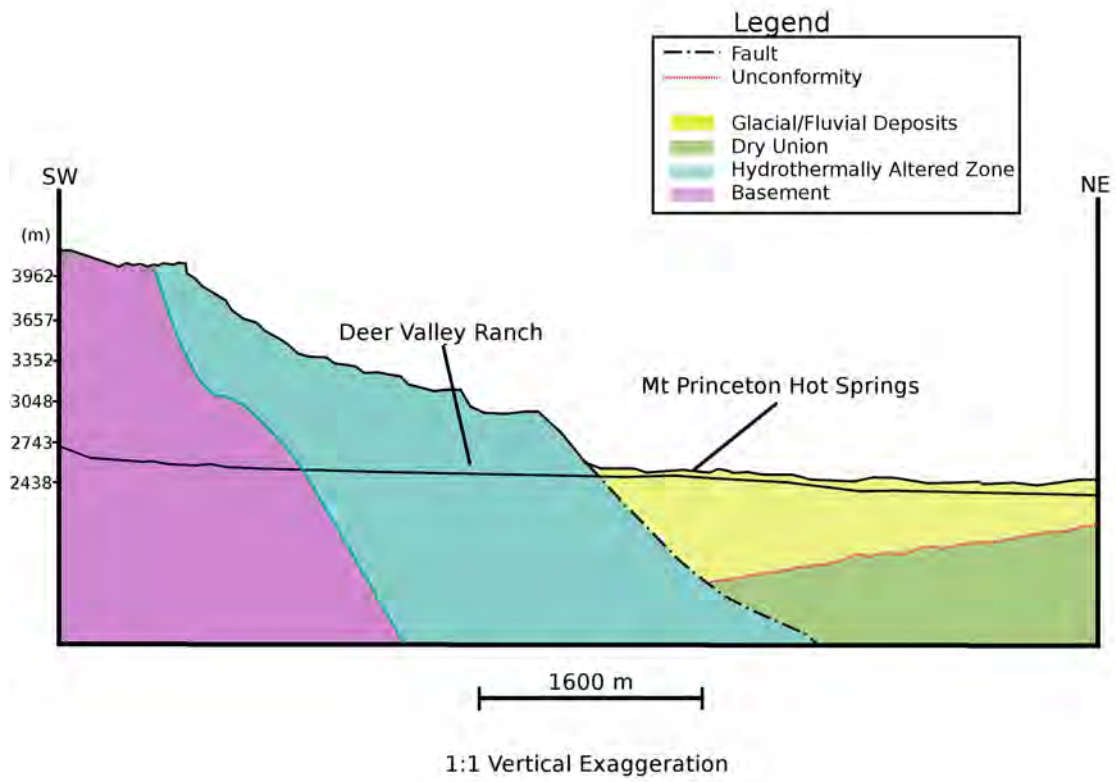

Figure 2.3.1: Geologic cross-section from deep seismic line using processed gravity data.

interpreted cross-section of the Upper Arkansas River Valley based on what we know about the geology on the surface, the seismic data collected in the field, and past hypotheses about the structure of the valley subsurface.

The figure below, Figure 2.3.2, shows where along the valley the interpreted cross-section was done.

The valley is composed of many of the sediments that were eroded off the surrounding Sawatch and Southern Mosquito Ranges.

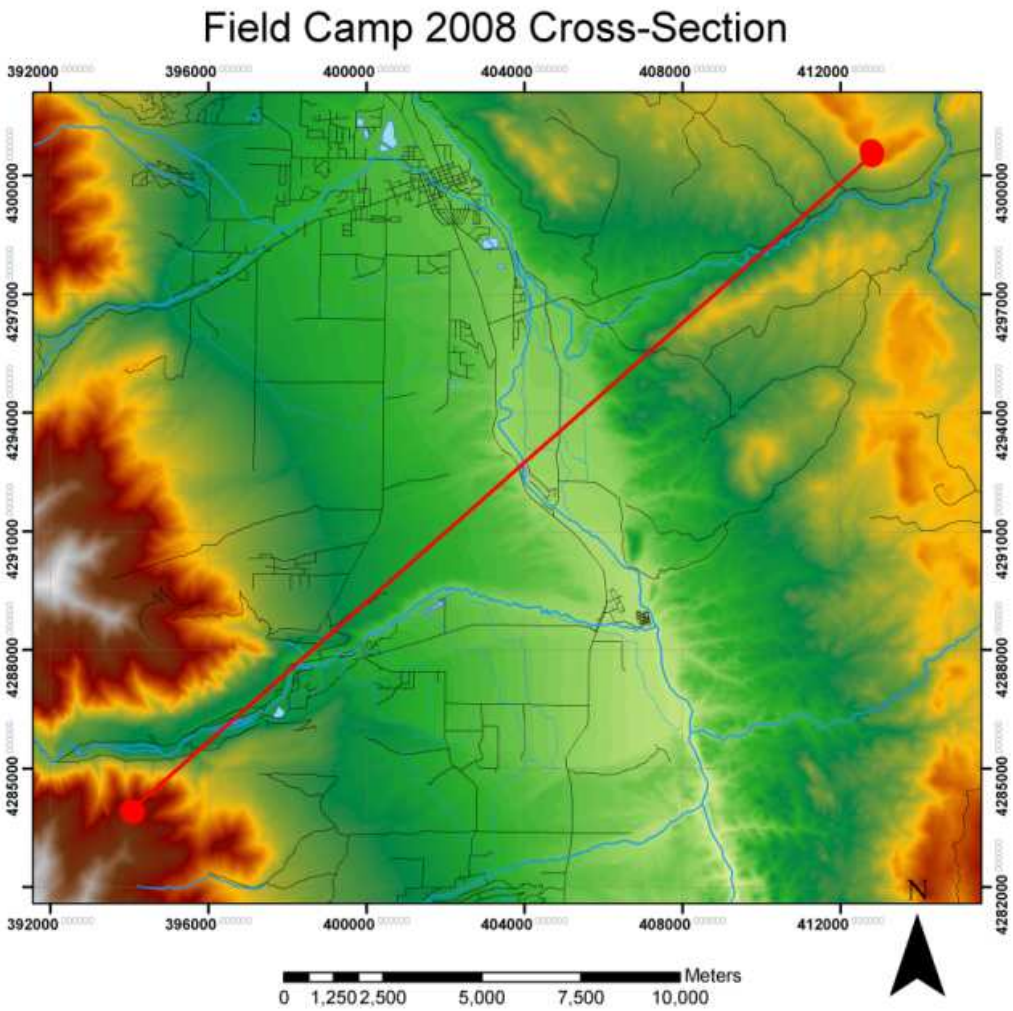

Figure 2.3.2: Location of interpreted cross-section in Upper Arkansas River Valley

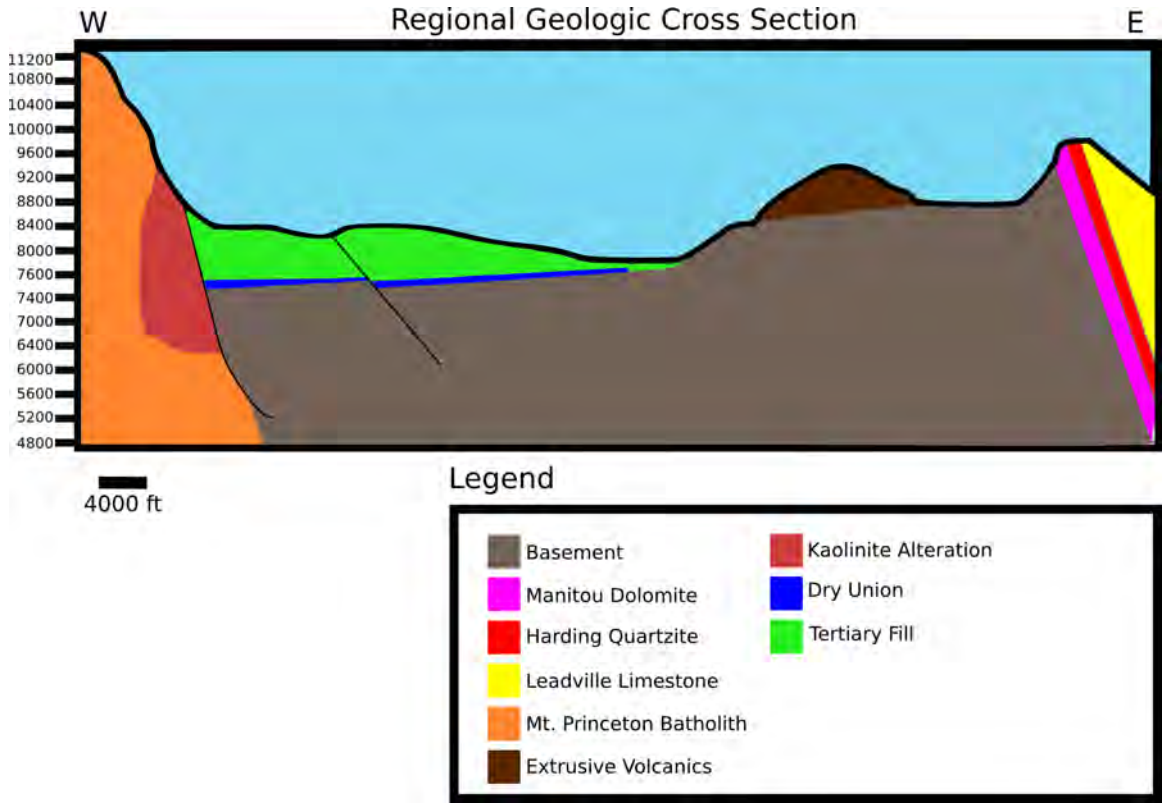

Figure 2.3.3: Interpreted geologic cross-section of the structure of the Upper Arkansas River Valley subsurface.

Chapter 3

Surveying

3.1 Introduction

Surveying is an indispensable component of any geophysical field investigation because the process of surveying provides the necessary geophysical information for each survey point, such as latitude/longitude coordinates, elevation, and total distance between measurements. In this year's field study, four kinds of methods utilized in the surveying are Handheld Global Positioning System (GPS), Differential GPS (DGPS), Total Distance Measurement (TDM), and Pace & Chain. A variety of methods and instruments, as shown in the following table, are employed to take the survey at different study areas for different purposes.

Study Area	**Method**
North Seismic Line	DGPS
Field 1	Handheld GPS
Field 1.2	DGPS
Dead Horse	DGPS
Long Self-Potential Line	Pace & Chain
South Seismic Line	DGPS
Drainage Ditch	DGPS and Pace & Chain
All Gravity Points	DGPS

Table 3.1: Different methods used in the survey

Since the process of surveying has determined the location information, another section of the whole field investigation, data processing for different geophysical methods, depends on several factors in the location information (e.g., latitude/longitude coordinate, elevation, and total distance). For instance, the gravity method has an important correction to be done, the free-air correction, which strongly depends on elevation at the gravity-measure point. In addition, any interpretation of data from the fields results needs to be implemented according to location information given by the surveying. Otherwise, if the survey locations are not clearly given through the surveying, the final interpretation results are inherently meaningless in some sense.

3.2 Handheld GPS

The Global Positioning System (GPS) [5] is the only fully functional Global Navigation Satellite System (GNSS). Utilizing a constellation of at least 24 Medium Earth Orbit satellites that transmit precise microwave signals, the system enables a GPS receiver (e.g., a Handheld GPS instrument) to determine its location, speed, direction, and time. Handheld GPS uses GPS signal from a minimum of 3 overhead satellites to obtain a fix which is usually relatively accurate within 30m. Actual accuracy can be achieved down to 5m but due to US Military intervention accuracy is restricted.

The position calculated by a GPS receiver requires the current time, the position of the satellite and the measured delay of the received signal. The position accuracy is primarily dependent on the satellite position and signal delay. To measure the delay, the receiver compares the bit sequence received from the satellite with an internally generated version. By comparing the rising and trailing edges of the bit transitions, modern electronics can measure signal offset to within about 1% of a bit time, or approximately 10 nanoseconds for the C/A code. Since GPS signals propagate at the speed of light, this represents an error of about 3 meters. Position accuracy can be improved by using the higher chip-rate P(Y) signal. Assuming the same 1% bit time accuracy, the high frequency P(Y) signal results in an accuracy of about 30 centimeters. Electronics errors are one of several accuracy-degrading effects outlined in the table below. When taken together, autonomous civilian GPS horizontal position fixes are typically accurate to about 15 meters (50 ft). These effects also reduce the more precise P(Y) code's accuracy. Typical errors of Handheld GPS caused by several effects are listed in Table 3.2.

Source	**Effect**
Ionospheric Effects	± 5 Meters
Ephemeris Errors	± 2.5 Meters
Satellite Clock Errors	± 2 Meters
Multi-Path Distortion	± 1 Meter
Tropospheric Effects	± 0.5 Meters
Numerical Errors	± 1 Meters

Table 3.2: Sources of user equivalent range errors (UERE)

Handheld GPS was used at field 1 which is in the North Site. Due to the inadequate accuracy of GPS, Total Distance Measurement (TDM) was also implemented in this area, which will be introduced later.

3.3 Differential GPS

Differential Global Positioning System (Differential GPS, DGPS)[2] is an accuracy-enhancement to Global Positioning System. When GPS first became available to consumers, it was heralded as the beginning of a new age of navigation. For the first time anyone could find out

where they were, anywhere on the planet – give or take about 80 meters. For mariners in bad weather, plus or minus 80 meters can mean the difference between safely pulling into the harbor or taking off the keel. To deal with this inaccuracy, several groups developed and deployed DGPS using a network of fixed ground reference base stations to broadcast the difference between the positions indicated by the satellite systems and the known fixed positions. These stations broadcast the difference between the measured satellite pseudoranges and actual (internally computed) pseudoranges, and receiver stations may correct their pseudoranges by the same amount.

DGPS works by having GPS receivers at stationary, known locations, near to where accurate position determination is desired. These stations broadcast the range errors they are seeing from each and every GPS satellite. Nearby DGPS receivers can give as good as between 10 to 2 meter accuracy. The exact accuracy attained is a function of distance from the DGPS stations, and how rapidly the stations broadcast their data. If more than one station is used and each station is set up correctly, with fast enough transmission, sub-meter accuracy is possible. Many DGPS stations intentionally transmit slowly to limit accuracy.

DGPS was intensively applied to almost all the study areas, only except for the field 1, in which we used the handheld GPS and TDM. For instance, in north and south seismic lines, flags were spaced evenly to represent source and receiver stations or measurement locations every 30 meters. The tools used on this log included caliper, natural gamma ray count, temperature, and fluid resistivity. The caliper tool measures borehole diameter and is used to look for changes in the borehole due to perforations or washouts. It can tell if the data is credible or not. Natural gamma ray count measures the radioactivity emitted from rock units and can tell if a particular rock is a reservoir rock such as a sandstone or a sealing rock such as a shale. The fluid resistivity rock measures the electrical resistivity closest to the borehole. Resistivity logs are excellent in determining a type of fluid in or near a well. Temperature logs determine the borehole temperature and can determine if the water is a hot water well [8].

3.4 Total Distance Measurement

Very similar to conventional distance measurement instruments, Total Distance Measurement (TDM), by an onboard computer, utilizes a laser to calculate distances and angles from a known reference point which can be converted to latitude, longitude, and elevation. In terms of mobility, the TDM is somewhat laborious to use and requires two separate operators. Furthermore, the use of a TDM instrument is on the more expensive side of surveying techniques. Like Differential GPS, a reference point and coordinate system must be applied when using the TDM.

Combined with handheld GPS, TDM was used at the field 1 in the north site. When used correctly, TDM can supply a very high accuracy, as high as the order of a centimeter, which implies that error in TDM data is usually caused by humans themselves. For example, when setting a reference point and a reference coordinate system for TDM operation, if the reference points and the reference coordinate system are not processed properly to each and

every following data point, a systematic error will come up. In addition, the prism held by the second operator must be oriented orthogonally to the laser from the onboard computer. If it is not oriented precisely, an alternative error will occur.

3.5 Pace and Chain

Among all the methods, Pace and Chain is the least expensive one yet and only slightly less mobile than the Handheld GPS. It merely requires a measuring tape by which an operator can measure off distances away from a particular reference point. Its simplicity, of course, comes along with inadequate accuracy. Therefore, this method is for one who only plans to obtain relatively rough distance information in a survey without a high demand of accuracy. Its lack of accuracy can be dependent on the terrain. On flat terrain, its accuracy can be fairly good given that the measuring tape is taut and that any associated human and instrument error is negligible. Otherwise, the terrain is a serious issue.

Pace and Chain was used for the long self-potential line at the north site and for the drainage ditch at the south site for preliminary surveying locations. Crews were sent out with a measuring tape or two and flagged a particular survey line using the Pace and Chain method. That is, each crew measured out station distance and placed a flag at each station using a measuring tape taking values from a starting point. This was done for the deep seismic and the gravity lines.

3.6 ArcGIS/ArcMap

ArcGIS is a group of geographic information system (GIS)[3, 4] software produced by ESRI. ArcGIS is built around the geo-database, which uses an object-relational database approach for storing spatial data. A geo-database is a "container" for holding datasets, tying together the spatial features with attributes. The geo-database can also contain topology information, and can model behavior of features, such as road intersections, with rules on how features relate to one another. At the desktop GIS level, ArcGIS consists of several integrated applications, including ArcMap, ArcCatalog, ArcToolbox, and ArcGlobe. ArcCatalog is the data management application used to browse datasets and files on one's computer, database, or other sources. ArcMap is the application used to view, edit and query geospatial data and create maps.

According to the data collected with all the methods above, the students used the ArcGIS/ArcMap system to display survey lines and grids completely with station locations and other pieces of information regarding each data station. In addition, a variety of features (e.g., topography, county roads, rivers and streams, lakes, drainage ditches, etc.) concern the groundwater and hydrological distribution in the area of interest, which are also included in the GIS result. By displaying a particular type of information on each layer of the software and combining these layers into one 2D representation, the students built a map of the study area which will help to explain the interaction between map components and how each ties into the big picture.

3.7 Conclusion

Surveying supplies the location information for every section of data obtained from the 2008 Chaffee County field camp investigation. The surveying results can help the data processing, since the data processing of one geophysical method may not only need the coordinates where the geophysical phenomena occur but may also sometimes benefit from the relationship between two different areas. It makes the interpretation result much more comprehensive, which helps us understand the groundwater and geothermal situation in Chaffee County.

Chapter 4

Well Logs

4.1 Introduction

Well logging, or formation evaluation, concerns the physical properties of the materials in the subsurface.Several tools are used, particularly nuclear tools, to gather information about the rocks that neighbor a well. These tools can produce information about the rock types, what kind of fluids are in those rocks, and how those fluids can flow through the ground. They are the most accurate remote sensing method the geoscientist can use and are a starting point for interpretations of seismic, electromagnetic, and spontaneous potential data.

Chaffee county offers several water wells throughout the region. The Colorado School of Mines in cooperation with the United States Geological Survey logged two wells near the survey area. Boise State University also took a VSP survey (see section 7) to obtain a velocity model. The well locations are shown below in figure 4.1.1 below.

4.2 Log Data

Figure 4.2.1 below shows the well logs taken from the Bill Moore Well. The tools used on this log included caliper, natural gamma ray count, temperature, and fluid resistivity. The caliper tool measures borehole diameter and is used to look for changes in the borehole due to perforations or washouts. It can tell if the data is credible or not. Natural gamma ray count measures the radioactivity emitted from rock units and can tell if a particular rock is a reservoir rock such as a sandstone or a sealing rock such as a shale. The fluid resistivity rock measures the electrical resistivity closest to the borehole. Resistivity logs are excellent in determining a type of fluid in or near a well. Temperature logs determine the borehole temperature [8].

Figure 4.2.1 indicates that there are two different rock units: the top unit is a shale unit while the bottom is a sandstone unit. The water level, as indicated by the fluid resistivity and temperature logs, point to a water table depth of 35.95 ft. The water is a hot water well with a bottom hole temperature of 145 °F.

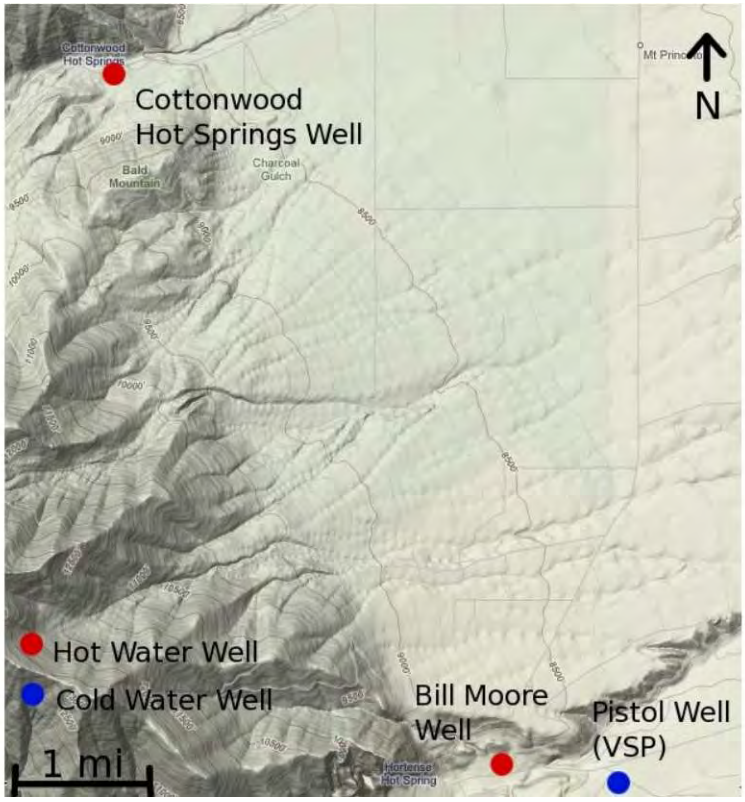

Figure 4.1.1: Locations of wells studied during field camp

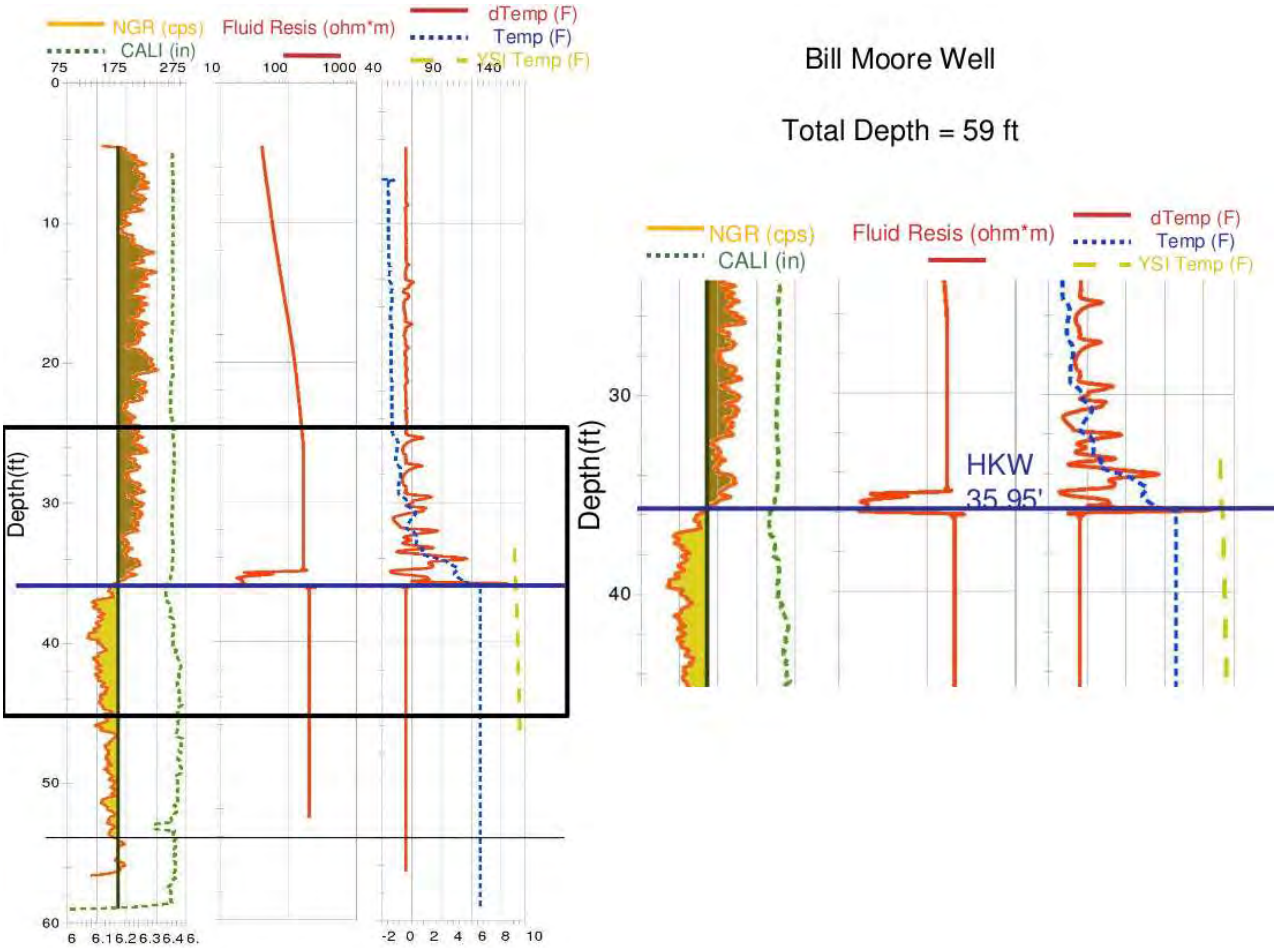

Figure 4.2.1: Well logs of the Bill Moore Well

Figure 4.2.2 shows the well logs from Cottonwood Hots Springs.

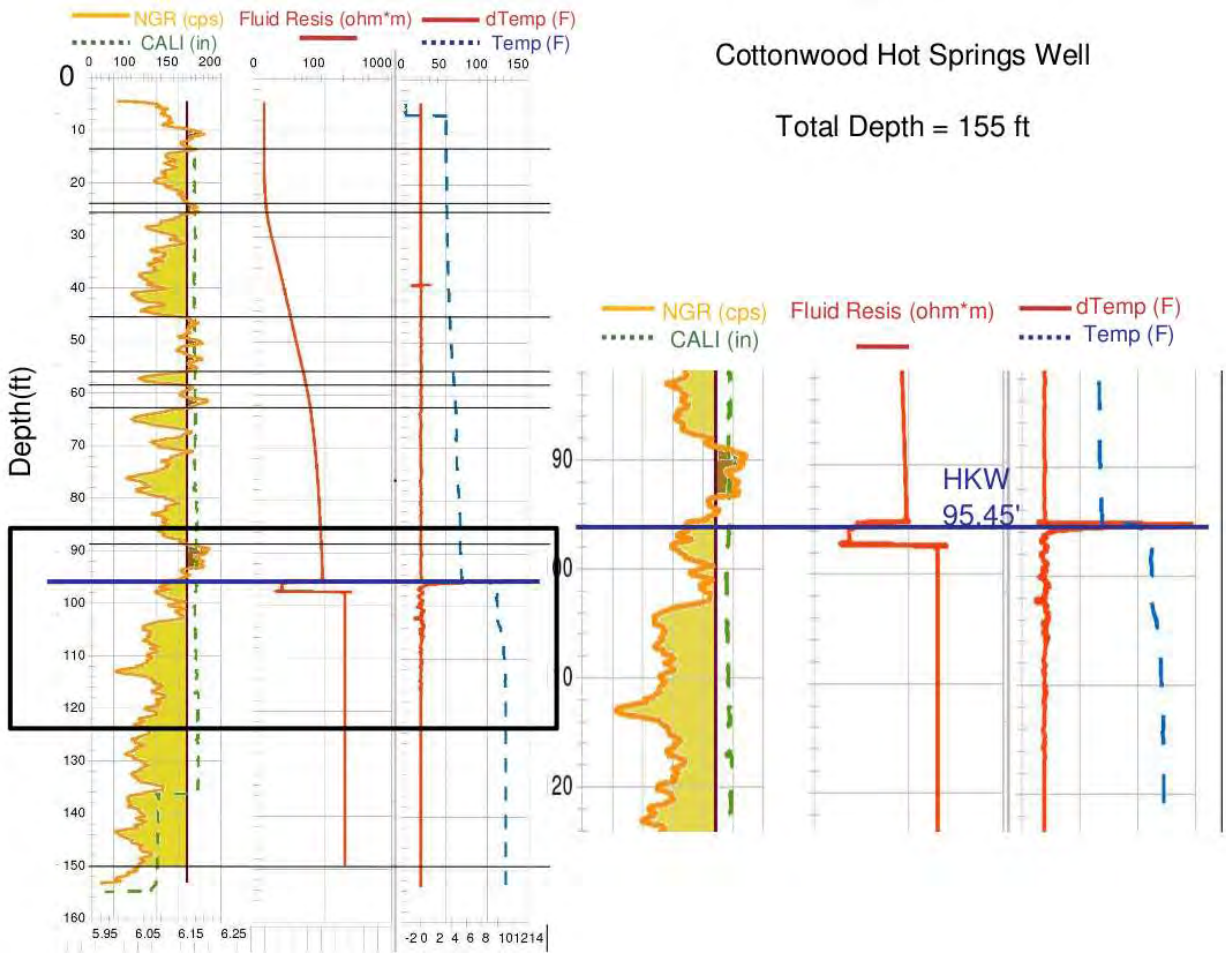

Figure 4.2.2: Cottonwood Hot Springs well logs

The well logs near Cottonwood Hot Springs show a more complex lithology on the gamma ray curve. The near surface geology for this well is different than the Bill Moore well. The sandstones tend to be interbedded with shale instead of being a "clean" sandstone. However,there is a clean water table level from the logs at 95.45 ft.

4.3 Interpretation of Wells and Geology

Using the well logs, we can also create a correlation of lithologies based on the Bill Moore Well and the Piston Well (see 7. These correlations are shown below in figure 4.3.1.

The knowledge of the well and vsp data and the a priori knowledge about the fault that separates warm and cold water wells from Dr. Henderson allows for a rough interpretation between the two wells. The Bill Moore well is on the upthrown block while the Pistol well is

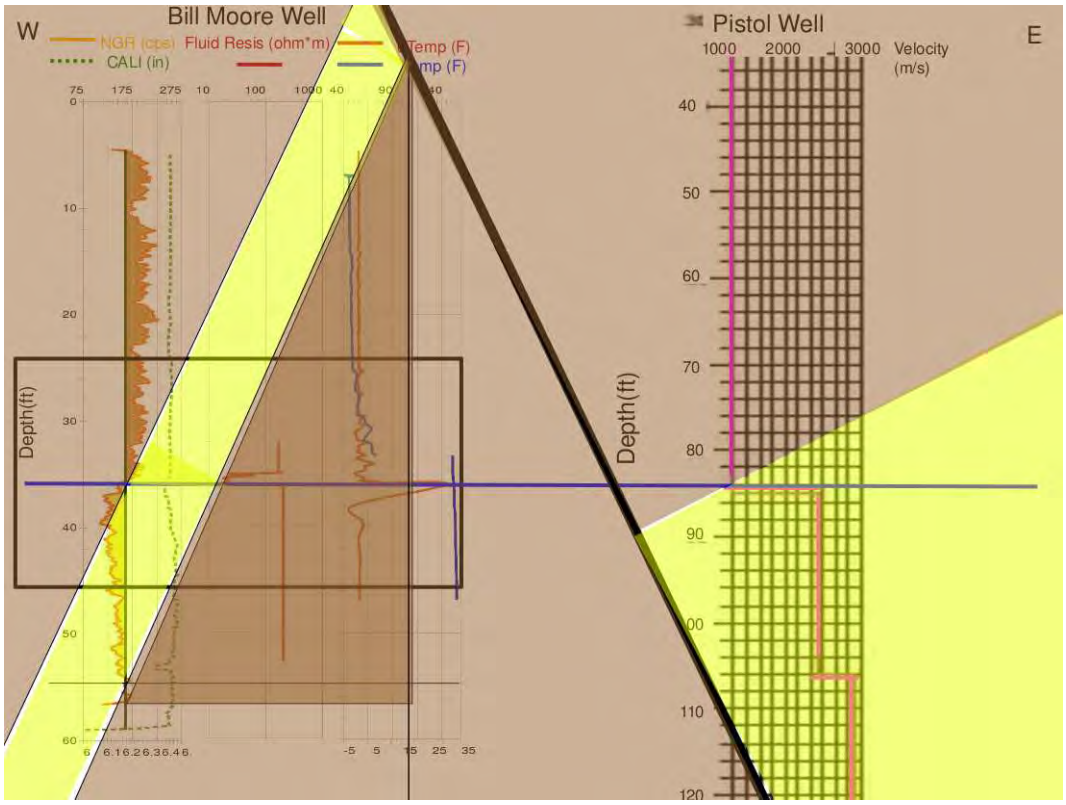

Figure 4.3.1: Lithostratigraphic correlation between the Bill Moore and Cottonwood Hot Springs wells (Ordinance datum: water table)

on the downthrown block. It seems that the fault that separates these two regions is a very significant fault that should appear in the DC and SP data.

This cross section also enlightens the geologic structure of this part of the valley. It seems that the hot water wells occur at higher depth while the cold wells have water tables at lower depths. It seems that there is coupling between groundwater and geothermal systems.

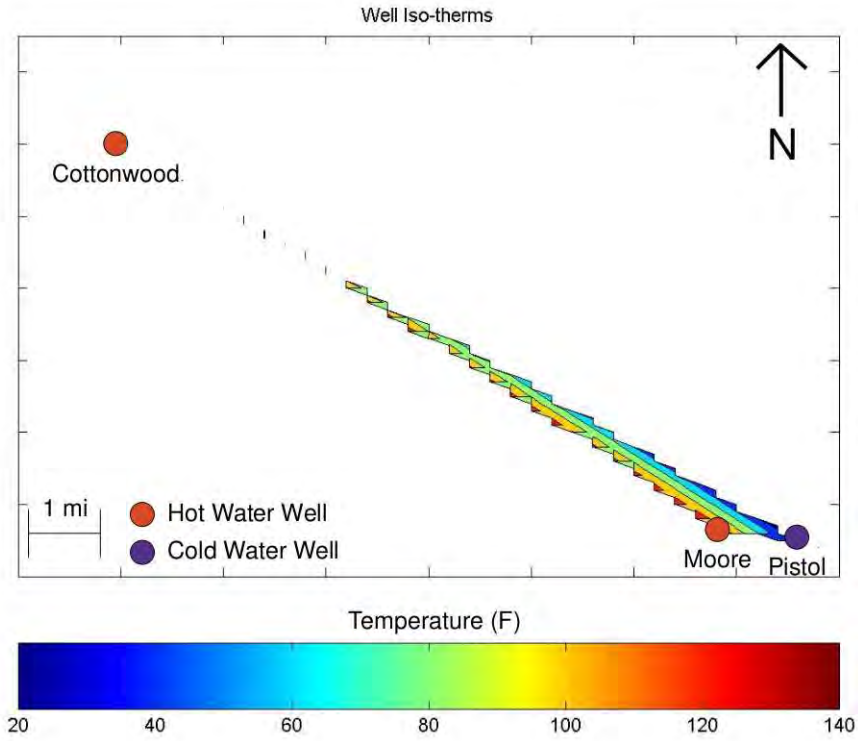

Figure 4.3.2: Isotherm map from well data

Although the data is extremely limited, these wells imply that hot water is to the west of the basin while cold water lies to the east. In a way, this data makes sense if there is a fault farther to the west of these wells acting as a source for hot water. The heat can diffuse as it continues into the Arkansas basin.

Integrating the well logs with surrounding wells gives a map of water table depth from the surface. This map is shown in figure 4.3.3.

The map may be incomplete towards the south, but we can see that the map suggests an elongated basin towards the south of the Mount Princeton vicinity. Note that the depth to water is deeper in the north whereas the water table is shallower in the south near Mt. Princeton Hot Springs. It seems that there may be a possible fault in this area. The deep seismic line that goes through this area is likely to see a fault in their data. This rough figure also shows that the wells seem to connect with the knowledge of the basin before this study.

By comparing the water table map with the isotherm map, we see that hot water tends to occur to the west of the basin. Water depth is shallower here as well, which confirms our conjecture of a coupled groundwater and geothermal model.

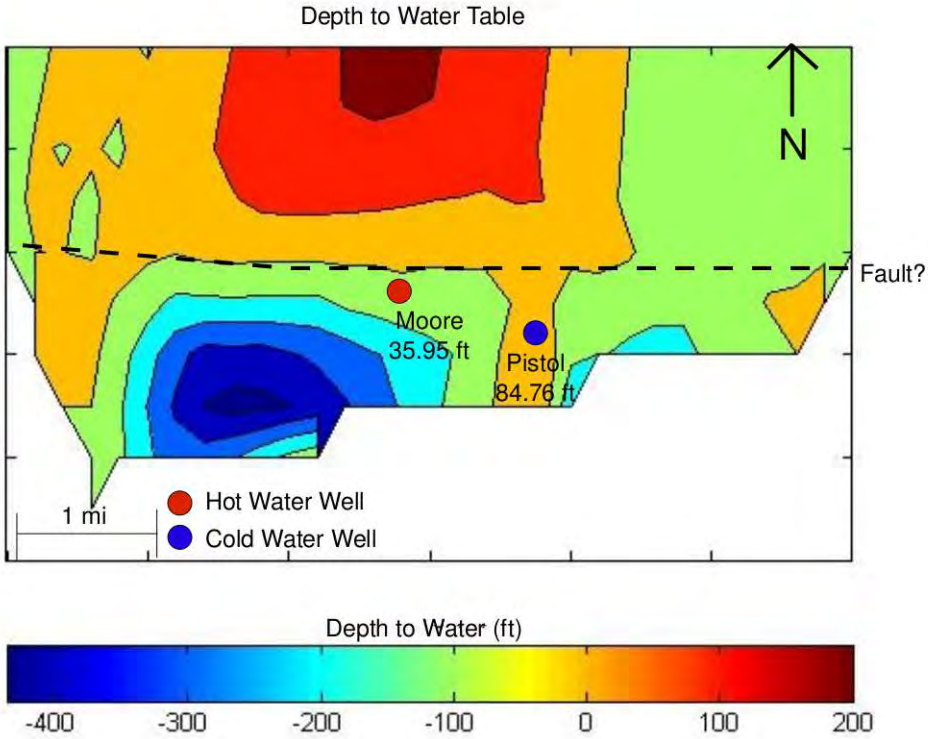

Figure 4.3.3: Depth to water table map from well data relative to Bill Moore Well

Comparing the well logs with the velocity model from VSP in section 7. The porosity increases with depth in the water charged sandstones. Overall, this region has a fairly decent water charged sandstone. The focus should be on the structure and the extents of this sandstone and see where the fluids might travel to. Those questions concern the geophysical methods in the future chapters.

Chapter 5

Deep Seismic

5.1 Introduction

The deep seismic reflection method utilizes elastic energy to create waves that propagate through the Earth. When these waves arrive at a boundary in the Earth between two rock units, the waves reflect or refract depending on the properties of the material. When the waves return to the surface they are recorded through the use of sophisticated analog-to-digital recording equipment, which allows geophysicists to visualize the data in near real time. After the data is collected in the field, it is extensively processed to recreate an image of the subsurface. The main goal of seismic reflection surveying is to recreate the apparent structure of the Earth as well as the stratigraphy. The ability of geophysicists to create accurate images of the subsurface has resulted in the wide spread use of deep seismic imaging in the oil and gas industries as well as other sectors of industry.

Since the deep seismic method provides information regarding the structure of the subsurface, the CSM team elected to pursue two seismic lines. The first line was on Chaffee County Road 290 for a length of 9.6 kilometers (6 miles). The primary purpose of this line was to gain an understanding of the complex regional geology of the Upper Arkansas Valley in the area surrounding the Chalk Cliffs.

The second line was in south of Chaffee County, near Chaffee County Road 220. In total, over 7.3 kilometers (4.5 miles) of data in southern Chaffee County was collected. The primary goal of this line was to develop an understanding of the basin geometry further to the south in an effort to further characterize the presence of the geothermal activity near Poncha Springs. The secondary objective of this line was to gain a background understanding of the geology of the southern region of the basin to determine where to focus future efforts for study.

5.2 Background

The seismic method relies on the generation of waves and the capturing of the information that they contain. A wave can be thought of as energy that moves through a material in a way that is governed by the material's properties. Conceptually, the easiest form of wave

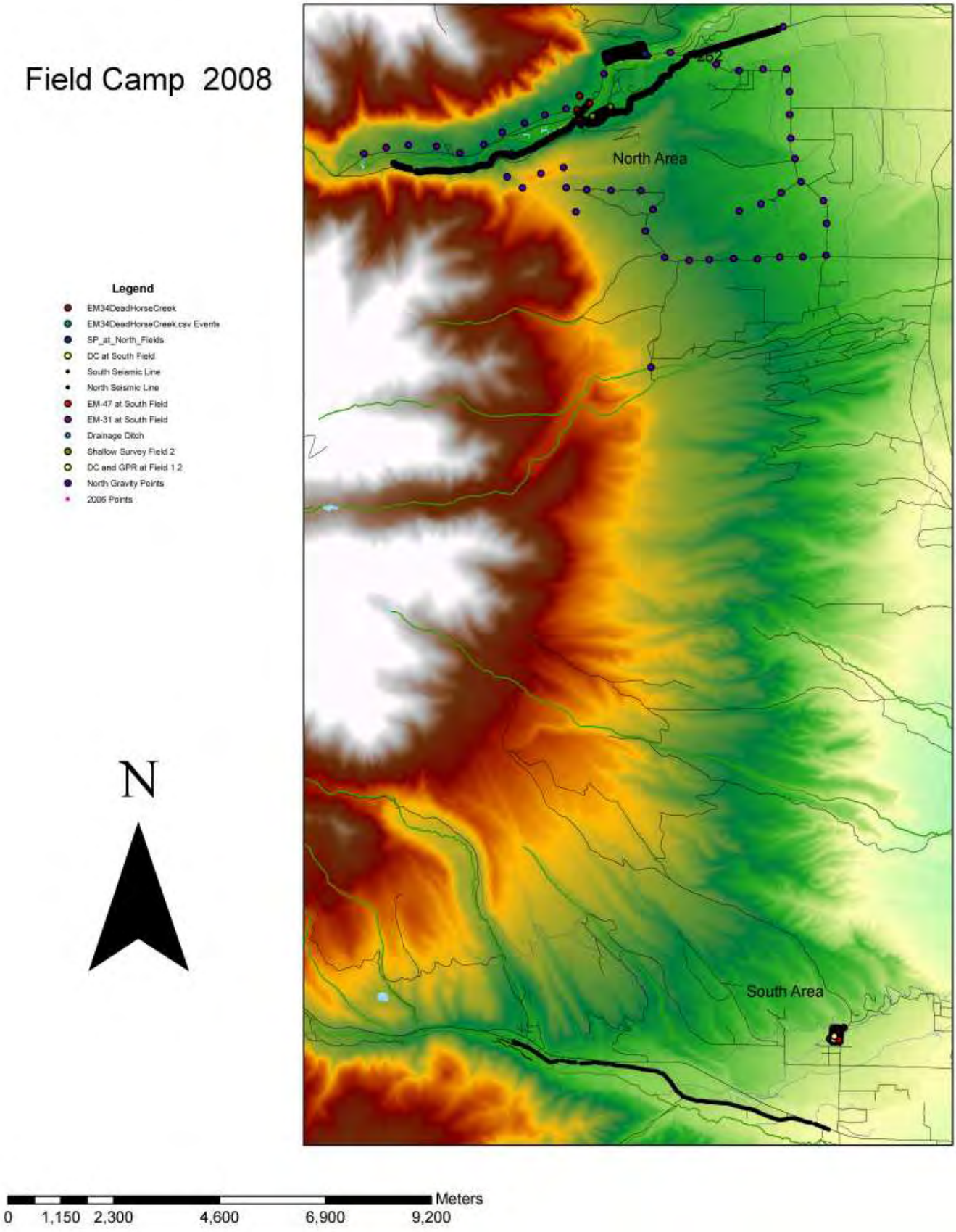

Figure 5.1.1: Field Camp 2008 Map displaying the North and South Seismic Lines

energy to visualize are waves moving on the surface of water. As the wave moves along the surface, the particles of water are being displaced. The displacement is what is referred to as amplitude. The number of times the peak of the waves travels by in a set time frame is what is refered to as frequency. The wavelength is related to the frequency, but is uniquely defined as the distance between two peaks of a wave.

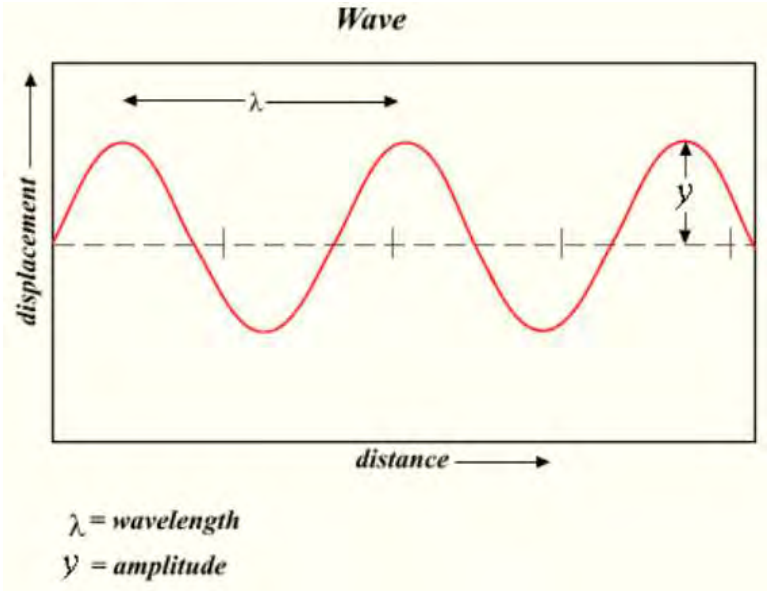

Figure 5.2.1: A diagram of a waveform[9]

For the seismic method, the waves that are of interest are elastic waves. Elasticity is the measure of a material's ability to deform under force and then return to its original state. A highly elastic material, such as a rubber band, will stretch or deform to many times its original size and still return to its original shape. Most, if not all, materials exhibit elastic properties at some scale. Rocks are no exception to this rule, they are slightly elastic at a very small scale. It is not uncommon for rocks to deform millimeters as energy from a wave passes through them. The rocks then quickly return to their original shape, which is referred to as elastic rebound. The elastic behavior of rocks can be characterized by acoustic impedance. Acoustic impedance is the ability of a material to resist changes in sound energy. Mathematically, it is defined as the product of the density and the velocity. Physically, changes in acoustic impedance are caused mostly by velocity changes in the various types of rock.

As the waves move through the Earth they arrive at fairly distinct boundaries between differing lithologies. At these boundaries there are changes in material properties, which causes some of the energy of the wave to be reflected back to the surface. Some of the energy is transmitted through to the next layer although its path is changed due to refraction. The governing laws in this situation are the reflection laws which dictate how much energy will be transmitted and how much will be reflected. In a simplified sense, these calculations depend on the ratio of the physical parameters of the two layers as well as the angle upon which the wave arrives at the interface. It is important to note that these interactions occur at all

interfaces, regardless of whether the wave is traveling down through the Earth or towards the surface.

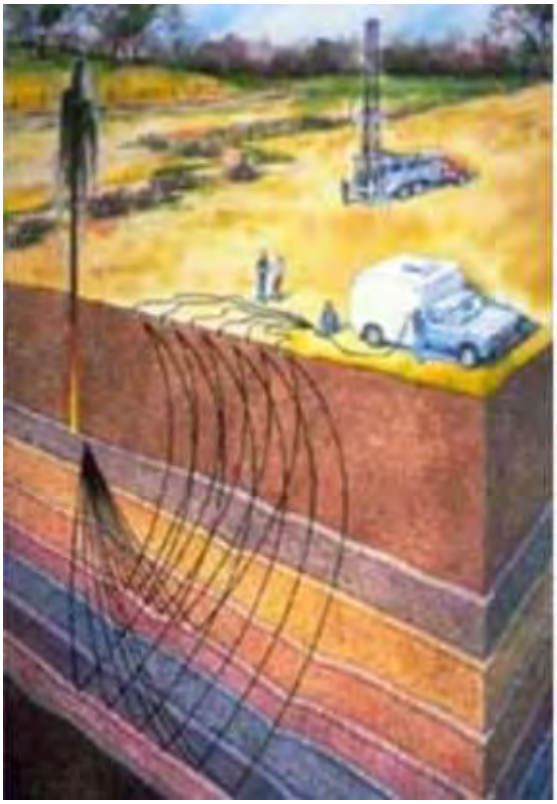

Figure 5.2.2: A schematic showing how seismic waves move through the Earth, reflect or refract, and then arrive at the surface to be recorded. This is the basic process for seismic surveying[10]

When the energy is reflected back to the surface by the "reflector" the parameters of the wave are changed. The wavelength, frequency, and amplitude are all affected. An additional term, polarity is a sign convention that only describes the direction relative to the original wave. For a layered Earth, in which the acoustic impedance of the rock is increasing the polarity of the returned waves should all be the same as the original wave. However, if there is a layer in which the acoustic impedance decreases relative to another layer, the polarity of the wave would change from +1 to -1. In this way, polarity can be used to tell information about the parameters of the reflecting layer.

For seismic surveys, the waves are generated using a source that is typically a vibroseis truck, explosive, or some other impulse upon the surface of the Earth. Each type of source has advantages over the others. However, many land seismic surveys are "shot" using vibroseis trucks because of the speed that they can obtain data, as well as their ability to vary the frequency of the shot. Typical frequencies used in land seismic acquisition range between a few hertz to eighty hertz. Regardless of how the energy is generated, it is recorded at the surface of the Earth using a geophone. A geophone is directly coupled to the ground using

a spike, and is therefore extremely sensitive to vibrations, Geophones can record minuscule perturbations in the Earth such as a human walking within a few meters. The geophones record the displacement of the ground as a function of time after the source fires. These recordings are referred to as shot records. However, time alone does not give us enough information to determine where exactly in the Earth a reflecting wave has returned from. Instead, it can only give us information enough to position the events in time. Theoretically, if there are enough recorded observations from the same object, the object can be located in space. However, there are always practical considerations, in particular noise to deal with.

Figure 5.2.3: A sample geophone, with a cut away view. Geophones use electromagnetic induction to generate electrical signals that can be captured and digitized. A quarter has been placed in the picture for scale[11]

In order to maximize the information that is gathered during a survey, geophones are placed in arrays that are referred to as a spread. Typically a spread can consist of anywhere from dozens to hundreds of individual geophones that are placed at some distance from the source, which is called the offset. By having geophones that are offset from the source the surveying crew can image multiple areas simultaneously, and image the same area using a wave with a different wave path. Spreads are furthered categorized by type, which refers to the spread geometry. The spread is designed to allow the recording of hundreds of data sets that supposedly image the same area. These duplicate recordings are called Common Depth Point Gathers (CDPs). Where the CDPs are located is determined by the offsets of the geophones as well as the spread geometry. The following figure depicts how moving the spread while moving the source of the wave will create duplicate images of the same area, but by the energy will have followed a different wave path to the location.

Once the data is collected, it can be organized by CDP into records. These records display the data collected by the geophones as traces which are a function of offset. As the offset

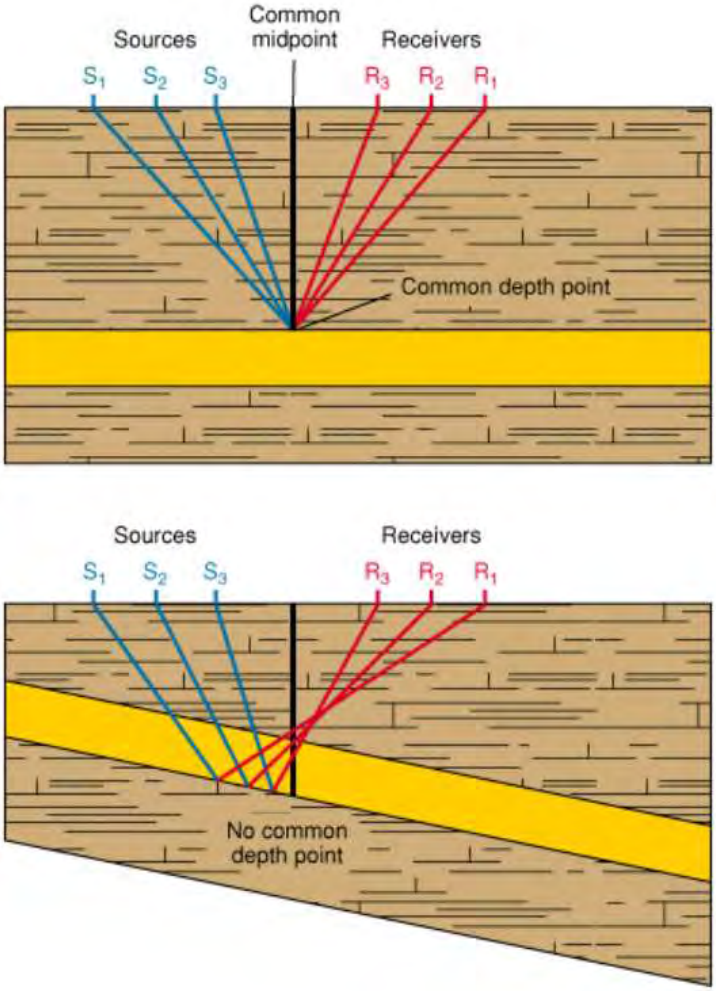

Figure 5.2.4: Illustration of how a common depth point works. Notice that if the reflector is not horizontal then the ray paths are not coincident[12]

increases, the waves take longer to return to the geophones, and therefore the data appears be shifted in time as a function of offset. For the direct arrival wave, produced directly by

the source moving along the surface of the Earth, the shift in time is linear. For a reflector at depth the shift in time is hyperbolic in nature. This shift in time, is referred to as move out, and must be corrected for before the full power of CDPs can be utilized. The most common scheme to correct for move out is called Normal Moveout (NMO). NMO uses the velocity of the medium to calculate what the hyperbola should be, and then uses the velocity to shift the position of the traces in time. This correctly lines up the events in time, in preparation for stacking.

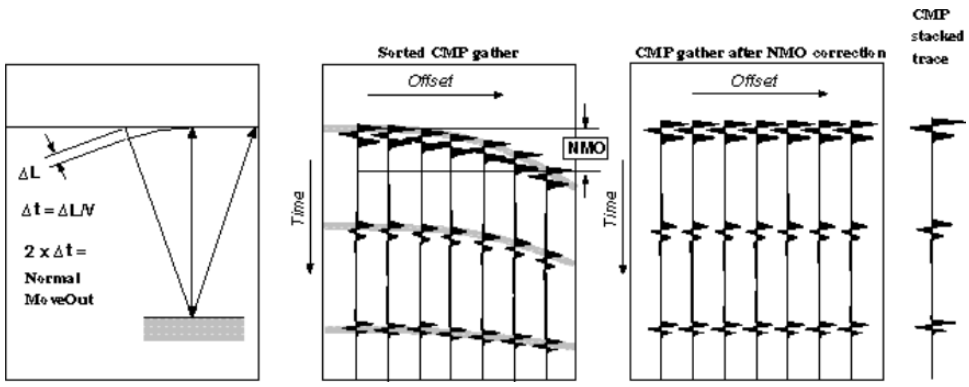

Figure 5.2.5: A graphic illustrating how move out presents itself in a shot record and how NMO corrects the move out. The stacked section has attenuated a great deal of noise[13]

Stacking is the ultimate goal of seismic processing because it dramatically increases the resolution and accuracy of the images that are generated. By adding the move out corrected traces together, and then normalizing the result, the signal to noise ratio dramatically increases. Mathematically, the signal to noise ratio will increase by the root mean square of the number of samples at each location. The number of redundant samples at any given location is referred to as the fold of the survey. Additional processing techniques, such as signal processing filters and migration, which attempts to reposition events in time, are also used. These are discussed more in depth in the processing section of this report. Ultimately, the images that are presented are the stacked CDP gathers that are positioned in space. Typically, they are placed in time. Sometimes, they are positioned as a function of depth, if a time-depth migration or conversion has been used.

5.3 Survey Design

When designing a survey a primary goal is to maximize the fold coverage over an area of interest. Typically, a geophysicist will spend days working on large scale designs. The first criteria is whether the survey will be two-dimensional or three-dimensional. The difference is huge in terms of both the man power required as well as the amount of information acquired. Another major criterion is what type of structure needs to be resolved. Different structures may require additional sampling in order to ensure accuracy. Further issues involve the amount of noise to be attenuated. In areas where the noise is expected to be significant, higher fold is recommended.

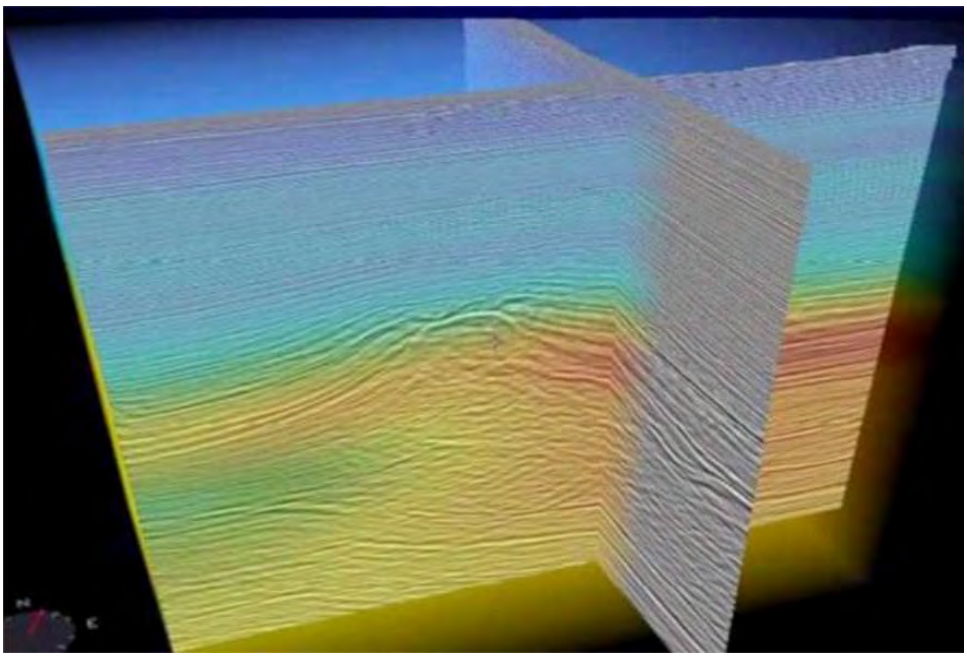

Figure 5.3.1: A three-dimensional survey creates a volume of data, whereas a two-dimensional survey creates a single line of data. 3D surveys are much better at delineating structure, but are tremendously more expensive and difficult to carry out[14]

Using these criteria, the CSM team elected to conduct two, two-dimensional surveys due to time and manpower constraints. The surveys were conducted using the following parameters: 30 meter station spacing, 6 phones per geophone string for 5 meters between an individual geophone, 30 meter shot spacing, 10 vibroseis sweeps from 5-80 Hz using a linear sweep for 5 seconds. The lines are divided into the North line, which began at station 930 and ended at station 1252 (9660 meters in length) and the South line that began at station 1930 and ended at station 2176 (7380 meters in length).

The overall goal of the surveys was to create 70 fold across the entire survey, for a total of 700 sweeps per CDP. However, the line extended two kilometers beyond the end of the road for the vibroseis trucks. To remedy the issue, the vibroseis trucks sat at the furthest location, station 1000 for the North line, station 2000 for the South line, and fired 70 shots as the geophones were picked up and replaced. This type of spread is referred to as an end-on spread. As the geophones were picked up from the end of the line and placed on the other end of the line, the shooting spread became a split spread. A split spread refers to the fact that the spread is split by the source. After the spread had been picked up from the west side of the vibroseis trucks, the spread became an end-on spread again.

Once the spread had moved 70 stations up line, from station 1000 to station 1070, the second vibroseis truck was brought back to station 1000 to shoot far offsets. The far offset data was instrumental in increasing the area that was being resolved. This same procedure was used on the South line.

5.4 Processing

Once the data had been collected in the field, it was processed. Since the technical skills and resources to process are not available at Colorado School of Mines, Sissy Theisen at GX Technologies helped during the processing phase of the project. Her experience and expertise proved to quite useful, during the task of processing the two lines of data in a very short time span.

To begin processing, the data was accumulated into one place. By collecting and printing the observer notes (detailed descriptions of how the survey took place), and reading in the raw data tapes, processing was set up. For processing, Landmark Graphic Company's ProMAX was used. This software is one of the industry standards in processing, and though a few GX proprietary algorithms were used, the software is common enough that it provides a fairly reliable benchmark for repeatability in processing. The exact parameters of each work flow for the lines can be found in the appendix.

Once we'd gotten the data together, ProMAX projects were created for each line and the processing began. For the next step, the geometry files, which give source and receiver locations in terms their UTM coordinates, were imported. This stage is critical, as it allows the processing algorithms to make the proper decisions about the layout of the survey. A few snags were encountered during this part of the process, mostly due to the use of non-sequential file ID numbers on the north line. This problem was quickly resolved and the rest

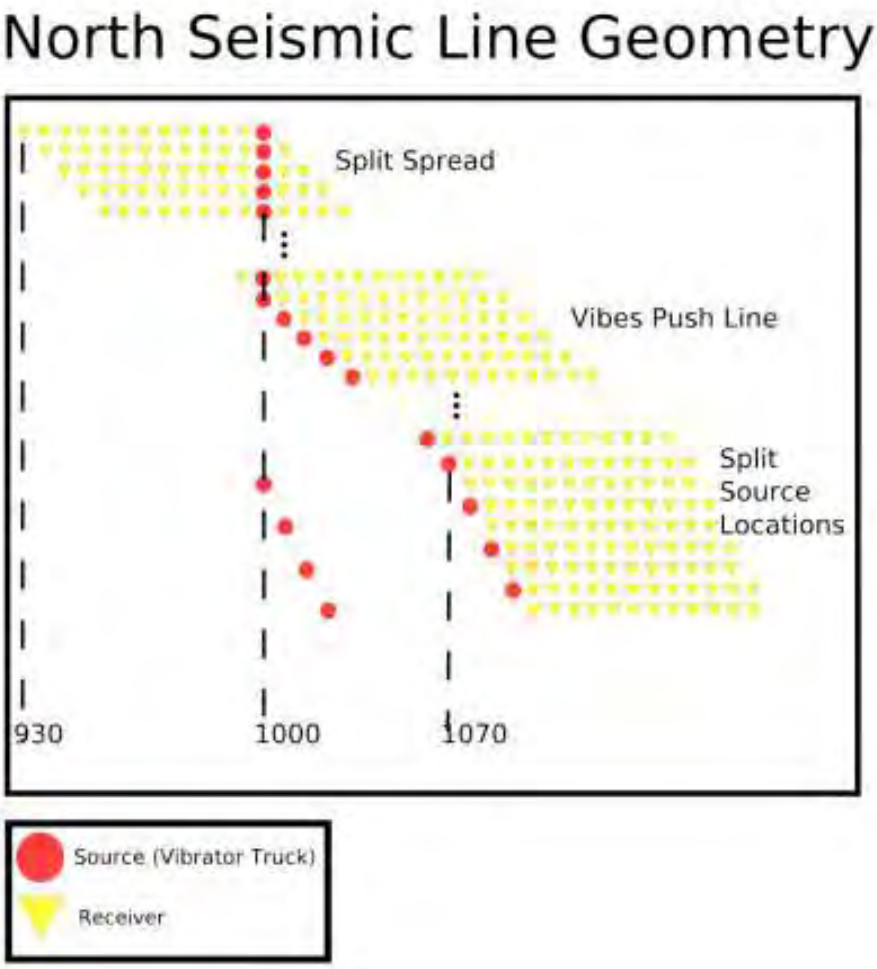

Figure 5.3.2: This diagram illustrates the types of spreads that were used for the 2D surveys that were conducted.

of processing continued.

The next step in preparing the data was to kill bad traces, and fix reversed ones. A “trace” is a record from an individual station. Due to wiring problems, and other errors, some of these traces are backwards (180 degrees out of phase) or simply pure noise. In order to fix these faulty traces, each shot gather (a collection of traces recorded from a single vibrator shot) was inspected, and the bad traces were manually selected. This way, the quality of the data was improved, and kept consistent.

For the next stage, the elevation statics needed to be applied. Elevation statics correct the seismic data for differences in elevation of the sources and receivers. These changes are called ”statics” because they do not change with time, they are simply a fixed correction across the dataset. Since all of the elevations were loaded in the geometry file, this was a fairly simple matter of setting up a few basic parameters (final datum elevation and replacement velocity). Once this was completed, the dataset was checked over with the statics and the traces fixes applied. The figure below shows some shot gathers after this correction was applied.

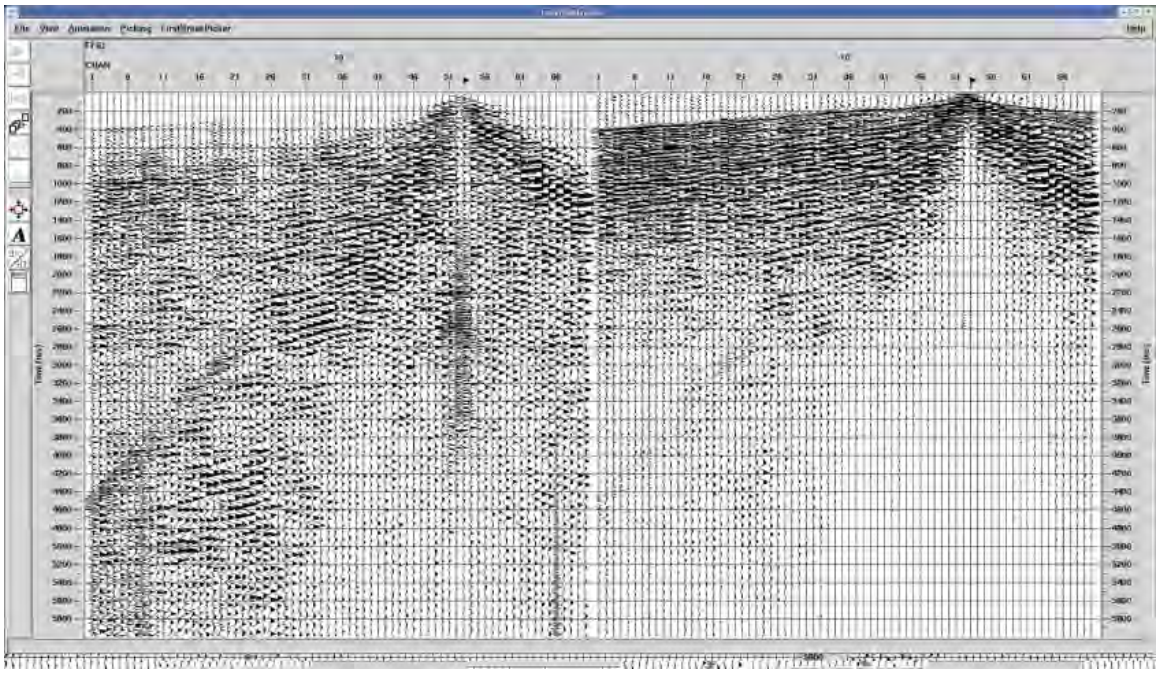

Figure 5.4.1: The North line shot gathers after the elevation statics have been applied.

At this stage, what is known as a “brute stack” was completed. That is,some very rough, basic velocities to flatten out any hyperbolas was chosen. This process of flattening the data is known as normal moveout, or NMO. The velocities chosen determine the extent of this flattening. Once each gather has been flattened in this manner, a stack with every trace in a gather is combined to make a stacked trace. These stack traces are then put together to create the seismic image. The purpose of this brute stacking process is to get a preliminary image as quickly as possible, and is not used as a final product in this case. To pick the velocities for this brute stack, ProMAX was used to find a velocity based on the shapes of

the hyperbolas in the gathers.

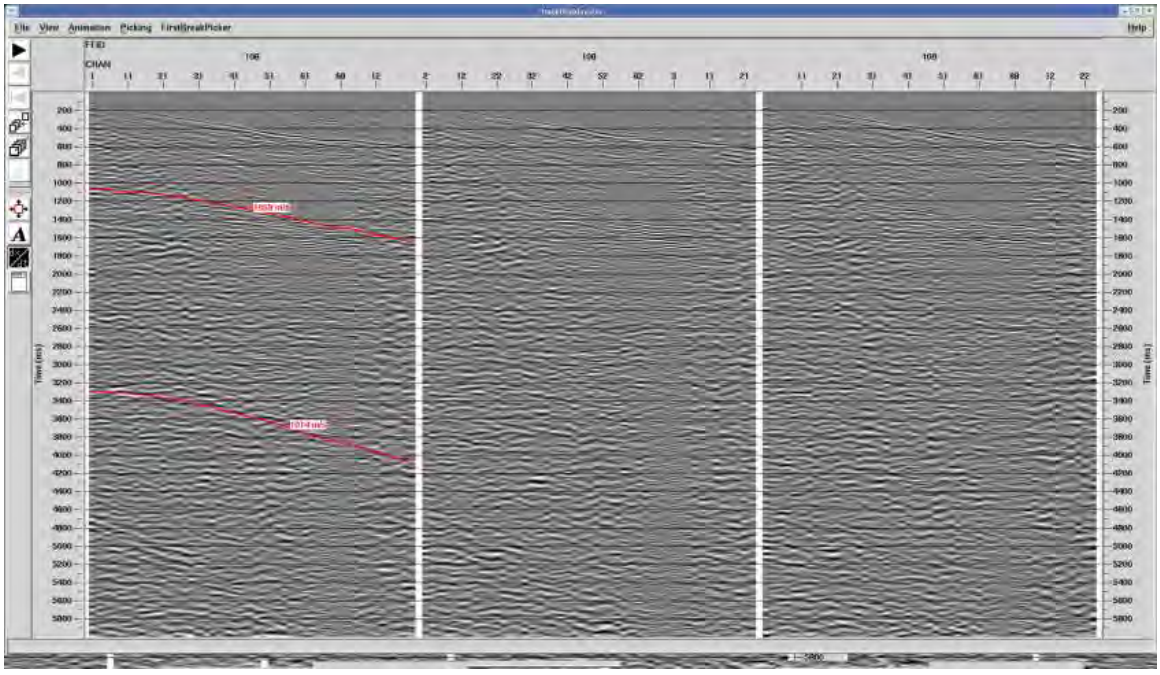

Figure 5.4.2: The process of picking velocities to be used in the brute stack for the North line.

Another step required for creating the process was creating the mutes. The purpose of the mute is to cut out, or "mute" section of the data that get stretched out too much by the NMO process. Since each trace is stretched in order to fit a flat line, the top portion of the traces get increasingly disproportionately stretched with increasing offset (that is, distance from the common midpoint). By picking a sloping mute zone at the top of each gather, the effect of stretching can be eliminated.

Once the brute stack was applied, the following results were obtained for the north line:

Already, some structure is visible in the data, though it is clear much work remains to be done. One particular problem that appears immediately obvious is the nature of the left hand side of the north line. It is clear that something is wrong with this data, as it is very high amplitude in relation to the rest of the line, and almost appears to be its own gather. This problem was investigated at a later time. Despite this oddity, the brute stack is a great example of the power of stacking in the seismic method, and how it helps represent the data as a useful image.

However, the brute stack is only a very rough result. To improve on it, velocities were picked. As stated above, the purpose of picking velocities is to help flatten out the hyperbolic gathers via the NMO correction. Using ProMAX's velocity picking tool, a velocity curve was created for multiple gathers in the data. This process transforms an inflated gather, like the following figure:

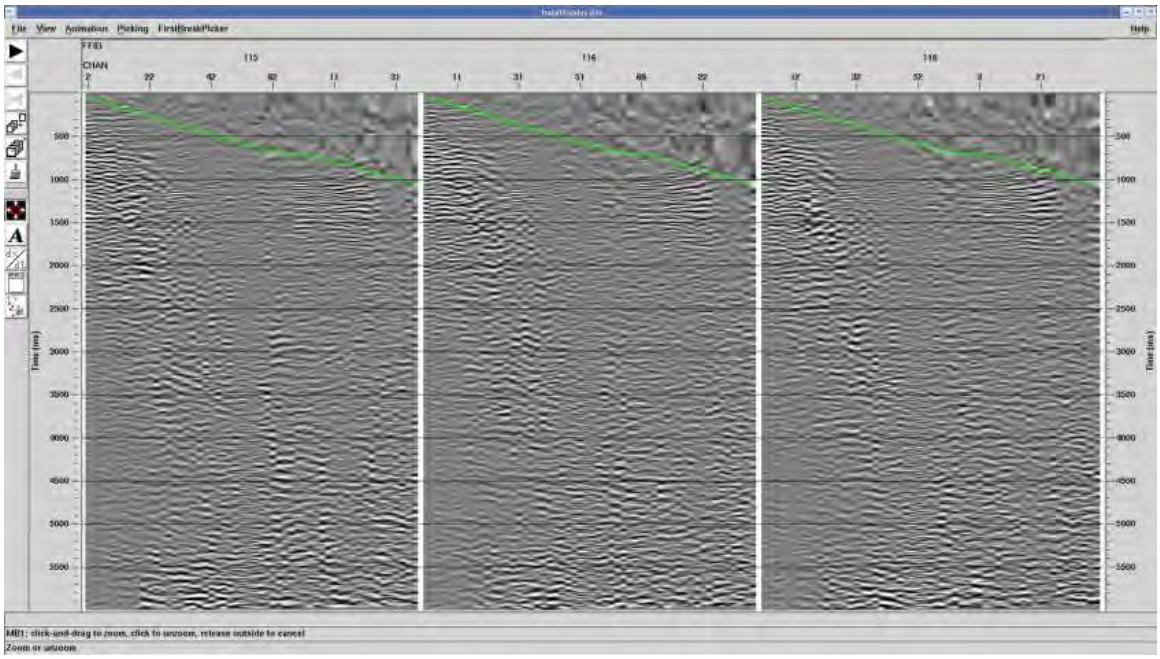

Figure 5.4.3: The process of picking areas to be muted to reduce the impact of the NMO on the data.

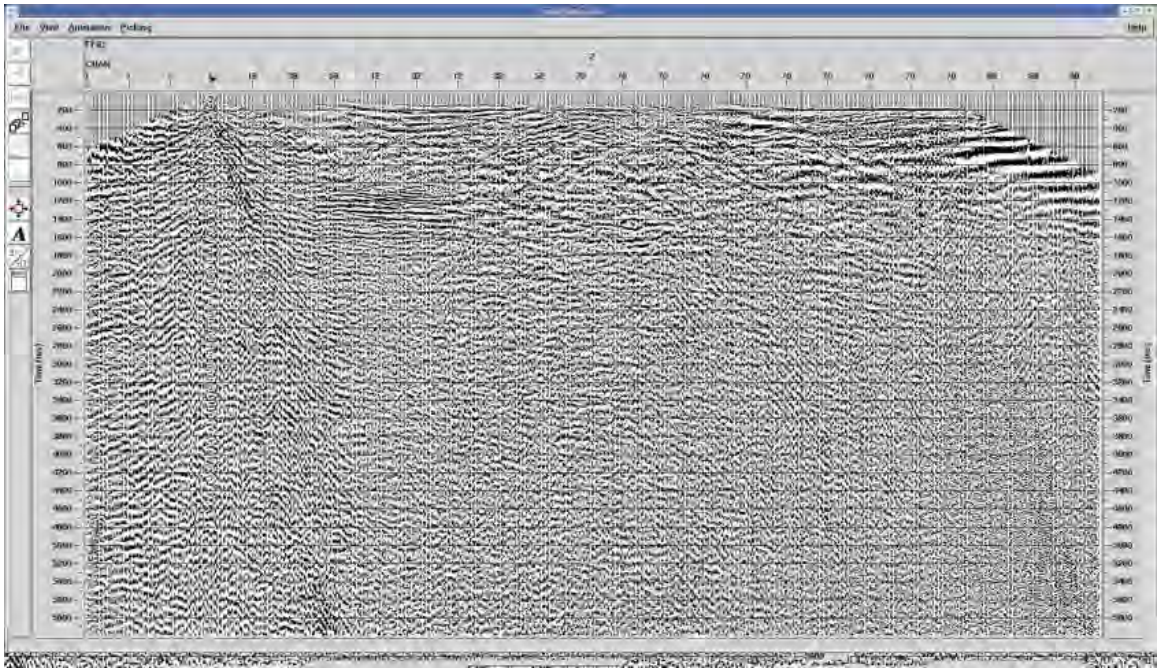

Figure 5.4.4: The brute stack for the North line. The brute stack is crudely processed seismic data.

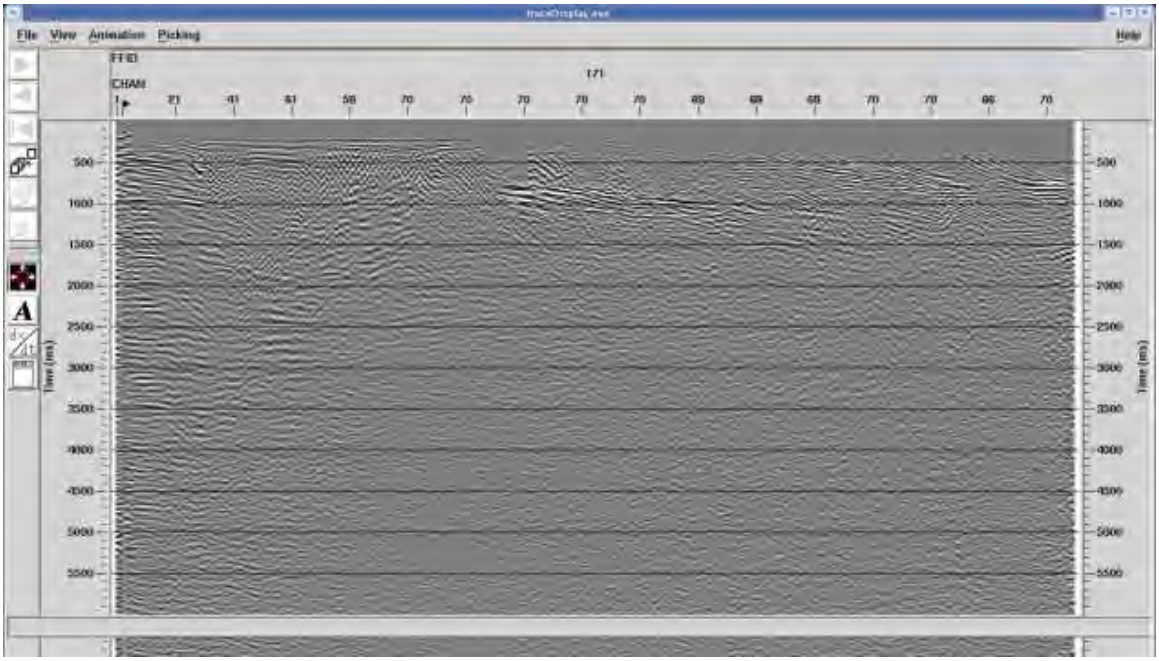

Figure 5.4.5: The brute stack for the South line.

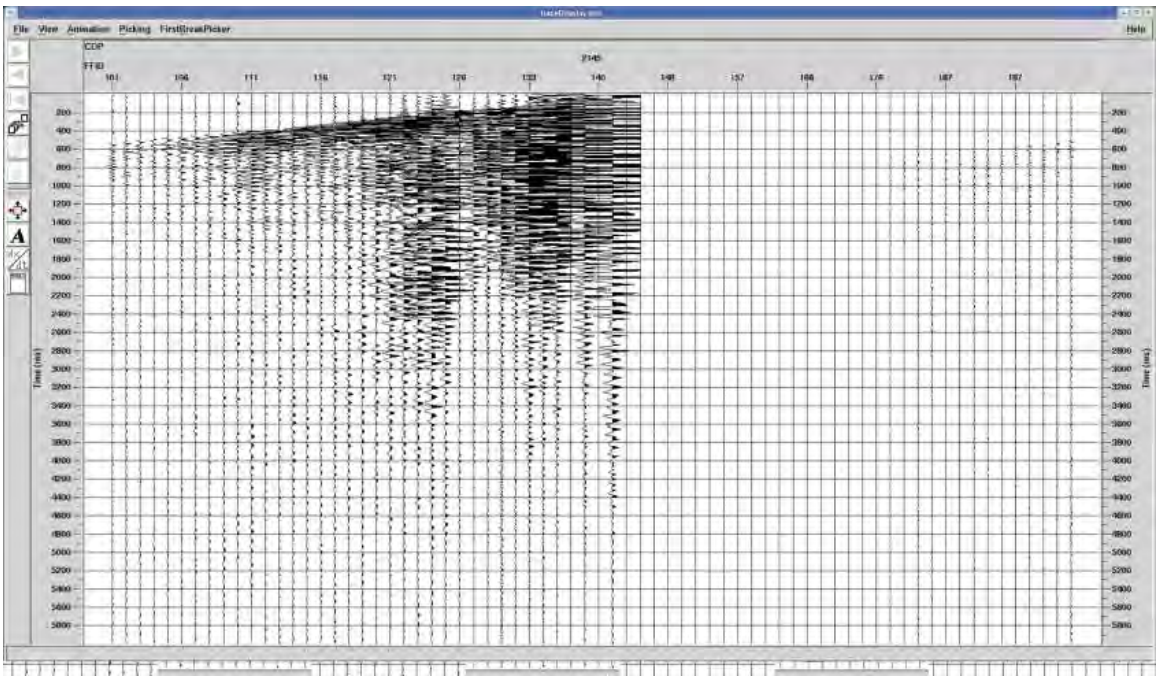

Figure 5.4.6: CDP 2145 from the North line without NMO applied. Notice the hyperbolic move out.

The next steps were mainly concerned with reducing noise in the data. Even with measures like in increasing fold coverage, and shooting with multiple vibrator sweeps, the data

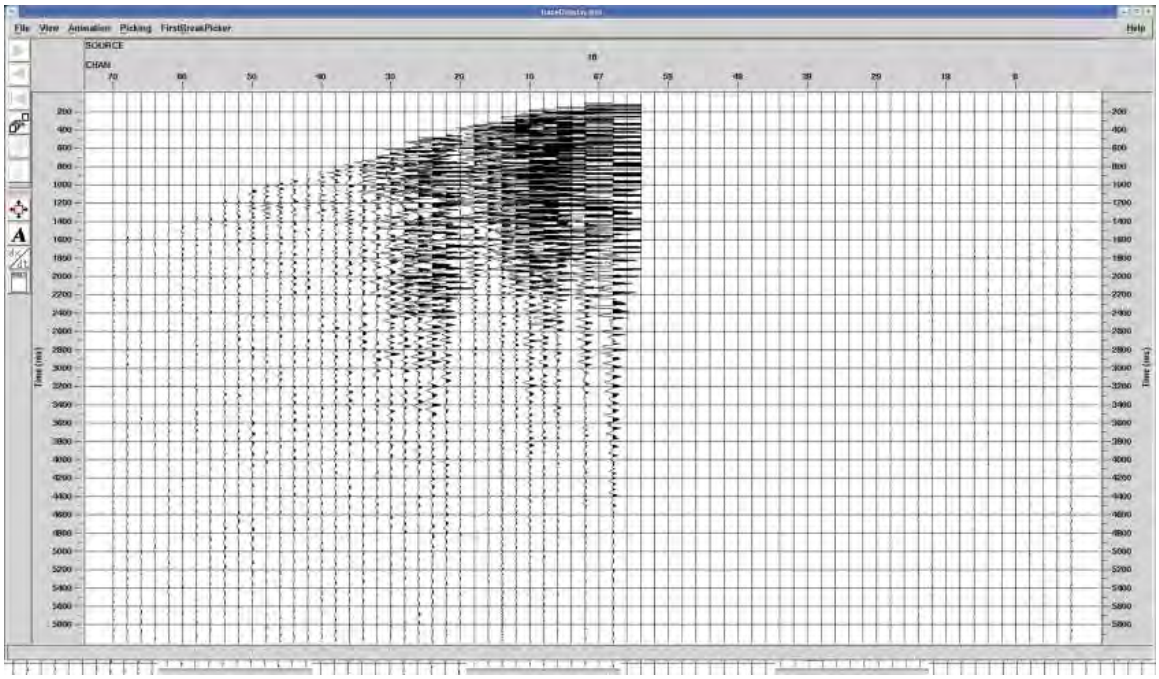

Figure 5.4.7: CDP 2145 from the North line with NMO applied using the correct velocity curve. Notice how the gathers have been flattened.

still contains a lot of noise. To fix these, several specific filters were applied, which are specifically targeted at sources of noise such as air wave noise, which is the noise cause by the vibrator sound traveling through the air being recorded by the geophones. In this processing, a deconvolution process was also applied. The purpose of deconvolution is to remove the effect of the source wavelet on the reflection data. Basically, this winds up make the data "spikier" and cleaner looking, as each wavelet is represented by one amplitude rather than a series corresponding to the frequency sweep of the vibrator source.

In commercial situations, processes such as noise attenuation and deconvolution require extensive trial and error to reach optimal setting. However, due to the extreme time constraints, a few best guess parameters were used. Even with this constraints, there were still visible improvements in the quality of the data. Residual statics was also applied, which creates further static corrections to the dataset.

At this point, there arose a question of the odd looking high amplitude section on the west end of the north line. After some testing and investigation, it became apparent that due to the use of so many shots sharing the same source point, the amplitude of these traces was so much larger than the rest that even the attempts at gain adjustment did not attenuate their effect. Further, these line contained lines that had a much smaller offset (30m) than the rest of the survey (120m). These factor combined created the odd looking section of data. To solve this problem, many of the redundant shot files were eliminated from the dataset, reducing this problem of extreme amplitudes. This solution appeared to have worked well, it was onward with the processing.

At this point, another stack was completed. The results of this stack for the north line, which is a greatly improved version of the brute stack because the velocities were picked, reduced noise, and applied another set of static corrections, are below.

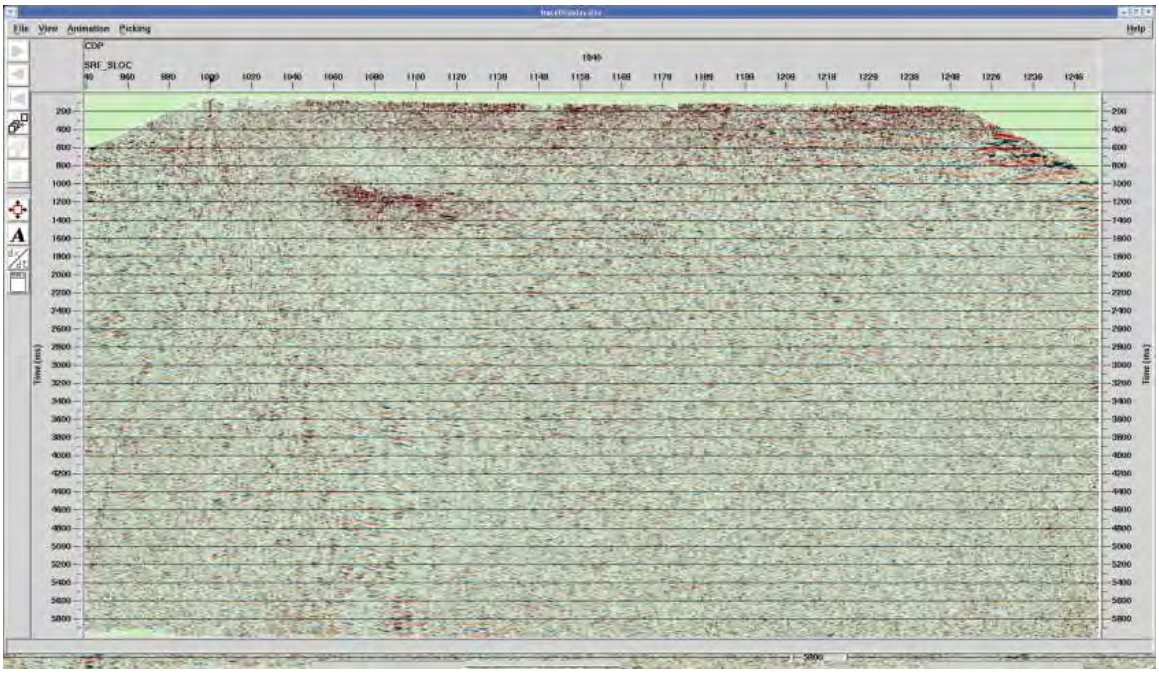

Figure 5.4.8: The updated North line brute stack. The noise has been dramatically reduced and the resolution has increased substantially.

Now, it was time to perform the time migration. The purpose of time migration is to place all the traces in their corrected location for each time. Since the NMO corrections attempted to flatten out each gather, the section is inaccurate for regions in which there are dipping (that is, non-horizontal) reflecting layers. The process of time migration fixes this discrepancy, and gives a more accurate, more easily interpretable image.

Two different time migration schemes, phase shift and finite difference, were attempted. The mechanics of these processes are beyond the scope of this paper, but some generalizations can be made about the usefulness of each method for these purposes. Finite difference migration is considered to be the more superior, more accurate, and more modern method. Phase shift migration is somewhat out of date, but still had an application when dealing with noisy data such as the data collected. The following are the results of each of these migration algorithms on each line.

As is seen, each of these migrated stacks has its own characteristic look. For current purposes, it was decided that the finite difference stacks had better resolution and a better representation of deep events for the north line. For the south line, the phase shift migration gave a better quality image.

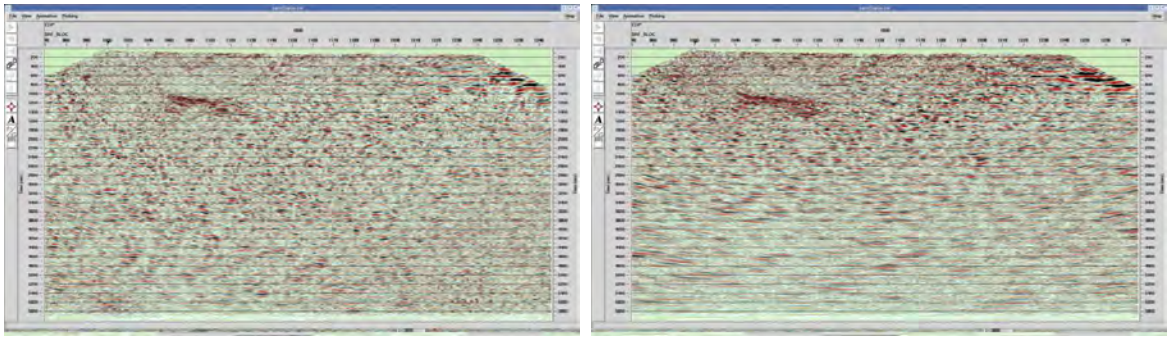

5.4.1 FD Model 5.4.2 PS Model

Figure 5.4.9: The North line following migration. The image on the left has been migrated using a finite difference model. The image on the right was migrated using a phase shift migration.

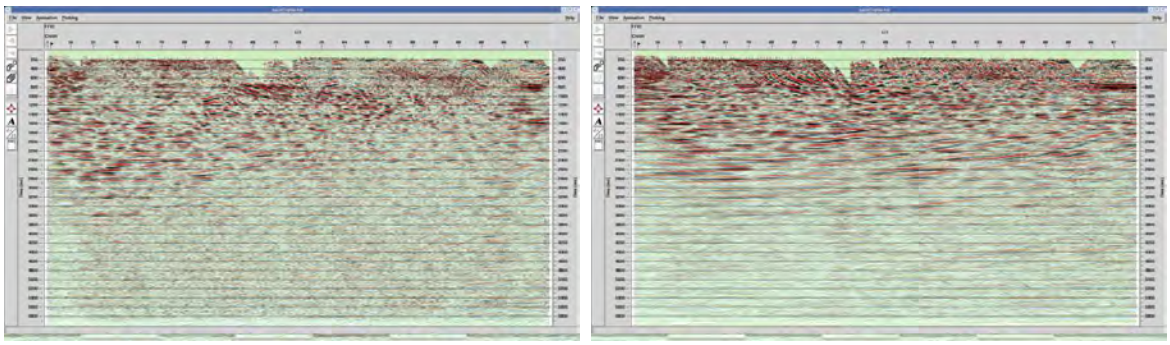

5.4.1 FD Model 5.4.2 PS Model

Figure 5.4.10: The South line following migration. The image on the left used a finite difference migration. The image on the right used a phase shift migration.

To improve the quality of the image, several smoothing and enhancement filters were applied to each section. These stacks were then looked at and used the previously picked velocity curves created a depth converted section. Now, it is very important to note that a depth converted section is not the same as a depth migrated section. The velocities used from the conversion are not the result of a rigorous velocity model, but rather interval velocities based on the root mean square (RMS) stacking velocities. The following figures are a result of this enhancement and conversion process. The north line uses the finite difference migration, and the south line uses the phases shift. These figures were utilized for the interpretation.

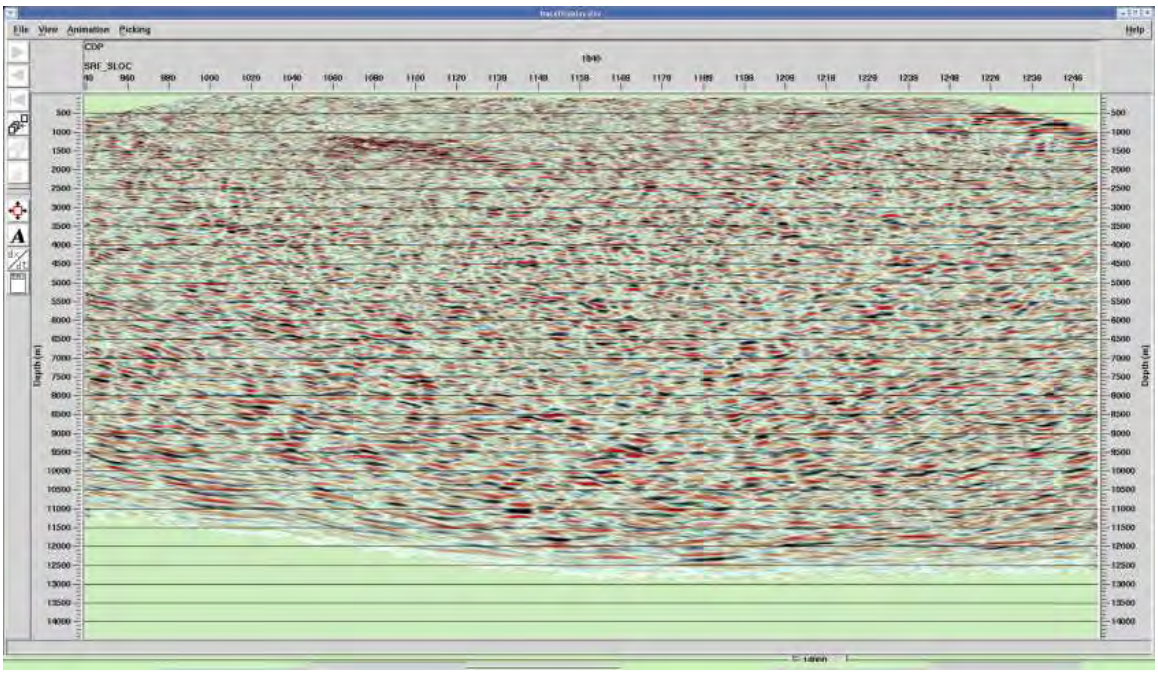

Figure 5.4.11: The migrated North line after having a time-depth conversion applied to it.

Overall, the processing clearly showed the complexity of the seismic method. Though it was possible to get final images, almost certainly the quality could improve through further processing. Since many portions of seismic processing are trial and error based, with lengthy waits for computation in between, time is an essential ingredient from creating the highest quality section.

Additionally, the data was quite noisy. Two dimensional land data is widely considered to be the worst quality seismic data, due to limited ability to characterize noise in multiple directions, as is the case with a three dimensional survey. Land based surveys, in contrast to marine surveys, face problems of noise from surface sources, error due to uneven surface, and other problem which reduce the quality of the data. This noise makes it difficult to resolve specific reflectors in the images.

Despite these setbacks, the final images, particularly the one for the south line, should provide some value. The south line has clearly defined layers and faults. The north line is much more noisy and difficult to interpret, but this was slightly expected given the difficult

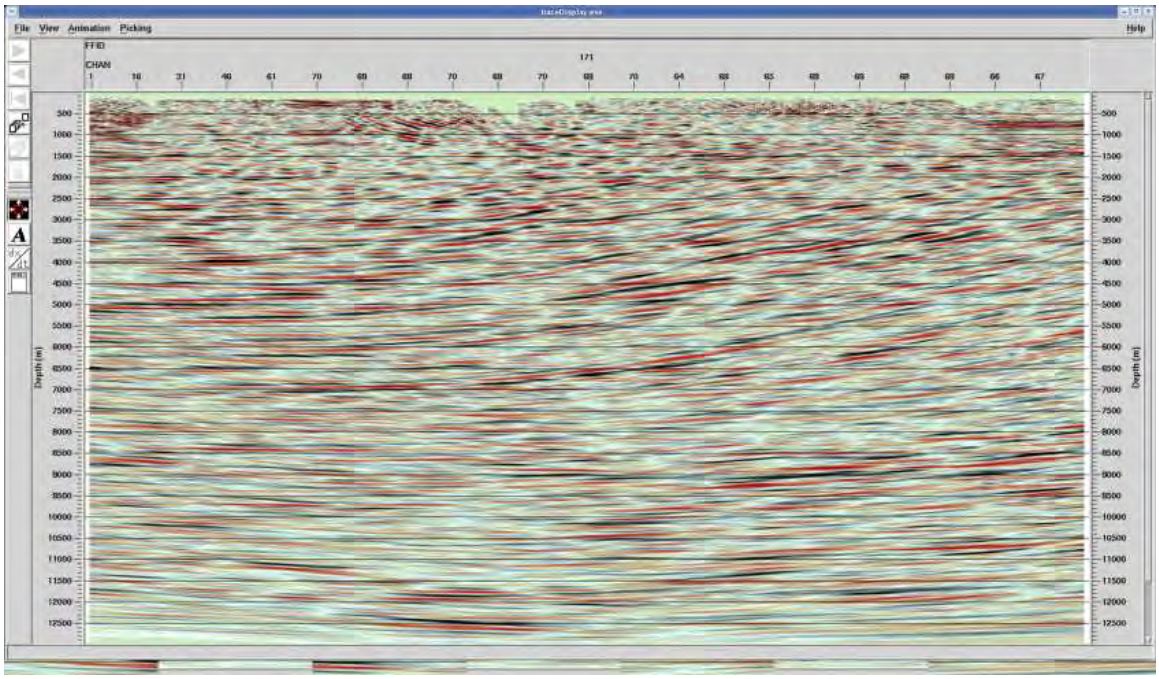

Figure 5.4.12: The migrated South line after having a time-depth conversion applied to it.

nature of the line. When the interpretation is combined with the near surface accelerated weight drop seismic, it will be possible to create a clearer picture of the geology of the line.

5.5 Error Analysis

As with all other geophysical surveys the largest problem in processing and interpreting seismic data is handling the noise. There are two types of noise, coherent and incoherent noise. Coherent noise is caused by a source that may or may not be known, however it always displays itself in a pattern that can be easily discerned. In the case of seismic noise, coherent noise can include the following: ground roll, noise from vehicles or humans, noise from various other events, and electromagnetic interference. Coherent noise can usually be attenuated using a variety of signal processing filters or mutes because it typically is only present in certain frequency ranges. For most surveys, there is noise present in the survey from power lines at 60 Hz as well as at the harmonics of 120 and 180 Hz. This noise could be attenuated but since there can be useful information at 60 Hz it is sometimes left unchanged.

Incoherent noise on the other hand is completely random and cannot typically be accounted for using signal processing techniques. However, CDP stacking does a great job of attenuating incoherent noise. In fact, the signal to noise ratio increases as the square root of the number of samples in the CDP. In order to illustrate this point, the processing team ran some statistics on a CDP gather with various numbers of gathers stacked together using ProMAX. The statistics provide some measure of the signal to noise ratio for the individual traces.

The statistics that were ran include: Amplitude Decay Rate, which measures how quickly the amplitudes decay in the trace; First Break Amplitude, which measures how large the largest event is; Frequency Deviation, which is equivalent to standard deviation for the dominant frequency; Dominant Frequency, which is a measure of which frequency is most prevalent in the trace; Spikiness, which is a measure of the amount of rapid change in the trace; and Trace Amplitude Energy, which is a measure of the total energy in the trace.

As the number of stacked shot gathers increases for the CDP the power of CDP begins to show itself, as the statistics rapidly converge to what appears to be the steady state solution. However, the statistics show that additional information would continue to refine the values for quite some time. This is very different from the situation that was caused by attempting to create fold by shooting 70 times at the ends of the lines while moving the geophones and not moving the vibroseis trucks. This form of stacking is in essence the same kind of stacking that was used when 10 sweeps were stacked together into one shot gather in the field. As the statistics show, this kind of stacking is of very limited utility.

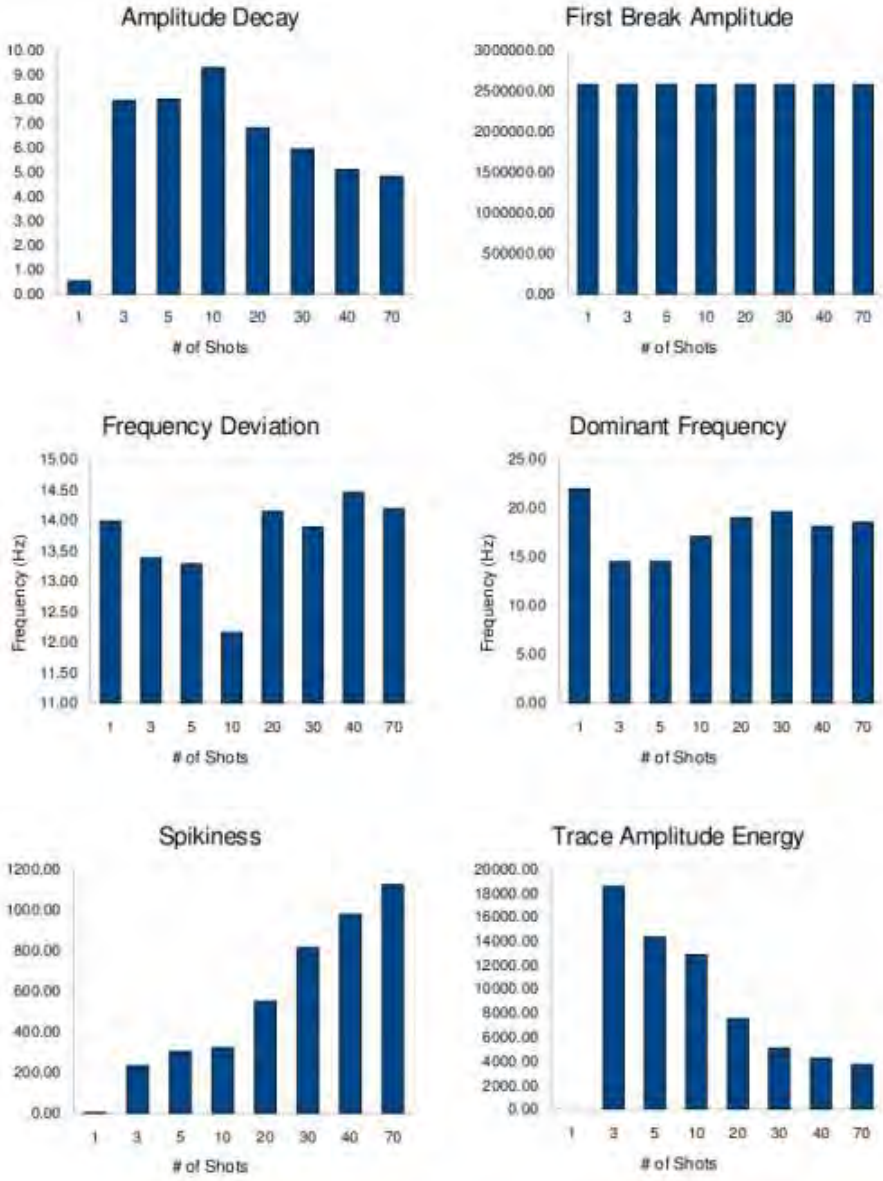

Figure 5.5.1: ProMAX statistics that were run for CDP 2145 on the North line with NMO applied, and a 30% mute applied. As the number of stacked gathers increases, the statistics appear to approach a steady state.

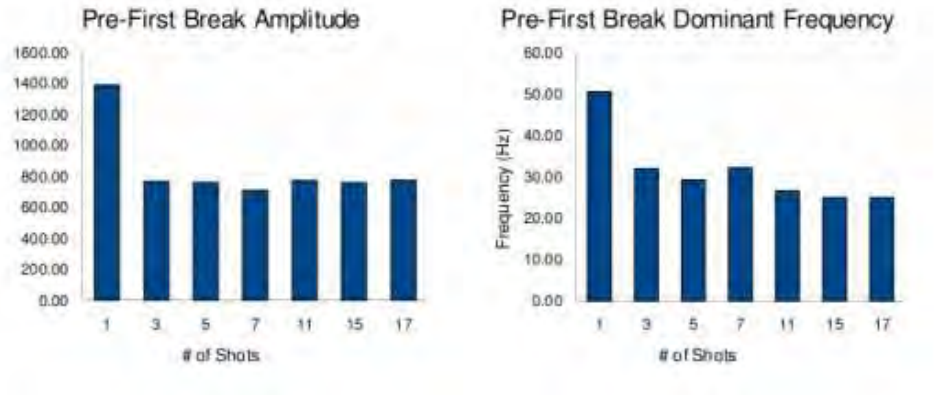

Figure 5.5.2: ProMAX statistics that were run for station 955 on the North line. The stacking was centered around shot gather 9 at this station. The pre-first break amplitude and frequency here are a measure of the ambient noise. As the statistics show, the ambient noise is attenuated rapidly by stacking these gathers together even though these gathers are really reshooting the same trace repeatedly. This kind of stacking is useful for attenuating incoherent noise.

Other sources of noise that should be mentioned include those that are caused by or during the survey itself. Multiples, or reflections that return back from the reflection off of another layer should theoretically be attenuated during CDP stacking. However, they may still appear depending on their characteristics. Therefore, one must be very careful to not interpret multiples as layers, since they are not a physical surface.

The major source of error in this survey though may be due to the choice of location for the survey. It was apparent from the beginning that the survey line may have run directly over a shear zone, or faulting area that causes the offset of the mountain range in that area. If this is the case, then the data will be very noisy and difficult to interpret due to the scattering caused by the underlying geology.

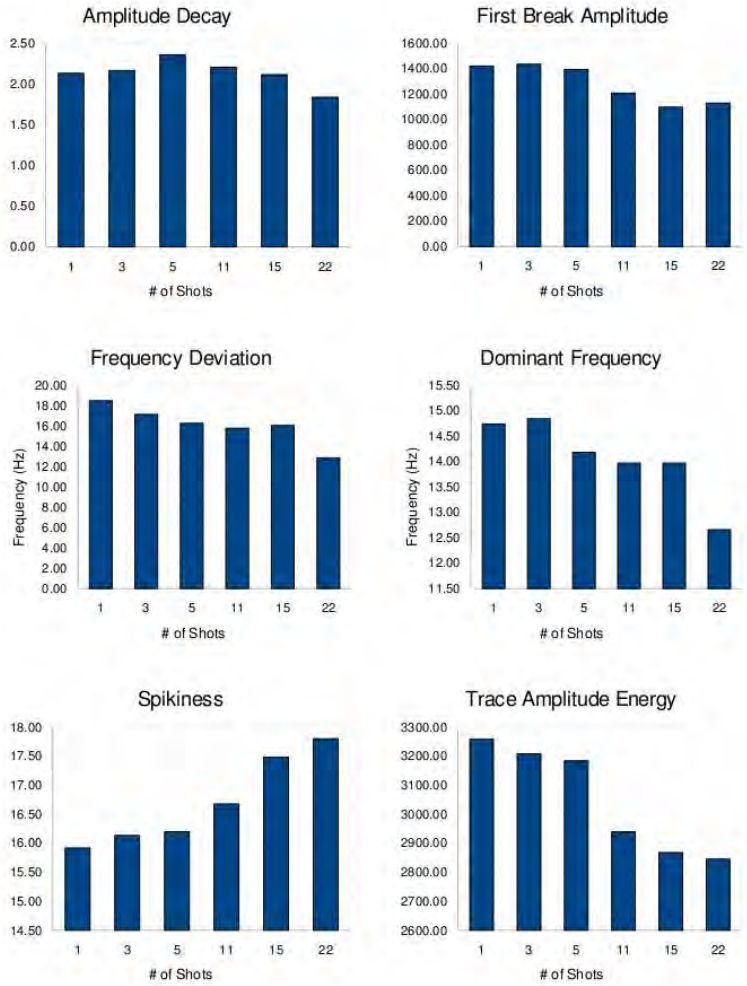

Figure 5.5.3: ProMAX statistics that were run for station 960 on the North line. The stacking was centered around shot gather 11 at that station. These statistics show that even though the random ambient noise is attenuated, that coherent noise is not attenuated through this form of stacking, which contrasts with CDP stacking.

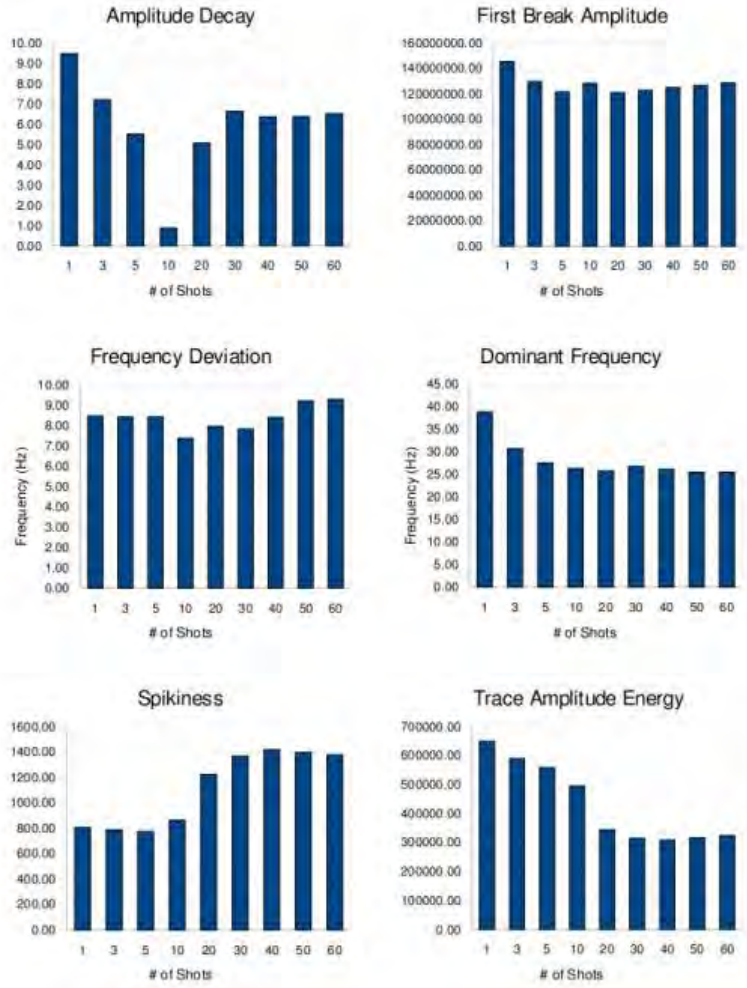

Figure 5.5.4: ProMAX statistics for station 999 on the North line. The stacking was centered around shot gather 8 because it appeared to be the noisiest shot. As the statistics demonstrate, there is very little gained from continuing this type of shot pattern after 20 or 30 shots because the coherent noise is not being attenuated.

5.6 Interpretation

As stated in the processing section, the interpretation of the north line is somewhat difficult, while the south line is a little more clear. To complicate matters, the results from the gravity and near surface seismic groups were integrated into the interpretation. This integration proved to be quite tricky at times, but in the end a consistent integrated interpretation was reached.

To start the interpretation, the basin/basement boundary was picked. Because basement rock tends to be dense crystalline rock, the reflector from the basement should be quite distinct. Also, since the basement is often more homogenous, and without layers, there should be no layered reflectors inside the basement area. Unfortunately, the dataset for the north line did not show any extremely distinct boundaries that could definitively be picked out as the basement at first glance. Layers were also seen that were quite deep within the section, which would not have been expected from the basement region.

In order to help understand the the section better, particularly with the issues concerning the basement depth, the shallow seismic section was examined. The shallow seismic team seemed to show a depth to basement around 200 meters, which was well above where coherent reflectors in the seismic section are seen. In attempt to solve this apparent contradiction, the gravity data along the line was inverted for the boundary. Unfortunately, the gravity inversion requires several parameters from the seismic, making it hard to get an independent verification of the boundary.

However, more data was interpreted, the situation improved. It was realized that since the shallow line only covered the first part of the deep seismic line to the east, and the strong reflectors were to the west, that there must be a fault that dropped the basement down. Additionally, some other faint structures that were thought to be faults aligned quite well with the known faults on the geologic map. Using this basic boundary data, the gravity team was able to get a better result for their cross section, which fit in well with the seismic interpretation, as will be shown later.

Next, is the interpreted seismic section. This section is correlated with the visible faults on the geologic map, with their extensions as interpreted on this section.

As is shown, the faulting pattern and basin fill is consistent with the expectations for an extensional rift system. Since it is believed that these faults allow for the geothermal activity in the region, confirming their location in this region, as well as getting estimated dips, should help in the geothermal decision making processes.

On the west end of the section, there is shallow fill overlaying the basement rock, with a depth to basement of approximately 200m. Moving towards the east, a large offset fault is seen, which corresponds to the large faceted spurs seen along the front of the mountains to the north and south. This fault drops the basement down much deeper. Inside this basin, the older Dry Union sediments overlying the basement, as well as the newer glacial and alluvial

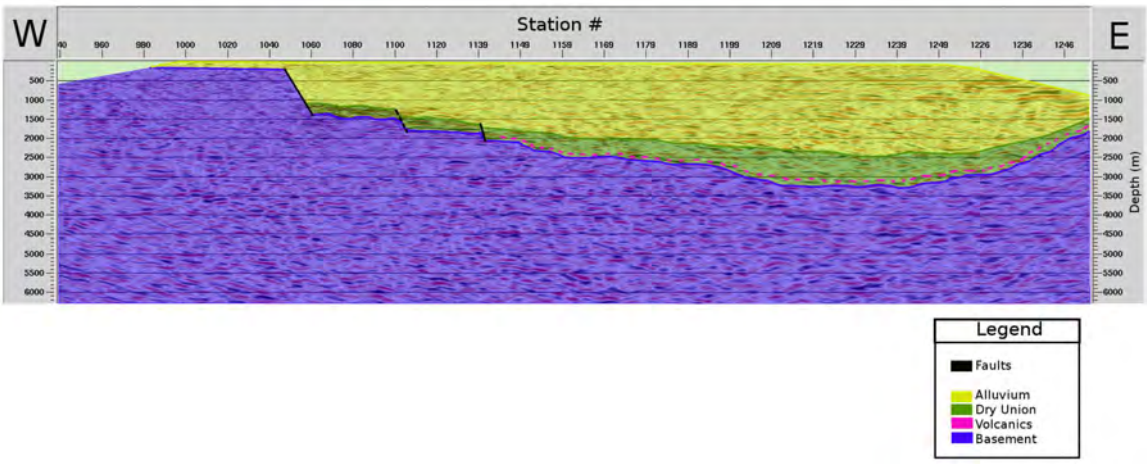

Figure 5.6.1: Interpreted North Line Seismic Section

fills in the rest of the basement. Some minor faulting is seen into the basin, consistent with the regional stress regime. There is a strong reflector just above the basement that could possibly be the lava flow seen outcropping further to the east.

Of course, there are still ambiguities. Since the top of the basement is not extremely well defined, a specific depth to basement cannot be stated. But, with the help of the gravity cross section, a general idea can be created. The following is the gravity team's model of the line, with faults picked based on their seismic locations. As is shown, the faulting pattern is consistent with what is expected from the geologic character of the region. Since the valley is a part of an extensional rift system, faulting on either side of the valley is expected, with the center portion dropping down to become a graben. This section appears to be consistent with this conclusion.

The south line proved to be a lot easier to interpret, with sequence boundaries and some possible structures clearly visible. Since this survey was done as a preliminary step, there are not many geologic interpretations to be made. There is no gravity model or shallow seismic to tie into the interpretation, so the following section should be taken as a possible guide.

As shown, there are similar sediments and basement basin structure in both lines. The depth to basement is similar to the north line, but the same magnitude of faulting is not seen in this section. In fact, it appears that the south section is further basinward because of the smoother structure. The structures of the fill sediments on top are clearly defined on the section, but a more detailed interpretation will come when more complimentary data is collected.

5.7 Conclusions

Overall, the effectiveness of the seismic method is shown in its ability to determine specific structures and boundaries. For this survey region, the seismic data did not show anything

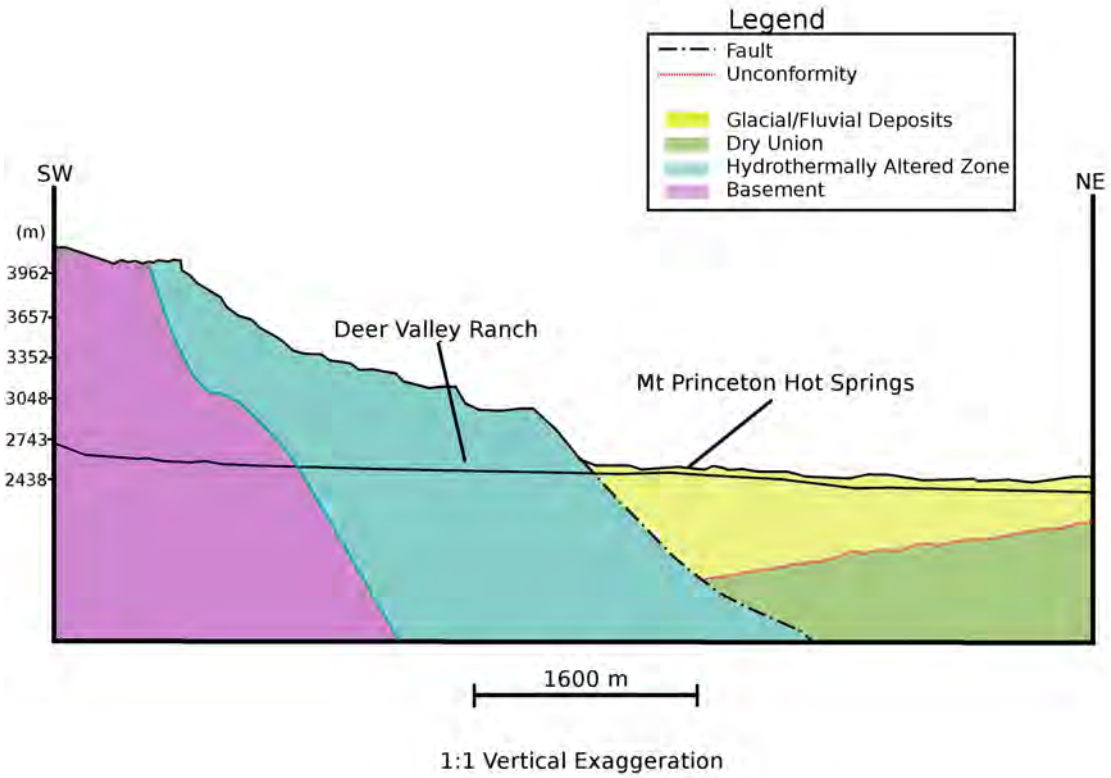

Figure 5.6.2: Gravity Based Geologic Cross Section

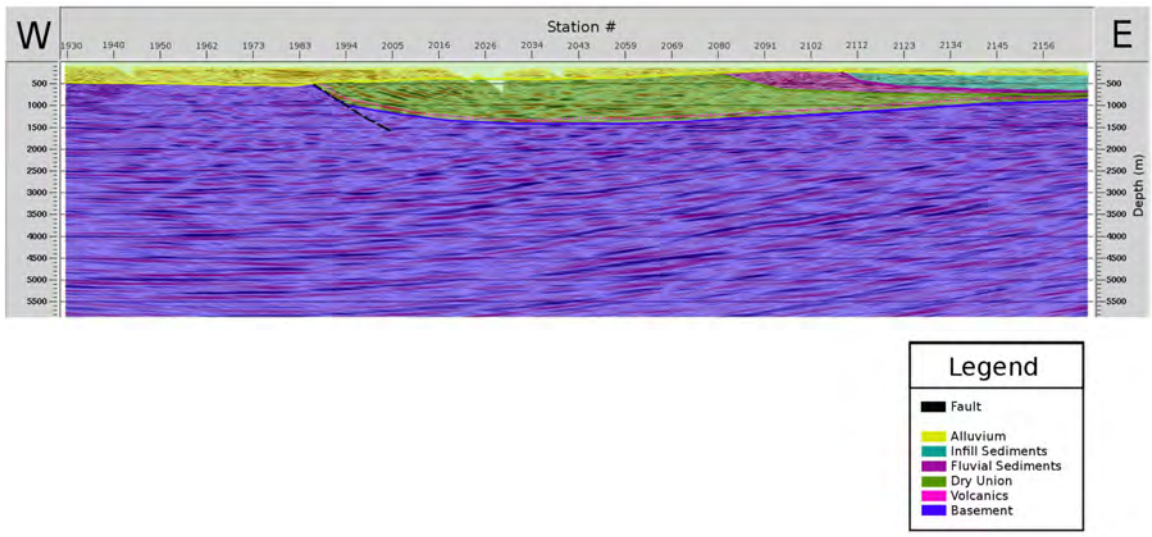

Figure 5.6.3: Interpreted South Line Seismic Section

revolutionary to the overall regional interpretation, but the data was able to prove regional faults seen on most geologic maps.

Of course, since the processing was rather rushed, a more thorough and careful treatment of the data could prove useful for getting more out of the dataset. Some of the hardest data to clean up is 2D land seismic data because of the surfaces irregularities of land, and the inability to characterize noise coming from outside the line. However, with more careful parameterization of the some of the processing flows, it is likely that the dataset could be greatly improved.

Future recommendations are to continue use of the deep seismic method, even though the data is a little noisy with the current survey design. The depth of investigation is unparalleled, and can help determine structure beyond what other methods are capable of. When designing future surveys, as much care as is possible should be taken to reduce noise, as this was the biggest issue with this data.

On the whole, the outcome and interpretation of these datasets were satisfactory, and hopefully this confirmation of the faulting and structure will prove useful to those hoping to better understand the geology of the Upper Arkansas Valley.

Chapter 6

Near Surface Seismic

6.1 Introduction

Deep seismic gives an understanding of the structure of the subsurface, but in this problem, we seek water that is only 30 to 150 ft to the surface. Near surface seismic methods can help characterize the subsurface around this target and give us an idea of where the fluids may be.

Near surface seismic is similar to deep seismic. The main difference between the two is how deep the the waves reach. The amount of money and time spent in order to apply near surface seismic methods is another important difference between shallow and deep seismic. Deep seismic uses vibroseis trucks that cost around $30,000 per day to operate and takes a long period of time in order to perform one shot at one station. On the other hand, shallow seismic uses a weight drop unit that costs $3,000 per day and takes about one minute per station. Shallow seismic methods are also more accessible. A weight drop truck is easier to transport to the field than a vibroseis and can go into heavy foliaged areas such as the Arkansas Valley.

Generally, shallow seismic methods reach up to 200 m in the subsurface. There are various types of shallow seismic sources. Sledge hammers, weight drops, and explosives are the most utilized sources. During our field session, we used the weight drop. An advantage to using shallow seismic is that it allows us to see the heterogeny of the shallow surface that can help in deep seismic processing.

6.2 Theory

6.2.1 Reflection of a Sound Wave

A source emits waves that travel into the subsurface until these waves reach a boundary between two different rocks or fluids as shown in figure 6.2.1. At that boundary, the waves will bounce off of the interface and travel back to the surface. This bounce is what is known as wave reflection. The time taken for the wave to travel from the source to the boundary

and back are recorded at the surface by geophones. We keep these times for processing.

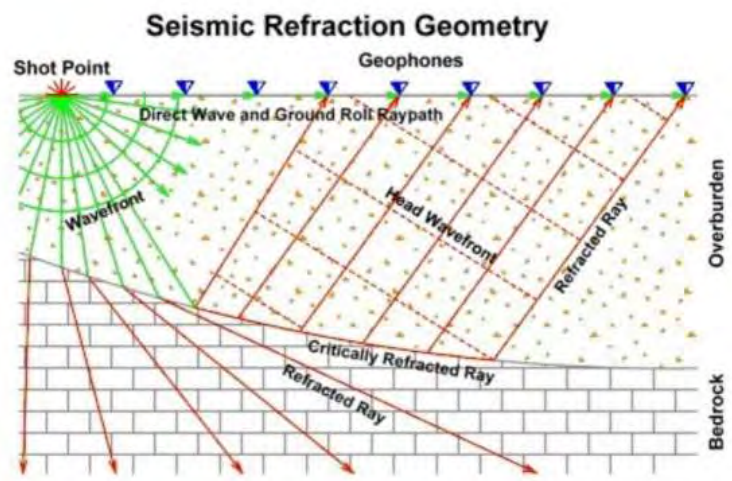

Figure 6.2.1: Seismic exploration theory

6.2.2 Refraction of a Sound Wave

Reflected waves are not the only waves generated At that same interface, some waves will travel into a deeper medium. Due to the differences in properties and in velocities of the rocks, these waves will bend. This is what is known as waves refraction. After that, the waves will either hit another interface and bounce back off of the new interface back to the surface where they will be recorded by the geophones, or they will continue traveling down the subsurfaces causing other refractions. These waves, as mentioned before, are recorded at the surface by a range of geophones that are distributed according to a specific spacing intervals.

6.3 Methodology

The seismic source, shown in figure 6.3.1 is a heavy 300 lbs weight that is flat and dropped on the ground from about 5 ft above the ground. The weight must land on the ground flat. A hydraulic system and chains lifted the weight. We dropped the weight eight times at the mid-point between two geophones. The mid-points between the geophones were our stations.

Our shallow seismic survey took place along our first deep seismic survey which was located in the Northern region of Chaffee County along CR 290 in west-east direction shown in figure 6.3.2.

Figure 6.3.1: Weight drop system used in near surface seismic exploration

120 geophones were distributed on that road with a separation of 5 m. Our source was placed at the mid-point of two geophones (2.5 m) where we recorded 8 shots between geophones. We recorded several shots to improve the signal-to-noise ratio. We had a total of 120 stations where we used our source. The weight drop truck was provided by Boise State University.

6.4 Processing

Seismic Unix processed the data through stacking the raw data and removing missing traces or correcting where polarization reversals occur. The seismic data was then time migrated to give the image shown in figure 6.4.1. High amplitudes are shown as blue where low amplitudes are in red.

6.5 Interpretation and Discussion

Figures 6.5.1 and 6.5.2 shows the unprocessed seismic data for two shots offset by 7.20 m.

The lines are interpretations of the velocity picked on peaks of the data. Notice that in these two sets of data that the data is asymmetric. There is a change in the velocity of the data as we can see when the lines changes from blue to green. The blue and green lines indicate rock unit velocities of 2300 m/s and 4100 m/s respectively. We would expect from these velocities that the velocity of 2300 m/s corresponds to a sandstone and the 4100 m/s corresponds to basement rock.

The velocity of the suspected sandstone is very interesting as it corresponds to the sandstone velocities in the interpreted VSP (see figure 7.6.1 in chapter 7). The contact near

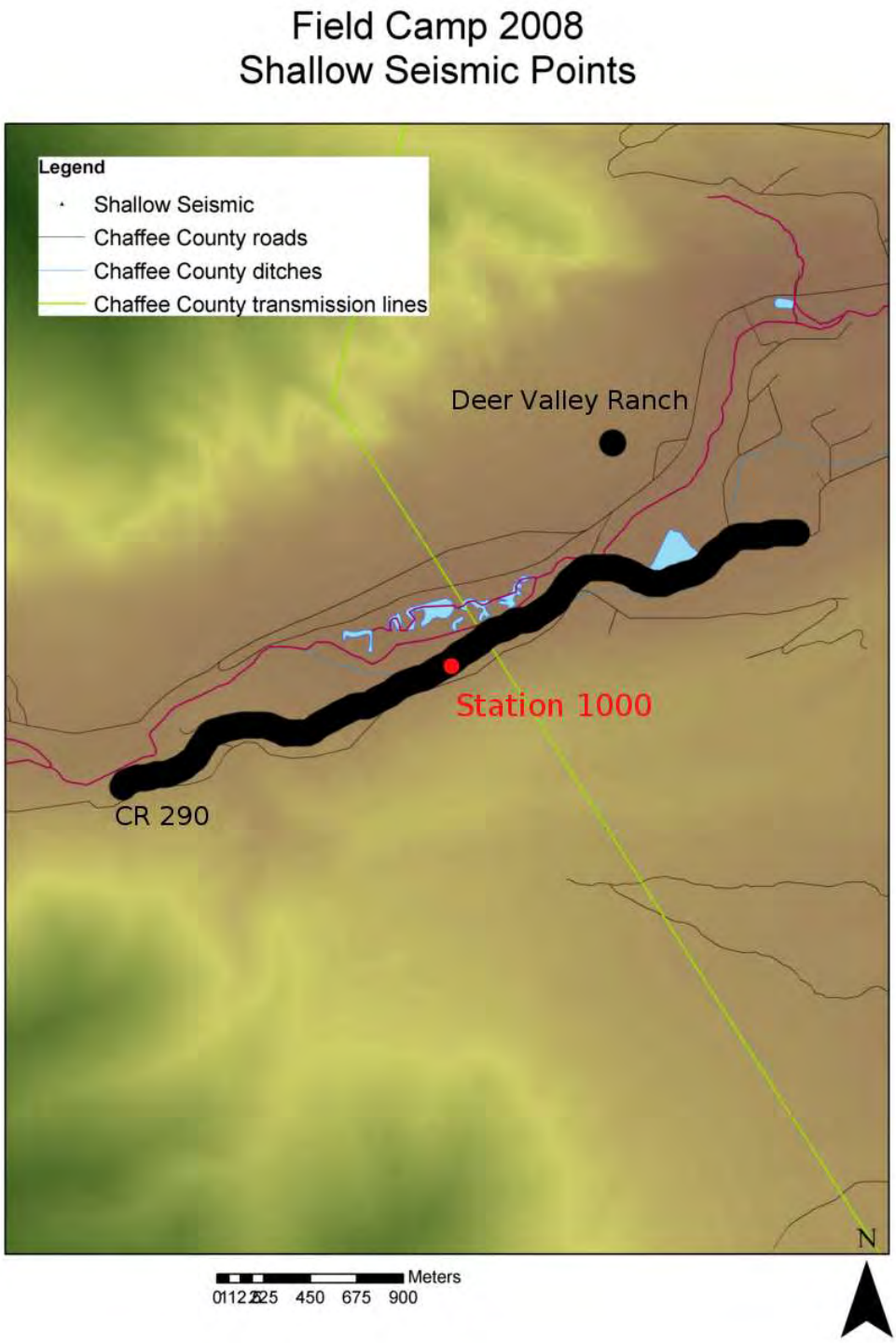

Figure 6.3.2: Near surface seismic line location

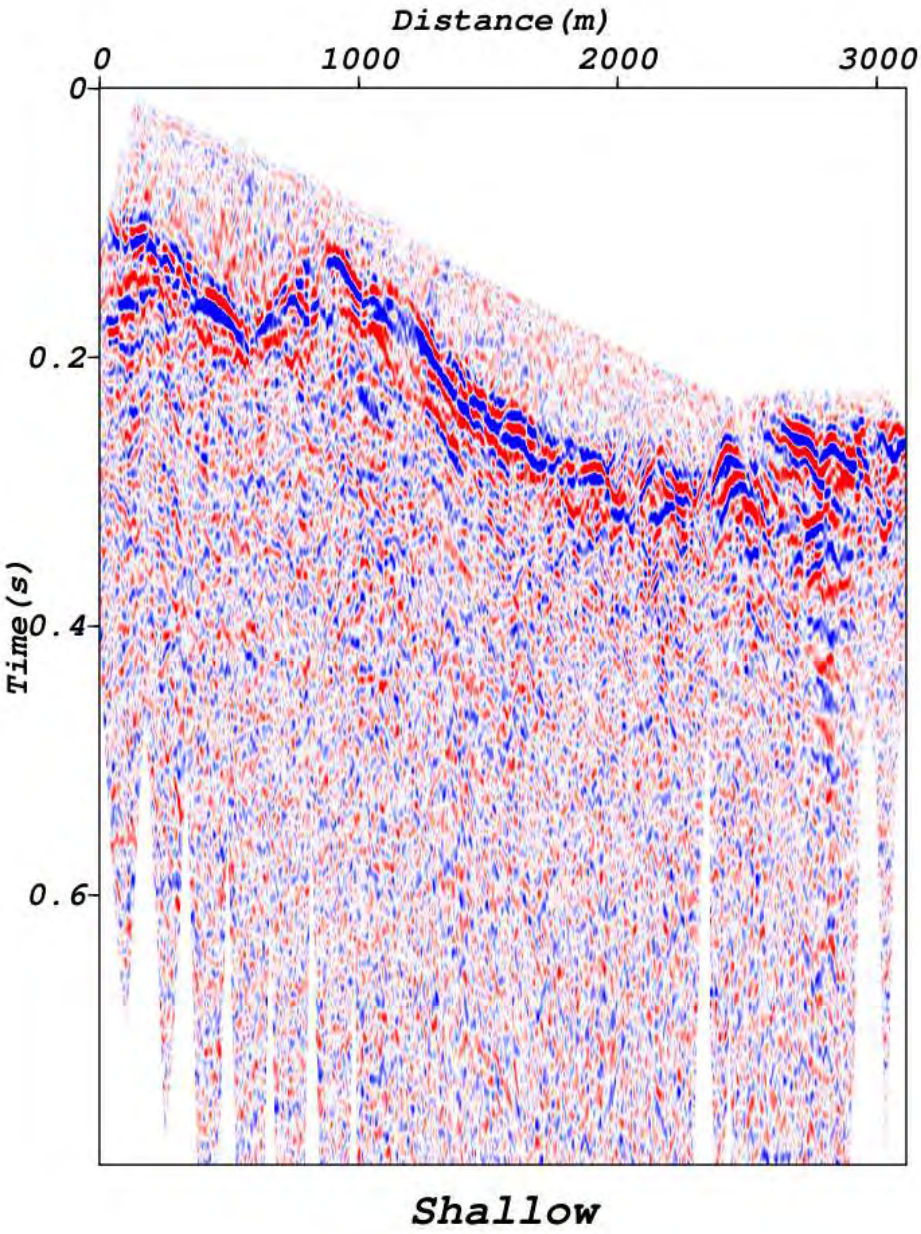

Figure 6.4.1: Near surface seismic image.

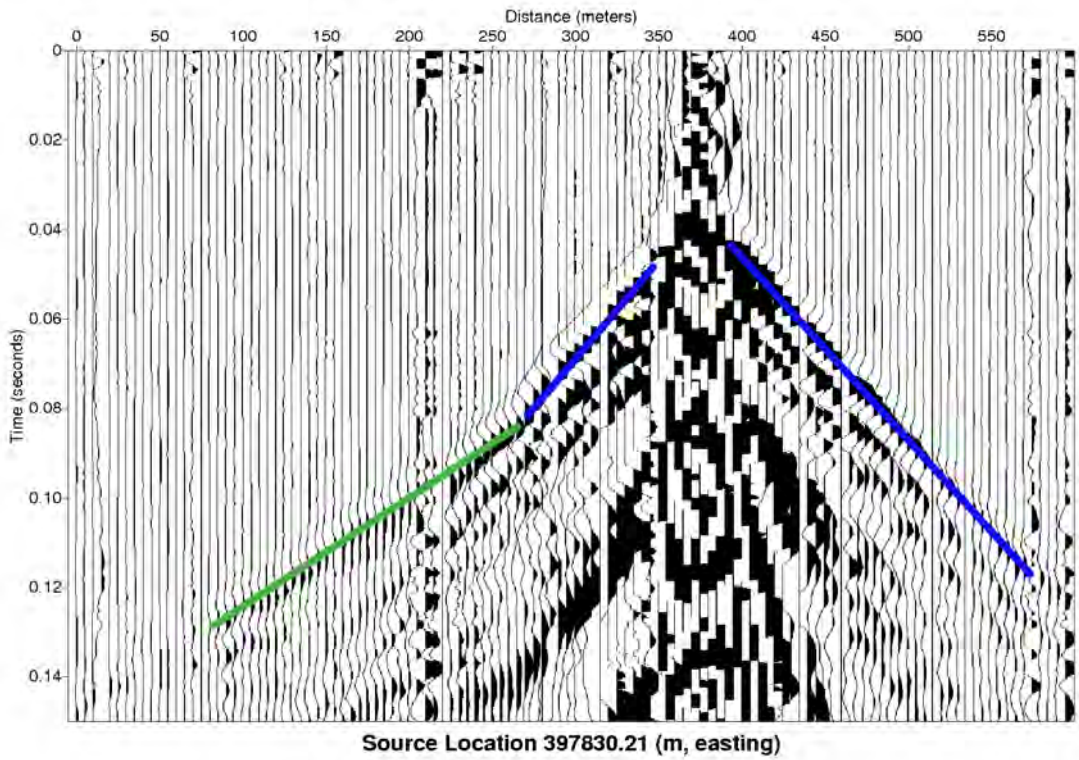

Figure 6.5.1: Unprocessed seismic data with velocity interpretations

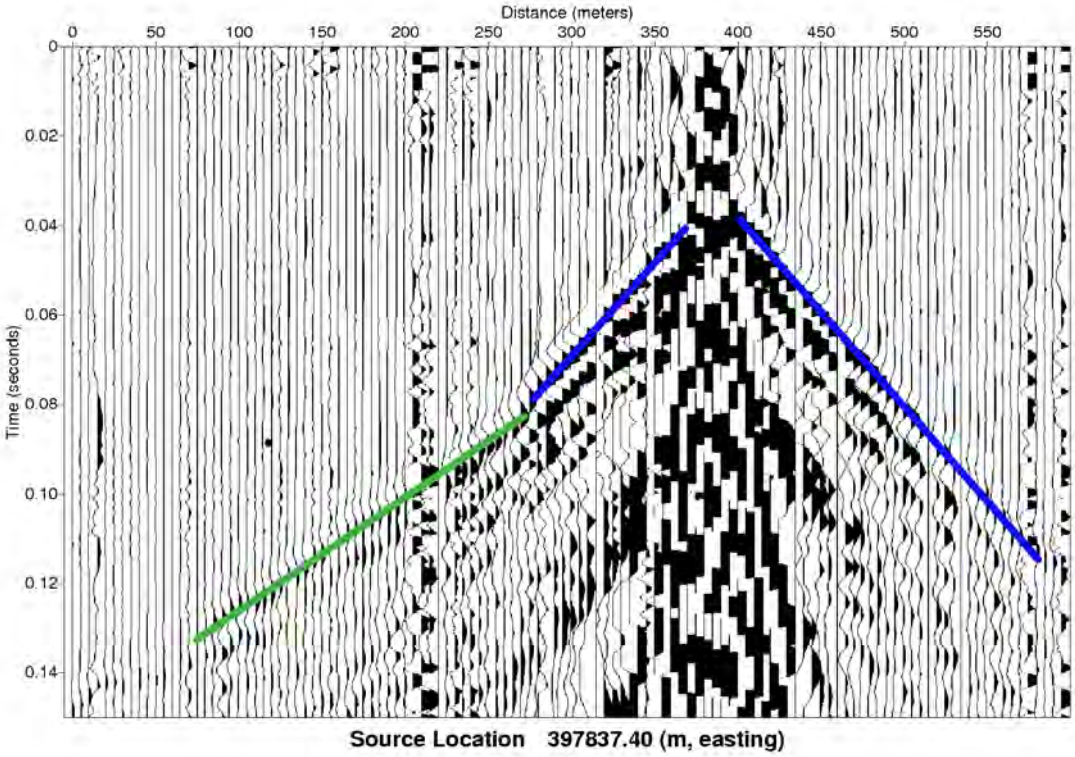

Figure 6.5.2: Unprocessed seismic data with velocity interpretations with source offset by 7.2 m from data in figure 6.5.1

260 m seems to reflect a lithology change if we compare this data with the velocity model derived from VSP. The velocities are then reflecting lithology. It is unknown if velocities or amplitudes are reflecting fluids.

Looking at figure 6.4.1 shows that there is a large event that follows the topography. We also looked for possible start of faults, which are shown below in figure 6.5.3.

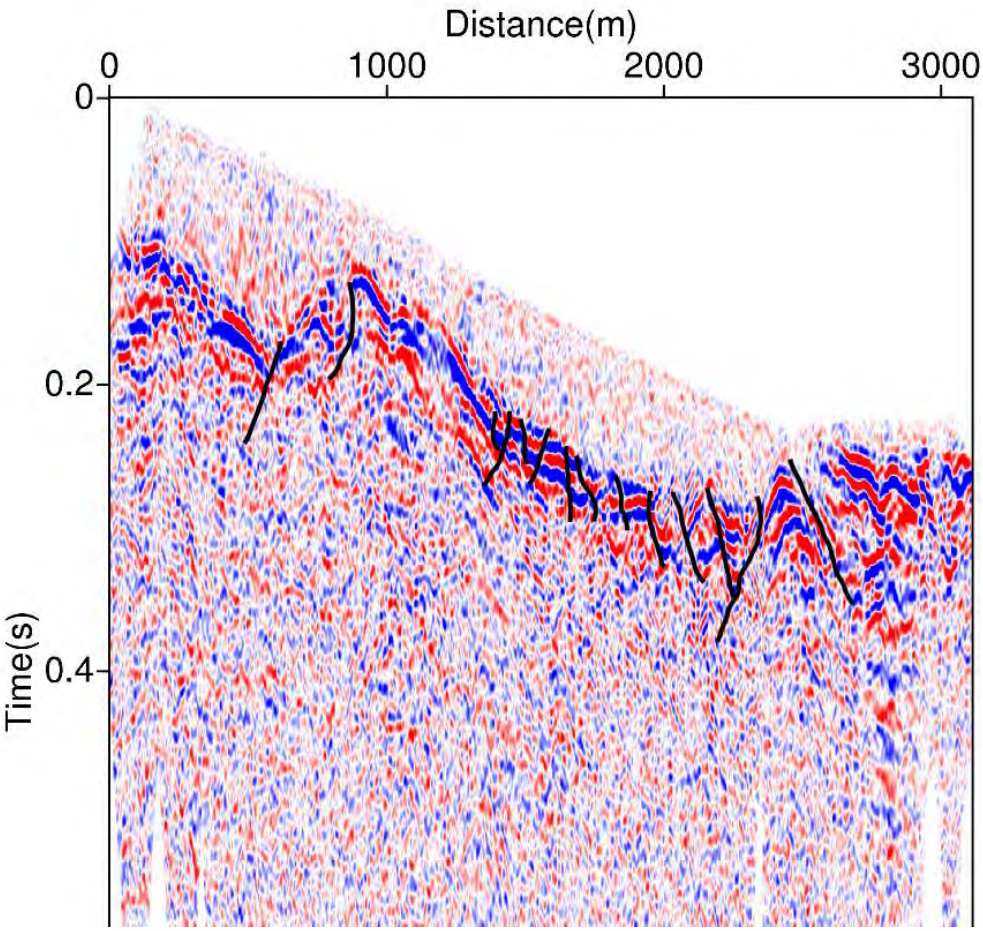

Figure 6.5.3: Fault interpretation along the near surface seismic line

Fault interpretation is based off the assumption that the stresses on the geology are extensional. We can see that the fault structure of the near surface is quite complex across this strike line. Some of the faults seem to lay underneath others while others may form odd stair step structures. We can also tell from the faults that the reflector in question may have been contorted a lot prior to faulting.

So what exactly is this reflector event? We speculate that it could be the boundary between the overburden and basement rock. Amplitudes can reflect either lithology effects or fluids. However, the water table argument does not make as much sense as a lithology hypothesis. There are ponds at the base of the slope, which would suggest that the water

table must be a lot deeper in the subsurface. Converting the seismic profile from time to depth and tying to the wells would help in seeing where the water table should be on the seismic.

Another interesting phenomenon is the amount of overburden or soil that is above this reflector. We would expect that a seismic cross section along the strike (that is, a line that goes across the slope of the mountain) to have an even distribution of overburden. If the conclusion that the reflector is a water table, then the seismic lines is suggesting that we can reach that water quicker towards the east because there is less overburden to drill through. The well would also cost less. We strongly recommend that one waits to drill a well though as this is a one line seismic interpretation. Well data in the area might help with the interpretation so that we can understand which regions are water bearing rocks and which ones are seals.

Chapter 7

VSP

7.1 Introduction

Seismic data acquired in the deep and near surface experiments can generate an image of the subsurface. In order to construct an image from that data, well data and petrophysical data must be acquired. One key piece of petrophysical data is a Vertical Seismic Profile.

A Vertical Seismic Profile (VSP) shown in figure 7.1.1 below uses a similar setup from the seismic experiments. Just like in exploration seismology, waves are recorded on seismograms as they travel through the ground to the receivers. The difference though is that the line of receivers are placed down a well instead of across the ground. Since the source is at or near the wellbore, the time a wave takes to reach specific depths in the borehole can be measured.

7.2 Location

The students performed a VSP at a cold water well in Chaffee County about 1.6 km "1.0 mi" east of Mt. Princeton Hot Springs known as the Pistol Well.

7.3 Methods and Acquisition

The students lowered a 37 hydrophone VSP tool into the Pistol Well until the bottom of the tool reached the bottom of the borehole. Once the tool was lowered, the students used a hammer next to the wellhead to generate a seismic source.

The students performed two VSP experiments at this well. The first experiment shown in figure 7.1.1 involved taking data from five hammer swings and then raising the VSP tool 0.1 m from the bottom of the hole. The students repeated this procedure until they took five shots and the tool was 0.4 m from the bottom. The students then raised the tool to 2.0 m from the bottom and recorded the waves from five hammer swings. Then, they raised the tool 2.0 m and repeated the experiment. They continued this procedure until the shallowest hydrophone was at the top of the wellbore. By moving the tool in 0.1 m increments, a dense sampling of the material of the lower borehole would be aquired.

In the second VSP experiment in figure 7.3.1, the students lowered the VSP tool to the bottom of the well and moved the hammer 2.0 m away from the well after swinging and

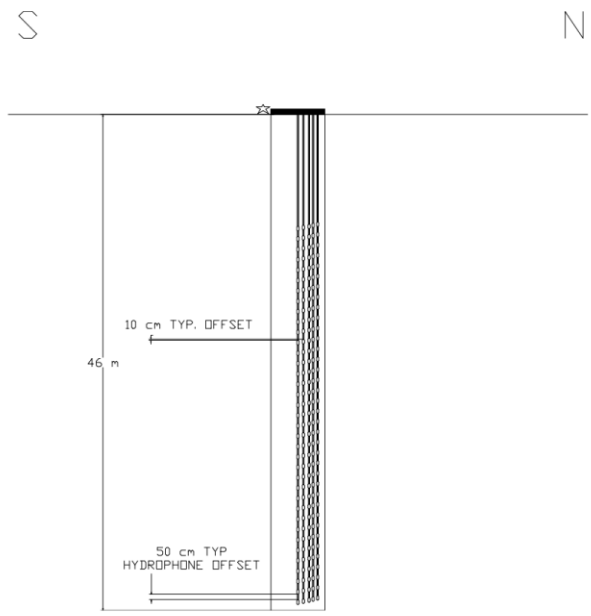

Figure 7.1.1: Vertical Seismic Profile Survey

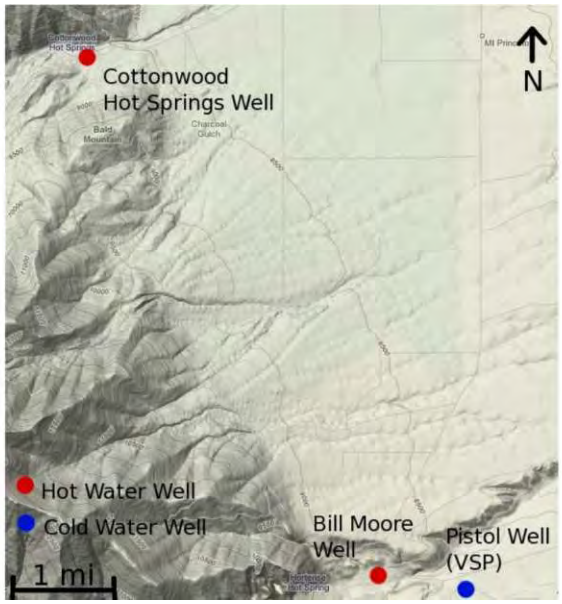

Figure 7.2.1: Studied Well Locations in Chaffee County

recording 5 times. they repeated this process until the hammer source was 22.0 m away from the borehole.

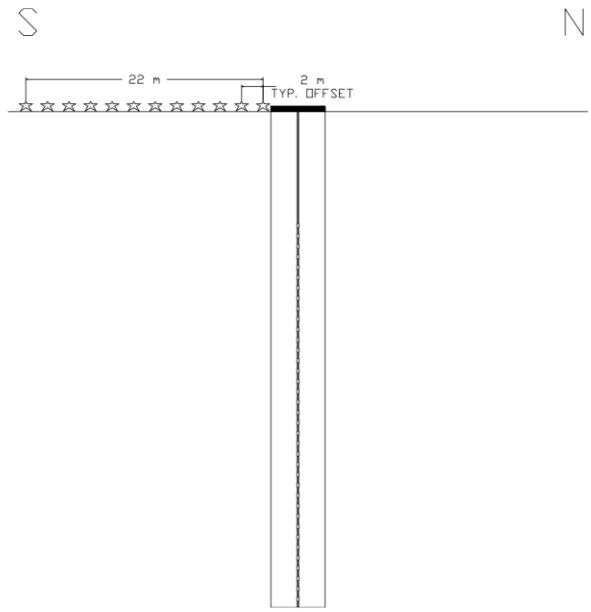

Figure 7.3.1: Second VSP experiment

7.4 Initial Results

Upon completing both experiments, the students then pulled out of the hole and noticed that hydrophones 36 and 37, the shallowest two hydrophones, were dry. All other hydrophones were wet. The water column was estimated in the well at 18.0 m making the highest known water in this well at 27.95 m. Calculating the depth to the water table would be possible knowing the spacing between each hydrophone. This depth to water is much deeper than the depth to water at Bill Moore's well which is about 1.6 km "1 mi" away.

In the VSP data, it was noticed that the amplitudes were following lithology and not the fluids. One reflector was noticed above the highest known water; this may be a change from shale to sandstone which is similar to the lithology in Bill Moore's well. Also, it was noticed that there was another submerged reflector in the VSP data from the first experiment. There are no direct indicators from amplitudes near 27.95 m deep.

7.5 VSP Data Processing

Following that, the raw data was loaded into Seismic Unix for processing. The raw stacked data is shown below in figures 7.5.1 and 7.5.2. The latter is a close up of times 0.0 s and 0.2 s.

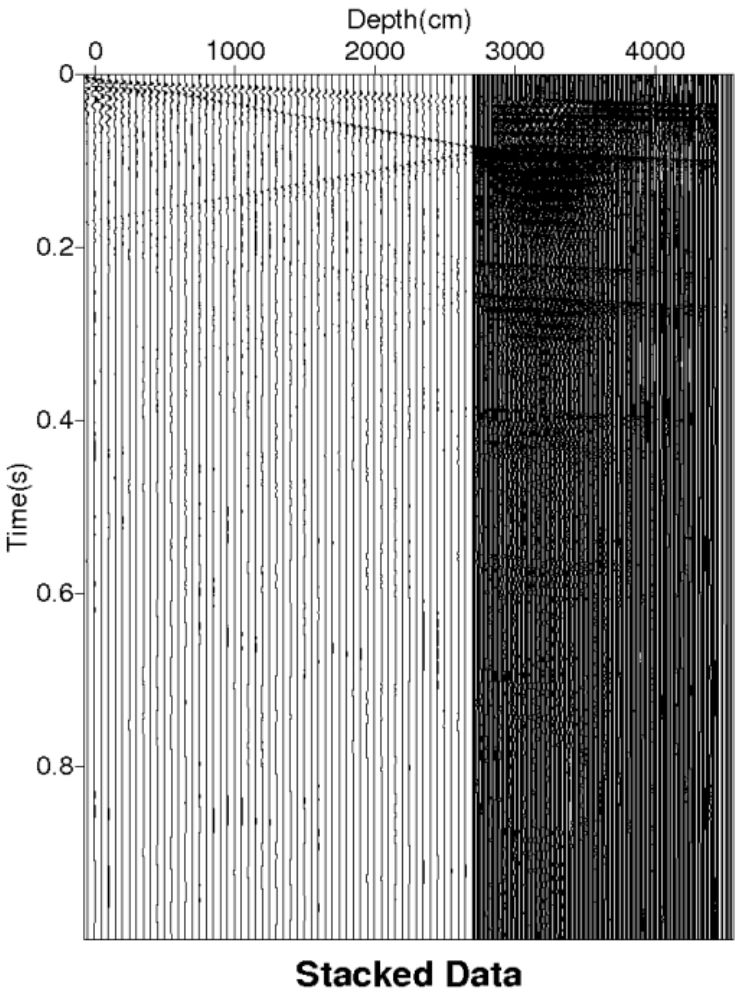

Figure 7.5.1: Piston well stacked VSP data

A dip filter separates the upward and downward waves to create the following set of processed seismic data in figure 7.5.3.

7.6 Interpretation and Discussion

Figure 7.5.2 shows two interesting events. The most noticeable event is the air wave that reflects and transmits at 28.0 m. This event seems to suggest a possible water contact as noticed from the raw data in figure 7.5.1 that the highest two hydrophones are out of the

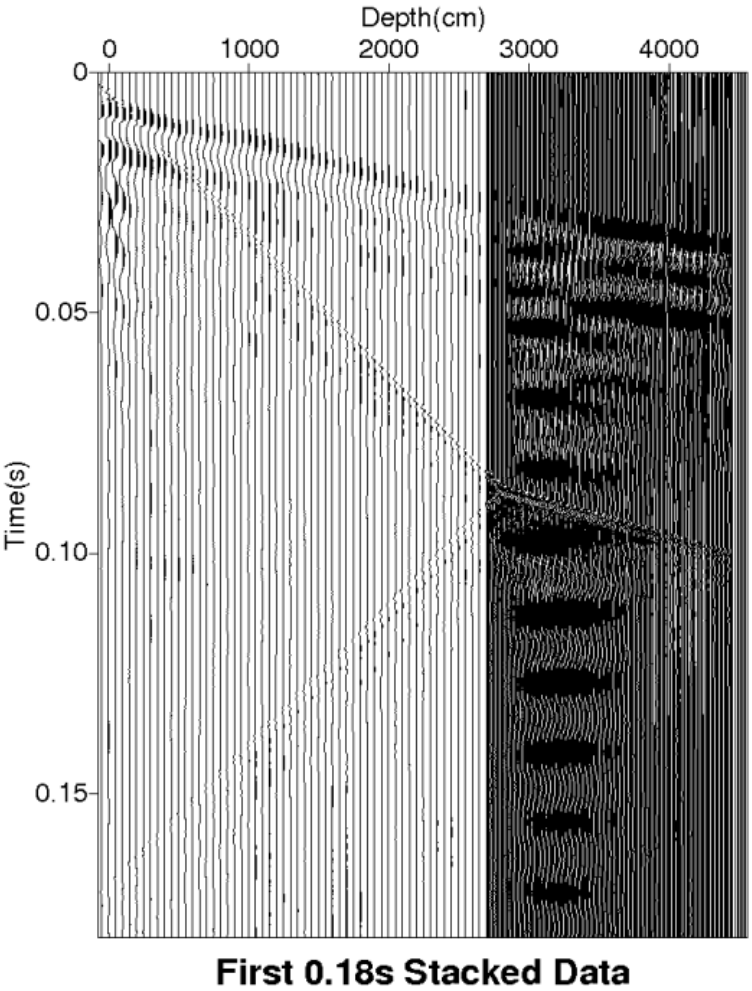

Figure 7.5.2: Piston well stacked VSP data between 0 s and 0.18 s

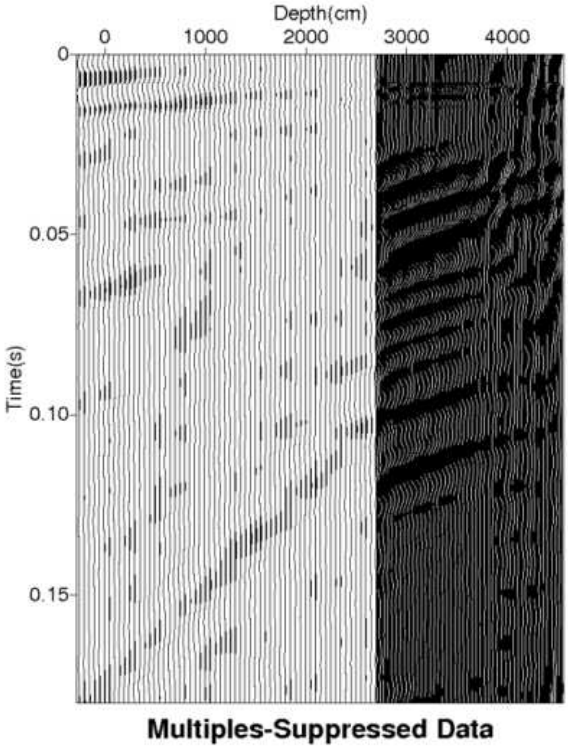

Figure 7.5.3: Seismic data after applying dip filter

water. There are no water reverberations on these traces. However, the velocity of the transmitted wave is 1250.0 m/s. This velocity is much slower than the velocity of water. Though there is possible evidence that this is a water contact, it is difficult to explain the difference from the observed and expected velocities.

Looking back at figures 7.5.2 and 7.5.3, one can see the presence of a reflector near 0.07 s below water level.

Using the interpreted lithology from Bill Moore's well and this VSP data, a three layer velocity model was constructed shown in figure 7.6.1.

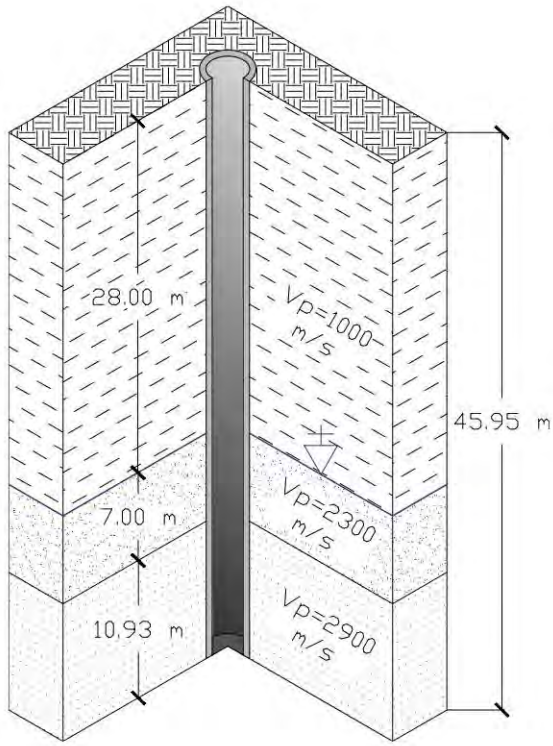

Figure 7.6.1: VSP Velocity Model

The students were able to see a lithology whose velocity increases as depth increases. It can be guessed that the lithology of the top layer is most likely a shale layer because of its low velocity. The higher velocity is expected to be that of sandstone. This lithology seems to fit the data from the nearby Bill Moore well. It would be expected that this sandstone would harbor water as there is the potential for water flow through this area.

Chapter 8

Ground Penetrating Radar

8.1 Background

Ground Penetrating Radar (GPR) is a geophysical method used to image the subsurface. This method has many of the same concepts as seismic methods, but rather than looking at how sound waves travel through a medium, GPR records the changes in a radio wave when it travels through the ground. Moreover, the images from GPR are similar to seismic images in that the horizontal axis reflects distance and the vertical axis reflects time. However, the GPR's radio frequency electromagnetic waves attenuate faster than sound waves, which result in smaller depth of investigation but a higher resolution at shallower depths.

When the radio frequency electromagnetic waves encounters a change in the dielectric permittivity part of its energy, the wave is transmitted and refracted while the other part is reflected back to the surface. The reflected part of the wave is what can be measured by a receiver on the surface as seen in Figure 8.1.1. The source and receiver are antennas of the same frequency. Different frequency antennas, such as 50, 100, or 200 megahertz, can be used depending on the desired depth of penetration and resolution. High frequency waves attenuate faster than low frequency waves. Because of this, a high-frequency antenna will have a shallower depth of investigation with a higher resolution. High-frequency waves have better resolution because the wavelength is smaller. Low-frequency waves have a large wavelength resulting in lower resolution. This causes the wave to see thinner layers and smaller objects. A wave will reflect when it detects a change in properties. As an example, by calculating the wavelength from the frequency, a 100MHz antenna has a wavelength of 3 meters while a 200 MHz antenna has a wavelength of 1.5 meters. As a rule of thumb, the resolution is one third of the wavelength. Because high-frequency waves can see smaller events, they will be reflected more often while traveling through the subsurface. Due to this increase in scattering, it will lose energy faster. Since the low-frequency waves attenuate slower they will travel farther.

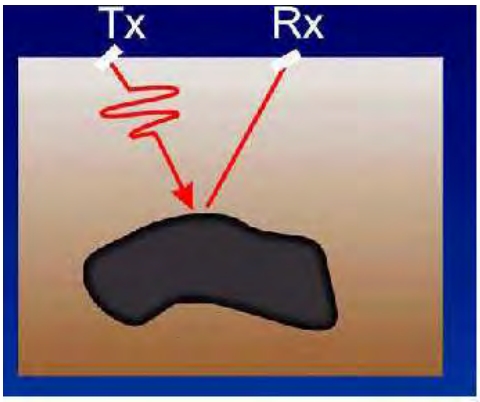

Figure 8.1.1: Ground penetrating radar uses radio waves to probe the subsurface. This represents detection of reflected or scattered energy[19]

The depth of investigation also depends on the electrical conductivity of the material that the wave is traveling through. As the conductivity of the material increases, the depth of investigation decreases because the electromagnetic energy dissipates into heat in a conductive medium, causing a loss in the signal strength. In addition, when the wave encounters an object with noticeable different dielectric permittivities it is reflected. With each reflection the signal loses strength.

8.2 Survey Design

While we are in the Upper Arkansas Valley we completed two different surveys. One survey was a constant offset survey while the other was a common midpoint survey. Both surveys were completed in the field next to Bill Moores well, survey field 1.2.

The constant offset survey was conducted along seven of the lines on field 1.2. For each line the two antennas were attached to a cart and pulled at a constant velocity. This setup can be seen in Figure 8.2.2. The distance between the antennas is related to the frequency of the antennas. It is assumed that the antennas were pulled at a constant velocity and the data is evenly distributed between the beginning and the end of the line. We used 50 MHz antennas at a distance of 6 feet between them with a transmitter voltage of 400 V for all lines on field 1.2. The data from the constant offset survey, when displayed, looks like a cross section of the subsurface.

To accompany the constant offset survey a common midpoint survey was acquired. In this case, the midpoint of the two antennas remains constant while the offset is varied, seen in Figure 8.2.3. To begin, the antennas are placed at a distance equal to the length of one of the antennas. The length of the antenna is related to the frequency. This length is the closest the antennas can be to each other without interfering with one another. When the antennas are at this distance it is known as zero offset. From that point the antennas are moved away from each other at intervals equal to the length of one of the antennas. This

Figure 8.2.1: Survey Grid on field 1.2

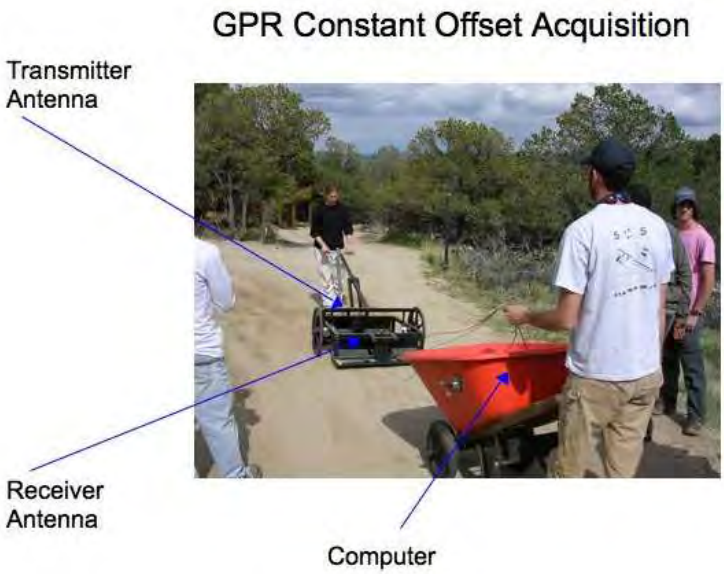

Figure 8.2.2: A GPR constant offset survey being conducted in the field.

data is useful for determining the velocity of the waves in the material.

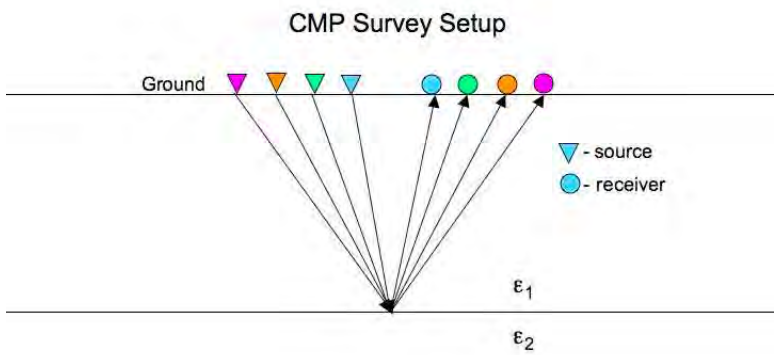

Figure 8.2.3: Survey Design of common midpoint gathers

8.3 Processing

The processing began with the common midpoint data (CMP). The goal from the CMP data was to determine the velocity of the waves in the subsurface. To accomplish this goal, the seismic processing suite known as Seismic Unix was used because seismic methods and

GPR are similar. The points along the direct arrival and any visible hyperbolas were picked resulting in points corresponding to offset and time. From these picks, the velocity of the wave can be calculated. The picks were made using Seismic Unix and then processed using a Matlab code. The code created a line of best fit to the picks, and then calculated the depth and velocity of the medium based on the slope and t-intercept of the line.

As a starting point, the CMP plots were viewed to estimate velocities and depth. The direct arrival will appear as a straight line and arrive first. The slope of this line is the inverse of the velocity. Any reflection off a horizontal layer will appear as a hyperbola in the CMP data. The direct arrival is shown in red while the hyperbola is shown in green in Figure 12.3.1. In this case the hyperbola asymptotically approaches the direct arrival at later times and larger offset. This implies that the layer is horizontal. In addition, once the velocity is known the depth of the horizontal reflector that created the hyperbola can be calculated.

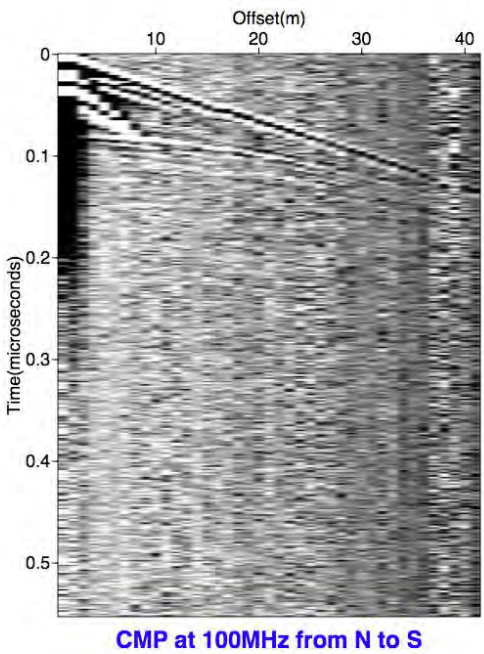

Figure 8.3.1: Example of collected CMP data at 100 MHz. From this, the picks are made which then go into the Matlab code.

CMP data was collected at 50 MHz, 100 MHz, and 200 MHz. The data collected from the 100 MHz antennas is shown in Figure 8.3.1, this data was chosen because the direct wave and reflection were more prominent. The velocity from the direct wave was calculated to be close to the speed of light. This indicated that the direct wave is the wave traveling through the air. The hyperbola located below the direct wave was calculated to be traveling at a similar speed. This means that the wave was traveling through the air when it was reflected.

The survey with 200 MHz antennas was used in the same location to collect common midpoint data. The survey was conducted once in a north-south orientation and again in an

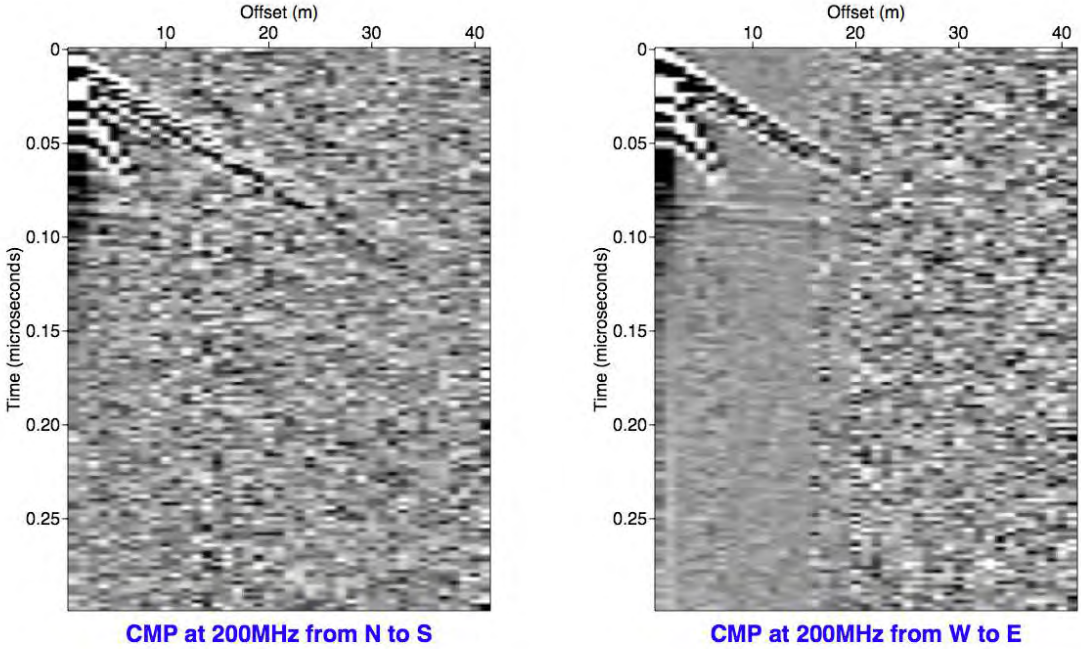

8.3.1 North-South orientation of 200 MHz CMP data. Hyperbolas shown in green.

8.3.2 East-West orientation of 200 MHz CMP data. Hyperbolas shown in green.

Figure 8.3.2: Multiple GPR CMP Stacks

east-west orientation, seen in Figure 8.3.2(a) and Figure 8.3.2(b) respectively. From this a direct wave through the subsurface is seen. From this wave the velocity is calculated to be near 1.5×10^8 m/s. The velocity was calculated to be in a similar speed for traveling in either direction. Because the data collected from different orientations appears similar and similar velocities were calculated, the medium is relatively isotropic.

When doing a constant offset survey the objects in the ground appear as hyperbolas, which can then be migrated using hyperbola mask migration in GRORADAR. To migrate the data, a hyperbola is fit to the target hyperbola based on dielectric permittivity and the radius of the object. The dielectric permittivity is then used to perform the migration, it also relates to the velocity. With migration the hyperbola is focused back on one point where the object is located. If the hyperbola is focused to a point, the permittivity of the medium was modeled correctly. When the velocity is calculated the image can be represented in depth rather than time, known as migration, making the data more useful for interpretation. A before and after migration image is shown in Figures 8.3.3 and 8.3.4.

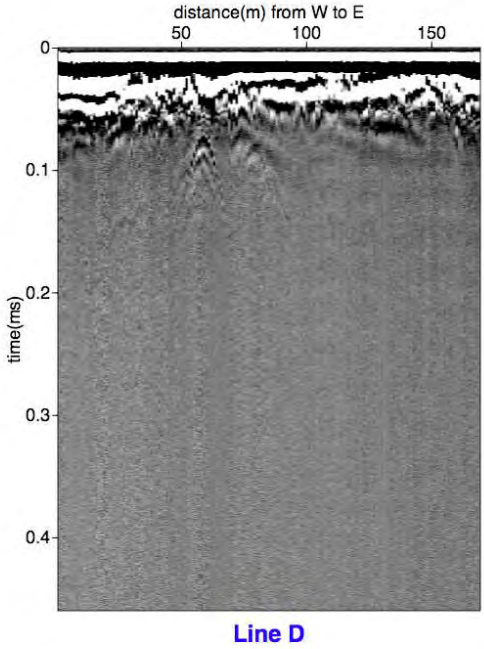

Figure 8.3.3: The raw data collected from line D on Field 1.2, image from Seismic Unix.

8.4 Interpretation

When looking at the CMP data the reflection can be explained as the wave bouncing off the operator located on the surface above the midpoint. This may be caused by the 100 MHz antennas not being shielded on the top, so it can receive data from the air in addition to data from the ground. The velocity from the CMP stacks was confirmed with the results from GRORADAR. This program assumes the magnetic permeability is 1.0 H/m. The equation for velocity can then be simplified to Equation 8.4.1.

$$v = \frac{c}{\sqrt{\epsilon_r}}[20] \tag{8.4.1}$$

Where:
v = Velocity [m/s]
c = Speed of Light (3.0×10^8 m/s)
ϵ_r = Permittivity Relative to Free Space

The velocity calculated from GRORADAR, was 1.3×10^8 m/s. From this velocity we can deduce the medium the wave traveled through to be dry sand.[21] From being in the field we would expect the subsurface to be composed of sand.

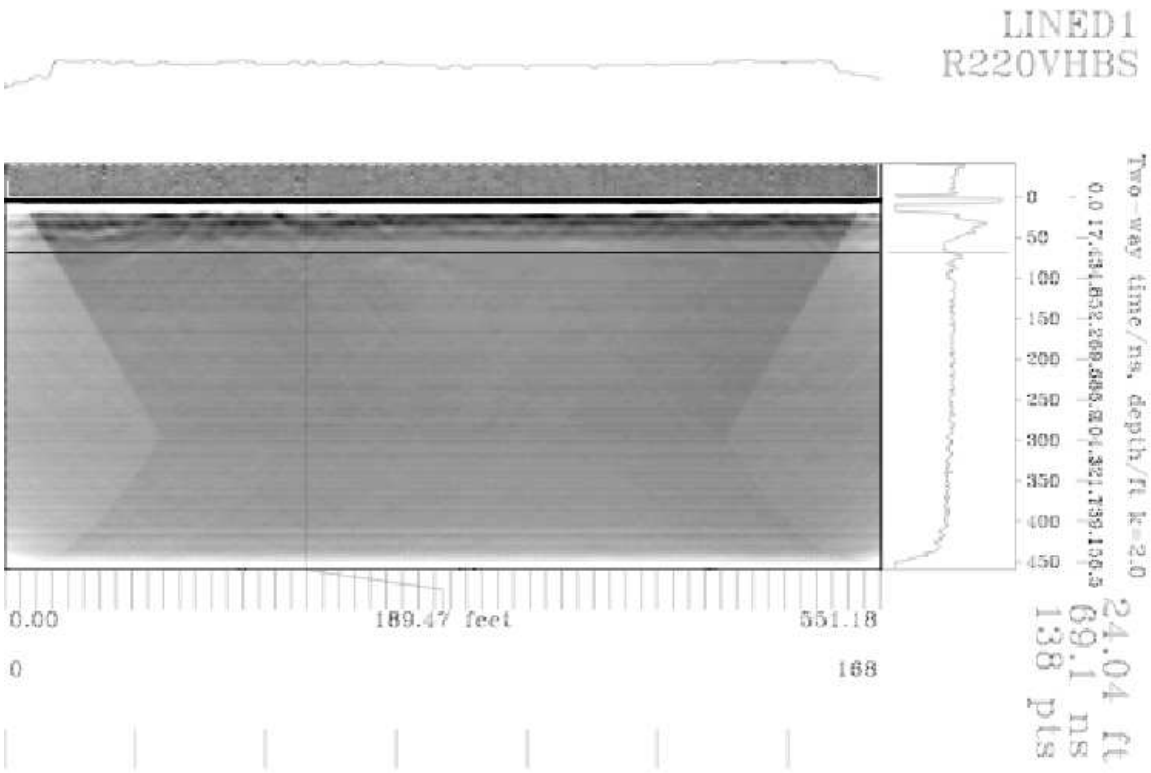

Figure 8.3.4: The data on the right is from the same line and has been migrated using GRORADAR. The cross hairs are at a possible depth to the water table where the time and depth shown to the right.

The top of the water table is expected to be where the cross hairs are in Figure 8.3.4. This was based on Bill Moores well where water is seen near 35 feet. After the migration was done the bottom of the horizontal layer is located at 24 feet so it is a good assertion that it is the top of the water table.

If there was a hyperbola that appeared at approximately the same depth in all of the lines, it could indicate a reflection from a fault or a pipe. None of the hyperbolas seen seem to be continuous or systematic so they probably represent isolated subsurface objects such as boulders. These anomalies tend to appear at a depth of 50-60 feet. From this depth, it can be concluded that the anomalies are not man-made. These boulders could be a result of fluvial deposits or mudslides in the area.

8.5 Error Analysis

Figures 8.5.1(a) and 8.5.1(b) show the same area of investigation, with the cart traveling to the east in Figure 8.5.1(a) and to the west in Figure 8.5.1(b). The figures are almost identical, indicating that the cart was pushed at a relatively constant speed and the data is repeatable.

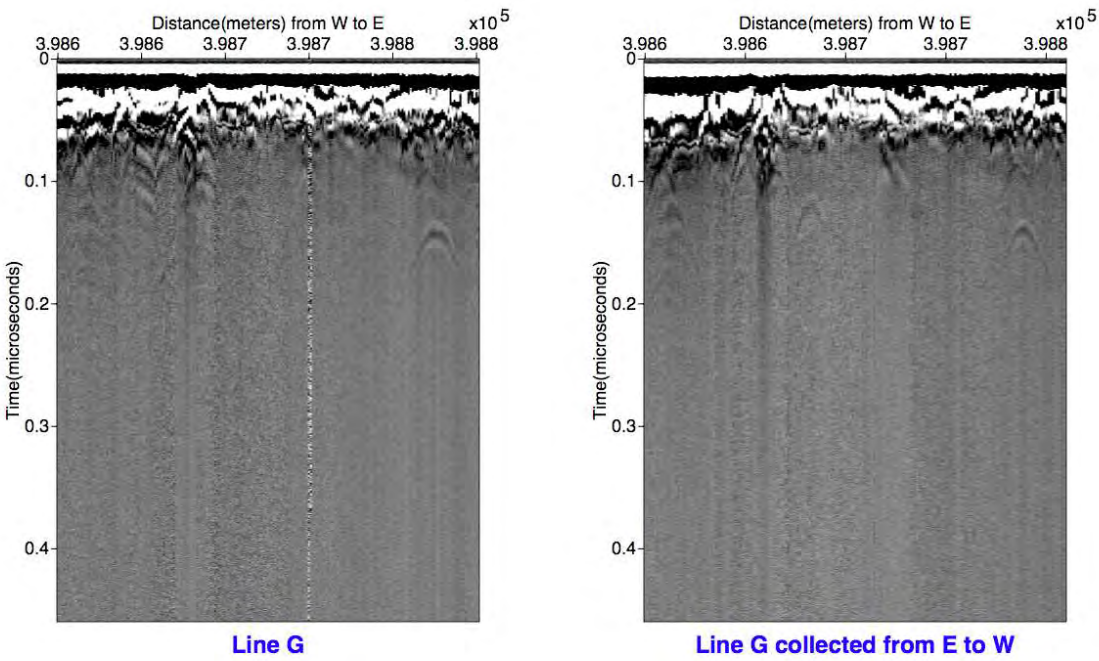

8.5.1 Line G collected from west to east.

8.5.2 Line G collected from east to west.

Figure 8.5.1: Line G Collected two opposite directions

The largest source of error occurs when assuming that the cart is pulled at a constant speed. The trace spacing was determined by dividing the total distance by the number of traces. The location of each trace could then be slightly varied during interpretation due to

the assumption of constant speed.

Also, since the antennas are not shielded, they will record signals from above the surface in addition to signals from the subsurface. This is a source of noise in the data. This noise could be from waves transmitted by radio, television, or various other sources.

Chapter 9

Electromagnetics

9.1 Introduction

Electromagnetic (EM) characterize apparent conductivity of a subsurface region. Students used electromagnetic methods to locate potential sources of geothermal fluids in the Upper Arkansas Valley basin and characterize water table flow in the region.

Geothermaly heated water often contains dissolved minerals and ions which cause a conductive anomaly in EM data. The objective is to locate these geothermal sources for future use in geothermal power. It is also necessary to understand the characteristics of flow in the water drainage system in the area of prospective drilling . Future wells and energy production should not disturb water table levels.

It is theorized that agricultural drainage and irrigation channels act as a sources for elevated water table levels in regions adjacent to the channels. As the amount of agricultural activity in the Upper Arkansas River Valley basin decreases, inhabitants are concerned that water tables in the basin area will drop and cause complications for water extraction through existing wells. This study conducted surveys around the area of a drainage ditch north of the south (Poncha Springs) deep seismic line. Another objective is to determine the depth of the water table around the drainage ditch and from that information characterize the effect of the ditch on the water flow of the surrounding area.

9.2 Dead Horse Survey Site

The "Dead Horse" survey site is located at a dry lake bed (the location of what was Dead Horse Lake). The goal in conducting electromagnetic surveys at this site is to supplement the nearby seismic acquisition data taken and characterize subsurface conductivity. The focus is on conductive bodies, which might indicate faulting and hydro-thermal activity.

9.3 South Drainage Survey Site

The south drainage survey site is located on County Road 250, north of its intersection with County Road 140. This site is the location of an agricultural irrigation channel. Our goal in surveying around this channel is to determine if it has water leakage and if that leakage

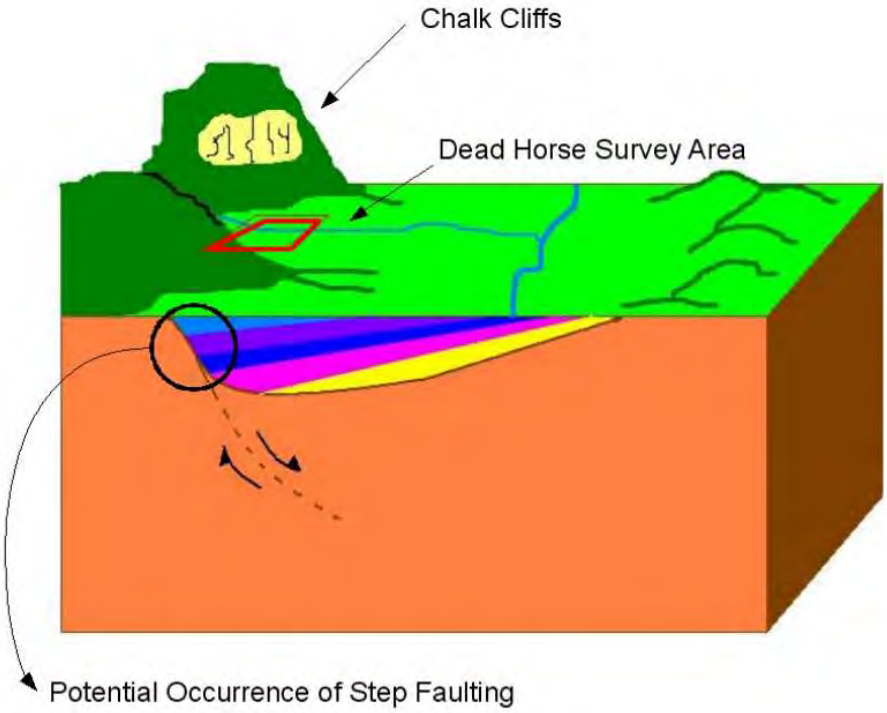

Figure 9.2.1: Location of Dead Horse Survey Site with relation to regional faulting

affects the local water table. Water leakage from irrigation channels may cause higher water table levels in adjacent areas allowing shallow access to water resources in the affected area. If water flow through channels discontinues due to agricultural decline, inhabitants of the region could expect a drop in water table level, which might cause lower production in existing wells.

9.4 EM-31 Introduction

Conducting an EM-31 induction survey will provide data of near surface conductivity in the area of observation. Using this method serves to model the characteristics of groundwater table as it approaches the surface. The EM-31 is a frequency domain method of acquiring EM field data. Frequency Domain Electromagnetics (FDEM) involves generating an electromagnetic field that induces currents in the subsurface, which in turn generates a magnetic field that are measured. These magnetic fields provide the subsurface information such as conductivity. Common applications of FDEM include water aquifer exploration, metal detection, and permafrost mapping [15].

9.5 EM-31 Equipment

The instrument model used for this survey was the Geonics EM31-MK2. This system is effective for use mapping near surface conductive anomalies such as near surface groundwater occurrences. The effective depth of the Geonics EM31-MK2 is approximately 6 m [16].

Figure 9.5.1: EM-31 instrument (http://www.geonics.com/em31.html [16])

9.6 EM-31 Draingage Channel Survey Set-Up

One surveyor can easily cary the EM31-MK2 and take data at a regular walking pace. This surveyor can collect data over the entire survey site expediantly. Figure 9.6.1 shows the data points the EM-31 collected on the west side of county road 250 on both sides fo the irrigation ditch.

Collecting data points on both sides of the ditch provides the direction of water flow in the area surrounding the ditch as well as areas where increased seepage occurs.

9.7 EM-31 Drainage Channel Observed Data

Figures 9.7.1 and 9.7.2 correspond to the raw data. The two figures must have position corrections in order to straighten the lines used for measurements. After the position corrections the expected anomalies such as the water flow became visible and easier for interpretation. Figures 9.7.3 and 9.7.4 show the data after corrections. For interpretation purposes the quadrature is more accurate and reliable than the in-phase component.

The program GMT created the plots in figures 9.7.5 and 9.7.6.

¿From figure 9.7.5 the conductive buried pipe is located close to the left bottom corner of the site. The location is 402900 m east and 4266450 m north. This location agrees with the conductive body seen in the DC images. Moreover, surface water leakage, represented in green, surrounds the pipe. Two circular resistive bodies appear on both sides of the creek. Across the creek, a metal pipe could have caused this resistive feature.

9.8 EM-31 Drainage Channel Inversion/ Interpretation

There appear to be two anomalies in the south west area of the EM survey. The smaller anomaly has a magnitude of 20 mS/m but is confined to a small area. It could be noise or a small conductive body such as a water sprinkler (see figure 9.7.3). The bigger anomaly has a magnitude of approximately 10 mS/m that corresponds to the leakage of the irrigation pipe

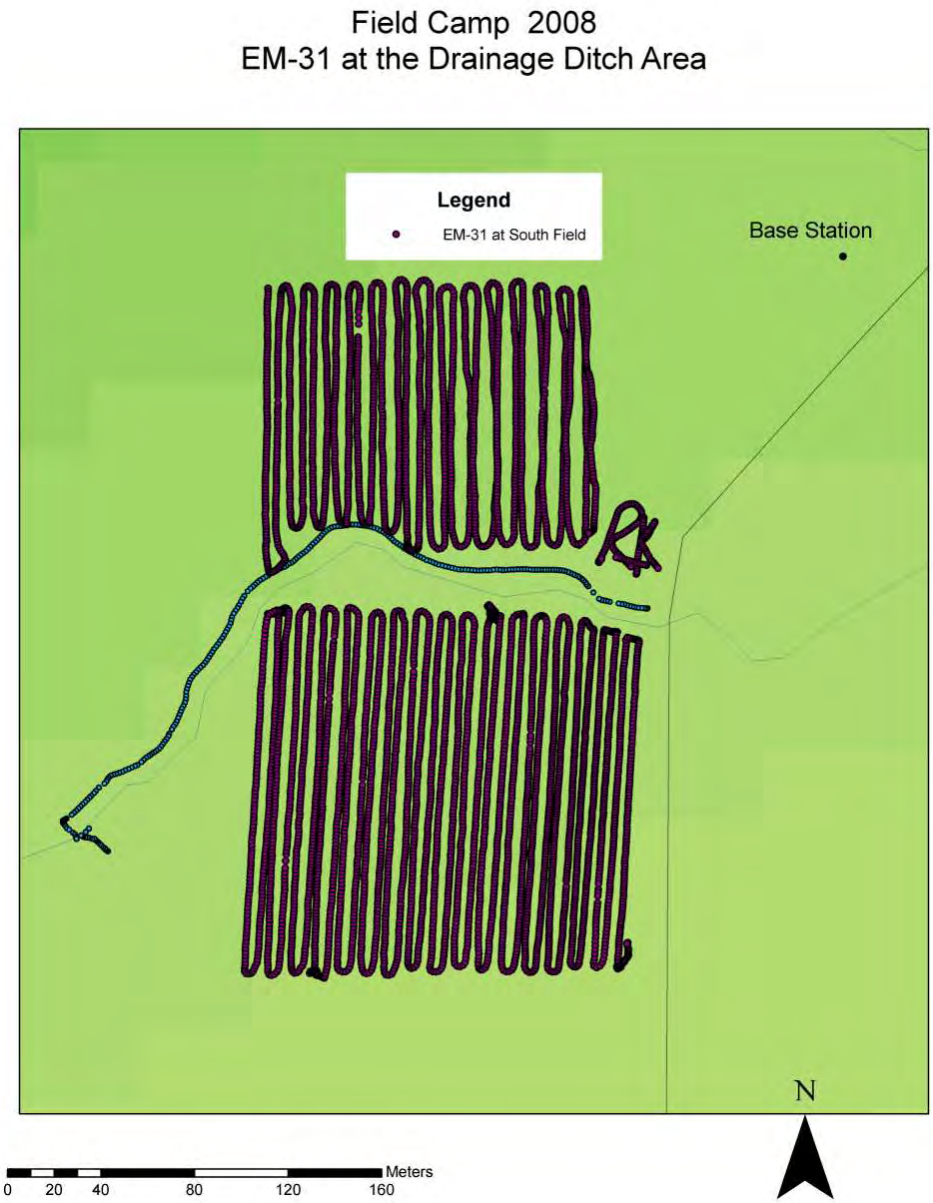

Figure 9.6.1: EM-31 Survey Line Locations and Geometry

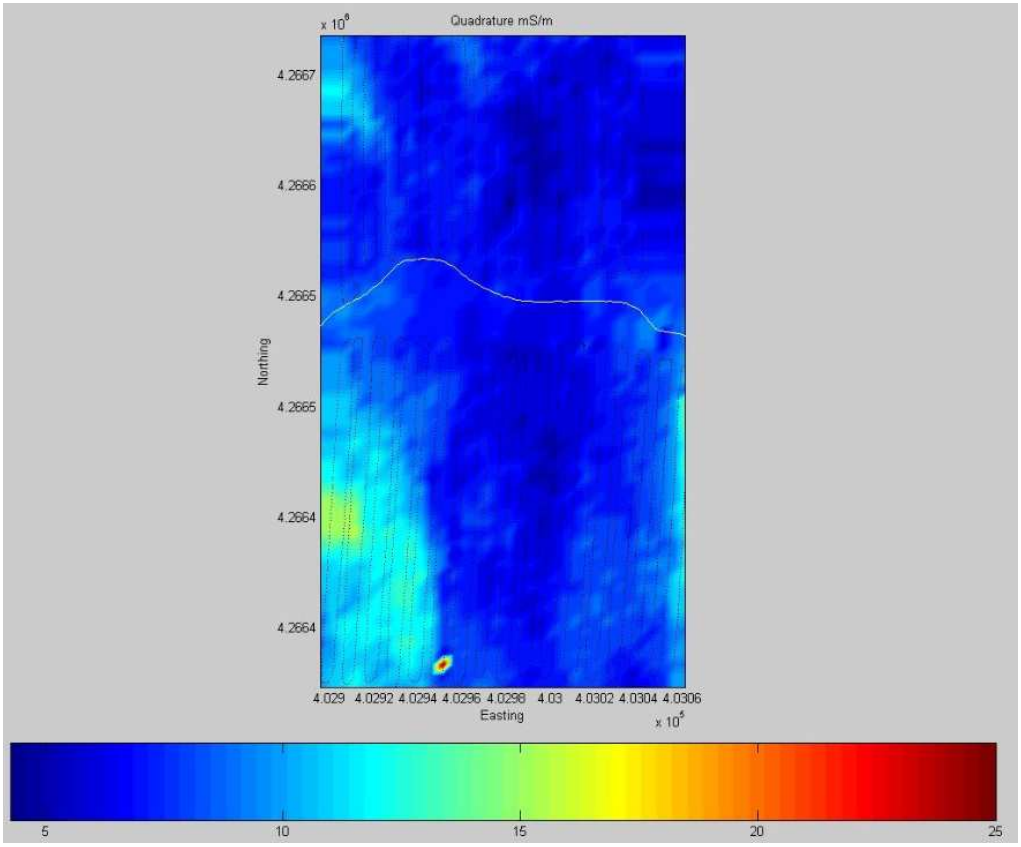

Figure 9.7.1: EM-31 Raw Conductivity Data Quadrature Component

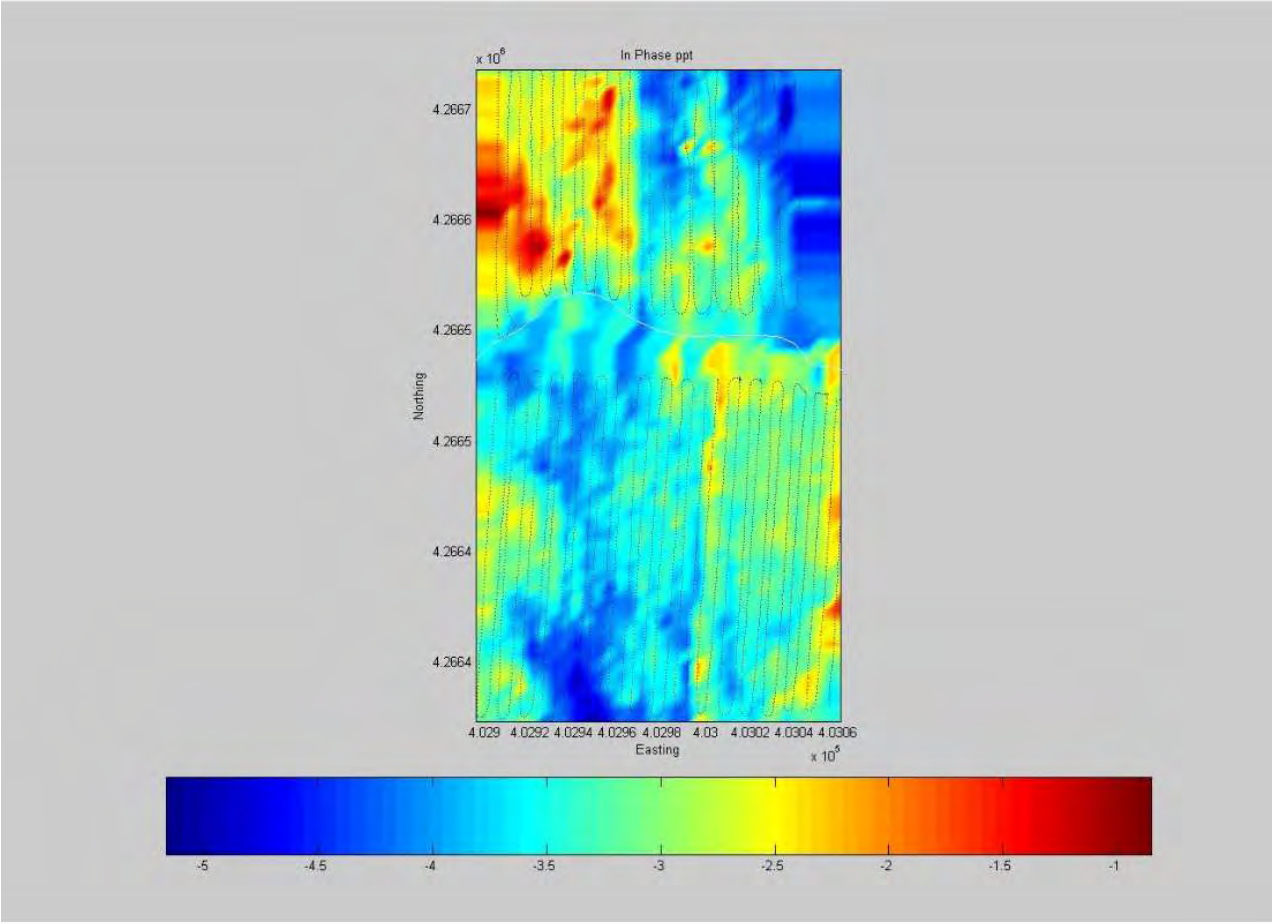

Figure 9.7.2: EM31 Raw Conductivity Data In-Phase Component

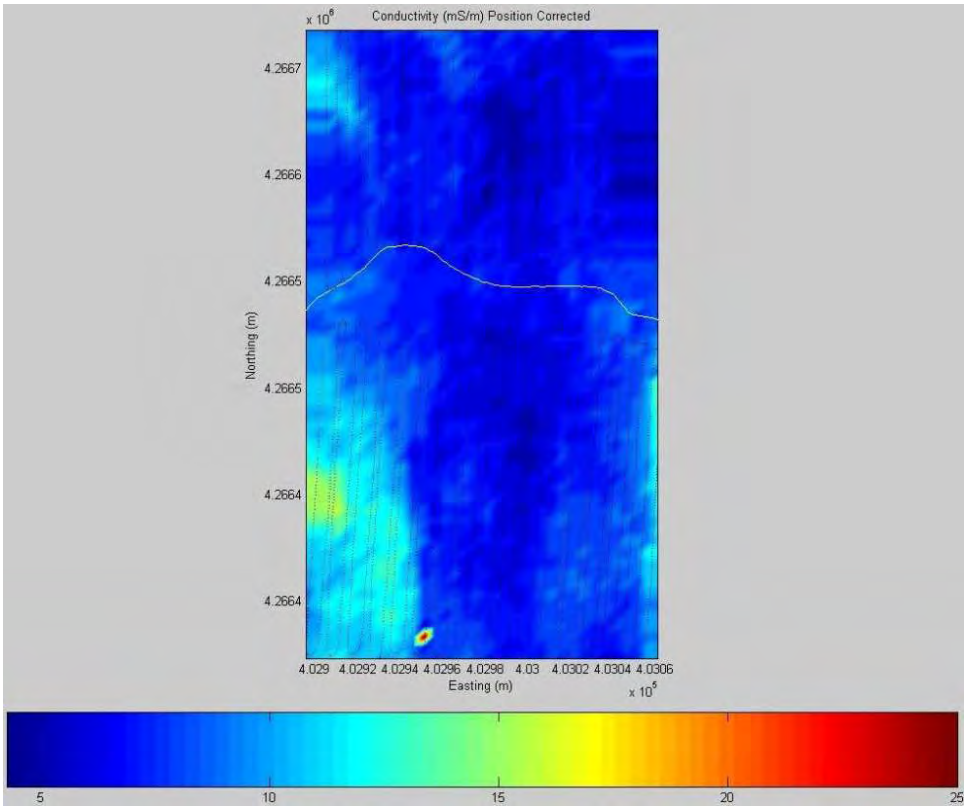

Figure 9.7.3: EM-31 Position Corrected Conductivity Data Quadrature Component

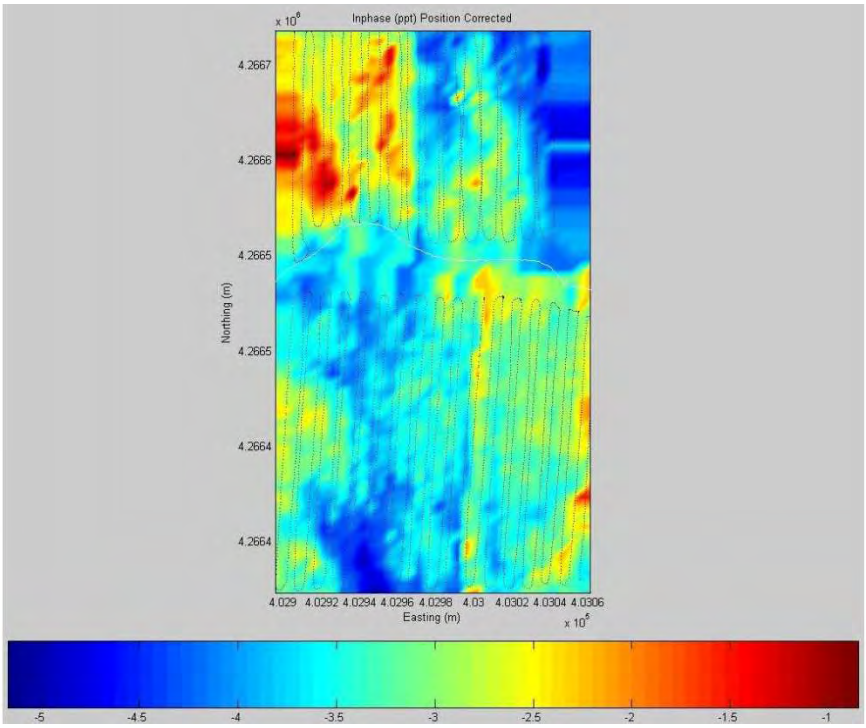

Figure 9.7.4: EM-31 Position Corrected Conductivity Data In-Phase Component

located at the south west area of this survey. These results cannot be confirmed using just the EM-31 survey. One must consider other survey results such as DC and if the data agree.

9.9 II.EM-31 Error Analysis

The main source of error in this survey is the offset in position between the differential GPS and the EM-31. The map shows that the GPS coordinates reflects the location of the EM-31 measurements. This is not the case as the GPS offset the EM-31. Also, surveyors are hard pressed to walk in lines that are perfectly straight. This offset contributes to stretching or squeezing the anomalies that are in the data. We have corrected for the offset by adding 0.2 m in the easting direction and 0.1 m in the northing direction. These values are based on measuring the east and north offsets for each surveyor and using the average to correct for position.

9.10 EM-34 Introduction

The EM-34 and EM-31 are very similar systems. Both are two loop systems which use similarly oriented transmitter and receiver coils. The EM-31 has a fixed distance between the transmitter and receiver coils. In contrast, the loops on the EM-34 are not fixed. A reference cable that varies the separation length between the loops connects the EM-34's loops. Increasing separation between transmitter and receiver loops increases the depth we

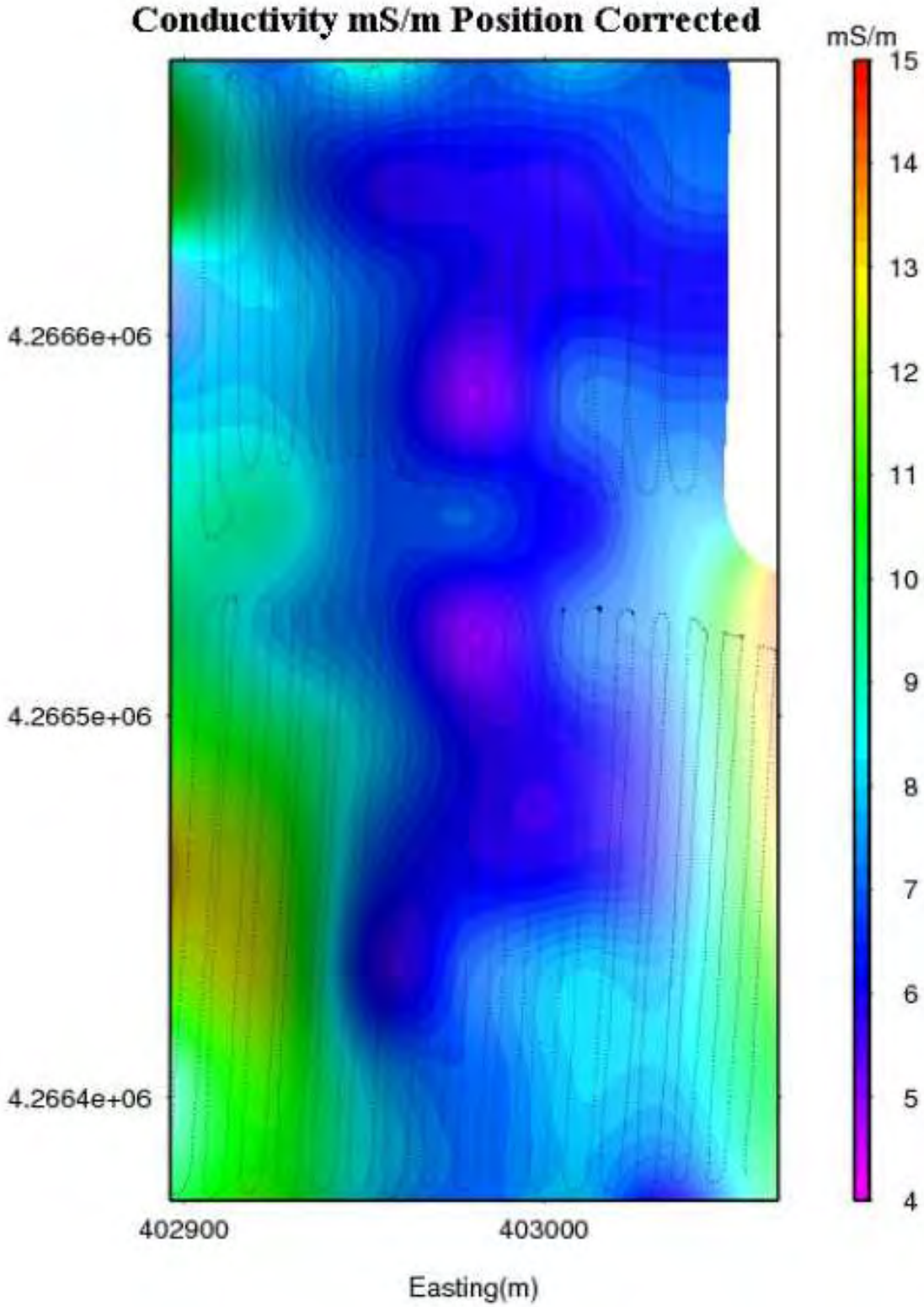

Figure 9.7.5: EM-31 Quadrature Component

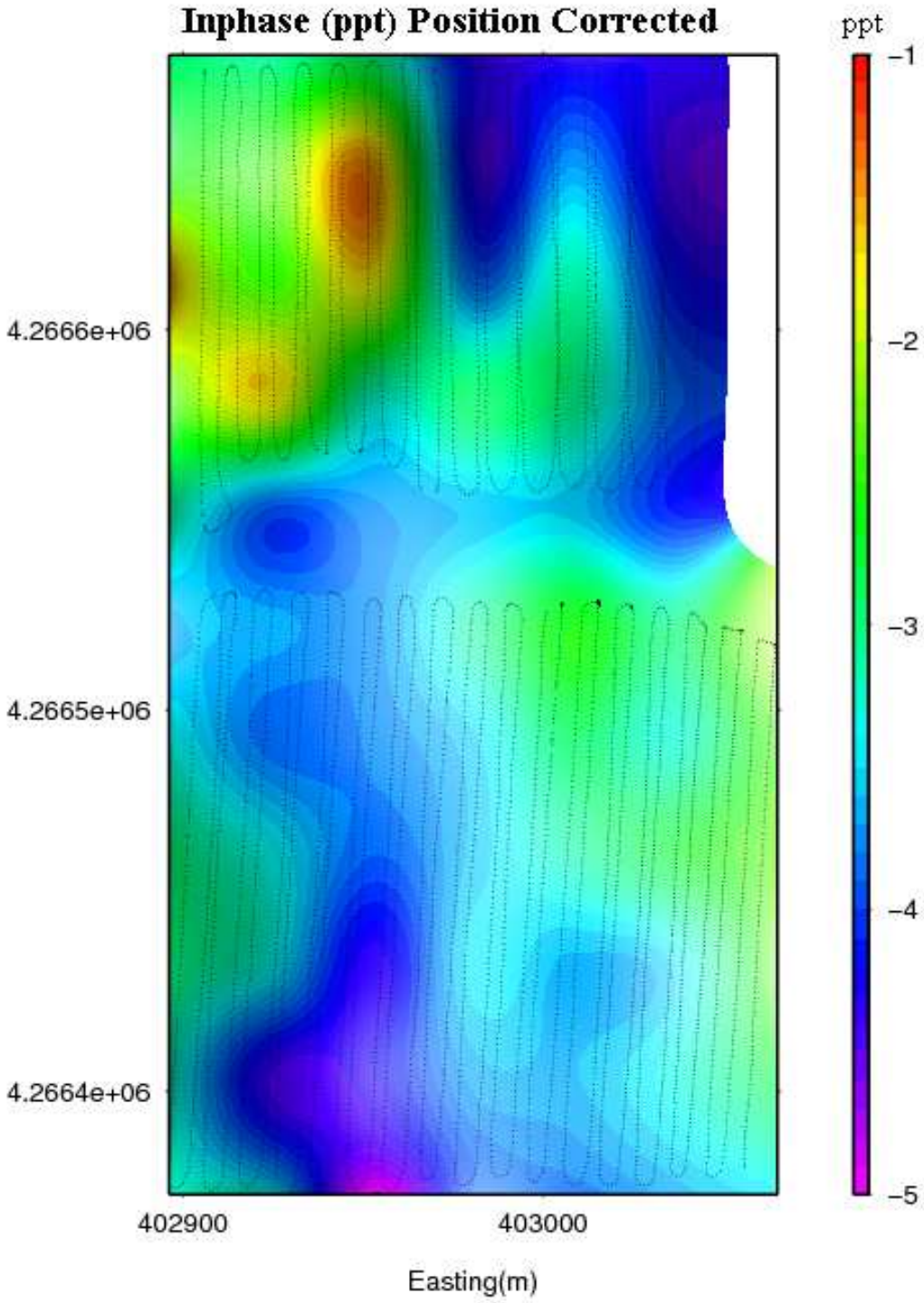

Figure 9.7.6: EM-31 In Phase Component

can see in the subsurface.

The interpretation of the regional geology suggests that there may be a series of listric step faults trending approximately North-South as a result of the extension in the Upper Arkansas Rift basin. We expect to see these faults in the data.

9.11 EM-34 Equipment

The EM-34 survey was conducted using a Geonics EM34-3. This instrument is appropriate for deep ground water mapping. Because of the variable lengths of of coil separation, the EM-34 is able to reach a depth of investigation of 60 m [17]. Figure 9.11.1 below displays the use of the method of use for the EM-34 system. The operators align the orange transmitter and receiver loops such that they are oriented in the same plane.

The direction in which the loops are oriented determine the orientation of the magnetic dipole produced by the loops. We took measurements in two loop orientation directions at each station. Vertical loop orientation gives us a horizontal magnetic dipole direction. Horizontal loop orientation gives us a vertical magnetic dipole.

Figure 9.11.1: Alignment of transmitter and receiver loops (http://www.geonics.com/em34.html)

9.12 EM-34 Dead Horse Survey Set-Up

At the Dead Horse North site the survey used 20 m spacing along each of the DC resistivity lines (Labeled DC Lines in figure 9.12.2. Because flag spacing is 10 m along these lines, there is some over lap in the conductivity measurements.

The surveyors collected EM-34 data at a 40 m spacing on line "R," which runs along the chalk creek river. Locations of the of the "R" line (river line), "X" line (cross line) and the Dead Horse DC resistivity lines are shown in figure 9.12.2 provided by survey organization team A consisting of Samuel Nilson, Jeremy Brown, Yong Ma.

The DC survey lines at Dead Horse took place on a field that has little topographic relief. However, the "R" and "X" survey lines cross an area which is topographically variable. Figure 9.12.3 shows the differential GPS data points for the Dead Horse DC Survey Stations.

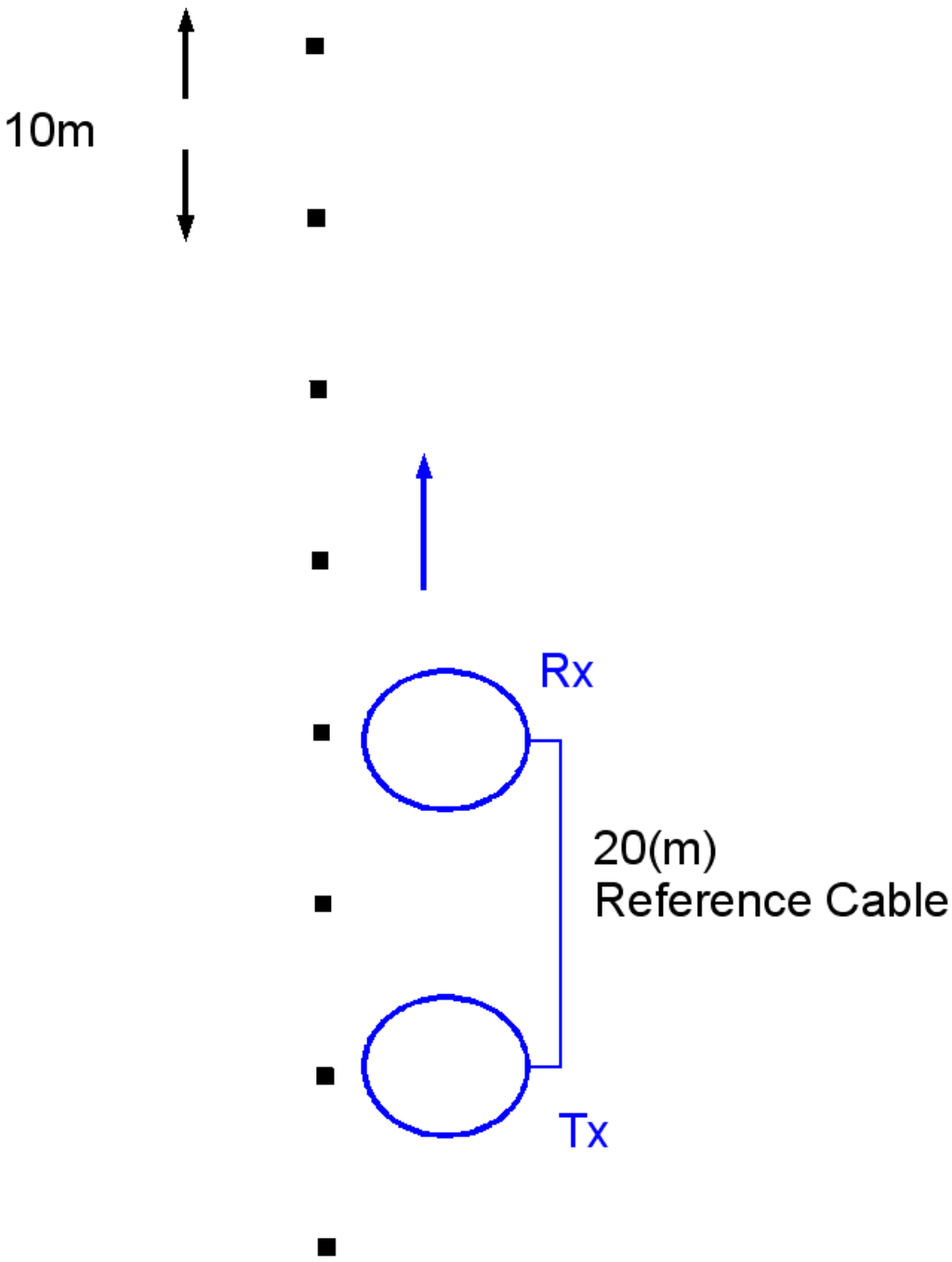

Figure 9.12.1: EM-34 survey method

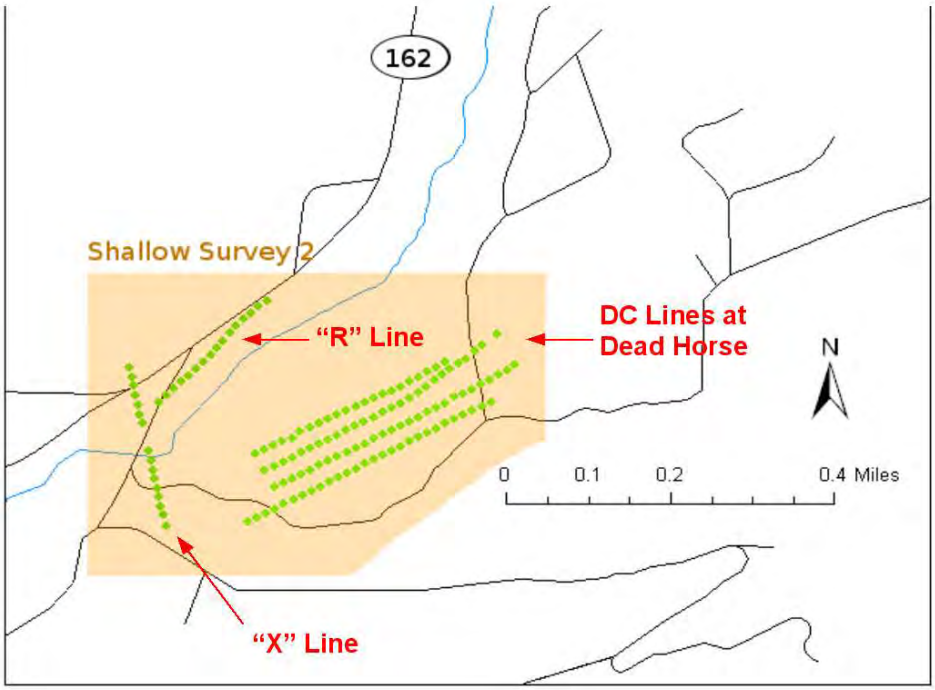

Figure 9.12.2: EM-34 line locations by, Survey Organization Team A

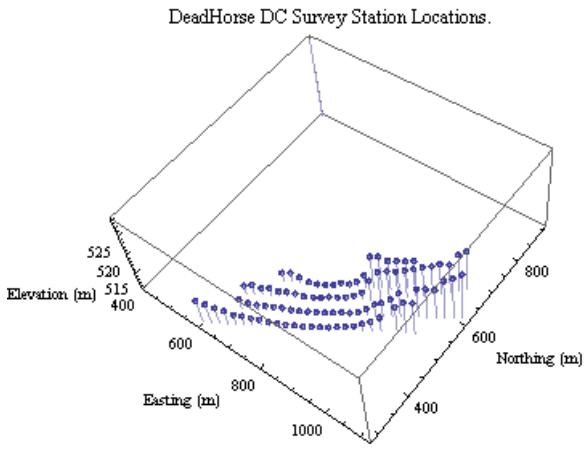

Figure 9.12.3: Dead Horse Survey Station Locations 3D Plot

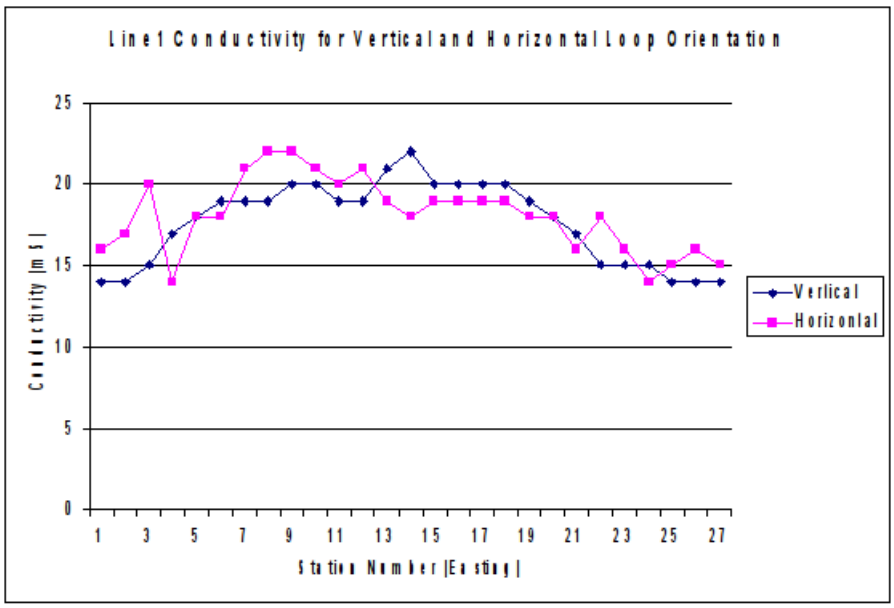

Figure 9.13.1:

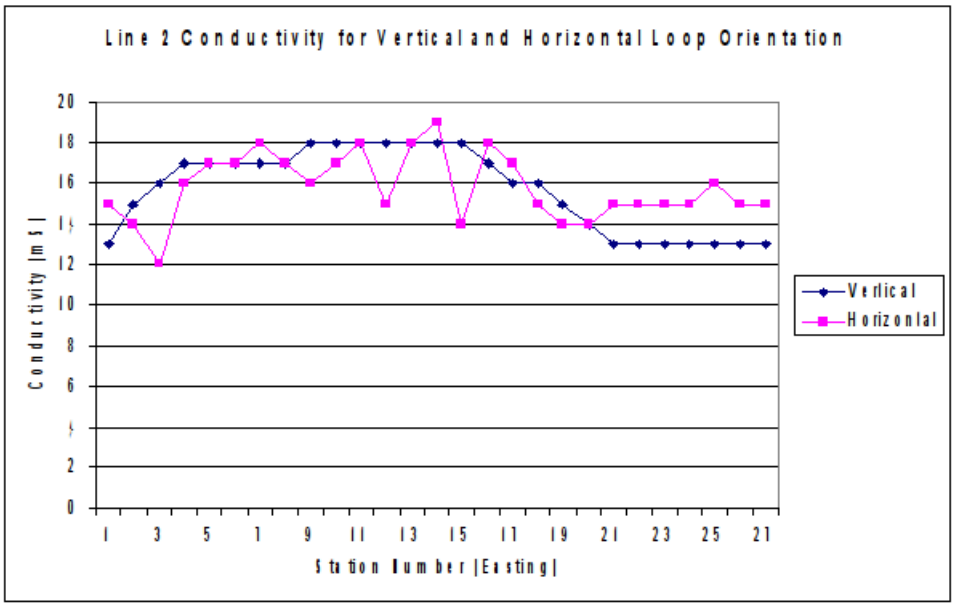

Figure 9.13.2:

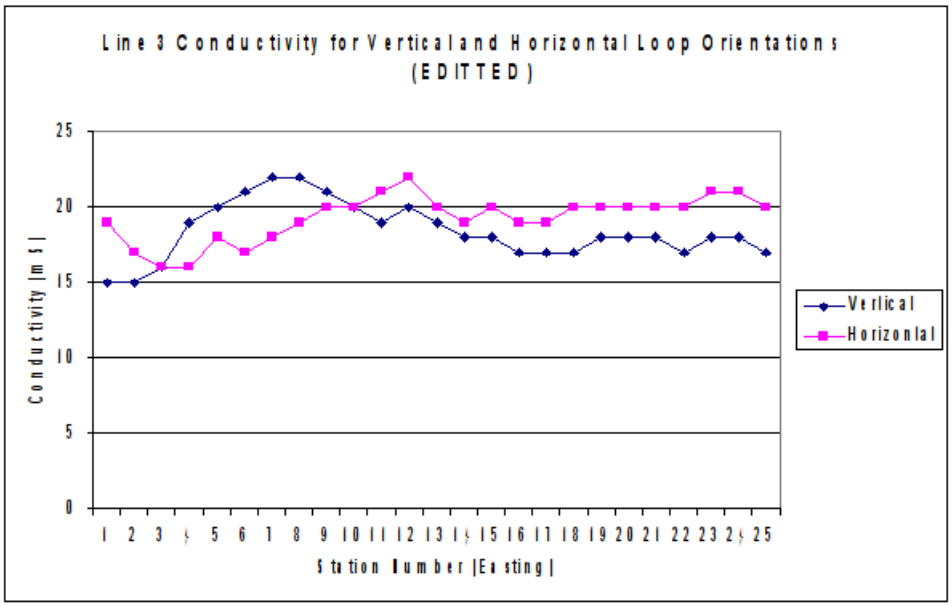

Figure 9.13.3:

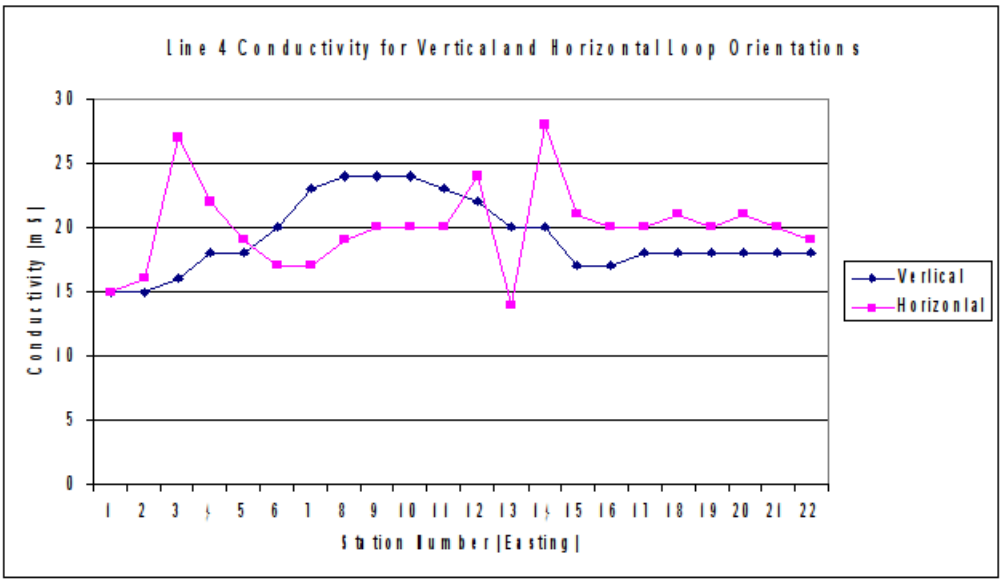

Figure 9.13.4:

9.13 EM-34 DC Lines Dead Horse Observed Data

The plots of conductivity lines 1-4 are shown in figures 9.13.1 through 9.13.4. The horizontal conductivity profiles in pink show erratic curvature and in some places poor correlation with the vertically oriented conductivity profiles shown in blue. Poor separation between the loop planes at the survey site is the most suspected culprit of the bad correlation. In order to conduct an EM-34 survey, the loops must be held so that they lie in approximately the same plane. Poor alignment results in substandard data.

9.14 EM-34 DC Lines Dead Horse Inversion/ Interpretation

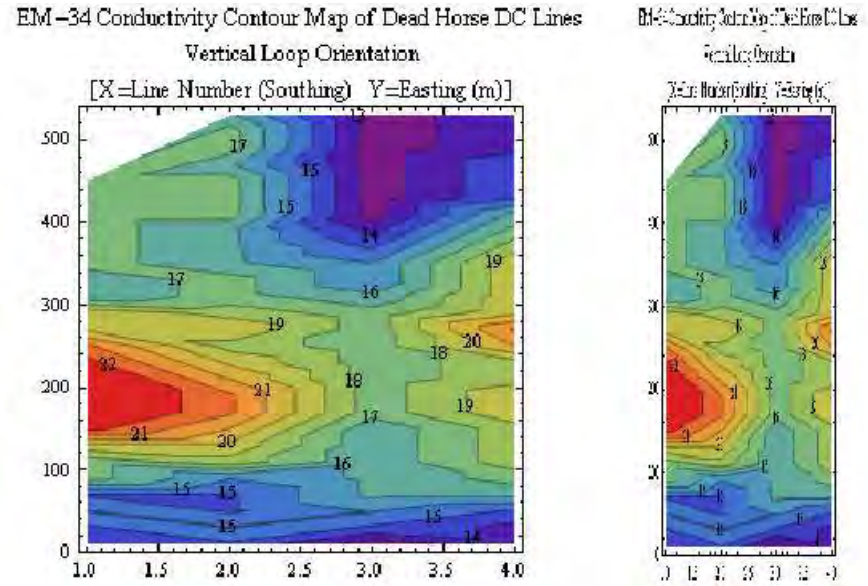

Figure 9.14.1:

The plots that combine the four lines determine that there is a generally resistive trend down the middle of the lake area. A high amplitude anomaly occurs on the north west part of survey area. This anomaly is clearly in the 3D conductivity map created with vertical loop orientation in figure 9.14.2.

9.15 EM-34 "R" and "X" Lines Observed Data

Figure 9.15.1 shows the topographic profiles and orientation of lines "X" and "R". Differential GPS provided the location data. In Figure 9.15.1 the line of survey stations with higher topographic relief is the "X" line. The "X" Line crosses Chalk Creek near it's center at its lowest point. The other shown line of survey points is the "R" line. The "R" line follows near the Northern bank of Chalk Creek river.

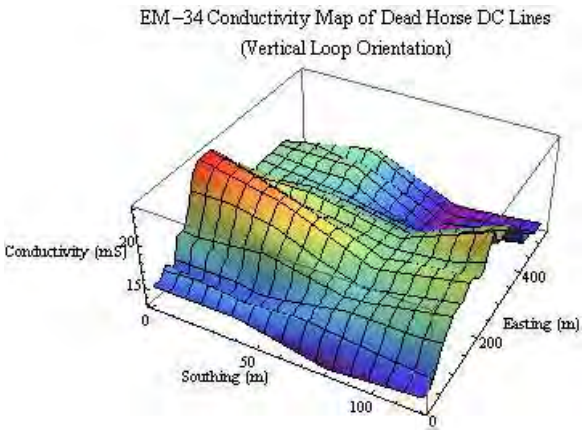

Figure 9.14.2:

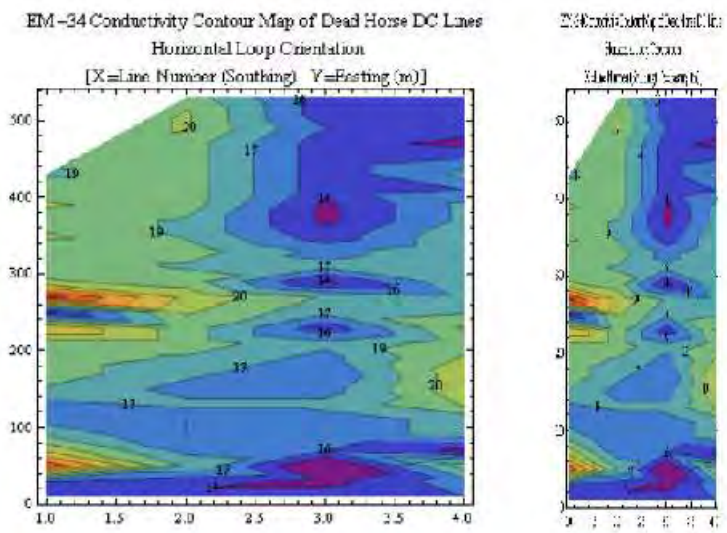

Figure 9.14.3:

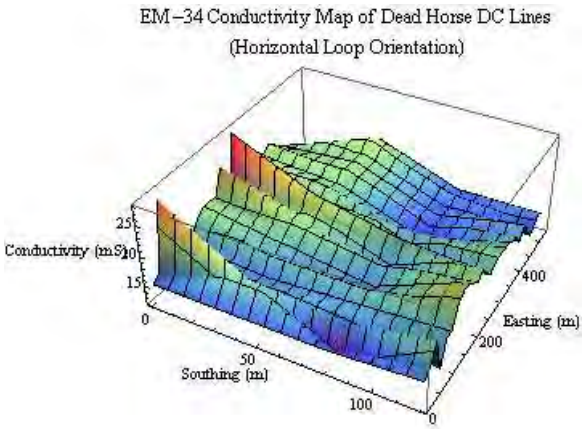

Figure 9.14.4:

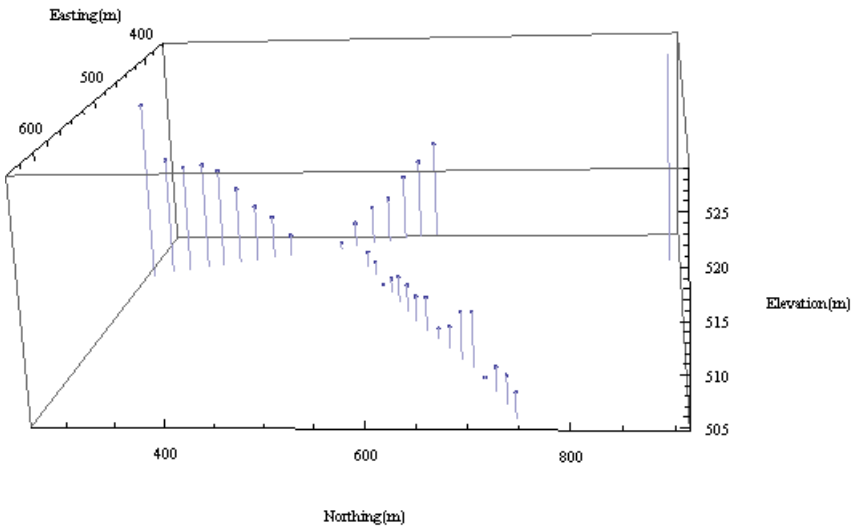

Figure 9.15.1: Line X and Line R elevation profile and orientation

9.16 EM-34 "R" and "X" Lines Inversions/Interpretation

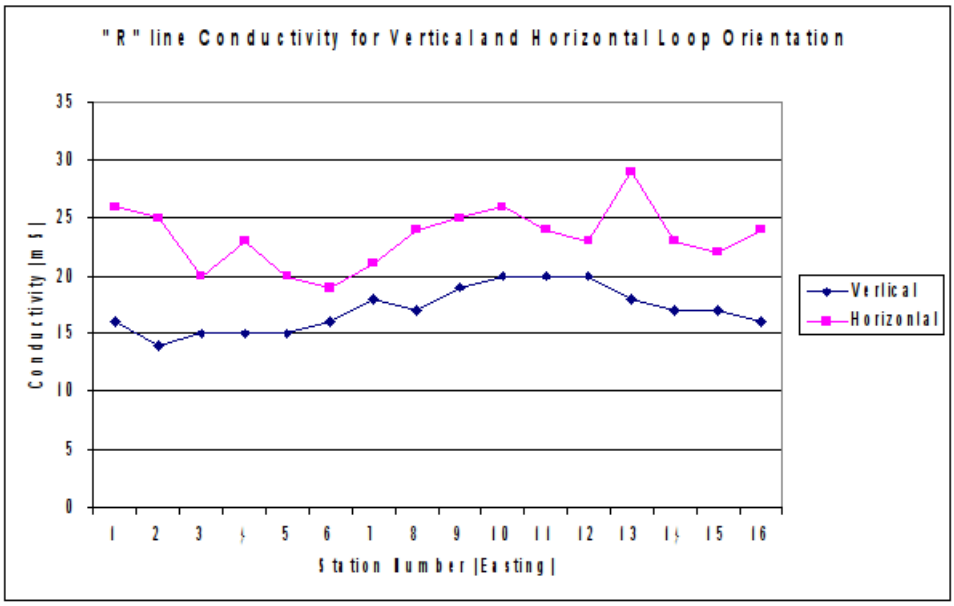

Figure 9.16.1: R Line Conductivity Profile

As expected the conductivity along the river bed at line R is relatively constant.

Despite what appear to be "bad data" points at stations 1 and 3, the contour profile depicted in figure 9.14.3 nicely shows the line crossing the river. This crossing takes place just after station 9. At this station we see a pronounced resistive section in the data. Survey stations 1 and 3 are located on a very steep hill that potentially causes poor separation. The resistive section also lies nearby a road where there might be utilities, which would greatly effect the reading.

9.17 EM-47 Introduction

The EM-47 is a time domain electromagnetic survey system. Time Domain Electromagnetics (TDEM) involves generating an electromagnetic field that propagates into the earth and induces currents at increasing depths over time. These induced currents generate a magnetic field that provides conductivity. Both the magnitudes and the decay of the induced currents contribute to give an idea of the conductivity and the geometry of the subsurface. For example, in resistive media, the current decays very rapidly. The converse is true for conductive media. The difference between FDEM and TDEM is that an FDEM transmitter coil radiates a fixed frequency electromagnetic field. The TDEM transmitter coil radiates a varying frequency electromagnetic field [18]. Exploration geophysics uses both time domain and frequency domain EM.

Figure 9.16.2: X Line Conductivity Profile

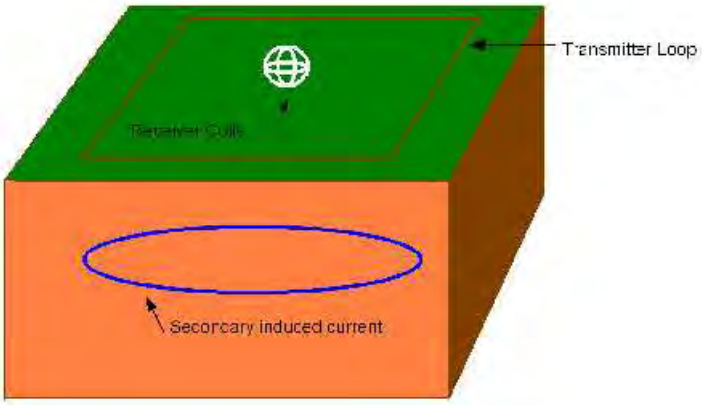

Figure 9.17.1: EM-47 Transient EM Sketch

9.18 EM-47 South Drainage Survey Set-Up

The surveyors used the Geonics Protem EM-47. For this survey we took 6 central loop sounding measurements using a 50 X 50 m loop as shown in Figures (9.18.1). For each of the soundings, we measured over 20 time gates using a repetition frequency of 285 Hz and 75 Hz. The transmitter period was 3.51 ms and the recording period was 0.8 ms with the 285 Hz. The 75 Hz had a transmitter period of 13.3 ms and recording period of 3.2 ms.

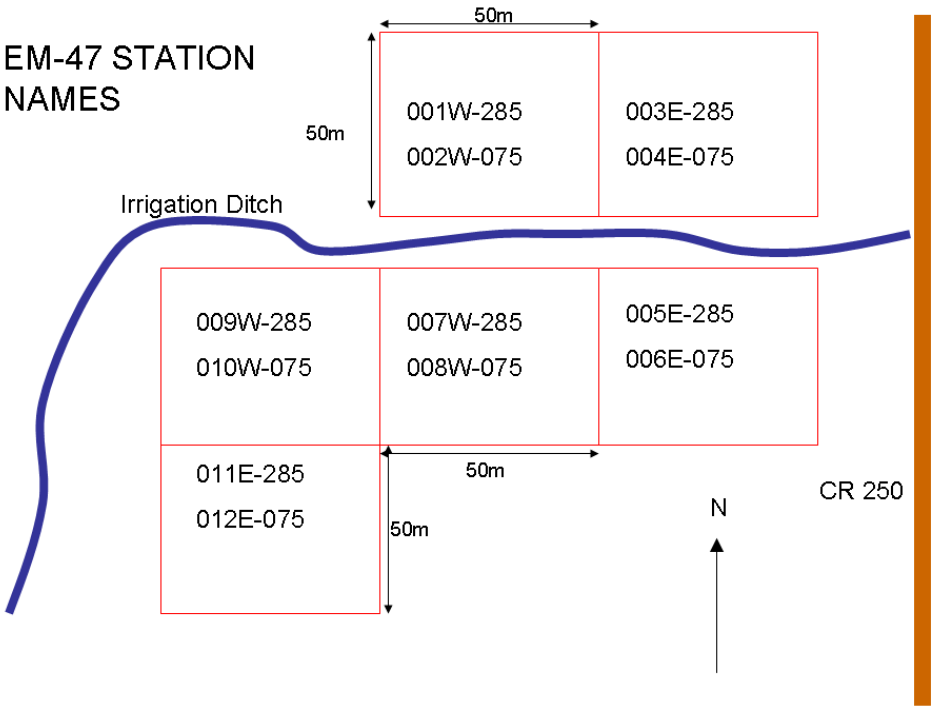

Figure 9.18.1: EM-47 Data collection station name convention

9.19 EM-47 South Drainage Observed Data

A log-log scale with time shows the synthetic data for both the flux converted 75 and 285 Hz. This plot determines how the secondary field decays in the ground. The 285 Hz data was recorded in μs and the 75 Hz was recorded in ms. Surveyors measured stations 1-4 on the north side of the drainage ditch and recorded stations 5-12 on the south side of the drainage ditch. The decay curves show how the secondary field (which is related to the eddy currents) behaves as it travels through the subsurface. As the slope of the curves changes, the conductivity of the sub surfaces changes. The figures 9.19.1 throguh 9.19.3 are a few measurements taken using a frequency of 285 Hz.

Figures 9.19.4 through 9.19.6 are plots of the central loop soundings using a frequency of 75 Hz. The jumps in the decay curves below are not possible as far as the behavior of the secondary field decays, and are electrical disturbances such as afternoon thunder storms.

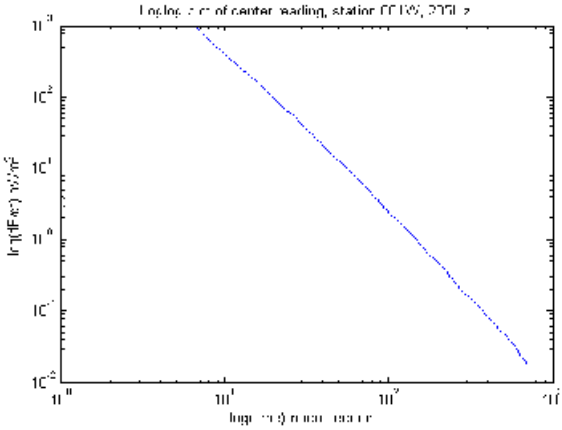

Figure 9.19.1: Station 001W log-log decay curve of secondary field 285 Hz

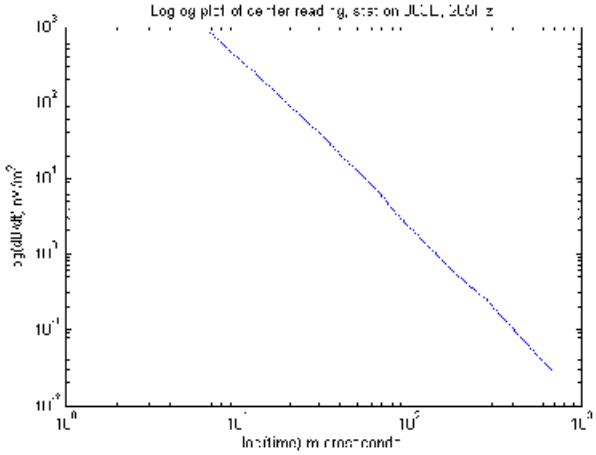

Figure 9.19.2: Station 003E log-log decay curve of secondary field 285 Hz

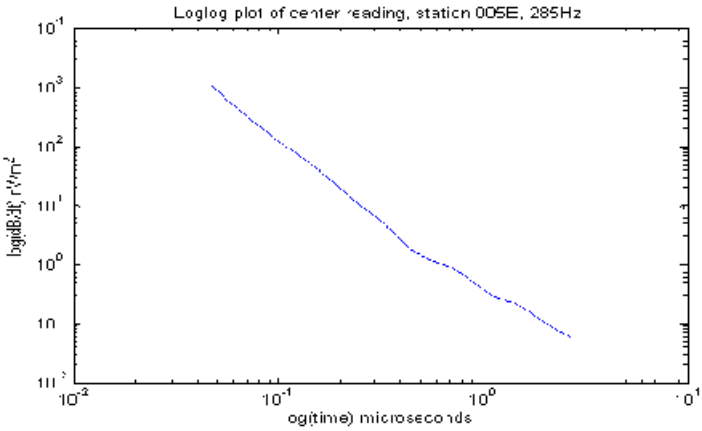

Figure 9.19.3: Station 005E log-log decay curve of secondary field 285 Hz

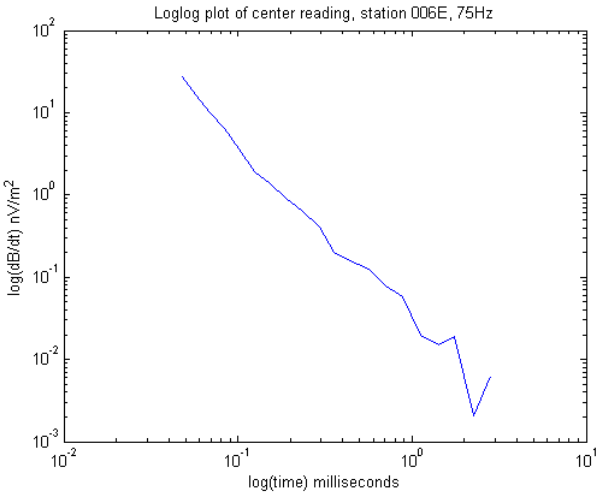

Figure 9.19.4: Station 002W log-log decay curve of secondary field 75 Hz

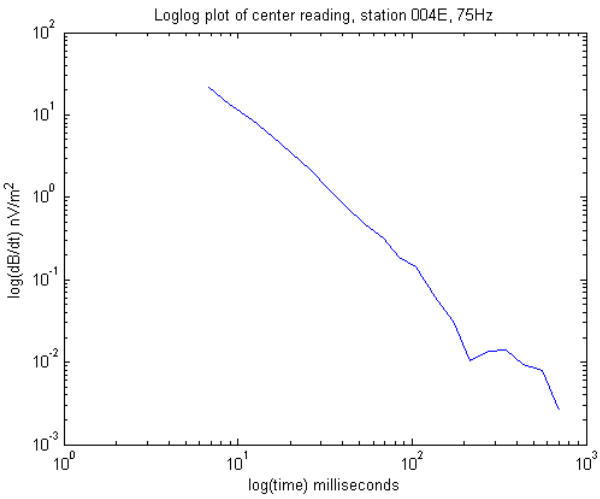

Figure 9.19.5: Station 004W log-log decay curve of secondary field 75 Hz

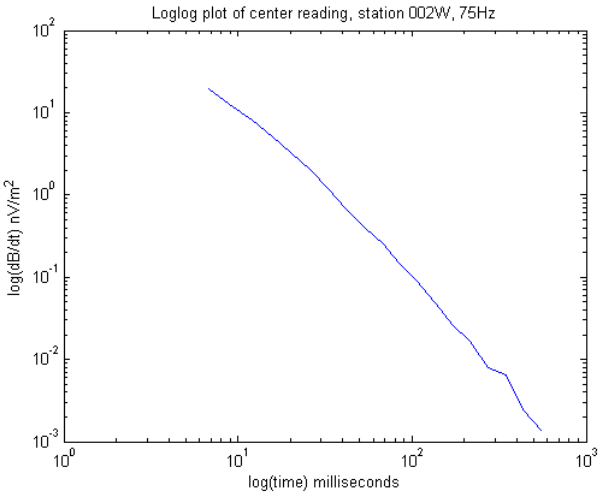

Figure 9.19.6: Station 006W log-log decay curve of secondary field 75 Hz

These figures are log-log plots of the change in magnetic flux with time (decay curves) in the z direction. A straight decay curve indicates a homogeneous half-space as shown in figures9.19.1 and 9.19.2. Figure 9.19.3 shows some variation in the decay, which indicates structure where this information can be used to invert the data.

9.20 EM-47 South Drainage Inversion/ Interpretation

The program EM1DTM inverted the data for all 12 stations north and south of the drainage ditch. The inversion program uses a 1 dimensional model with time-domain observations. The inversion produces both data misfit and the measure of the amount of model structure. The output of the inversion shows an electrical conductivity model of the central loop soundings acquired at the south drainage site. The scale on the data misfits is $\mu V/m^2$ and ms. The scale on the resistivity is in $\Omega * m$ vs m. All inversions had the same conductivity model with 40 layers and the bottom layer was at 400m.

The large error bars on the output plot show a poor data misfit for the last part of this inversion. The initial portion of the plot is accurately modeled and can be used for later interpretation.

> Inversions are like friends, you dont want them too close and you dont want them too far. -Dr. Yaugoo Li

The flux calculated from stations 001W and 002W along with the time gates were combined into One observation file combined the flux calculated from stations 001W and 002W along with the time gates. The time used in the flux gates were in μs and the remaining units were the same.

The students used the 1D inversion on the Em-47 to determine if there is evidence of water seepage from the drainage ditch. The resistivity values on the models north of the site (figure 9.20.6) you can see the resistivity values range from 83 to 85 $\Omega * m$ and the conductive

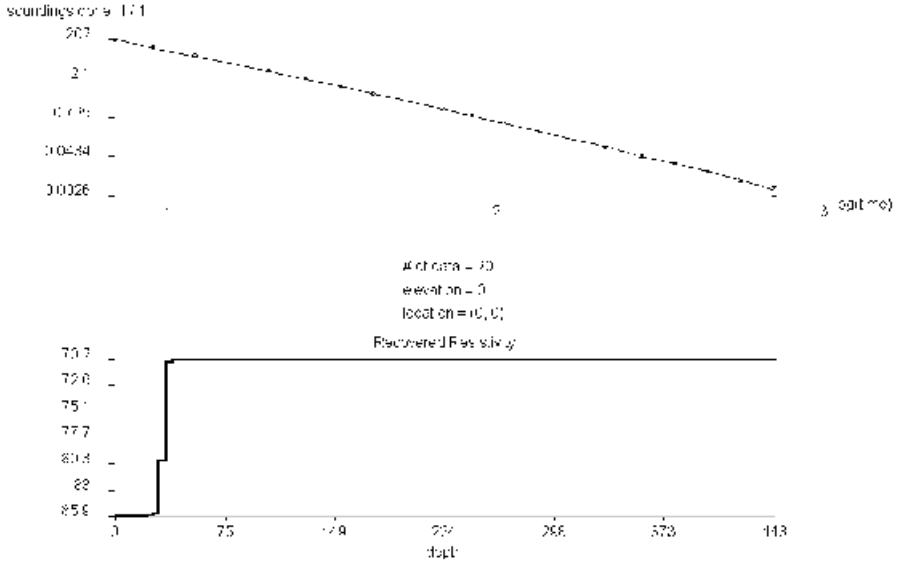

Figure 9.20.1: 1D Inversion on station 001W (285 Hz)

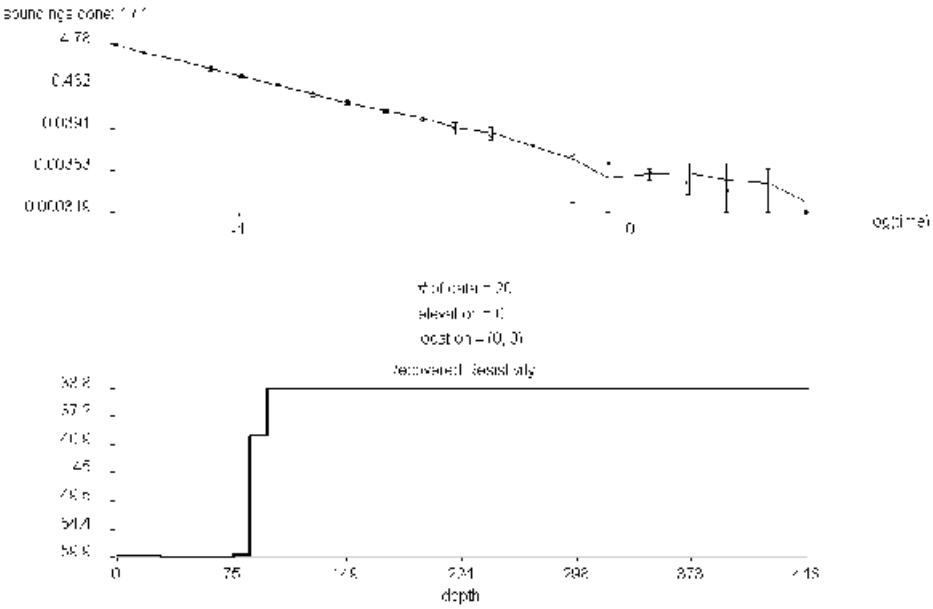

Figure 9.20.2: 1D Inversion on station 004E (75 Hz)

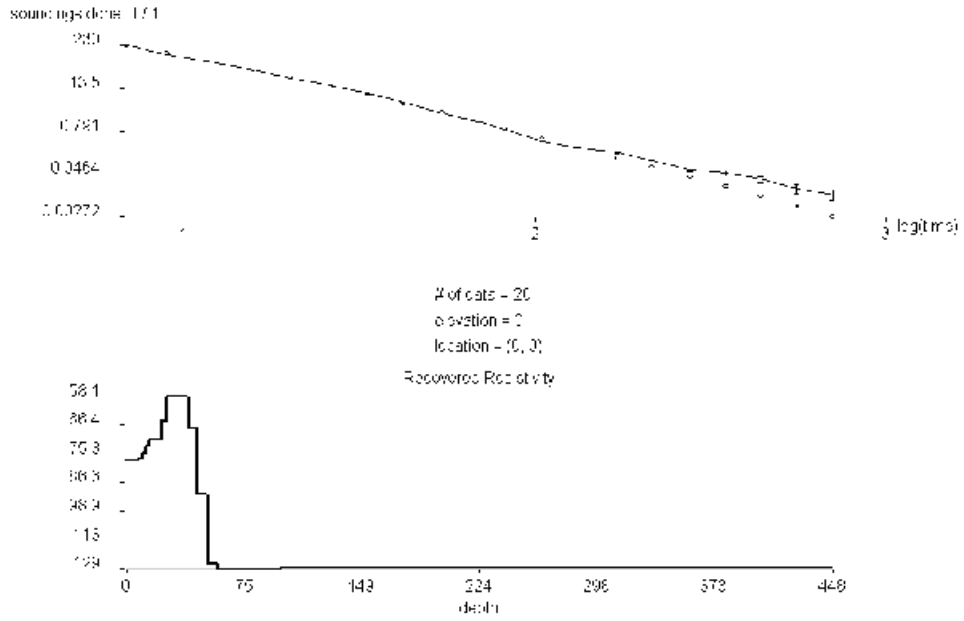

Figure 9.20.3: 1D Inversion on station 005E (285 Hz)

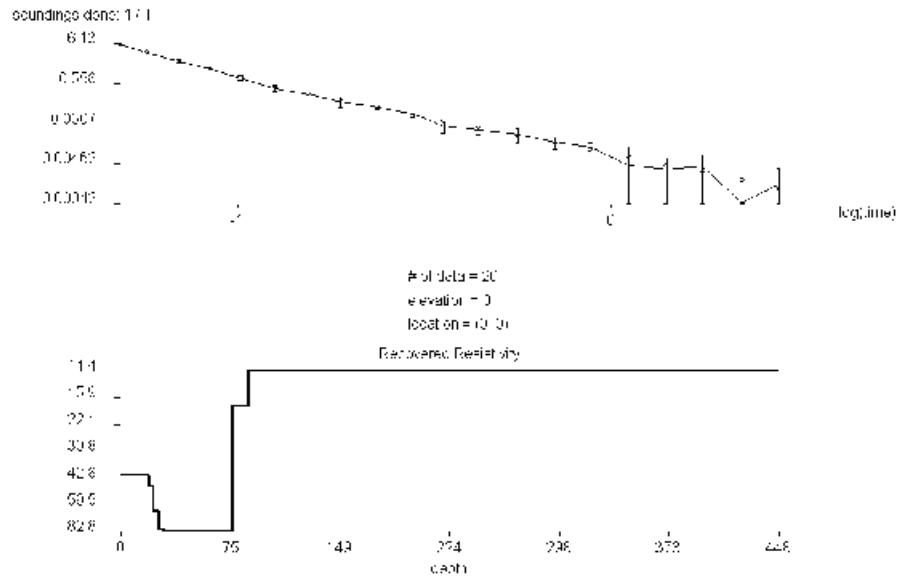

Figure 9.20.4: 1D Inversion on station 005E (285 Hz)

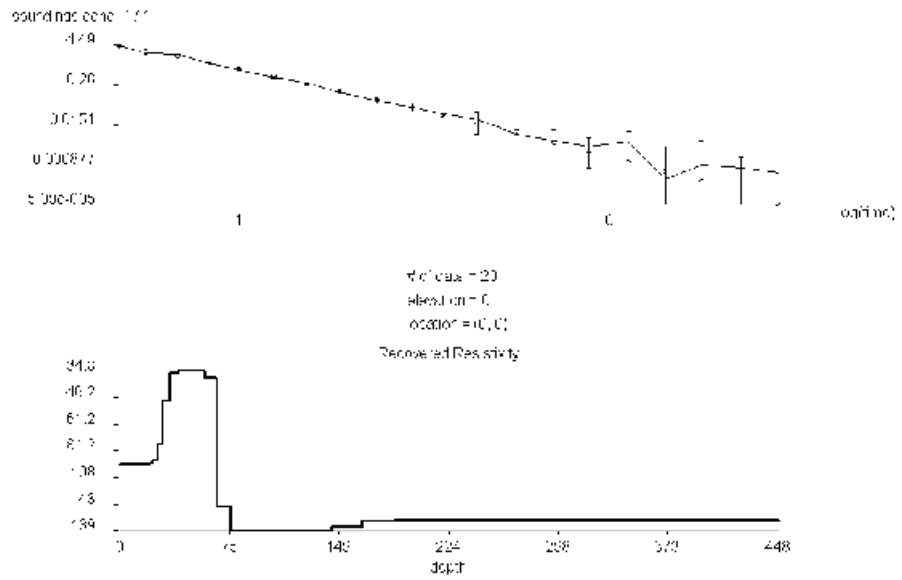

Figure 9.20.5: 1D Inversion on station 010W (75 Hz)

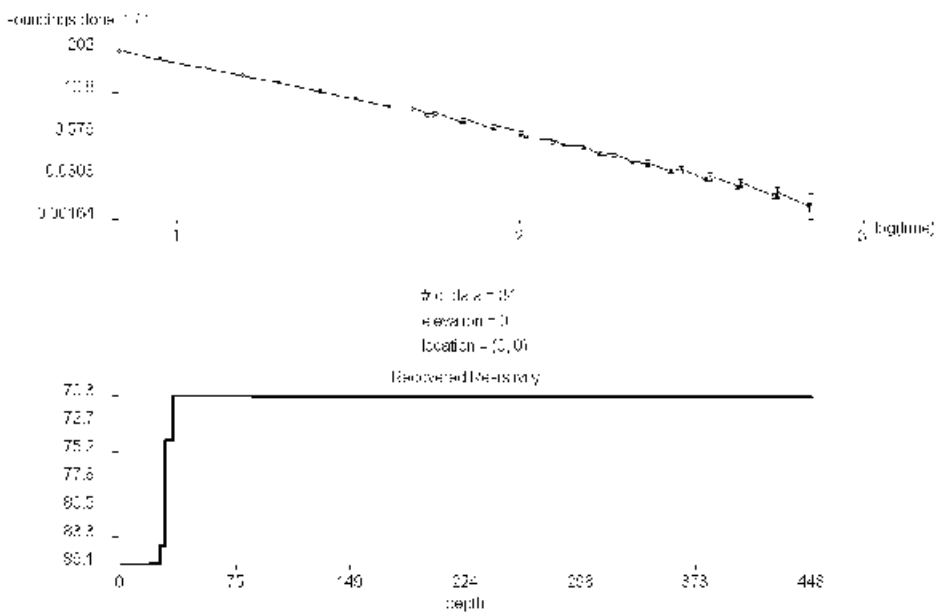

Figure 9.20.6: 1D Inversion on station 001W and 002W (285 & 75 Hz)

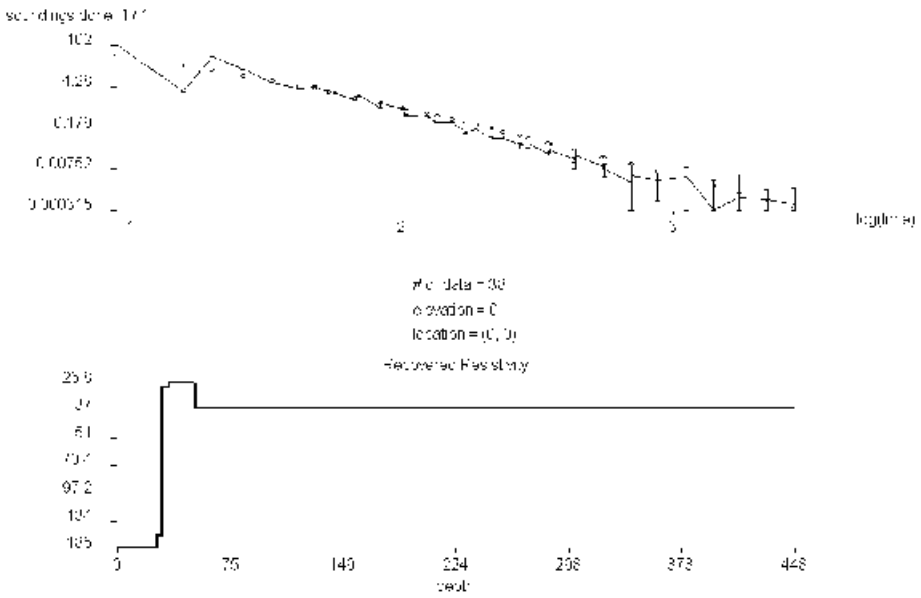

Figure 9.20.7: 1D Inversion on station 009W and 010W (285 & 75 Hz)

layer is roughly 70 to 75 $\Omega * m$. If you notice the models shown for the stations south of the drainage ditch (figure 9.20.7) you will notice resistivity values ranging from 134 to 185 $\Omega * m$ and the conductive areas are ranging from 26 to 51 $\Omega * m$. From the north side of the ditch to the south side of the ditch the ground is becoming more saturated with water as the more conductive layers show. These layers could be seepage from the drainage canal. This evidence is just one piece of the puzzle and can not be completely confirmed without the remaining pieces. We need to integrate this data with other geophysical methods.

9.21 EM-47 Error Analysis

The main source of error for the survey aspect was the thunderstorms that struck the skies in southern Arkansas Valley that late afternoon. These storms interfered with the EM-47 data and can be seen with the later stations in the decay curves. There is also some error in the inversion part which can be seen by the error bars.

Chapter 10

DC Resistivity

10.1 Introduction and Theory

DC resistivity is a valuable tool in the exploration for groundwater and geothermal activity because the resistivity of the subsurface is very sensitive to its water content. By looking at the vertical and lateral resistivity data one can spot the water in the subsurface because it will take the form of a more conductive anomaly. DC resistivity can also define layers in the subsurface because different rock types have different resistivities.

The DC resistivity method involves driving current into the ground and measuring how the conductivity structure affects the potential (voltage) difference between two electrodes.

The theory behind the DC resistivity method is rooted in Ohms Law,

$$\Delta V = IR \tag{10.1.1}$$

where ΔV is the potential difference across a resistor, R is resistance, and I is the injected current. The resistivity, ρ, can then be derived through Equation # 10.1.2.

$$R = \frac{\rho l}{A} \tag{10.1.2}$$

where l is length and A is cross-sectional area. Although these are very basic equations, they explain resistivity changes in the subsurface, imaged by putting a known current into the ground and measuring the resulting potential difference. The calculations for a forward model would be done with the vector form of Ohms Law in Equation # 10.1.3

$$\vec{J} = \frac{\vec{E}}{\rho} = \sigma \vec{E} \tag{10.1.3}$$

where $\vec{J}$ is current density, $\vec{E}$ is the electric field, ρ is the resistivity and σ is the conductivity. If induced current hits a boundary where the conductivity changes, the location can be considered a point source for an electrical field. This electric field causes charges to accumulate at the boundary which can be quantified by measuring the potential difference at

the surface. This allows for the calculation of the resistivity or conductivity of the subsurface material through the relationship shown in Equation # 10.1.4

$$\vec{J} = -\sigma \nabla V \tag{10.1.4}$$

For a homogenous material with a given resistance, R, when current is passed through the material there is a defined drop in voltage (Equation # 10.1.1) that can be used to calculate the true resistivity, as seen in Equation # 10.1.2. Ideally, the goal of a DC resistivity survey is a model of the true resistivity of the earth. However, when performing a survey, the measured potential difference is affected also by the geometry of the electrode array and the calculated value is called *apparent resistivity*. Apparent resistivity, unlike true resistivity, is not a physical property. There is a geometric factor determined for each type of electrode array that can be used, in combination with the measured apparent resistivity, to obtain a true resistivity used for interpretation.[22]

10.2 Survey Design

There are several ways to set up the electrode geometry when carrying out a resistivity survey, but they all involve two current electrodes and two potential electrodes. Figure # 10.2.1 shows a variety of the commonly used configurations. The dipole-dipole array has the set of current electrodes and the set of potential electrodes separated by a known distance (with the same electrode spacing). The array offers poor vertical resolution but excellent depth penetration. The Wenner array has the two potential electrodes located between the current electrodes and the spacing between each of the four electrodes is equal. The Wenner array has excellent vertical resolution and can detect layered media very well, but does not penetrate very deep. The Schlumberger array is similar to the Wenner array, but the spacing between the two potential electrodes is relatively small. A Schlumberger sounding offers both moderate depth of investigation and decent vertical resolution, offering a compromise between the dipole-dipole and Wenner arrays.[24]

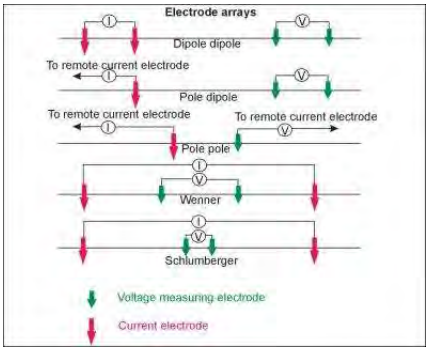

Figure 10.2.1: Common electrode arrays used for DC resistivity surveys[23]

We used multiple arrays in Chaffee County, including some uncommon ones not mentioned above. However, the inverted data is from dipole-dipole surveys.

The data inversion and locations of all the DC resistivity surveys performed at the 2008 Field camp are:

- Dead Horse Lake

4 lines

20 meter spacing

40 meter spacing between lines

28 electrodes in lines 1-3, 21 electrodes in line 4

oriented approximately 65 degrees east of north

3D inversion

- Field 1.2

  9 lines

  20 meter spacing between electrodes

  20 meter spacing between lines

  14 electrodes per line (rollover)

  3D inversion

- Long Line C

  Extends from field 1 to field 1.2

  20 meter spacing between electrodes

  42 electrodes on line (rollover)

  2D inversion

- Drainage Site, Poncha Springs (Figure # 10.2.2)

  5 lines

  28 electrodes in lines 1-3 and 5, 42 electrodes in line 4 (rollover)

  Lines 4 and 5 crossed irrigation channel

  5 meter spacing between electrodes

  10 meter spacing between lines

  2D inversion of lines 4 and 5

  3D inversion of all lines

10.3 Data Processing

We inverted the DC resistivity data using the DCIP3D software version 1.0. The software inverts the potential data that was collected and obtains conductivity values. The software accounts for noise and uncertainty and therefore does not fit the data perfectly. The formula needed to develop the conductivity is non-linear so it is linearized using a Gauss-Newton approach. For each data set, an appropriate mesh must be selected with small cell thickness nearest the surface and larger padding cells further from the electrodes. The number of cells used to create an inverted model is greater than the number of data collected. A topography

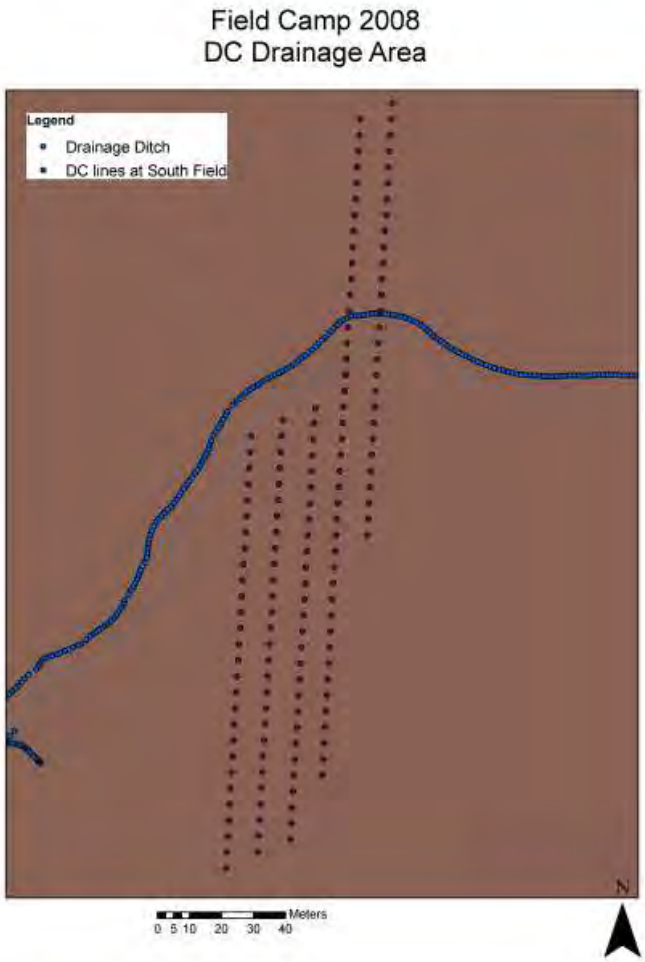

Figure 10.2.2: Survey design at the drainage ditch site near Poncha Springs

file can be input to define elevation variations at the surface on the model.[25]

The primary problem with the inversion is non-uniqueness, meaning there are infinite solutions. Some constraints can be placed on the data, for example by using a reference model, to improve the reasonability of the inversion.

10.4 Data and Interpretations

10.4.1 Dead Horse Lake

Dead Horse Lake consists of what was previously a lakebed, but has been drained. Data was collected along 4 lines, each 540 meters long. The 3D inversion is shown in Figure 10.4.1. The conductivity data is on the same scale as the drainage ditch site and there is no apparent significant anomaly. There is a slightly more conductive region in the center of the lake, likely where the ground is more saturated (Figure 10.4.2). The region is between the surface and 90m depth. The tiny anomalies to the northwest are due to electrical boxes on the surface. There is no apparent region of large-scale water accumulation.

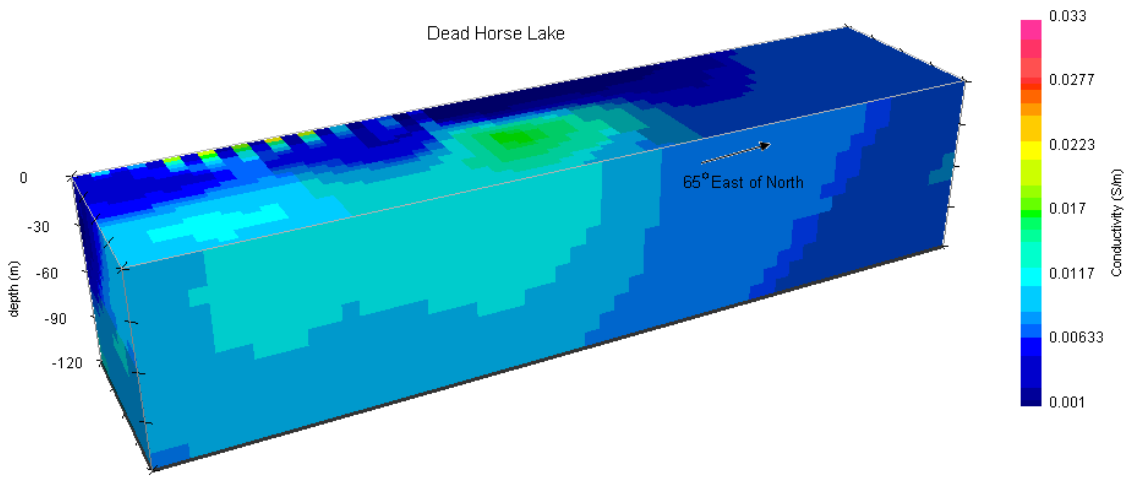

Figure 10.4.1: 3D inverted data for Dead Horse Lake, line 2. There is a large resistive layer in the subsurface.[27]

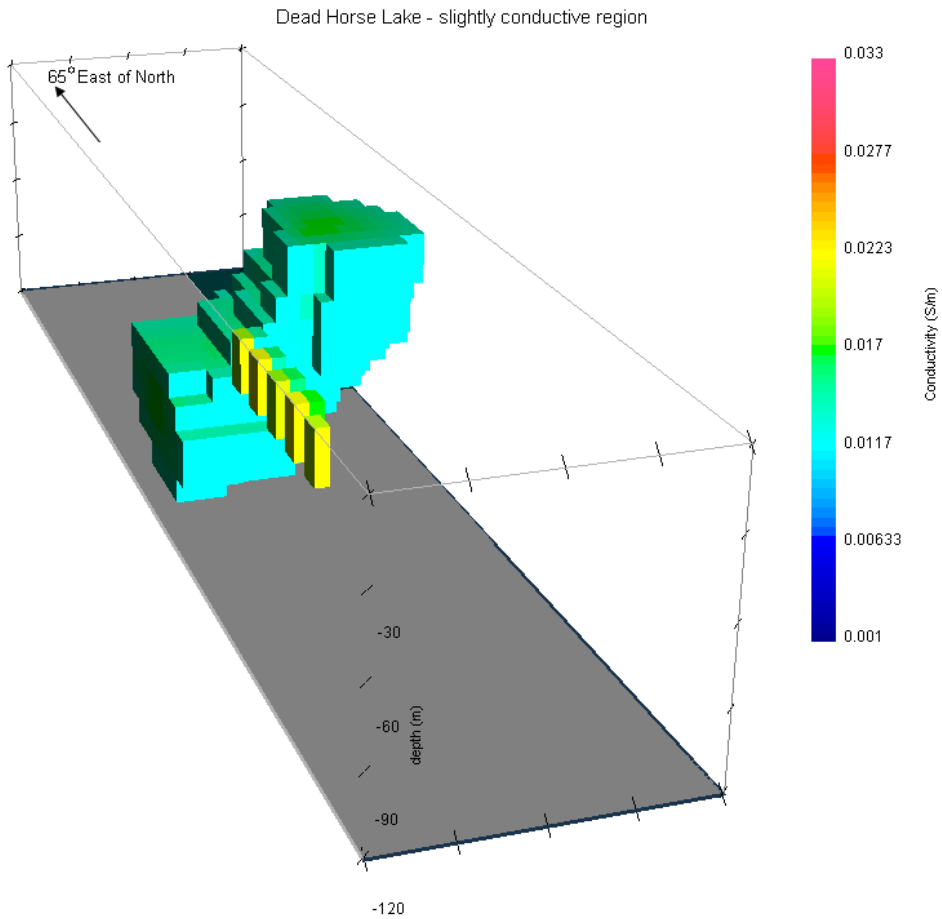

Figure 10.4.2: 3D inverted data for Dead Horse Lake. This 3D model shows the approximate shape and extent of the higher conductivity region.[27]

10.4.2 Lines 4 and 5 at the Drainage Site

Line 4 of the DC resistivity survey runs from south to north so that the generated profile faces to the west. The line crosses the irrigation ditch at approximately 170 meters. As seen in Figure 10.4.3, there is a significant amount of water in the subsurface along the south part of the line. At some location, the water appears to then be infiltrating to greater depths (between 25 and 40 meters). There is a line of flow running south of the irrigation ditch, indicating runoff. It is unlikely, from the shape and size of the near-surface anomaly to the south, that the anomaly is caused strictly by water infiltration from the ditch. One observation made in the field was that in the southwest corner of the survey there was a pipe sticking out of the ground from which water was flowing. This leads us to believe that the near surface conductive anomaly towards the west is prominently due to the surface spill from this pipe and not the ditch itself. However, the defined water flow off either side of the irrigation ditch demonstrates a contribution from the ditch to subsurface water in the region.

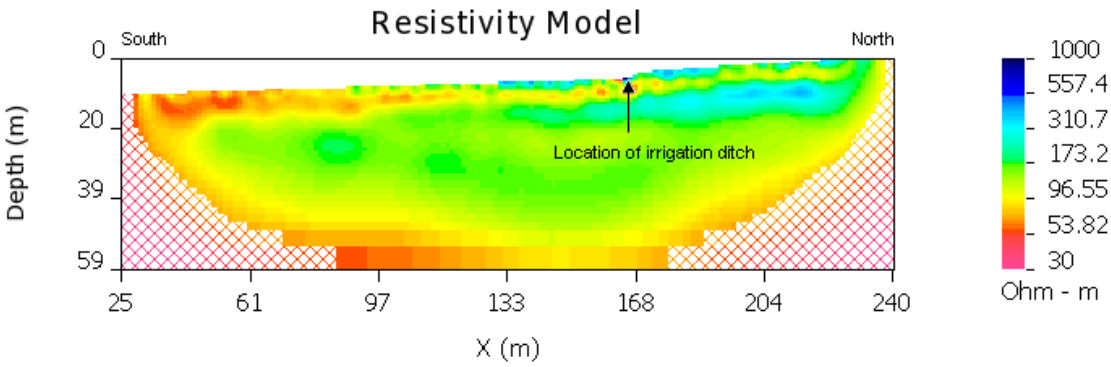

Figure 10.4.3: Inverted data for Line 4 (south site). The irrigation ditch is indicated. Profile faces west.[26]

Figure 10.4.4 shows the inverted model for line 5, 10 meters to the east of line 4. It shows a very similar anomaly but with higher resistivities. The near surface anomaly to the south has a higher resistivity for line 5 because the upwelling of water on the surface is farther away. There is a smaller volume of water accumulating at depth, also indicated by higher resistivity values. However, the runoff from the irrigation ditch is still apparent in both images.

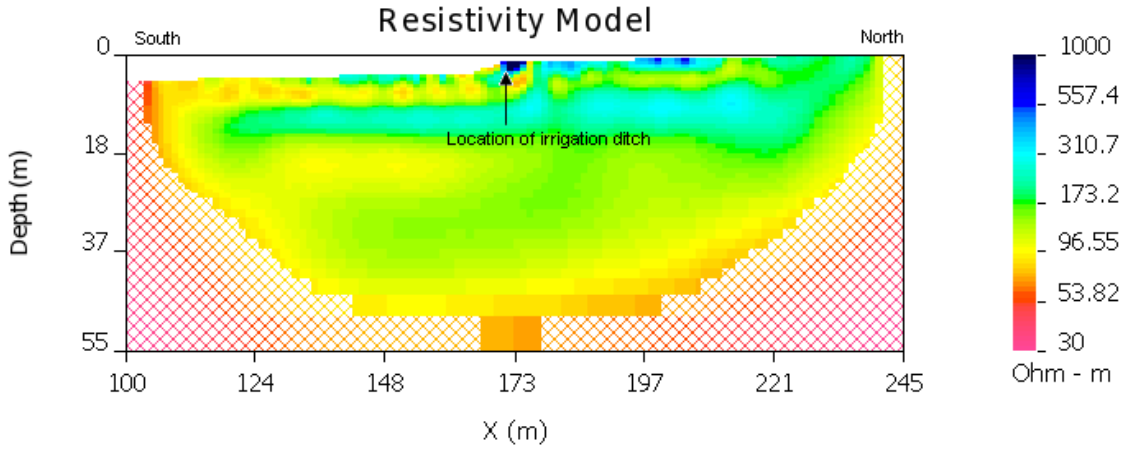

Figure 10.4.4: Inverted data for Line 5 (south site). The irrigation ditch is indicated. Profile faces west.[26]

10.4.3 3D Inversion at Drainage Site

The 3D inversion correlates well with the 2D inversions done on lines 4 and 5. The 3D inversion shows that water is leaking from the irrigation ditch to the north, downhill to the south at some locations (Figure 10.4.5). Line 1 is nearest the pipe with upwelling water that we observed on the surface. The conductive anomaly does not appear to be connected to the drainage ditch, but is likely due to water from the pipe. Line 2 is farther from the pipe but has a larger anomaly, meaning there could be leakage from the drainage ditch. This trend continues for lines 3, 4, and 5, and the anomaly extends further towards the ditch for each line. The leakage from the ditch is therefore inconsistent.

Figure 10.4.6 shows the most conductive regions. It confirms that the greatest amount of accumulation is at the east end of the survey site and that there is leakage from the drainage ditch, as seen in Figure 10.4.5. This also corresponds to the 2D inversions in Figures 10.4.3 and 10.4.4, which give a more detailed view of the water flowing downhill from the drainage ditch along lines 4 and 5.

The DC resistivity data confirm that there is water leakage from the drainage ditch, which could contribute to local well water. It is important to note that the survey was done in a very small area and that the amount leakage was not consistent and was less significant to the west. A regional overview of the significance of leakage from the ditch requires additional data.

10.4.4 Line C

For the survey on the long self potential line, or line C, the first 28 electrodes were laid out starting with electrode 1 at the east end of the line and extending to the west. After the first survey was complete electrodes 1-14 were moved to the west of electrode 28, which is called a roll-along. The spacing between the electrodes is 20 meters making the total distance covered 820 meters (Figure 10.4.7).

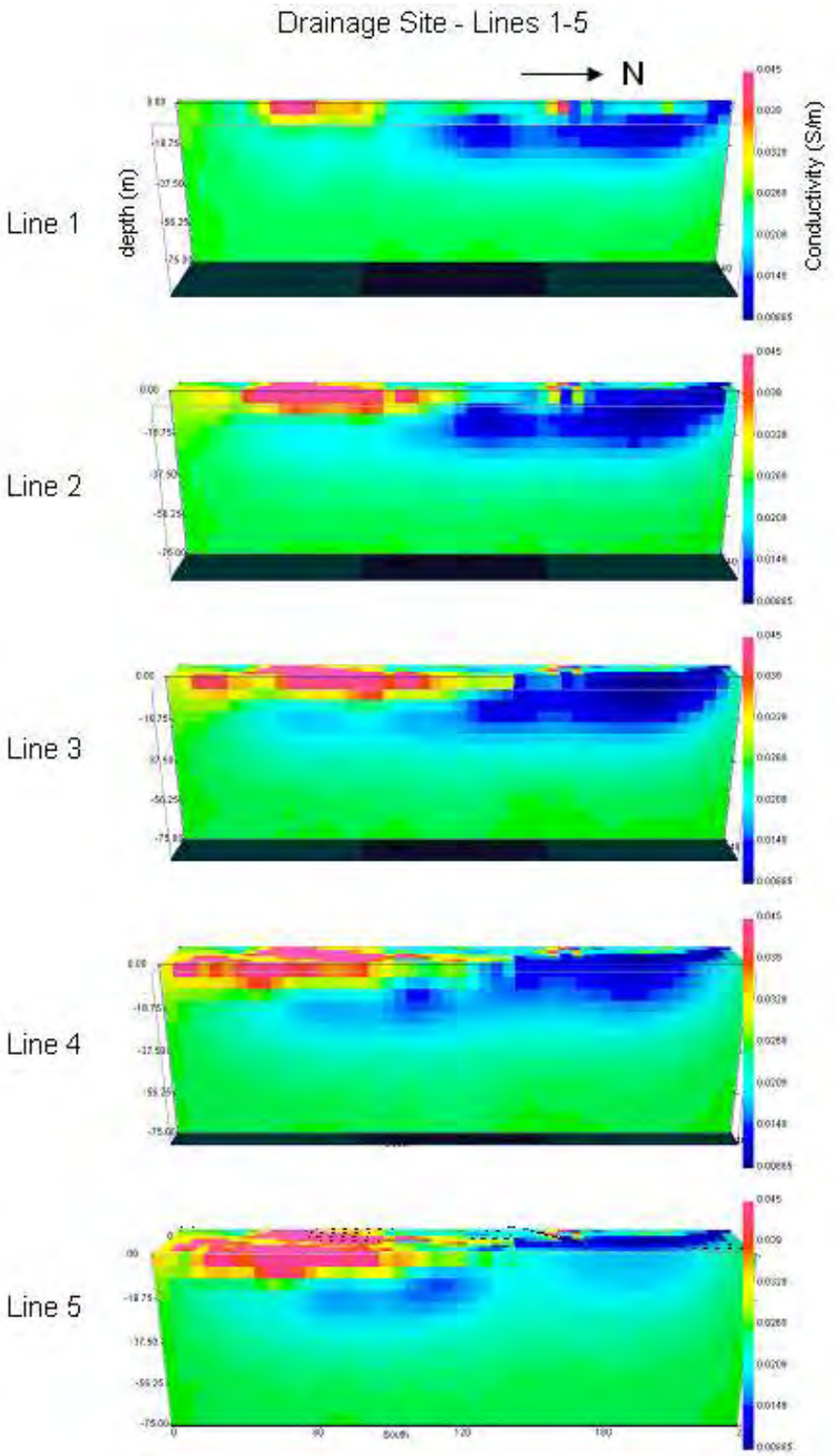

Figure 10.4.5: A 3D inversion of the DC resistivity survey done at the drainage site. The section is sliced by line.[27]

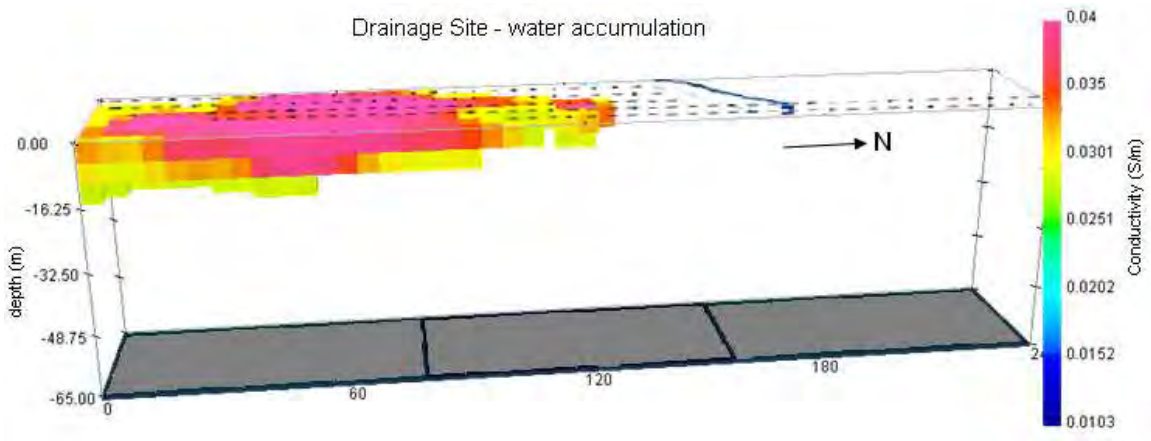

Figure 10.4.6: The isolated conductive body show with the irrigation ditch location on the surface and survey lines (lines 4 and 5 intersect the ditch).[27]

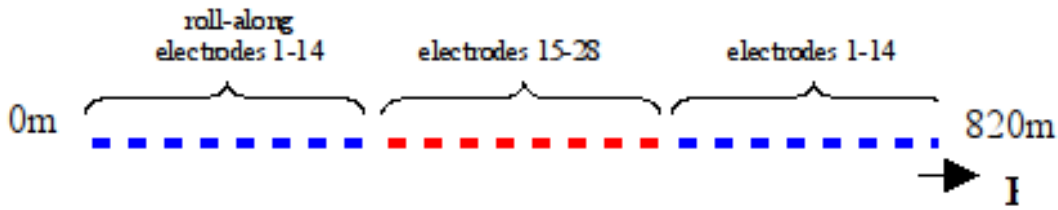

Figure 10.4.7: Electrode set-up for Line C (north site)

The line is not perfectly straight and it also crosses a private property from approximately 450 meters to 500 meters. The property is surrounded by a barbed wire fence and the line crosses about 10m to the south of the house.

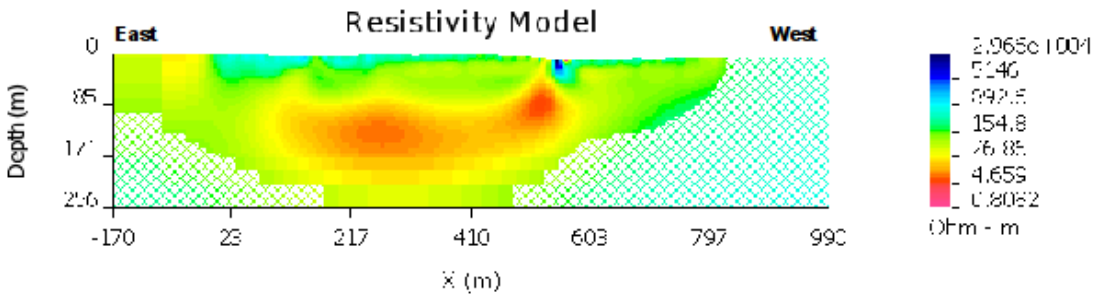

Figure 10.4.8: Inverted data for Line C (north site). House is blue (resistive) anomaly and red shows water accumulation. Profile faces south.[26]

Figure 10.4.8 shows a 2D inversion along line C, with an approximate depth of investigation of over 200 meters. The model runs from east to west and therefore faces south.

The inversion shows a thin, resistive layer over a highly conductive body. The top of the conductive anomaly is anywhere from 10 meters deep at its shallowest point to 90 to 100 meters deep toward the center of the line. The highly resistive area near the surface at about 550 meters is due to the house.

10.5 Error Analysis

The primary source of error in the field for DC resistivity surveys was due to surrounding objects such as electrical boxes, power lines, drainage pipes, or fences. There is always potential for human error. Field notes helped keep track of possible problems, such as the electrical boxes on the Dead Horse Lake survey seen in Figure 10.4.2. It is important to note that when inverting data, it is not ideal to fit the data exactly. Inversions must account for the fact that data contains noise and therefore cannot give a perfect model of the subsurface.[25] Inversion programs account for this and we assumed a 5% error in our 3D inversions. There is always an inherent problem of non-uniqueness. A very deep, highly conductive body would give the same model as a shallow, less conductive body. This is one of the reasons it is so important to use multiple types of surveys (e.g. EM-34 and self-potential) to compare to DC resistivity data. With different types of data, it is easier to narrow down the actual shapes, sizes, magnitudes, and depths of anomalies.

10.6 Conclusions

The DC resistivity data gives a very good idea about water accumulation in the various survey areas. At Dead Horse Lake there is no significant water accumulation, which corresponds to self-potential data showing no movement of water in the area (Figure 10.4.1). There is a slightly saturated region where the lake was once located (Figure 10.4.2). At the south site, there is apparent water flowing from the drainage ditch into the subsurface but the flow is inconsistent along the ditch (Figures 10.4.3 through 10.4.6). It is possible that drainage ditch runoff contributes to well water in the region but more data is required to confirm this. There is a large, distinct anomaly along Line C, or the long self-potential line, just north of Chalk Creek (Figure 10.4.8). This anomaly could show the location of a fault where hot water is rising to the surface. The data correlates with self-potential data in the region. When combined with electromagnetic data, DC resistivity will present a clearer idea of the locations of near surface water and self-potential data will clarify the directions of water flow.

Chapter 11

Self Potential

11.1 Introduction

Self-potential is a geophysical method that measures the naturally occurring potential differences on the earth's surface, with no artificial source of current involved. The DC resistivity method and the self-potential (SP) method share many of the same concepts. In both methods, the potential difference between two electrodes is measured. However, in the DC resistivity method, an artificial current is introduced into the subsurface. The SP method, on the other hand, measures only current due to natural sources, such as those caused by flowing water (streaming potential) or electrochemical processes. Streaming potential is caused by uneven charge accumulation due to flowing water through a porous medium. As a result, the direction of the flowing water by observing the location and magnitude of potential anomalies. Electrochemical reactions also lead to measurable potential differences, but these potentials do not necessarily correspond to groundwater flow. By creating an extensive map of these potential anomalies, it becomes possible to characterize both the flow patterns and electrochemical activities of a region. The behavior of this anomalous potential is govern by the Poisson's Equation for electric current, which is as follows.

$$\nabla \cdot (\sigma \times \nabla \Psi) = \nabla \cdot J_s \tag{11.1.1}$$

Where:
σ = Conductivity
Ψ = Electrical Potential
J_s = Current Density

11.2 Overview of SP Method

Conducting an SP survey is simple. There is a base electrode and a moving electrode. A voltmeter is used to measure the potential difference between the two electrodes. By using non-polarizing electrodes such as a copper and salt solution (copper sulfate, in this case) conductivity and signal strength are improved. Surveys can be either along a profile line or a grid. In the field camp surveys, both layouts were used. Having a significant change in

the potential values from the background potential represent an anomaly. In the direction of water flux along a fault, a positive anomaly is expected.

Since the SP method measures the relative change in potential values, it is not a good indicator of depth investigation. For example, one would measure similar values of potential if there is a large deep water table or a small, shallow water table. Either way, the potentials are the same, and there is no way to tell the difference without other data to constrain the model. And as the depth of the water flow increases, the amplitudes of the anomaly decrease. The SP method alone does not give a unique solution for the flow model. In order to reduce the non-uniqueness of the solutions, it is necessary to have a borehole to get the depth of the water table or use a 3D inversion from DC resistivity data.

11.3 Survey Design

Two advantages to using the SP method are its instant results and system portability. The instant results played a large factor in proceeding with the SP surveying. Initially a self-potential survey was performed in the west high-resolution field (see Figure 11.3.1). When an anomaly was seen during the survey, the SP lead (Dr. Andr Revil) ran the P2 profile survey to the east, and subsequently determined that a new high-resolution survey field should be created to the east in an open field.

Previously the shear zone of the north and south extension faults had been thought to reside in the valley, but these SP results initially determined otherwise. Dr. Revil then set out to profile the gullies running from the valley up into the cliffs, hoping to extend his proposed shear zone location. The portability of the SP system used during field camp allowed for these profiles to be run easily. With the rugged terrain encountered, it would have been very cumbersome to run DC or EM surveys. For the SP surveys, the roll of electrode wire used for all SP surveys had been previously marked in 10-meter increments. With no survey stations available, the SP crews simply set a base reference at the beginning of a survey line, and proceeded to follow the gully up into the cliffs. Readings were taken every 10 meters for better coverage should the shear zone be encountered. As noted below, this impromptu survey design provided good profiles and indeed located the shear zone and extent of it to the west along the cliffs.

Once the eastern high-resolution field was laid out, an SP survey was run at that location. Again, an anomaly surfaced while reading the data. This in turn prompted Dr. Revil to expand the western field to further record the anomalous area, and also run some linking profiles between the two fields. 10-meter readings were again taken for the detail provided.

For the deep seismic line, only 30-meter reading intervals were taken. Not only were these stations already GPS'd, but due to its location in the valley, no hot spring anomaly was expected to be found. At the same time, several tying profiles were run in order to be able to interlink the reference locations of all profiles run for SP and get an overall reference data point for later processing.

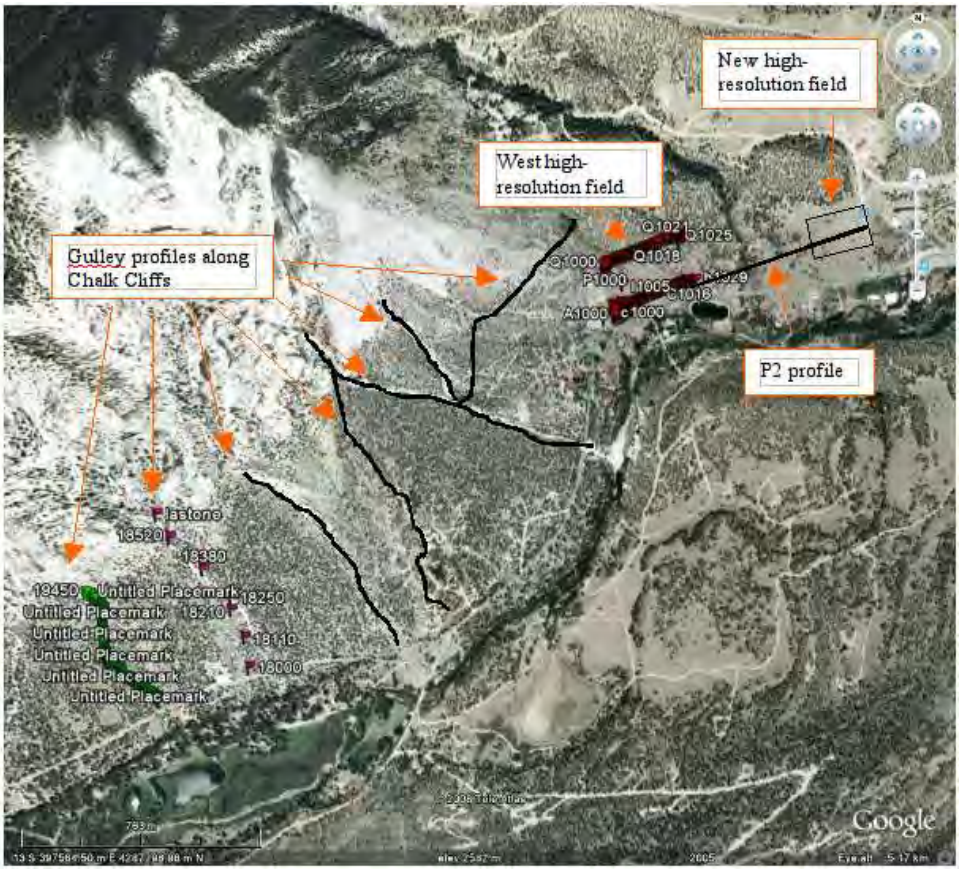

Figure 11.3.1: Geophysics valley view with partial SP survey included

11.4 Processing

The main processing problem was finding positions for the measurements. The SP method does not require specific positioning since the trends in the data are large scale. With limited time in the field, the GPS crew did not take coordinates for most of the SP lines, so UTM coordinates were retrieved based on an aerial photograph. Google Earth was used to complete this task by simply tracing out the path taken and marking the estimated flag locations. There were sparse handheld GPS points taken, but the aerial photograph was usually more accurate.

For the North (shown in Figure 11.3.1) and South (west of Poncha Springs) surveys SP produced a few different pieces of information. In the high resolution area on the North side SP is used to find upwelling of water. Hot springs are caused by a water source in the ground that gets heated and shoots to the surface through a fault; SP will pick up a high positive anomaly at this location. A crucial distinction to make is that there must be water flowing to pick up an SP signal. A fault can be present, but if the water flow decreases or is cut off then the fault will appear to fade out. In this geological setting the water contains silica and as the water approaches the surface it cools making the solubility of the silica lower. As the silica precipitates out of the water it can plug the fault and stop water flow, thus there will be no SP signal.

The South high resolution survey focused on how water was flowing around a drainage ditch. For this application the signal on a broad scale is simple to interpret. The source of water should produce a large negative response and create contour lines indicating the seepage direction. If there were no seepage, the data would show a strong negative anomaly next to the drainage ditch with relatively constant values over the rest of the grid.

On the North side west of the high resolution survey there were a series of gullies surveyed to trace the major fault over that region. The interpretation of the data is slightly different than that of the upwelling of the high resolution survey due to the slope. Right at the fault there will still be a high positive anomaly, but just above that there will be virtually no water flow compared to the water flowing from the fault, so the SP signal will drop dramatically once the fault is passed. There was no DC survey taken at these locations so the data can only be used to trace the fault.

The magnitude of the anomaly has little significance without employing other methods such as DC Resistivity, due to the non-uniqueness of the potential measurement. Coupling these methods together can produce a model of the depth of the water table and basic flow pattern.

11.5 Interpretation

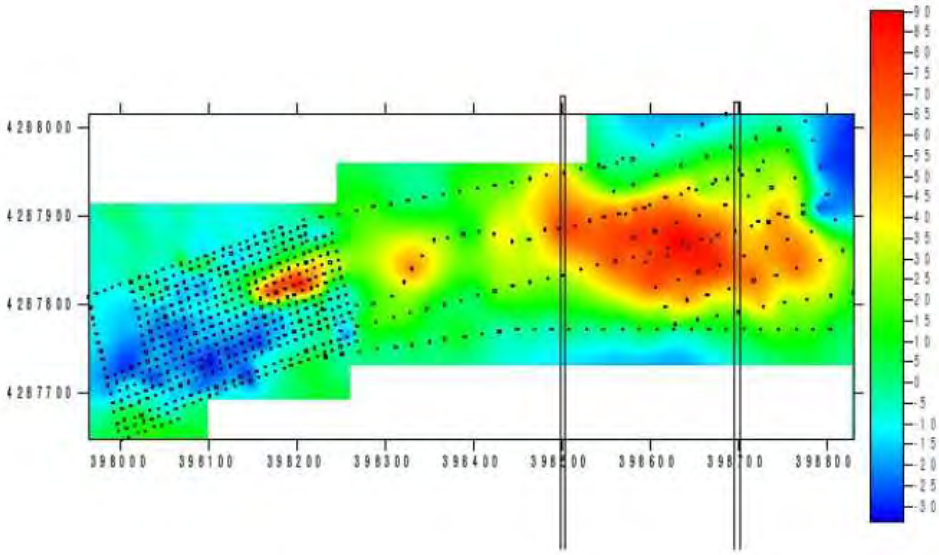

Figure 11.5.1: SP Anomalies on Map View, North Sites

The figure above demonstrates where measurements were taken on the high-resolution grid to the west and in the connecting profiles to the lower resolution grid to the east. As mentioned before, the high resolution grid to the west was not very helpful in terms of immediate information, but it did provide us the motivation to continue to collect data to the east. There is a highly positive anomaly located to the east that extends about 300 meters to the west. The smaller anomalies to the west indicate that this area has hot water that is most-likely dominated by an extensionally-derived crack in the subsurface. The reason that the anomalies are not continuous is a result of silica precipitation along the crack, which effectively "plugs" exposed areas, ceasing water upwelling in that area. The green X is the proposed hot water well drilling location.

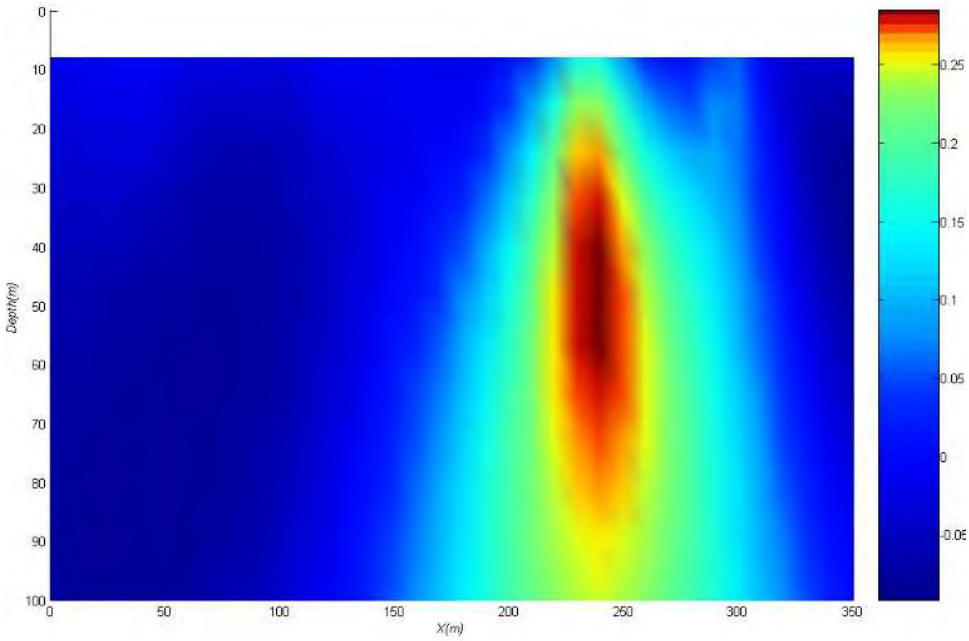

Figure 11.5.2: Tomography profile along line 1

The figure above represents the cross-correlation tomogram that represents probability for the location of the target anomaly. This tomogram was taken along the UTM line 398500 mE going south to north along the high resolution grid. The reason for this orientation is to better characterize the crack by correlating the lines perpendicular to it to avoid aliasing. There is also a tomogram for a line on the other side of the main anomaly along UTM line 398700 mE which can be viewed in the appendix.

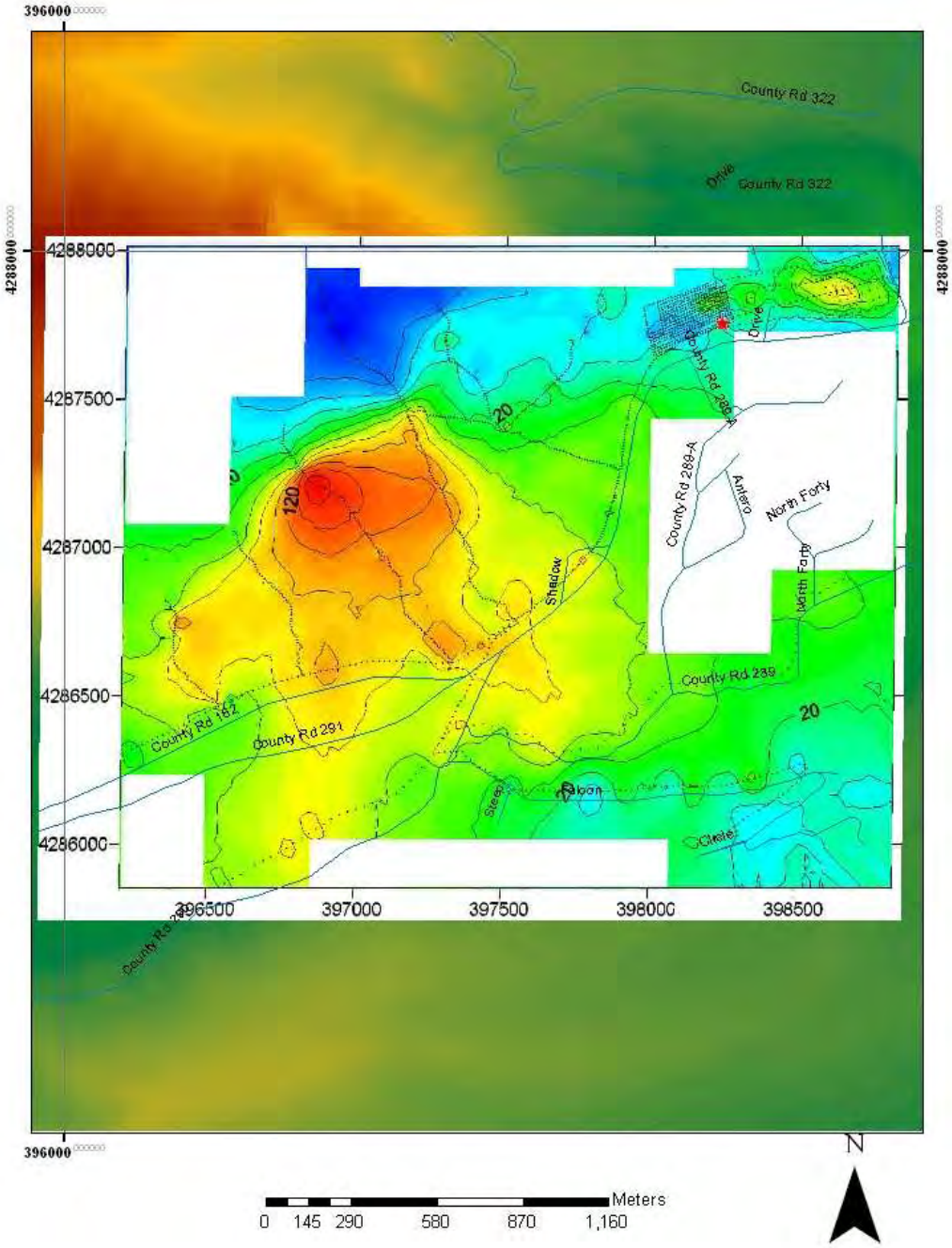

Figure 11.5.3: SP Anomalies on Map View, South Sites

The figure above represents not only the high-resolution grids, but also the valley profiles that were completed in order to locate the shear zone. Mount Princeton is to the north of the highly positive anomaly which is indicative of the shear zone along the major fault. It is highly likely that hot water is upwelling right at the base of Mount Princeton and traveling south along the water table. This area is different from the high-resolution zones because it is dominated by a major fault, and the high-resolution zones are dominated by extensional processes.

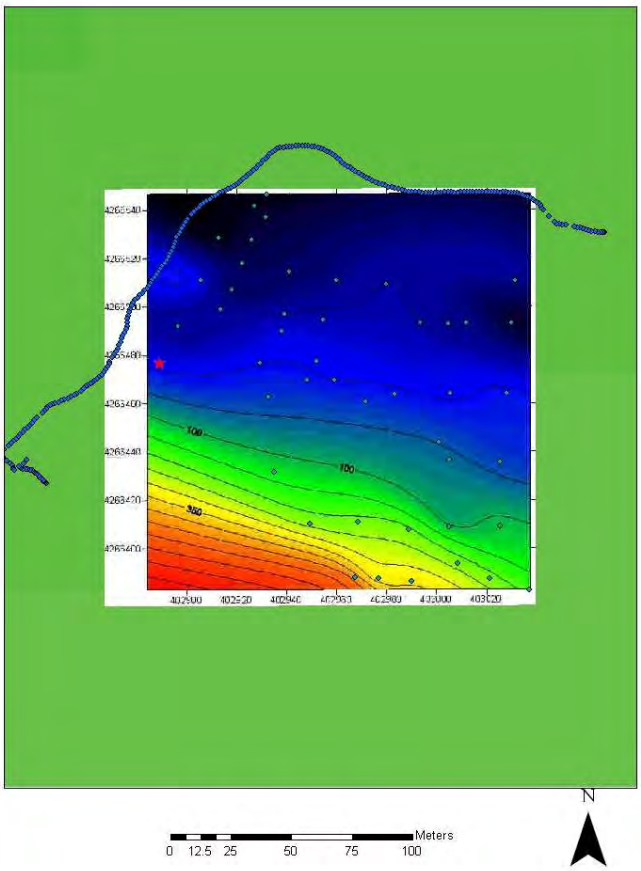

Figure 11.5.4: SP South Grid

The goal of the South grid was to determine water seepage out of the drainage ditch. Figure 2 shows a positive trend towards the Southwest corner. The strong negative response is the drainage ditch and the water looks to be flowing out of the ditch to the Southwest. The data coverage is somewhat sparse to the Southwest corner though, so the values more than likely taper off rather than increasing quite rapidly. The depth cannot be determined uniquely without using the results from the DC 3D inversion and time constraints did not allow us to do this. However, comparing the map view of the 3D inversion and the EM31 data with SP to see if the data correlate may prove useful.

11.6 Error Analysis and Issues

Due to insufficient satellite coverage for much of the gully profiling, very few GPS readings were taken while running the surveys. Even though primarily 10-meter readings were taken, due to the rugged terrain including numerous tree clumps and bushes many times the 10-meter reading intervals were also around ±3 meters differences.

Another error source was encountered when converting the UTM measurements from the GPS readings to decimal lat/long. The SP processing committee used *http://www.cellspark.com/UTM.html* as it was the most consistent among all converters trialed, but there were still some obvious differences seen between computers.

Google Earth was used to generally plot the lines using some GPS readings taken, and then filled in with proper interval spacing. It was found that those station locations that were measured tended to be somewhat inaccurate when compared to SP crew memories and overall views of the plotted lines. Even manually locating a point in Google Earth gave much room for inconsistencies when transferring specific locations to the data spreadsheet.

These surveying and processing procedures do not allow for an exact repeatable survey, but with this SP survey that was not a concern due to the generality of the data gathered. Should further surveying be undertaken at more specific locations based on the overall findings, it would be more efficient to simply take the SP equipment to the field and perform very localized surveys. Utilizing this method, exact locations of possible well boreholes could be accurately determined.

11.7 Conclusions

Interpretation of this data could not have been accomplished without correlating the SP data with DC and EM. Fortunately, the datasets seemed to correlate among the same anomalies in generally the same areas so there must be a high probability that the anomalies are actually there. The conclusions derived from the south grid in Poncha Springs are that water is leaking from the ditch and that the flow is approximately south by southwest.
The high resolution zone provides excellent data quality that correlates almost exactly with the data from the long C line that bridges both grids. Unfortunately, since the 3D DC data was corrupted, it was impossible to base the interpretation on anything besides the SP data alone. Therefore, after applying the cross-correlation tomogram for the two profiles on both sides of the anomaly, the highest probability for the target anomaly depth was somewhere between 40-50m in depth. In conclusion, since the target anomaly shows up in the same location in the DC and SP data, the greatest potential for a test well should be located right on the long C line at station C1047.
The mapping that involved the whole valley is much lower resolution, so the goal of the

interpretation was merely to emphasize the anomaly at the edge of the cliffs as a possible upwelling of water due to a shear zone created by the offset of the Mt. Princeton and Mt. Antero faults. This shear zone has the greatest signal in the area which is probably due to the deepest, hottest water situated underneath those cliffs. More mapping must be carried out in the areas surrounding Deer Valley Ranch in order to increase the probability of success for a geothermal plants test well.

Chapter 12

Gravity

12.1 Introduction

The gravity method utilizes variations in the Earths gravitational field in order to determine physical properties. By measuring these variations and comparing them either locally or absolutely, areas of anomalous densities can be identified. A gravimeter is the instrument used to measure the gravitational field by measuring the acceleration due to gravity at a particular point. In geophysics, the acceleration due to gravity is measured in milliGals, where 1 Gal = 1 cm/s2. Though the acceleration due to gravity is considered to be constant, it actually fluctuates depending where on Earth it was measured. Earth is a flattened sphere with a bulge around the equator, causing the distance between the center of the Earth and surface to be greater at the equator than at the poles. The acceleration due to gravity is directly proportional to the mass and inversely proportional to the earths radius squared at a particular point as seen in Equation 6.C.1 where M is mass, R is earths radius, and G is a gravitational constant. In order to obtain a more accurate gravity value, the values measured are put through differing corrections. The corrections include tidal and drift, latitude, free-air, terrain, and the Bouguer.[28]

$$g = -\frac{GM}{R^2} \tag{12.1.1}$$

12.2 Survey Locations

Gravity station measurements were taken along the north seismic line, the south seismic line, and random points in the surrounding area. The north seismic line ran along County Road 290 off of Highway 285. The south seismic line ran along County Road 220 off of Highway 50. Along the north seismic line, gravity measurements were collected at every third flag which were 30 meters apart. Along the south seismic line, gravity measurements were collected at every fifth flag then switched to every sixth flag, which were also 30 meters apart. In addition to the gravity measurements along the seismic lines, a team collected gravity in random locations around Mt. Princeton. Combining the data from all these locations can help us to create a rough map of the total gravitational field in the area. While

a 3D inversion requires more gravity stations and a more structured mesh, it is possible to do a 2D inversion along the seismic line.

12.3 Base Station and Tie-In Measurements

While taking gravity measurements, it is important to tie back to a base station. This allows for instrument and tidal corrections to be made to the data. A base station is a station you continually come back to and retake measurements. This allows you to find the differences in the values for each base station throughout time. This difference is used to calculate the drift and subtract it from the anomaly reading. Using the G-491, base stations are taken roughly every hour. Using the CG-5, base stations are required less frequently over time. To begin and end every day, data points are taken at a main base station. It is also necessary to take readings at the same point with both the CG-5 and C-491 to create reference points in order to tie in the measurements from both instruments. The difference between the readings of the gravimeters at the same locations is subtracted from one of the data sets in order to balance them out. This removes any error that may be caused by the differences between the mechanisms of the gravimeters. Typically, an absolute gravity measurement is taken at an absolute gravity station in order to correct the observed gravity values. As an absolute gravity measurement was not taken, all gravity values discussed are relative.

12.4 Data Reduction and Corrections

12.4.1 Counter reading correction

The two gravimeters used to collect gravity information were the CG-5 and the Lacoste-Romberg G-491. The G-491 displays observed gravity values that need to be converted to milliGals using a table and equation. The observed gravity data values were converted to milliGals using the counter reading (observed gravity) on the gravimeter, A, and a table with lists of values. The table includes the nearest integer smaller than the reading, B, the corrected gravity value in mGal, C, and the factor for Interval, F. Using these values, the correct relative gravity value is calculated according to Equation 6.C.2. All other corrections are calculated and subtracted from this calibrated value.[29]

$$\text{Gravity} = C + F * (A - B) \tag{12.4.1}$$

As for the CG-5, it is one of the newest gravimeters on the market today and displays the relative gravity in milliGals and needs no counter correction to the actual reading.

12.4.2 Instrument Drift & Tide correction

As the oceans feel a tidal effect from the sun and moon, solid earth also feels a tidal effect from their gravitational pull. This tidal pull has a direct affect on gravity readings by causing slight changes in the direction and amplitude of the gravitational field at a given point on earth.[28][29]

The gravimeters used, measure the strength of the gravitational field at a point measure in milliGals and easily detect these small fluctuations. Through time, these fluctuations may cause the gravity measurements to appear either higher or lower than they truly are.

Similar to the tidal effect, instrument drift can also cause the measured gravity values to appear higher or lower than they truly are. Unlike tidal effects, instrument drift is a by product of the gravimeters and the mechanism used to measure the gravitational field. For example, the Lacoste-Romberg G-491 uses a spring mechanism to measure the small fluctuations in the gravitational field. Through time and use the spring can become stretched out causing the observed value to be less accurate.

The tidal effect and instrument drift have similar trends and can be corrected for together. In order to calculate this correction, it is necessary to have measurements repeated at a base station every few hours. The equation used to calculate the tidal and drift correction is given in equation 6.C.3 where t is time of observation between base stations, g_b and g_e are the gravity readings at the beginning of a survey loop and end of a survey loop, and times t_b and t_e are the times of g_b and g_e, respectively. Reading g_1 is the very first, main base station reading.[28][29]

$$\Delta\text{Gravity tidal/drift} = g_b + (t - t_b)\frac{g_e - g_b}{t_e - t_b} - g_1 \tag{12.4.2}$$

12.4.3 Latitude correction

Earths rotation causes an angular velocity that affects the gravitational field. These angular velocities are caused by accelerations from the tides (taken care of in the Tide/Drift Correction) and the earths rotation. The angular velocity is naturally larger at the equator and decreases to zero at the poles. Considering this factor, the gravitational field is naturally larger at the equator and decreases with latitude towards the poles. The latitude correction is applied to remove the natural difference from angular acceleration in order to get a more accurate anomaly value. The equation for latitude correction can be seen in Equation 12.4.3 where ϕ is the latitude in degrees.[28]

$$\text{Gravity Latitude} = 978032.68\frac{1 + 0.00193185138639\sin^2\phi}{\sqrt{1 - 0.00669437999013\sin^2\phi}} \tag{12.4.3}$$

The distribution of the latitude correction values are shown in Figure 12.4.1.

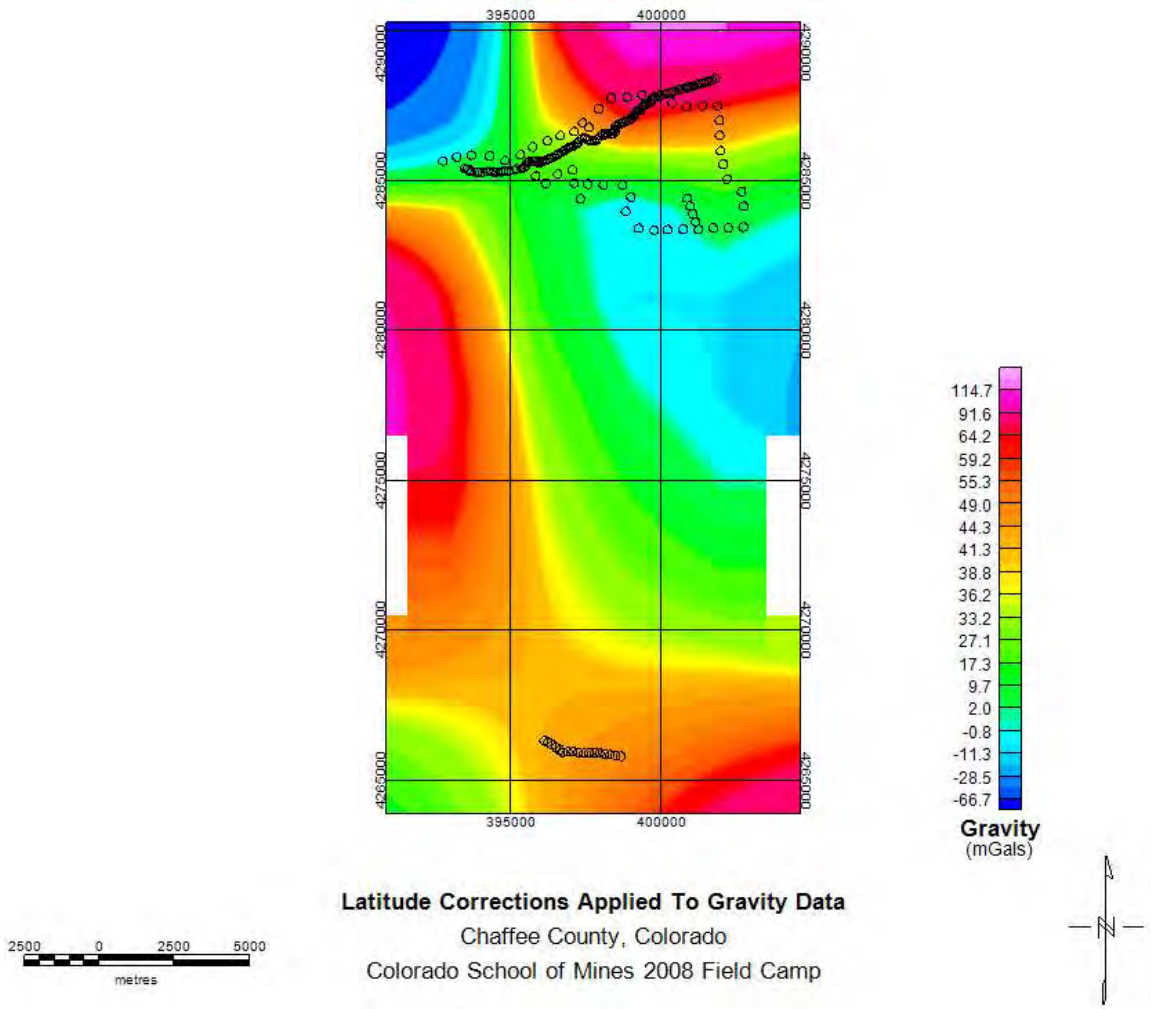

Figure 12.4.1: Latitude Correction Contour Plot

12.4.4 Free-air correction

There is a difference in the gravitational field depending on the radius of the earth at a particular point seen in the 1/R2 term in Equation 6.C.1. To remove the difference in elevation according to radii, a precise elevation is needed for each gravity station. The elevation at each station was measured using a differential global positioning system (GPS). The differential GPS can measure elevations to within centimeters depending on obstacles such as dense forests and heavy cloud cover. The accuracy decreases with increased interference, which can be seen in the data.[28][29]

The free-air correction removes the difference in elevation from one gravity station point to another, which reduces the data to a constant elevation datum. The difference between gravity measured at the station and what would be measured at sea level determines the free-air correction. It is important to note that the free-air correction assumes the space between the gravity station and sea level is filled with air. For our ground survey, the mass that occupies this space is dealt with in the Bouguer correction. Equations 12.4.4 and 12.4.5 shows the formula used to apply the free air correction, where h is the elevation above sea level in meters.[28]

$$\frac{dg}{dh} = \frac{2gh}{R} - \frac{3gh^2}{R^2} = -0.3086 \tag{12.4.4}$$

$$\text{Gravity Free Air} = \frac{dg}{dh}h = -0.3086h \tag{12.4.5}$$

The distribution of the free-air correction values are shown in Figure 12.4.2.

12.4.5 Bouguer correction

The free-air correction assumes there is no mass between the sea level datum and the elevation of the measurement point. The Bouguer correction takes into account the distance between the measuring station and sea level as it pertains to mass. The purpose of the Bouguer correction is to correct for the gravitational pull of the rock mass rather than the elevation by filling the void space left by the free-air correction with rock of appropriate density.[28]

Two assumptions are associated with this correction: the area between the measurements elevation and sea level can be represented by an infinite slab and secondly, that the slab has a reasonable density distribution (Chapin, 1996.) The simple Bouguer Correction can be applied using Equation 12.4.5, where ρ is the density of the slab and h is the elevation above sea level in meters. An average rock density of 2.65 Mg/m^3 is typically used across a geometric slab to calculate the Bouguer correction.[29]

$$\text{Gravity Bouguer} = -0.04193\rho h \tag{12.4.6}$$

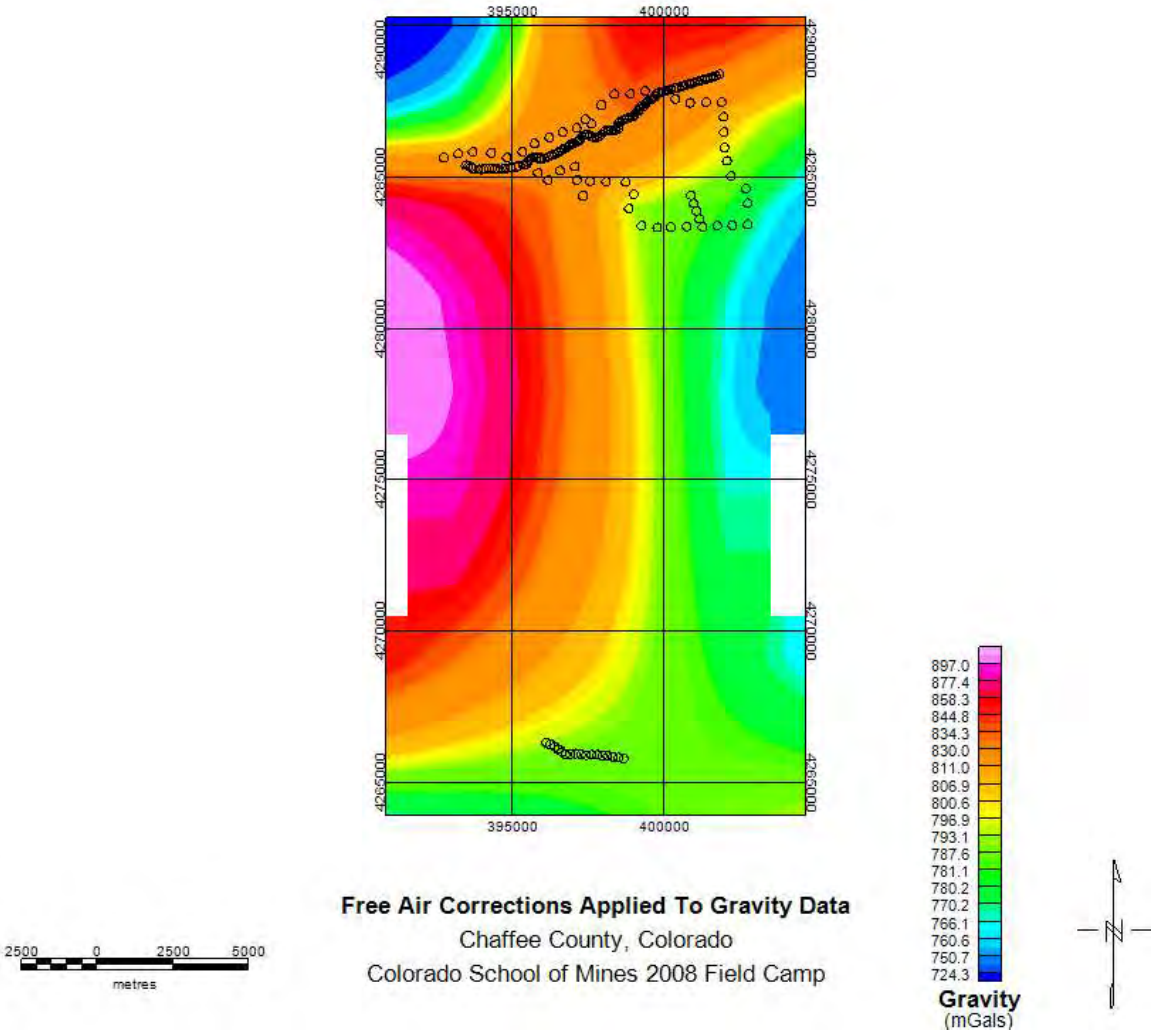

Figure 12.4.2: Free Air Correction Contour Plot

Figure 12.4.3: Example of Bouguer Correction

Combined with the free-air correction, a total elevation correction can be applied to the data according to the Equation 12.4.7.

$$\text{Gravity Total Elevation} = g_F - g_B \tag{12.4.7}$$

The distribution of values obtained from the Bouguer correction is shown in Figure 12.4.4.

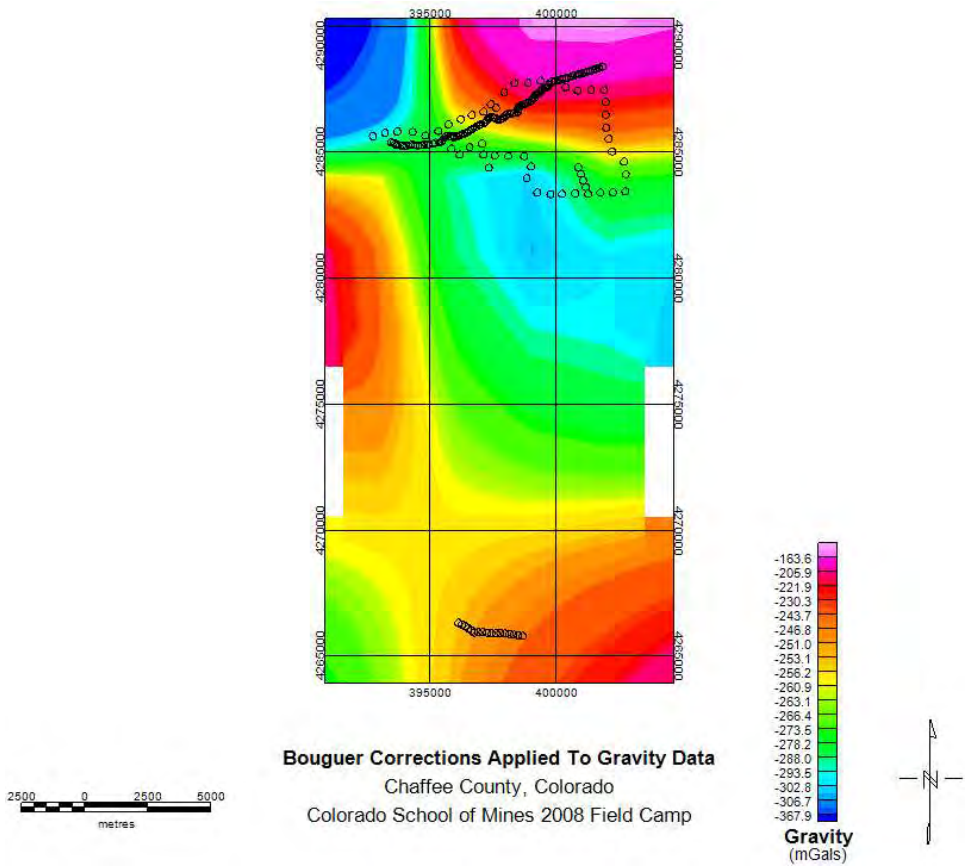

Figure 12.4.4: Bouguer Correction Contour Plot

12.4.6 Terrain Correction

A terrain correction is applied where there are significant differences in elevation across the gravity survey. In a flat area, the slab model used in the Bouguer correction will suffice. In areas with hills and valleys, the terrain correction is necessary to correct what the slab model missed. The Bouguer correction takes into account the gravitational pull in only one direction, as the slab is uniform, while the terrain correction takes into account the gravitational pull in two components, as there may be an excess or deficiency of mass nearby.[28]

The terrain corrections were processed using a high power mapping software program called Oasis Montaj; which is created by Geosoft. Oasis Montaj performs the terrain

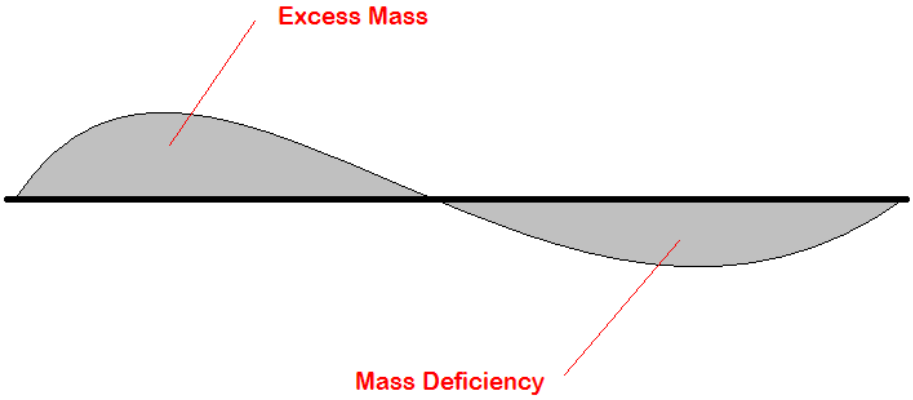

Figure 12.4.5: Example of Terrain Correction

correction by subtracting the excess mass or adding the mass deficiency to the gravity readings. The values of the excess mass or mass deficiency are calculated by using a regional correction grid of the surrounding terrain. This regional correction grid is created in Oasis Montaj by loading a regional and local digital elevation model (DEM) of the area. The DEMs were acquired from the USGS Seamless database with a resolution of 1/3 arc second or 10 meters.

The distribution of values from the terrain correction is shown in Figure 12.4.6.

12.5 Interpretation of Gravity Data

Once values for all the corrections are obtained, they can be subtracted from the observed gravity value in order to get a better idea of the gravitational field and density distribution across the area. Measurements from gravity stations along the north seismic line were used along with modeling software to invert the data. The model was created using a local easting scale. The first gravity station at local easting 0 has UTM northing of 4285443.03 and easting of 393382.94.

GMSYS was the software used to create a model of the subsurface that matches the gravity values measured. In order to create a model, the topography dataset (which included the UTM Easting and Elevation values) was imported along with the gravity station dataset (consisting of UTM Easting, Elevation, and corrected gravity anomaly values). These datasets give the basic topography of the region and the data points to fit the model to. Modeling like this is non-unique, meaning there are many geologic explanations that could fit the gathered data.

The distribution of corrected gravity along the north seismic line is shown in Figure 12.5.1.

A geologic cross section created while in Chaffee County and seismic data were used to

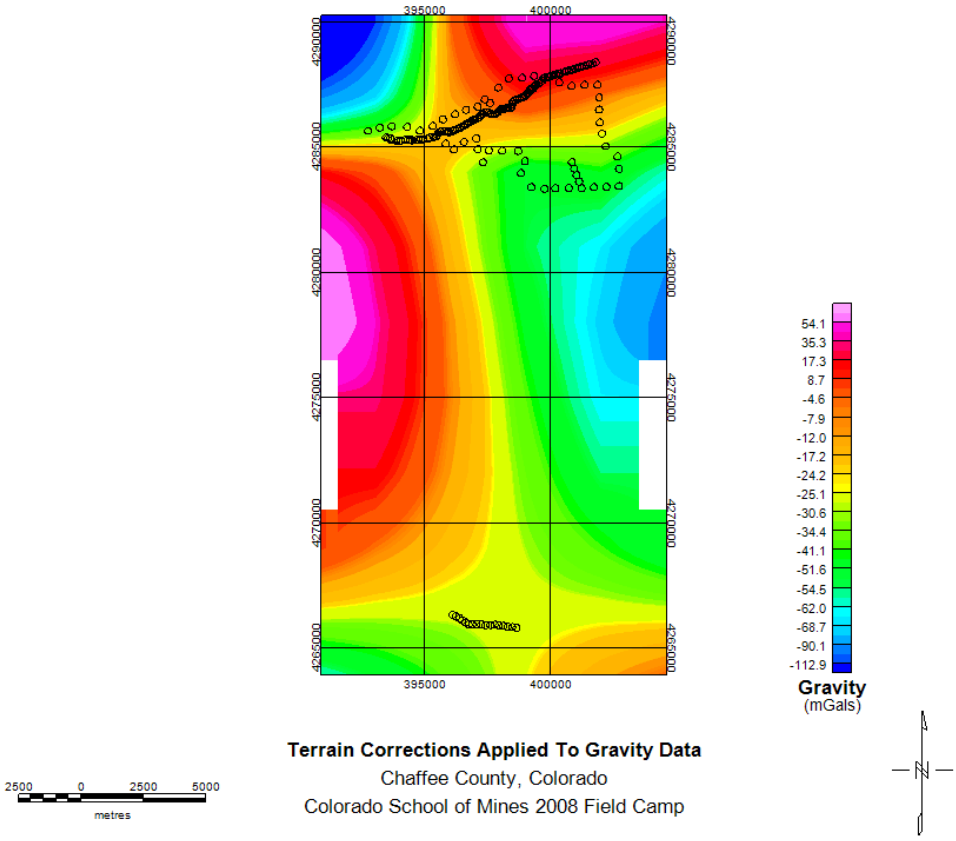

Figure 12.4.6: Terrain Correction Contour Plot

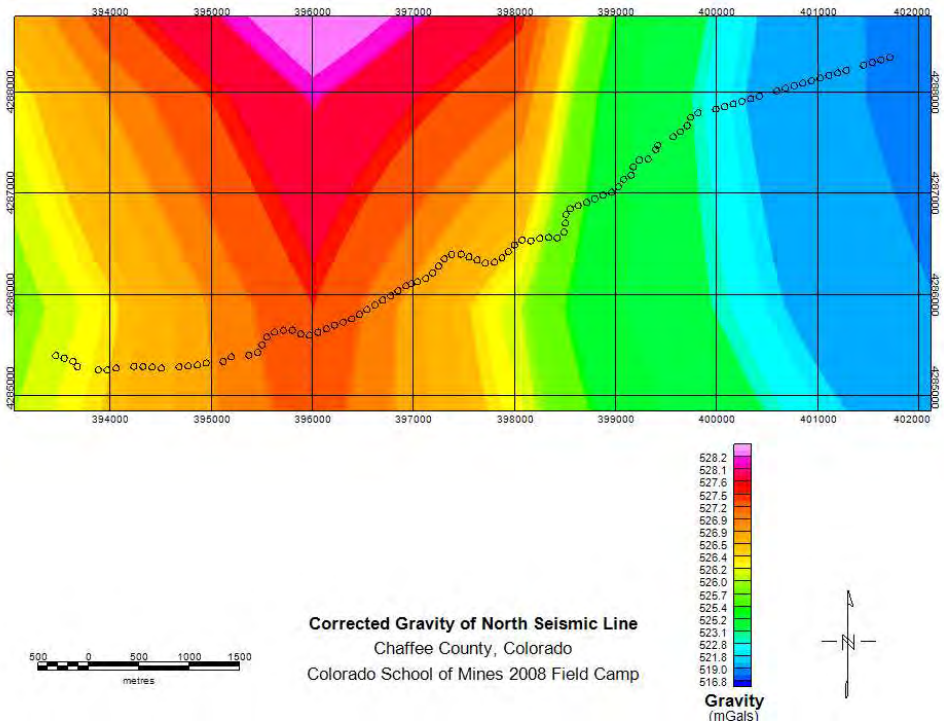

Figure 12.5.1: Corrected Gravity Data Contour Plot

help create a basic model. Dr. Batzle provided appropriate densities for the various rock and sediment types. The densities used are as follows: alluvium: 2.2 g/cc, dry union: 2.4 g/cc, basement rock: 2.7 g/cc, granitic intrusion: 2.5 g/cc. Our finished model shows a series of faults running across the middle of the cross section. These faults were also seen in the seismic data. The model seen in Figure 12.5.2 shows the depth to basement rock ranging from approximately 200 m to 500 m. It includes the Dry Union Formation, the alluvium that covers the basin floor, basement rock, and the Mount Princeton batholith to the west. The Dry Union Formation has a thickness of approximately 100 m in our model. Since modeling is non-unique, simply changing the densities and thicknesses of the rock units could provide alternative models that may also fit the data.

By adjusting the model, we were able to create a cross section with a very similar gravity profile to the data we collected. Several faults were added according to previous knowledge, which helped the model to better fit the data. The highs and lows seen in the gravity profile of Figure 12.5.2 correspond to the contours in Figure 12.5.1 created by Geosoft using the same data points.

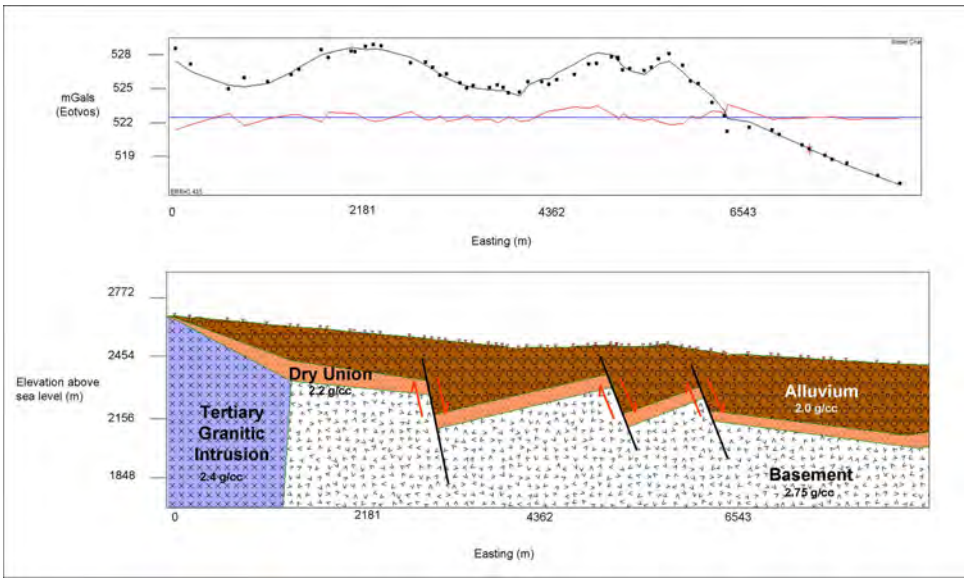

Figure 12.5.2: Gravity Profile

12.6 Error Analysis and Issues Encountered

he use of two different instruments for data collection is a source of error. As mentioned previously, the gravity values taken by one instrument needs to be corrected according to the values collected by the other instrument so the measurements can be compared locally. This leveling process introduces some error into the overall measurements. Each correction applied to the data introduces a small error to the data on the order of tenths to hundredths of a milliGal. The G-491 can only measure down to the hundredths place and is less accurate

than the CG-5. The CG-5 gives a standard deviation for the measured value. As the observed gravity values are used throughout processing, the error associated with the values propagates through the data.

A differential GPS unit was used to measure the elevation and coordinates of each gravity station. In wide open spaces, with a clear view of the sky, the differential GPS is able to pinpoint locations and elevations to within centimeters. The heavily wooded area near Mount Princeton provided challenges in getting a solid triangulation. Due to this obstacle, some stations were not readily recorded and may have been taken in floating mode, which is less accurate.

The terrain correction was done using Geosofts Oasis Montaj software. Many problems were encountered when putting the data in the correct format and importing it. Once the data was correctly loaded, the terrain correction was executed only to find that the DEM used to create the regional correction grid was too small. To the east, 30 gravity stations were off the regional correction grid. New DEMs were downloaded from Seamless and terrain correction values were obtained. Like the other corrections, the terrain correction has error associated with it as well. The DEMs used had a resolution of 10 meters; if 30 meter resolution had been used, the error associated with the terrain correction would be higher.

The figures displayed above were created using Geosofts Oasis Montaj. The contours were interpolated from the few data points and should not be considered final. Different programs interpolate and contour in differing ways; what is shown here is one possible distribution of the gravitational field.

12.7 Conclusion & Recommendations

Along the North Seismic line we created a model that consisted of three faults. This is only one possible model of the subsurface. Several more models could be created to incorporate different fault configurations, geologic bodies, and densities. More faults could be added to try to reduce the error in our plot. The error associated with our geologic model was .433. A higher error could mean the model created did not fit the model well enough while a lower error could mean the model created does not fit the data because there is a certain propagation of error in processing.

Not enough data points were collected to create a 3D model or accurate contour map of the area. It may be beneficial to collect data in a defined grid over the area in order to create a 3D model and contour map purely from collected data.

Chapter 13

Integration

13.1 Proposed Geothermal Well Location

In order to better understand the geothermal structure at the north site it is beneficial to compare and contrast the results of the self potential (SP) surveys and the DC survey taken along the long line. The SP data can tell us where water is flowing laterally but it is limited when it comes to depth. The DC data can help to fill in this gap.

When the 2D inversion is compared to the SP data we see a strong correlation between the locations of the highly conductive bodies and the high voltage regions respectively. As mentioned in Chapter (11), the high voltage areas form a linear feature that we believe to be a crack created by the rift system in the valley. The discontinuous nature of the crack is likely due to silica plugs that have precipitated from the groundwater. The DC inversion also shows a discontinuous conductive body along the line with the highest conductive region, near 100S/m, at a depth of approximately 85m. The presence of water could still be feasible in conductivities ranging from 15S/m up, which means that we are seeing water as shallow as 20 to 40 meters. The fact that we believe this to be the location of a fault or crack, along with the evidence of geothermal activity in Bill Moores well and the Mount Princeton Hot Springs leads us to assume that the water we are seeing in these conductive regions is hot. Our conclusion therefore, is that this would be an excellent location for geothermal production.

To further expand on the conclusion above we have come up with a proposed well location that would take advantage of the hydro-thermal system in the area. Figure (13.1.2) shows the location as it relates to the SP results and Figure (13.1.1) shows the same on the DC cross section. The well is located where the largest anomalies are present in both data sets and as illustrated in the map in Figure (13.1.2) the well is conveniently located in a large vacant field. The UTM coordinates for the location are 4287860.783 northing and 398631.726 easting.

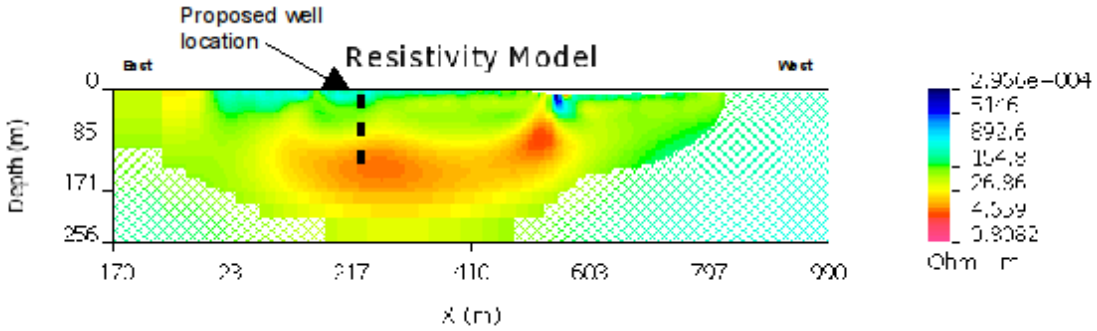

Figure 13.1.1: Inverted 2D section of the long line with the proposed well location indicated.

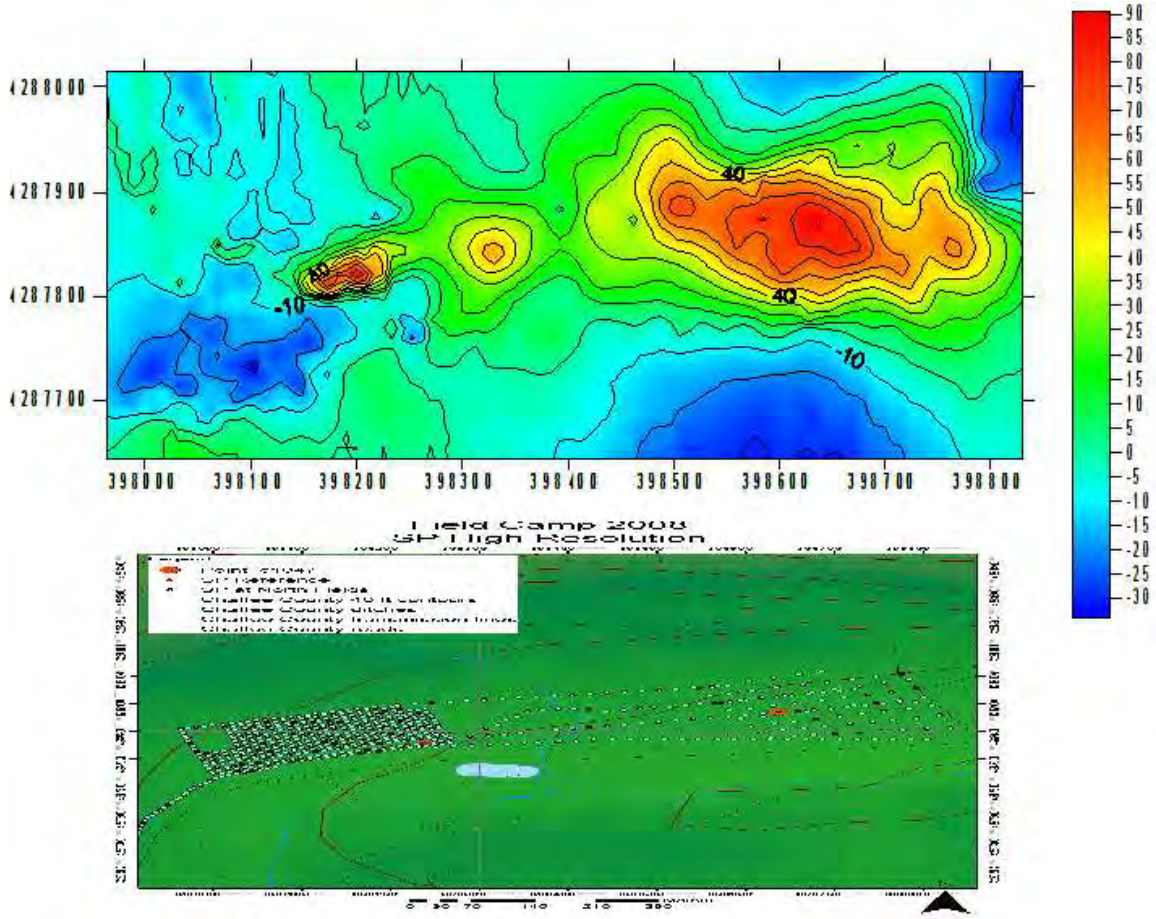

Figure 13.1.2: (Top) The SP data contour map (units are in millivolts). The approximate proposed well location is indicated by the black star. (Bottom)GIS map with the proposed well location indicated by the red circle with the black star. The red star is the location of the SP reference electrode.

13.2 Drainage Site Integration

13.2.1 Problem Description

The students in the geophysics department with the Colorado School of Mines were asked to investigate a site just west of Poncha Springs on county road 250. The possible problem associated with this site is the irrigation canal that runs roughly west to east is potentially leaking out into the adjacent field just south of the ditch. Local residents are concerned with this issue in that it could produce a false depth to the top of the water table. Another concern is if the groundwater tables recharge in that area is influenced by the leakage of the irrigation canal, and if so what would happen to the recharge of the water table if that source is removed. Our main goal with this investigation is to determine whether or not the irrigation canal is leaking. Prior to the survey, we looked at satellite photos of the area and noticed the field to the south of the drainage ditch is much greener than the north side. We later found out that the owners of that south field do not irrigate.

13.2.2 Survey Site Layout

DC and EM-47 measurement locations: **Note**: 3 of the 6 central loop locations are the only ones that coincide with east DC lines

13.2.3 EM-31 and DC data Comparison

Figures (13.2.3) and (13.2.4) show how the inverted data looks for the south site area just west of Poncha Springs. The EM-31 image in Figure (13.2.3) shows a 2D plot of the inverted data for the south site. The Fine lines that loop back and forth indicate the GPS coordinates taken continuously while completing this survey. The Inversion was plotted using GMT for Figure (13.2.3) and the location for the y-axis is in a UTM coordinate system. The DC image below in Figures (13.2.4)-(**??**) shows a 3D plot of the area that corresponds to the GPS locations in Figure 1. The Inverted data was plotted using a 3D mesh tool, which can be seen in slices that are associated with line numbers in Figures (13.2.4)-(13.2.8).

The EM-31 shows some water seepage but its not coming from drainage ditch, its coming from the pipe on the east side of the field. The slices that show line 1 and line 2 show this same seepage coming from the pipe. The conductive bodies on the south east side of the plots both appear to be at the same location on the south grid. On DC lines 3-5 there is obvious change for the conductivity values on one side of the canal compared to the other. The south side of the canal shows a much more conductive body that starts at the canal and flow to the south. On the north side of the canal the soil is much more resistive which indicates a much drier material in that location. The EM-31 data shows nothing in terms of canal seepage, which could be due to the depth of investigation, which is 6 meters. Overall for this comparison between the DC data and the EM-31 data we are only able to confirm that part of the anomaly we are seeing is coming from the surface flow generated by the

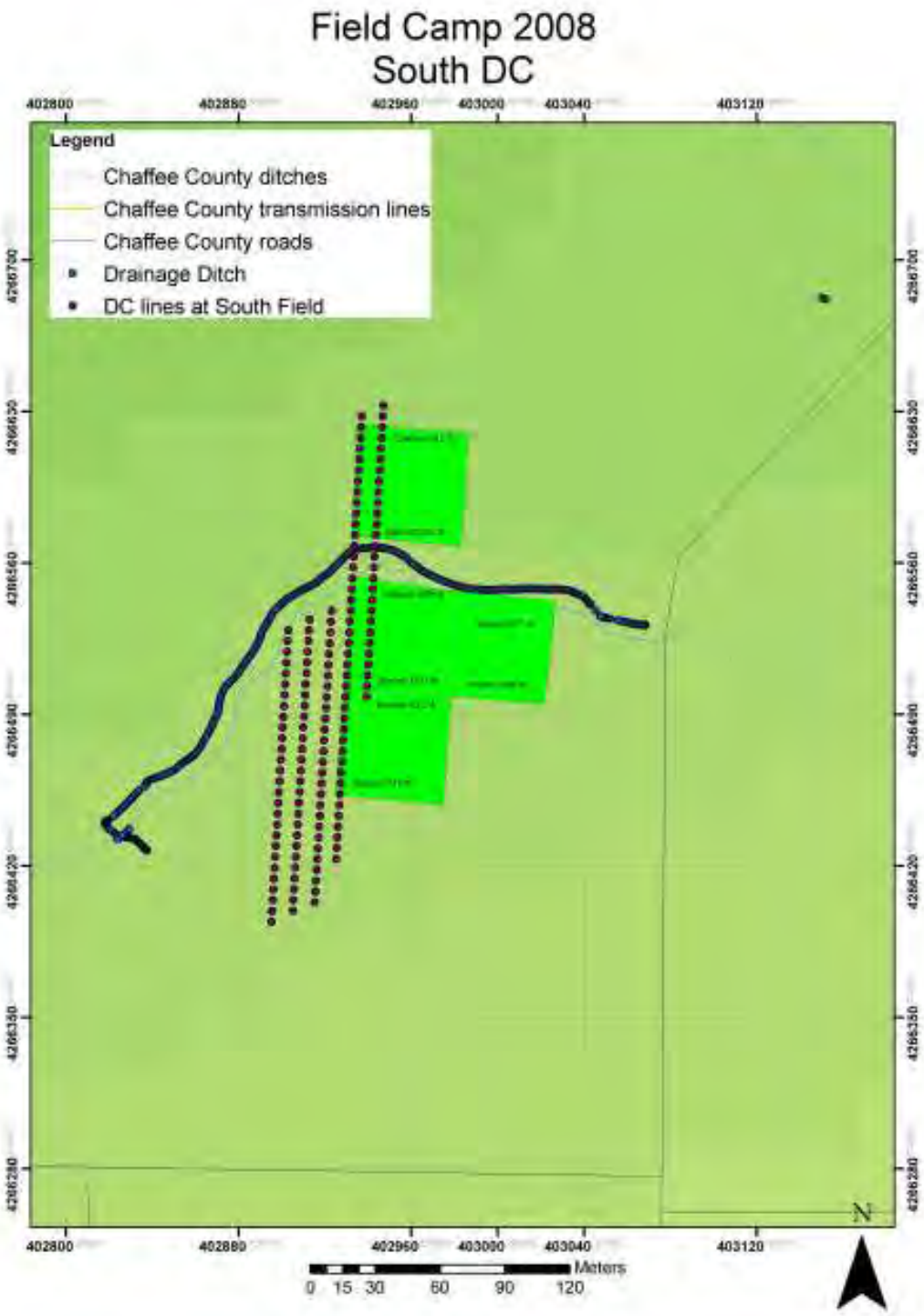

Figure 13.2.1: Survey layout for DC and EM-47 (South Site)

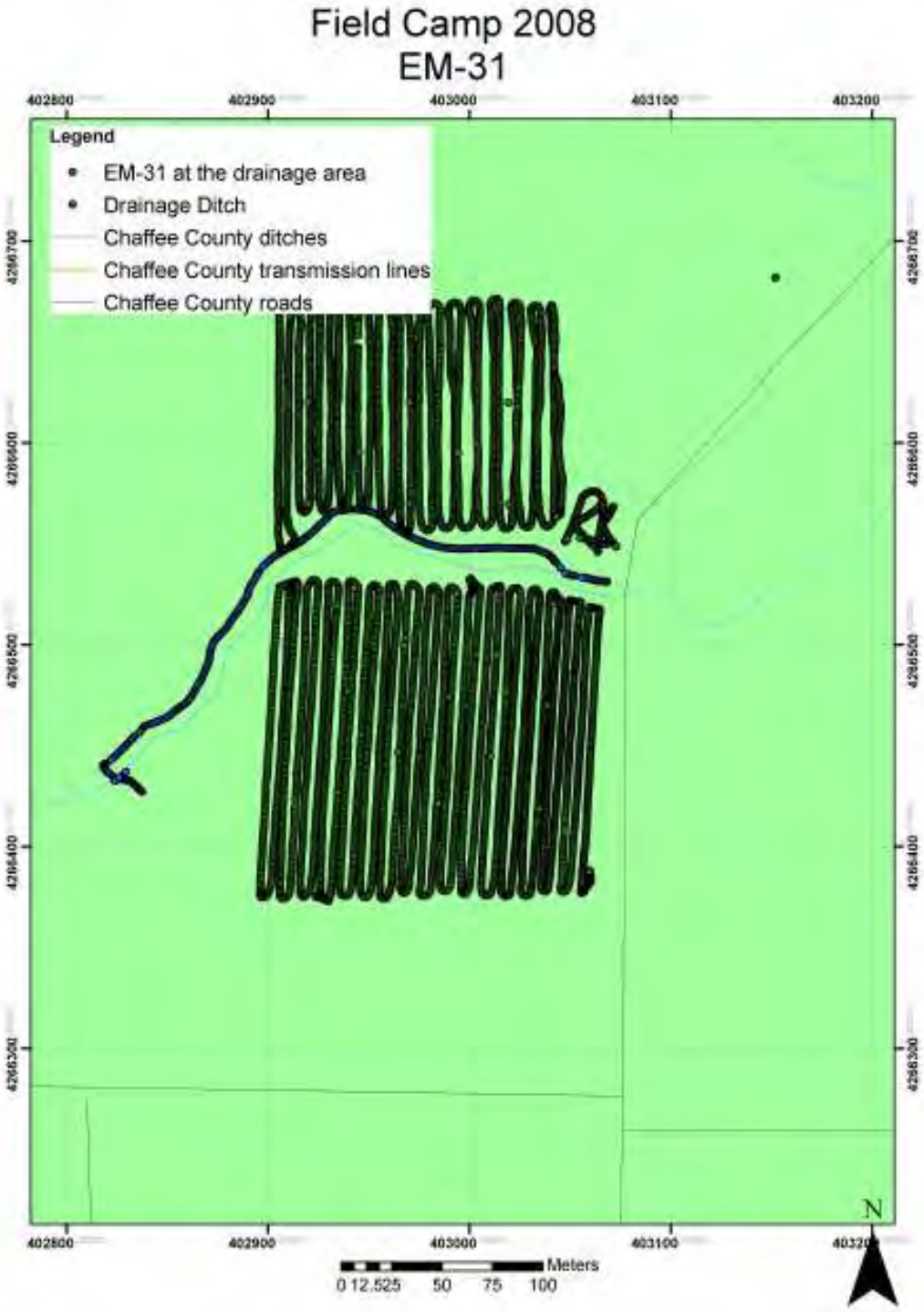

Figure 13.2.2: Survey layout for EM-31

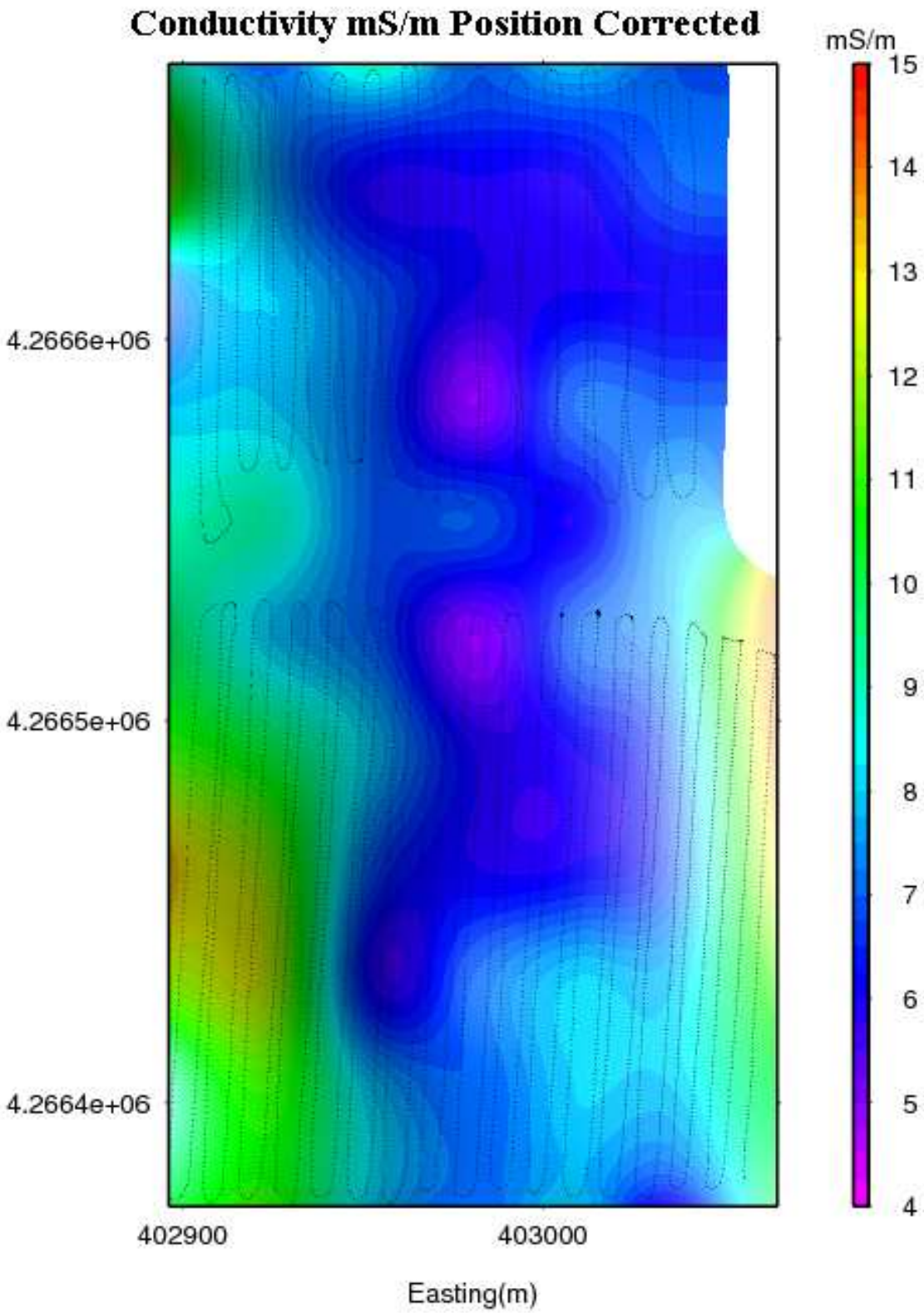

Figure 13.2.3: 2D plot for EM-31 on South site

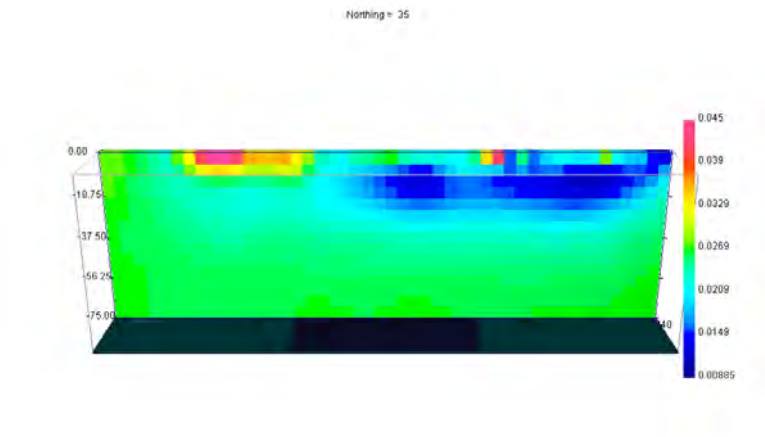

Figure 13.2.4: DC Line 1

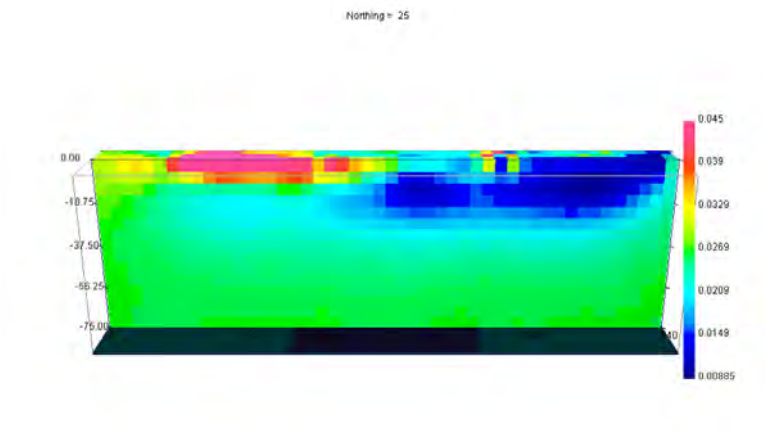

Figure 13.2.5: DC Line 2

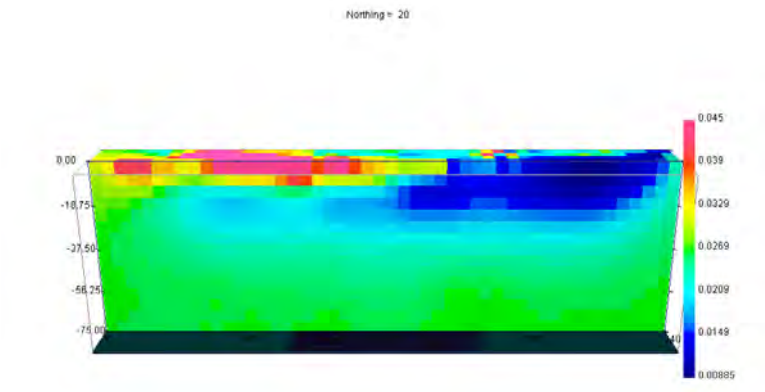

Figure 13.2.6: DC Line 3

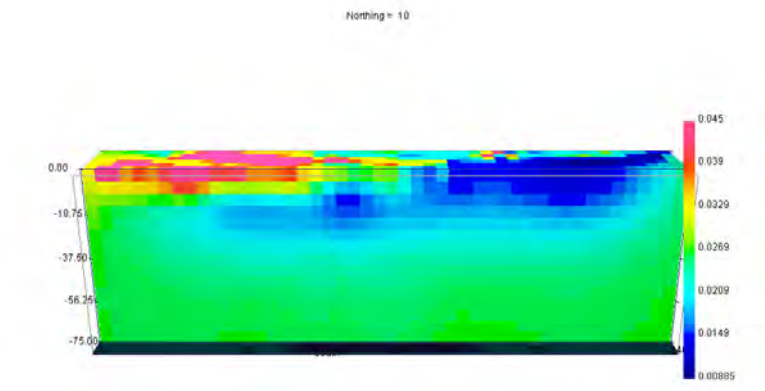

Figure 13.2.7: DC Line 4

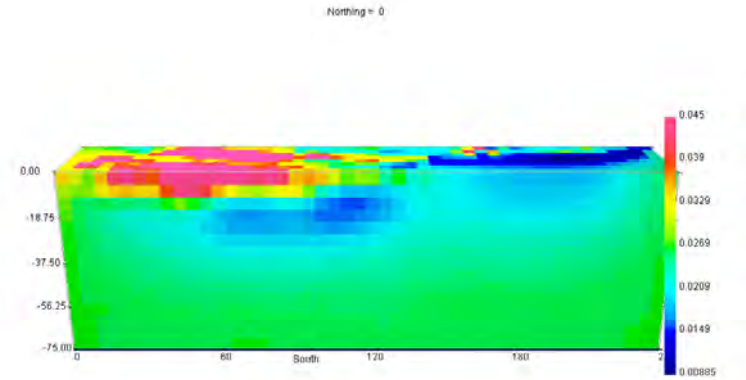

Figure 13.2.8: DC Line 5

pipe on the west side of the field.

13.2.4 EM-47 and DC data Comparison

As seen in Figure (13.2.1) four of the EM-47 loops cross lines 4 and 5 on the DC survey. Therefore the data from the soundings 001, 002, 007, 008, 009, 010, 011, and 012 are the only ones we can compare with the DC data. Soundings 001 and 002 are on the north side of the creek and the inversion results here correlate very well with the large resistive anomaly that can be seen in the 3D inversion of lines 4 and 5 in this location. The resistivity values on the north side range from 30 - 125 Ωm for the DC data, and the resistivity values from the EM-47 are around 65-85 Ωm. This confirms that there is little to no leakage from the ditch on the north side.

On the south side of the ditch we are seeing a conductive plume indicating that there is leakage present, but as mentioned in the previous section there is also water seeping into the ground on the west side of the field where a pipe is bringing water to the surface. The DC values from the south side of the drainage ditch range from 20-130 Ωm, and the data inverted from the EM-47 indicates a resistivity value ranging from 35-130 Ωm. The values for the EM-47 show a large increase in the conductivity when moving north to south across the drainage ditch. The inverted DC data and the EM-47 data correlate very well with each other. Overall, from reviewing the inverted data there is significant proof that the drainage ditch is leaking from the south side.

13.2.5 Concluding Results

The data collected at the drainage ditch located west of Poncha Springs gives supporting evidence to the fact that the ditch is leaking from the south side. The water from the drainage ditch is seeping in different locations along the canal and is seeping down into the subsurface. Therefore the seepage from the ditch is getting into the water table increasing

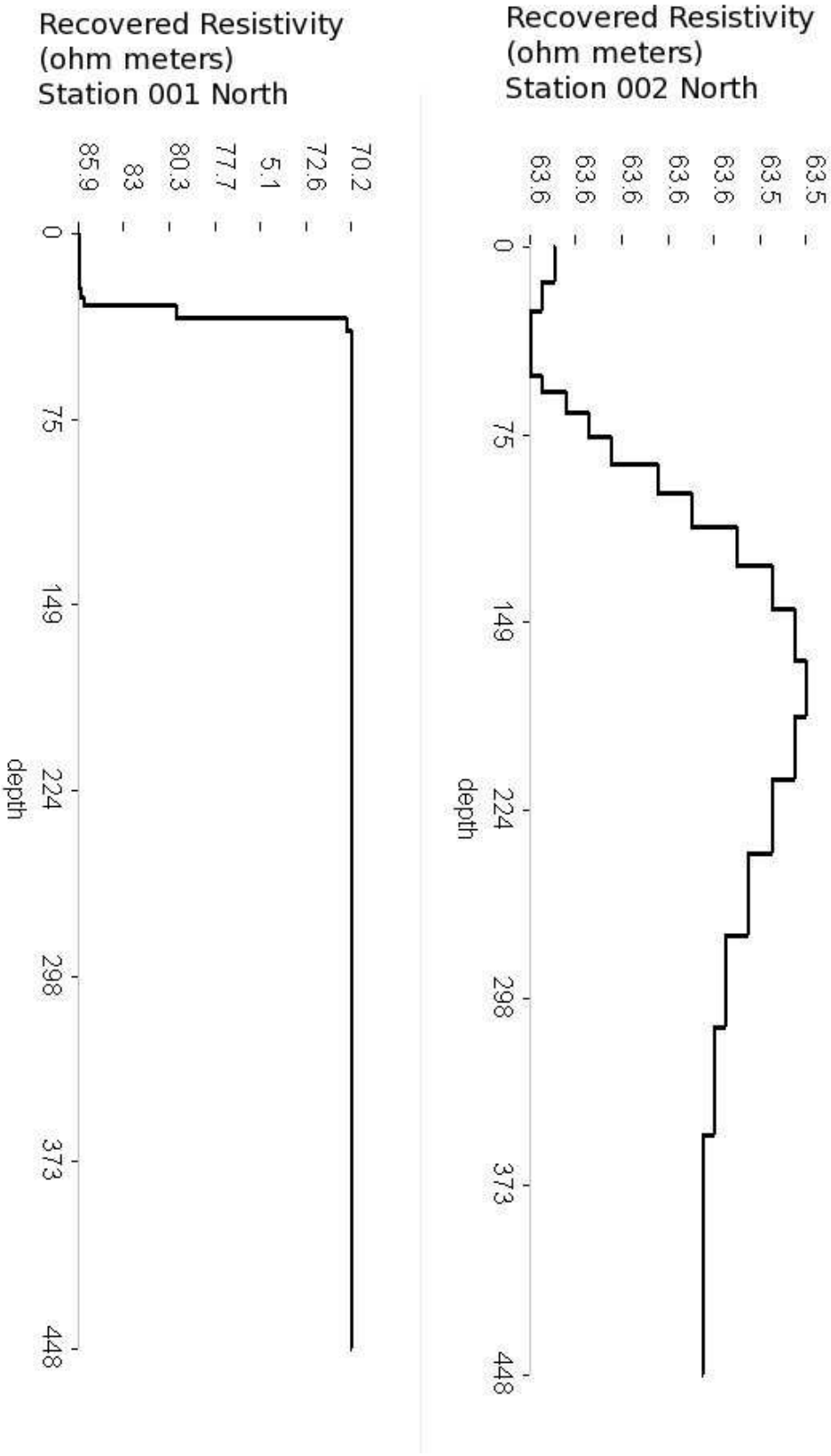

Figure 13.2.9: 1D inversion for stations 001 and 002 north of ditch

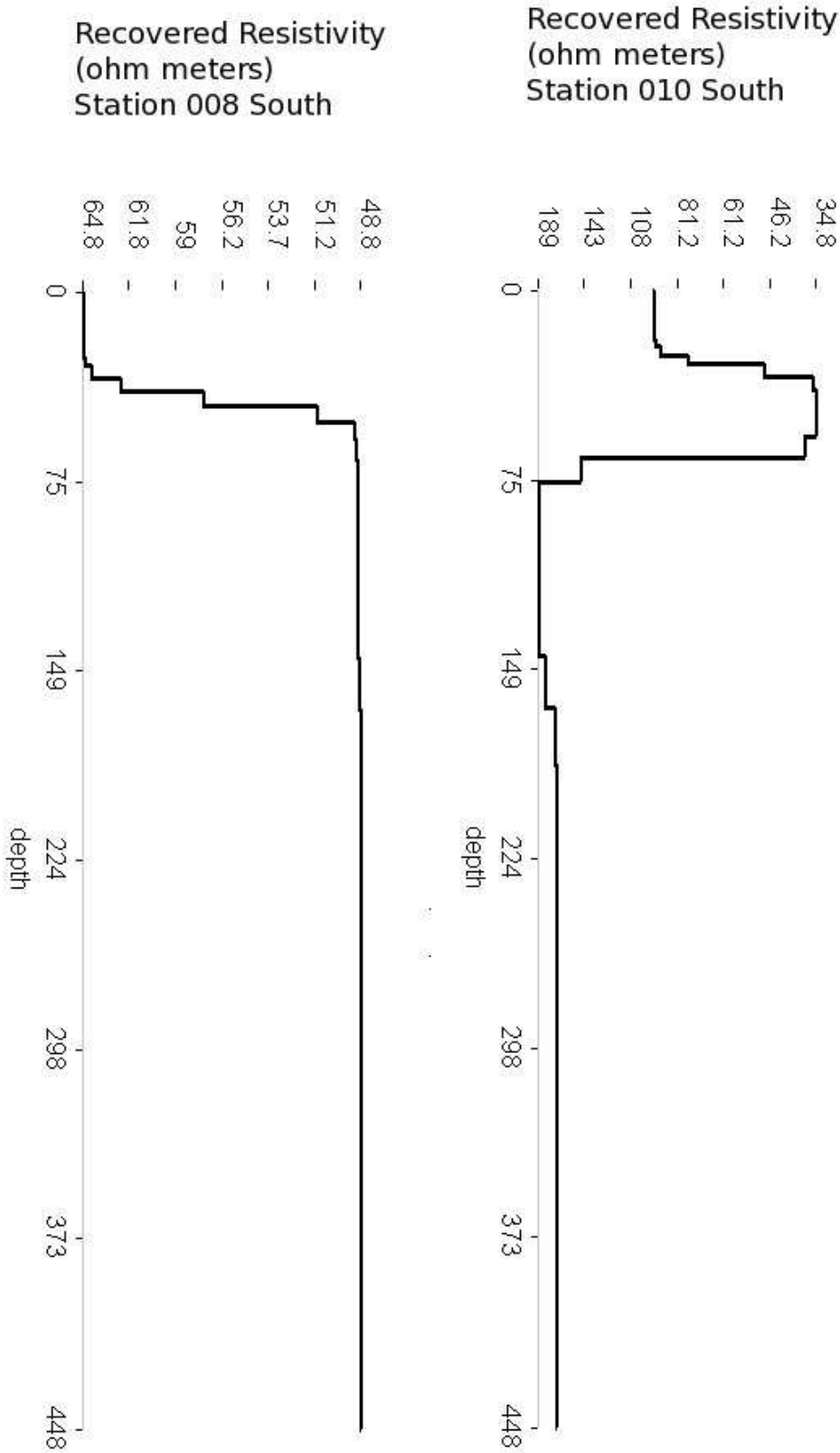

Figure 13.2.10: 1D inversion for Station 008 and 010 south of ditch

the total volume for the table. The amount of water that is seeping into the table is unknown but, we know that if this issue was fixed, the water table would definitely decrease in volume. The direction of the flow is evident from the SP survey conducted in the same location, which is flowing to the south by south-west. Figure 11 below shows this trend as you move from low to high in a southern direction. Image 12 shows what the plots for EM, DC, and SP look like overlaid on top of each other at the drainage location.

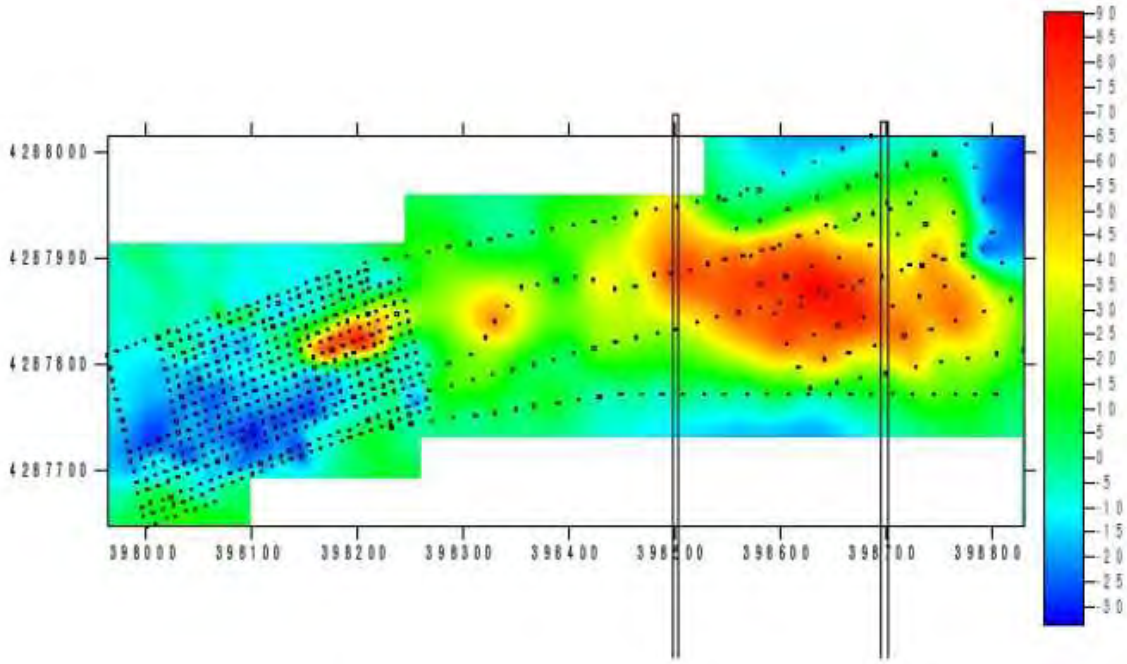

Figure 13.2.11: Trend in Water Movement taken by SP Crew

Chapter 14

Future Objectives and Plans

14.1 Objectives: Field Camp 2009

For the past four years the upper Arkansas River Valley has been the focus of study by several junior classes in the Geophysical Engineering Department of the Colorado School of Mines. The 2005 junior class studied one particular area of the valley using the same geophysical methods discussed so far. Similarly, the class of 2006 studied a different area, having moved south of the 2005 area. The junior class of 2007 attempted further investigations to the south. The 2008 junior class studied the Poncha Pass transfer zone at the southern extent of the valley, as well collected data in Chalk Creek Canyon to further the comprehensive understanding of the area. The succession of field camps in Chafee County was designed to gain a complete and accurate picture of the entire Upper Arkansas River Valley, starting at the northern end of the valley and moving south. However, more challenges still remain. In order to make a thorough analysis of the Upper Arkansas River Valley, the 2009 junior class should correlate seismic profiles together, implement electrical surveys with a finer grid, and investigate more areas to the east and south.

14.2 Field Camp 2009 Recommendations

Near Surface/Electrical

- Implement surveys west of the Southern Mosquito mountain range and east of the Arkansas River in order to get a comprehensive overview of the valley.
- The second high-resolution grid was not as finely sampled as the first high-resolution grid, so it might be beneficial to have a 10-meter spaced grid in the same area as well as where they connect, to get a better idea of the location of the major geothermal anomaly. It should also be extended more to the North to clearly delineate the edges of the anomaly.

Gravity

- It would be helpful to deploy a gravity crew along the eastern side of the basin in order to correlate with previous years gravity data.
- A profile constructed across the valley from east to west would provide valuable information about the sediments and hydro-geologic system.

Seismic

- Implement a north-south profile on the western side of the valley that runs perpendicular to data collected so far, therefore correlating the measurements from 2005, 2008, and possibly others. It could be located along CR-270 and CR-321 which travel north-south.
- Most of the profiles have been located to the west, so it would benefit to have an eastern profile oriented east-west, such as near Trout Creek Pass.

Surveying/GPS

- Handheld GPS systems are not accurate enough for the type of precise data we expect to reproduce.
- Planning of areas to GPS would be highly recommended, as many processing groups came back to CSM and found they did not have sufficient data, or the data had errors. A large part of processing is recording where the measurements were taken, and a lot of error is involved when the points need to be re-created.

Chapter 15

Appendix A - List of Figures

List of Figures

Chapter 16

Appendix B - Geologic Time Scale

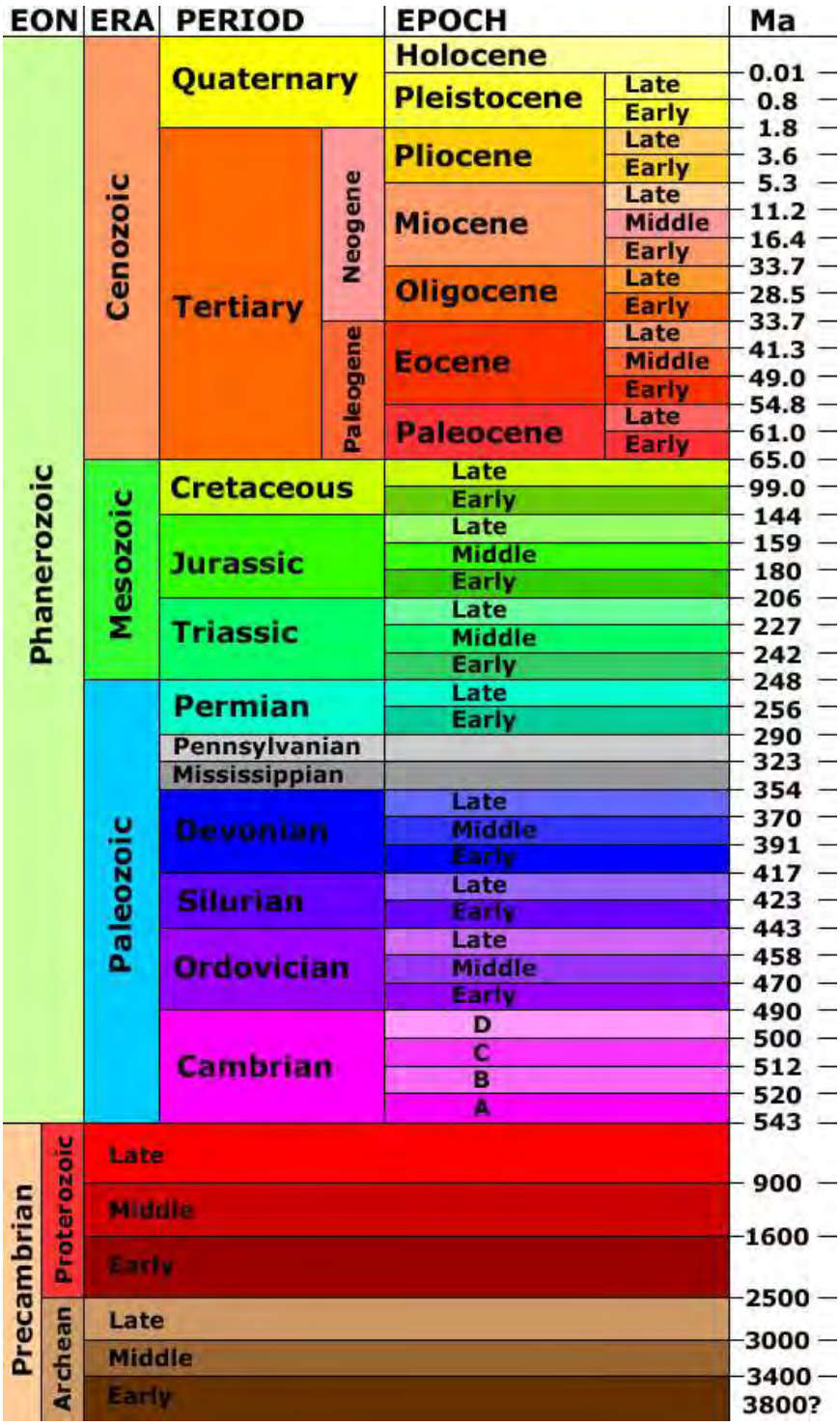

Figure 16.0.1: Geologic Time Scale[30]

Chapter 17

Appendix C - Maps

Figure 17.0.1: Drainage Area Map

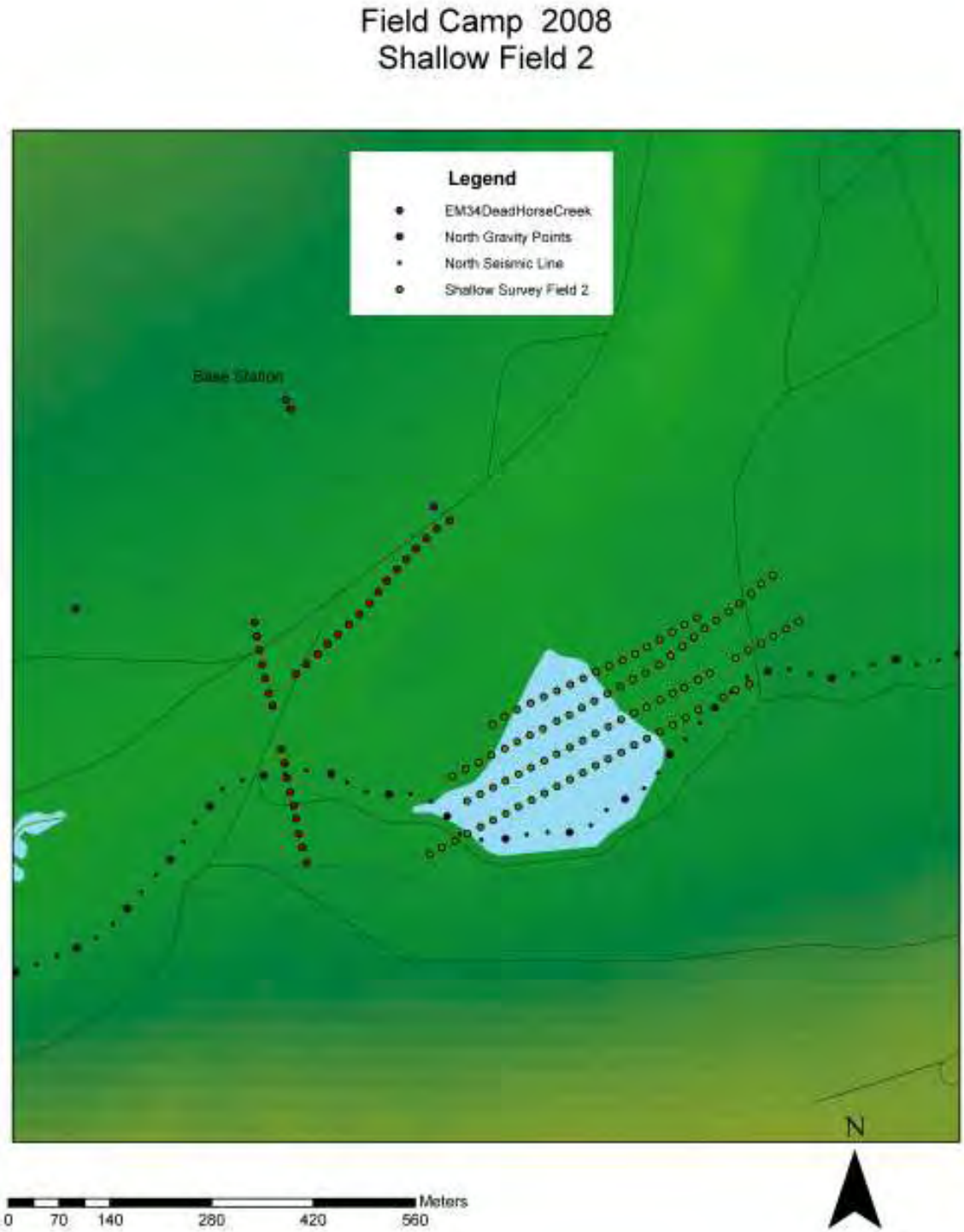

Figure 17.0.2: Shallow Field 2 Map

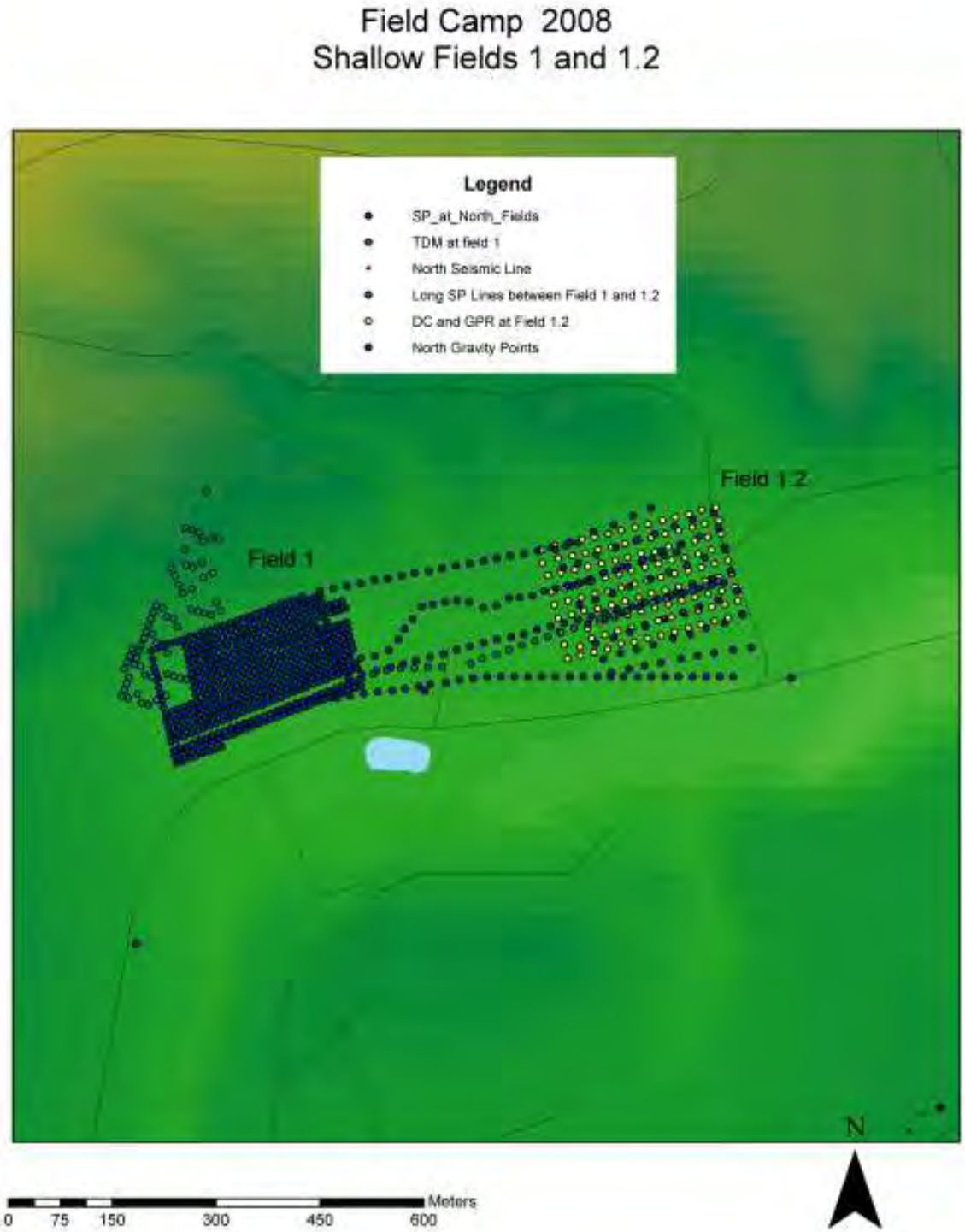

Figure 17.0.3: Shallow Fields 1 and 1.2 Map

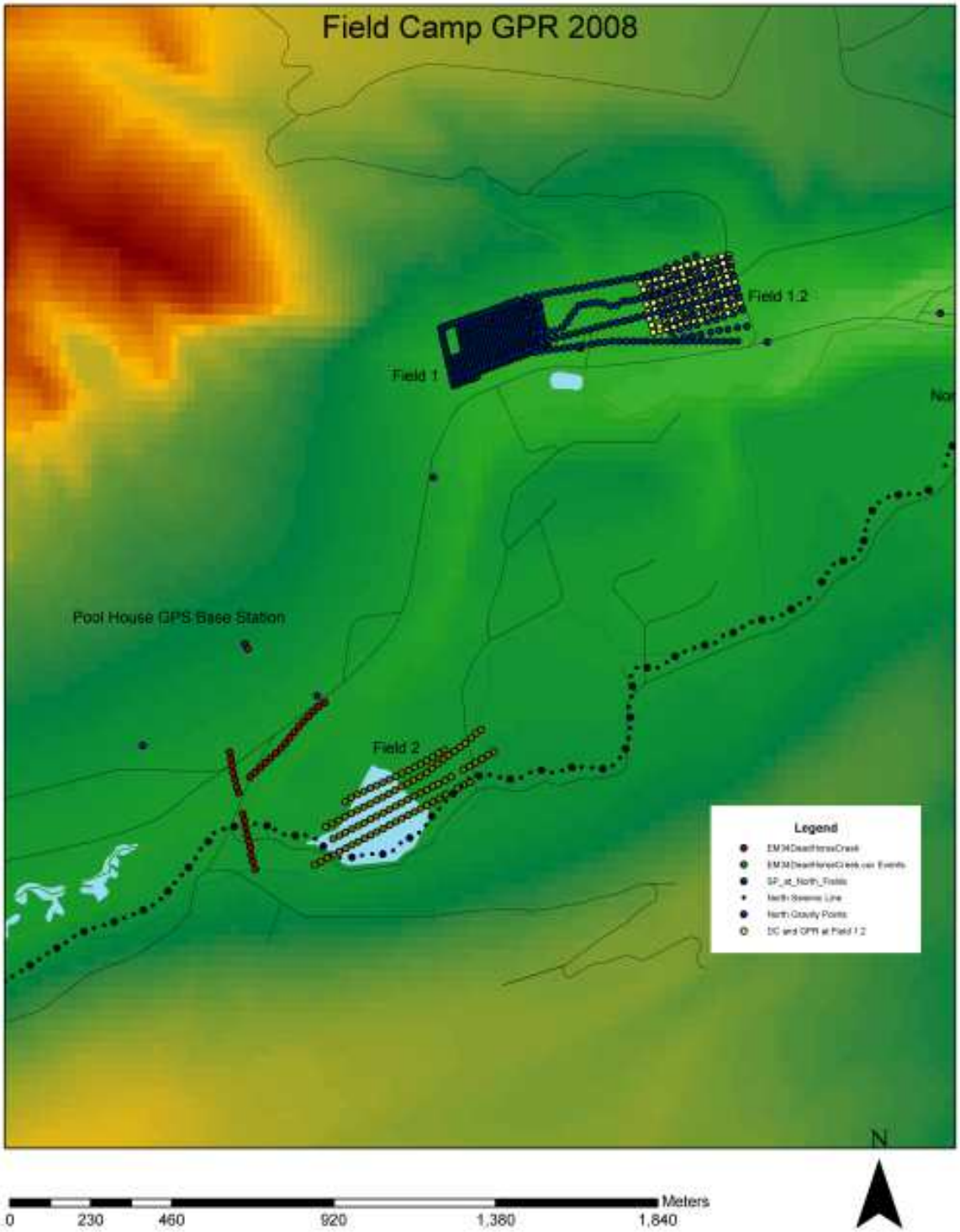

Figure 17.0.4: GPR Map

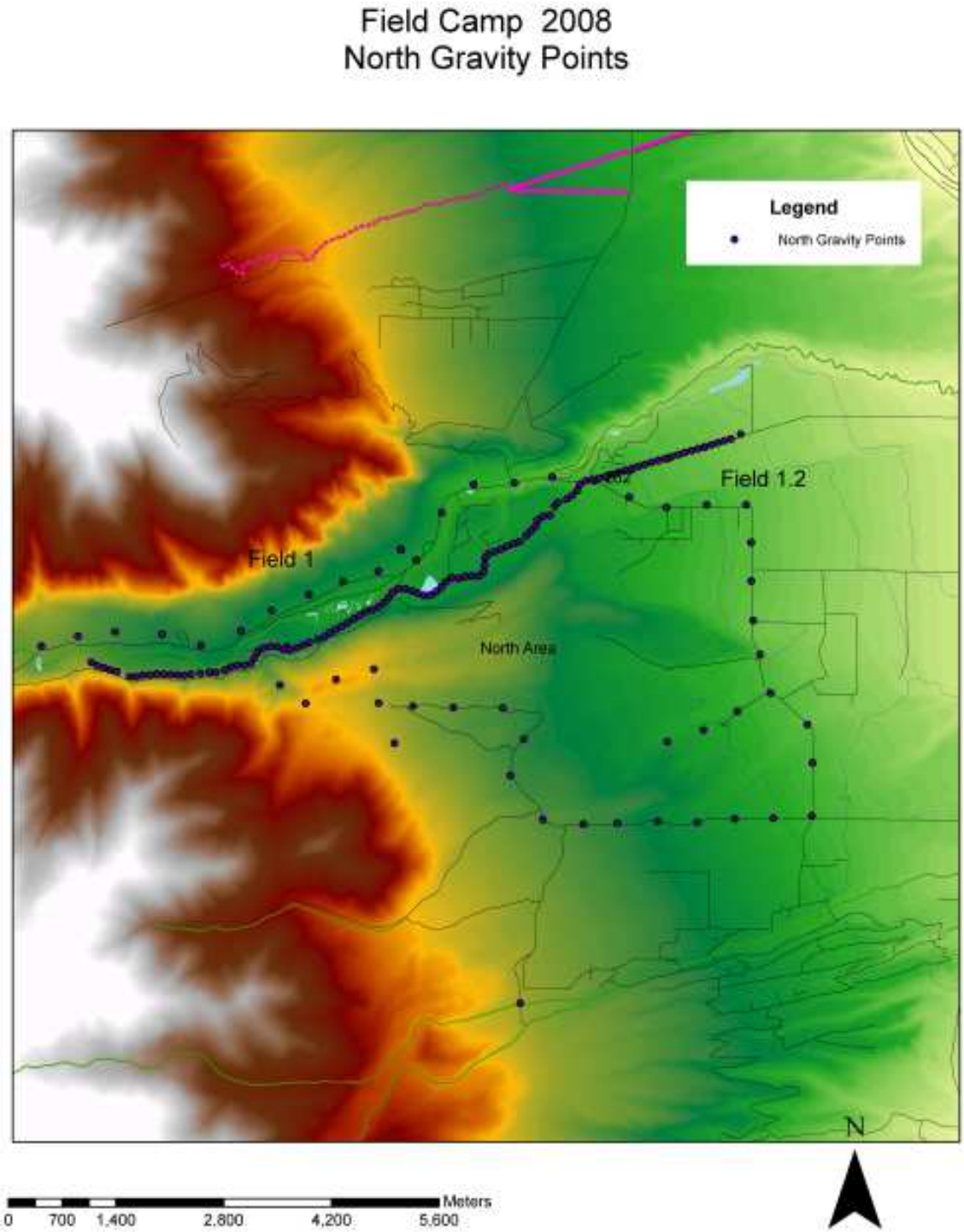

Figure 17.0.5: North Gravity Points Map

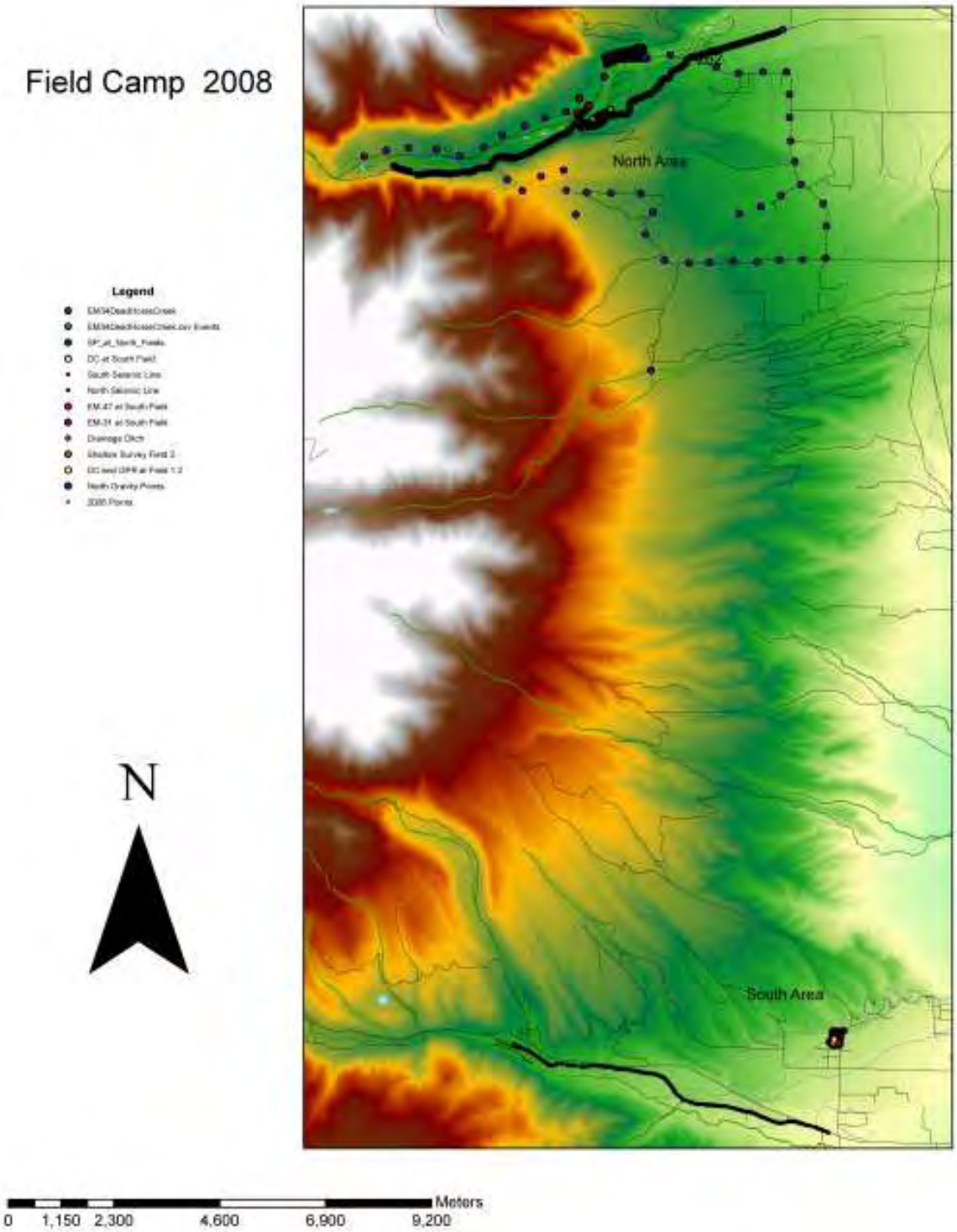

Figure 17.0.6: Field Camp 2008 Map

Bibliography

[1] ePodunk, "Chaffee County, CO," www.ePodunk.com. [Online]. Available: http://pix.epodunk.com/locatorMaps/co/CO_9387.gif. [Accessed June 4, 2008].

[2] J.C. Kammerer, "Largest Rivers in the United States," USGS. [Online]. Available: http://pubs.usgs.gov/of/1987/ofr87-242. [Accessed: May 30, 2008].

[3] Center for Gravity, Electrical, and Magnetics Studies, "Upper Arkansas River Valley," Colorado School of Mines. [Online]. Available: http://www.geophysics.mines.edu/cgem/projects/arkansas.html. [Accessed: May 30, 2008].

[4] CSM Geophysics Field Camp 2007, "Characterization of the Upper Arkansas River Valley," Colorado School of Mines. [Online]. Available: http://pal.boisestate.edu/mediawiki/index.php/Kasper. [Accessed: May 30, 2008].

[5] Garmin Ltd, "What Is GPS?", *Garmin*, 2008. [Online]. Available: http://www8.garmin.com/aboutGPS/. [Accessed June 2, 2008].

[6] Trimble, "Why we need Differential GPS?", *Trimble*, 2008. [Online]. Available: http://www.trimble.com/gps/dgps-why.shtml. [Accessed June 2, 2008].

[7] Environmental Systems Research Institute, Inc, "ArcGIS: The Complete Enterprise GIS", *ESRI*, 2008. [Online]. Available: http://www.esri.com/software/arcgis/index.html. [Accessed June 2, 2008].

[8] G. Asquith, D. Krygowski, *Basic Well Log Analysis*, 2nd ed., Danvers, Massachusetts, AAPG, 2004.

[9] Wikipedia, "Wave," *Wikipedia.org*, 2008. [Online]. Available: http://en.wikipedia.org/wiki/Wave. [Accessed June 2, 2008].

[10] Northwestern University, "Seismic Reflection," *Northwestern University - Department of Earth and Planetary Sciences*, 2007. [Online]. Available: http://www.earth.northwestern.edu/people/seth/107/Seismology/seismicreflection.htm. [Accessed June 2, 2008].

[11] L. Thomas, "Geophones," *Introduction to Geophysical Exploration*, 1999. [Online]. Available: http://www.earthsci.unimelb.edu.au/ES304/MODULES/SEIS/NOTES/geophone.html. [Accessed June 2, 2008].

[12] Schlumberger Ltd, "Diagrams of common depth point and common midpoint," *Schlumberger Limited*, 2008. [Online]. Available: http://www.glossary.oilfield.slb.com/DisplayImage.cfm?ID=228. [Accessed June 2, 2008].

[13] M. Tanahashi, "Seismic Method and Hydrate," *Methane Gas Hydrate*, 2001. [Online]. Available: http://www.gsj.go.jp/ tana/hydrate/seismic/seismic.method.html. [Accessed June 2, 2008].

[14] Halliburton, "ProMAX Family Seismic Data Processing Software," *Halliburton*, 2008. [Online]. Available: http://www.halliburton.com/ps/Default.aspx?navid=221&pageid=862&prodid=MSE%3a%3a1055450737429153. [Accessed June 2, 2008].

[15] Electromagnetics TDEM, Northwest Geophysical Associates, Inc. Online document, accessed May/30/2008: http://www.nga.com/Geo_ser_EM(FDEM).htm

[16] http://www.geonics.com/em31.html, Last Accessed: May 28, 2008, 10:13AM

[17] http://www.geonics.com/em34.html, Last Accessed: May 28, 2008, 09:53AM

[18] Electromagnetics TDEM, Northwest Geophysical Associates, Inc. Online document, accessed May/30/2008: http://www.nga.com/Geo_ser_EM(TDEM).htm

[19] A.P. Annan, *Ground Penetrating Radar Principles, Procedures & Applications*. Sensors & Software Inc, 2003, pp. 1-9.

[20] Olhoeft, Gary. Velocity. February 13, 2001. www.g-p-r.com/velocity.htm [Accessed June 4, 2008].

[21] J. M. Reynolds, An Introduction to Applied and Environmental Geophysics. West Sussex, England: John Wiley & Sons Ltd., 1997, pp 704.

[22] R. Phillips, "Electrical Resistivity Method," 2007. [Online]. Available: http://epsc.wustl.edu/ẽpsc454/Phillips/lecture_phillips_resistivity.pdf [Accessed May 28, 2008].

[23] "Identifying Roadbed Underlain by Expansive Clays (Determine Clay Content in Swelling Soils)...," *Federal Lands Highway Program*. [Online]. Available: http://www.cflhd.gov/agm/engApplications/RoadwaySubsidence/522IndentRoadbed ExpanClays.htm. [Accessed May 28, 2008].

[24] J. M. Reynolds, An Introduction to Applied and Environmental Geophysics. West Sussex, England: John Wiley & Sons Ltd., 1997.

[25] UBC-Geophysical Inversion Facility, Department of Earth and Ocean Sciences, University of British Columbia, DCIP3D: *A Program Library for Forward Modeling and Inversion of DC Resistivity and Induced Polarization Data over 3D Structures*, ver 1.0, Vancouver, British Columbia: GIF.

[26] *DCIP2D*: 2d Inversion of DC Resistivity and IP Data, ver. 3.2. GIF, 1998.

[27] R. Shekhtman, *MeshTools3D*, ver. 20010712. UBC-GIF, 2001.

[28] J. M. Reynolds, An Introduction to Applied and Environmental Geophysics. West Sussex, England: John Wiley & Sons Ltd., 1997, pp.31-115.

[29] Field Session 2007, "(Characterization of the Upper Arkansas River Valley: Gravity Survey," Department of Geophysics, Colorado School of Mines, 2007.

[30] "Geologic Time Scale," USGS. [Online]. Available: http://www.google.com/images. [Accessed June 4, 2008].